HUMIC ACID PROTONATION, METAL ION BINDING AND METAL COMPLEX DISSOCIATION KINETICS

A thesis

submitted in partial fulfilment

of the requirements for the Degree

of

Doctor of Philosophy

at

Lincoln University

New Zealand

by

Andrew William Rate

Lincoln University

1990

Abstract of a thesis submitted in partial fulfilment of the

requirements for the Degree of Ph.D.

HUMIC ACID PROTONATION, METAL ION BINDING AND METAL COMPLEX DISSOCIATION KINETICS

by A.W. Rate

Two humic acids have been studied in terms of: (i) their ability to bind H^+, Cd^{2+} and Cu^{2+}, and; (ii) the rates of dissociation of their Cu^{2+} complexes.

For both Summit Hill and Waimari Peat humic acids, the protonation reactions of the carboxylic acid functional groups were sensitive to changes in solution ionic strength, such that COOH groups dissociated more readily at higher ionic strength. This behaviour was shown to be consistent with that expected for flexible, macro-ionic molecules with acidic functional group heterogeneity. For Summit Hill humic acid, both the acid strength, and abundance, of COOH groups increased with decreasing molecular size.

The observed complexation of Cd^{2+} and Cu^{2+} with sodium or calcium humates of the humic acids was found to be very heterogeneous with respect to binding affinity. Both metal ions bound significantly to humates in the presence of excess concentrations of Na^+ or Ca^{2+}, and displaced H^+ from humates at neutral pH, suggesting inner-sphere complexation. The observed enhanced binding of Cd^{2+} and Cu^{2+} to humates, as temperature increased, was found to be more consistent with a very slow component in the complex formation reaction than with thermodynamic effects.

The kinetics of competing-ligand induced Cu^{2+}-humate dissociation reactions were also found to be very heterogeneous with respect to first-order rate constants. A new model for metal-humate dissociation kinetics, based on a lognormal distribution of first-order dissociation rate constants, was

developed and shown to give a good description of kinetic data. Dissociation reaction rates were found to increase with increasing Cu^{2+}:humate ratio, salt concentration or temperature; a decrease in reaction rate was found when pH or pre-dissociation Cu^{2+}-humate reaction time was increased.

Modelling of humic acid protonation, metal complexation, and Cu^{2+}-humate complex dissociation kinetics data was found to be useful, using suitable models, for predictive or comparative purposes. All equations used for modelling were considered to give strictly empirical descriptions of data.

ACKNOWLEDGEMENTS

I am gratefully indebted to Annelies, whose love, patience, and expert typing have been essential during my completion of this degree (which has lasted almost as long as our marriage).

Thanks are also due to those who have acted in a supervisory role during the course of this project: Dr Ron McLaren, whose comments, encouragement and practical assistance were very refreshing (and very necessary); Professor Roger Swift, for very helpful (and long-distance) comments on the manuscript, and without whom the project would never have started; and Dr Roland Harrison, for helpful discussion and criticism. I am especially grateful to Dr Kip Powell for advice and encouragement from start to finish.

Expert and indispensable technical assistance was provided by Ms Leanne Hassall, Mr Huntly Horn, Mr Rob McPherson and Mr Alan Wise.

I appreciated useful and helpful discussions regarding my work with Dr Clare Backes, Dr Bob Leonard, Dr Geraldine Ritchie and Dr Rob Sherlock.

The staff at the Centre for Computing and Biometrics were also extremely helpful. Mrs Brenda Lord and Mr Paul Helleur gave expert help with word processing and graphics; Mr Martyn Brown and Mr John Baird ably assisted with FORTRAN, and Dr Dick Sedcole and Mr Bruce Robson gave useful statistical help and discussion.

Finally, thanks to those friends, relatives and acquaintances (you know who you are) who made life in and out of Lincoln University bearable over the past few years, and kept sanity an achievable option.

TABLE OF CONTENTS

CHAPTER THREE
MATERIALS AND METHODS

CHAPTER FOUR

COMPUTER PROGRAM DEVELOPMENT AND TESTING

CHAPTER FIVE

PROTONATION BEHAVIOUR OF WAIMARI PEAT AND WHOLE AND SIZE -FRACTIONATED SUMMIT HILL HUMIC ACIDS

CHAPTER SIX

COPPER AND CADMIUM BINDING BY SUMMIT HILL AND WAMARI PEAT HUMIC ACIDS

CHAPTER SEVEN
KINETICS OF COPPER(II) DISSOCIATION FROM SODIUM AND CALCIUM HUMATES

CHAPTER EIGHT
CONCLUSIONS

LIST OF FIGURES

LIST OF TABLES

LIST OF SYMBOLS

In the text, SI symbols and units have been used wherever possible. Square brackets [ ] always denote concentrations. The names of elements are abbreviated to the conventional periodic table symbols.

Symbol	Explanation
a	constant in integrated form of Elovich equation
a_j	activity of species j
A	fitting parameter in Sips/Freundlich equations
b	constant in integrated form of Elovich equation
B([M])	terms in numerical finite difference equation
C(k,t)	concentration distribution function for kinetic spectrum
C_L	sum of protonated, deprotonated and metal-complexed ligand concentrations over all ligands
C_{ML}	stoichiometric concentration of bound metal
Cu_L	labile copper
Cu_{NL}	non-labile copper
Cu_{NR}	effectively non-reactive copper
DF	degrees of freedom
E_a	activation energy
F	variance (F) ratio
F	Faraday constant
F(k,t)	distribution function for kinetic spectrum
I	ionic strength
k_F	first-order forward rate constant
k_R	first-order reverse rate constant
k_i	first-order rate constant for reaction of metal ion with ligand $k_\mu$mean of normal distribution of first-order rate constants
L_i	
K_a	acid dissociation constant (= $1/K_{HL}$)
K_{H_nL}	stepwise protonation constant for formation of H_nL
K_i	formation constant for species ML_i
K_{ML}	formation constant for ML
K_s	self-association formation constant
K_x	crosslinking formation constant
K_μ	mean of normal or Sips distribution of binding constants
$\overline{K}$	weighted average equilibrium function
K'	differential equilibrium function
L	generalised deprotonated ligand
L_i	i^{th} deprotonated ligand
L_i'	sum of concentrations of deprotonated and protonated forms of i^{th} ligand
L_{obs}	observed ligand concentration (kinetics)
M	generalised metal ion
MS_B	error mean square
MS_R	regression mean square
MS_T	total mean square
n	number of ligands L_i in discrete multiligand models
	molecularity of complex ML_n
	average number of acidic groups per macromolecule

Symbol	Explanation
N(κ)	distribution function for continuous multiligand models
P	generalised reaction product
P_s	self-association probability
P_j	adjustable parameters in model(s)
pK_{app}	apparent dissociation constant
pK_{HH}	apparent dissociation constant at half-neutralisation
pK_{int}	intrinsic dissociation constant
R	generalised reactant
R	gas constant
r_1	singly lagged residual autocorrelation
SS_B	error (residual) sum of squares
SS_R	sum of squares for regression
SS_T	total sum of squares
t	time
T	absolute temperature
w	regression weighting factor
z	electrostatic charge
α	degree of dissociation
	constant in Elovich equation
β	fitting parameter in Sips/Freundlich equation
	constant in Elovich equation
β_{H_nL}	overall protonation constant for formation of H_nL
β_n	overall formation constant for complex ML_n
γ	Gaussian distribution spread parameter
e_j	molar absorptivity of species j
f	nuber of crosslinking sites per macromolecule
f_1, f_2	terms in numerical finite difference equation
χ_j	mole fraction of species j
θ	number of data
κ	log K (equilibria) or log k (kinetics)
η	electrostatic interaction term
ψ	electrical potential
$\overline{\nu}$	formation function (= $\Sigma_i[ML_i]/C_L$)
σ_K	standard deviation of normal distribution of binding constants
σ_k	standard deviation of normal distribution of rate constants
τ	dimensionless time parameter (= kt)
ω	composite electrostatic interaction term
[j]	concentration of species j
$[j]_B$	concentration of species j in bulk solution
$[j]_S$	concentration of species j at charged surface
$[j]_0$	concentration of species j at time = 0
$[j]_t$	concentration of species j at time = t
$[j]_\infty$	concentration of species j at time = ∞

CHAPTER ONE

INTRODUCTION

1.1 General Introduction

It has long been recognised (Bremner *et al.*, 1946; Beckwith, 1955) that the complexation reactions between soil organic matter and metal cations are important in soil systems. The extent to which a metal cation is complexed can determine whether it is present at deficient or toxic levels for soil organisms (Adriano, 1986). This is important in the context of availability of trace elements to plants. In addition, soluble organic complexing agents may provide a mechanism for the transport or leaching of metal ions which would otherwise remain immobile within soils (Stevenson, 1985). Such transport processes may also facilitate plant availability, by moving metals into the vicinity of plant roots.

Since humic substances form a substantial proportion of the organic complexing agents present in soils (Brady, 1974; Stevenson, 1985), an understanding of the reactions between these materials and metal ions are of importance in understanding soil processes, and for making predictions regarding metal ion speciation. Although the complexation reactions between humic substances and metal ions can be modelled empirically (Sposito, 1986), a complete mechanistic explanation of the processes involved remains elusive. This particular research problem is considered by some authors (Perdue and Lytle, 1983b) to be intractable, due to the complexity of the reactions involved.

The metal ions for which complexation reactions with humic substances will be most critical are those normally present in trace quantities in the environment. Trace metals can be subdivided into two

categories: essential, and non-essential, depending on whether or not they are necessary participants in biochemical processes. Both types of trace metal ions may be toxic to plants and other soil organisms if present in excess (Purves, 1985).

Copper (as the divalent cation Cu^{2+}) is a trace element which is essential for plant nutrition, although if present in excessive amount it may cause toxic effects for plant and other soil organisms (Purves, 1985). Copper is known to form strong complexes with soil humic substances (Stevenson and Ardakani, 1972), and 20-50% of soil copper may be associated with organic matter (Adriano, 1986). Copper(II)-organic complexes have been implicated in plant deficiencies of copper, especially in soils such as peats with high organic contents (Brady, 1974). In contrast, the toxic effects of high levels of copper may be ameliorated *via* complexing reactions with humic substances (Adriano, 1986).

In contrast, an element such as cadmium, also existing largely as the divalent cation, is not known to be necessary for any biological processes and is toxic at quite low levels (Purves, 1985). Although it has been suggested that the dominant mechanism of cadmium(II) - humic substance interaction is an ion-exchange process, it has also been found that organic interactions can limit plant uptake of cadmium (Adriano, 1986).

Copper is commonly applied intentionally to soils in fertilisers (Brady, 1974), and efficient use of such soil amendments demands a more thorough knowledge of the relevant reactions. In addition, both copper and cadmium are known (de Haan and Zwerman, 1976) to be present in agricultural, urban or industrial effluent and accurate prediction of environmental impacts also requires such detailed information.

1.2 Scope of This Work

1.2.1 General

The project was intended to focus on the complexation reactions of two humic acids with copper(II) and cadmium(II). One humic acid was the Summit Hill tussock grassland soil humic acid, which is a Reference humic substance of the International Humic Substances Society. The second humic acid used was extracted from the Waimari Peat soil. A survey of the literature (Chapter 2) was considered to justify the following research objectives.

1.2.2 Research Objectives

1. To characterise the protonation behaviour of the two humic acids: quantitatively, in terms of abundance and strengths of acidic groups, and qualitatively, in terms of macro-ionic behaviour and solution conformation.

2. To investigate the effect of molecular size fractionation on the protonation behaviour of the IHSS Reference humic acid.

3. To examine the effect of temperature on the complexation reactions of the two humic acids with copper(II) and cadmium(II), especially for humates in the solid phase, and to provide explanations for the observed behaviour.

4. To measure rates of dissociation of metal-humate complexes from solid and dissolved humates, and examine the effect of varying certain experimental conditions (such as pH, initial metal:humate ratio and ionic strength) on these rates.

5. To evaluate, or develop, and apply models for humic substance protonation, metal complexation and complex dissociation kinetics, and use these models as an aid in formulating conclusions about the mechanisms of complexation reactions.

6. To relate the observed protonation, metal complexation and complex dissociation kinetics behaviour of the humic acids to mechanistic and structural hypotheses.

7. To develop and implement experimental and numerical analysis techniques suited to the previously stated objectives.

CHAPTER TWO

LITERATURE REVIEW AND INTRODUCTION TO HUMIC SUBSTANCES

2.1 Preliminary Descriptions

It is should be noted, before starting, that a large number of books and major reviews are available which cover similar aspects of the properties of humic substances to those covered here. This review, therefore, does not aim to be comprehensive, but to introduce the reader to some chemical and physical properties of humic substances which relate in some way to this project.

2.1.1 General Definition of Humic Substances

Humic substances are complex mixtures of a broad and very variable group of organic compounds, which are classified under a single definition on the basis of common macroscopic properties. The following properties are shared by humic substances: they are macromolecular, weakly polyelectrolytic, polydisperse, structurally heterogeneous, chemically and biochemically stable and intensely coloured organic substances formed from biologically derived residues by a combination of biochemical action and abiotic chemical reactions. Excluded from this concept of humic substances are well defined organic substances such as: proteins, polysaccharides, lipids or any other pure compounds. Humic substance macromolecules, however, may contain structural elements which are identical with, or

closely resemble, known molecules (Schnitzer, 1978; Thurman and Malcolm, 1983; Stevenson, 1982, 1985; Aiken *et al.*, 1985).

2.1.2 Occurrence of Humic Substances

Humic substances are ubiquitous in terrestrial, aquatic and marine environments, including soils, peats, groundwaters, lakes, streams, estuaries and oceans and their associated sediments (Aiken *et al.*, 1985; Thurman, 1985). They occur in these environments both by formation *in situ* and translocation from other environments by various forms of water movement such as soil leaching and stream transport. Soil humic substances are almost exclusively formed within soils. They are a major carbon pool in the global environment (Aiken *et al.*, 1985; Hayes *et al.*, 1989a) and contribute humic substances to most other systems except pelagic environments (Harvey and Boran, 1985).

2.1.3 Formation of Humic Substances in Soil and Sediments

Humic substances in any environment are predominantly formed from the residues of dead plant materials, due to the dominance of plants (primary producers) on a mass basis over animals in most ecosystems (Clark, 1979). As these biological residues decay biologically and chemically, numerous types of organic compounds are released. These include: saccharides (cellulose, starches, sugars); phenolic compounds (lignins, flavonoids, tannins) and the related quinones; amino acids and proteins; lipids, triglycerides and other hydrocarbons; and more simple organic compounds such as citric and oxalic acids (Stevenson, 1982, 1985; Mathur and Farnham, 1985). Humic substances are considered to form from these precursors, and several processes are believed to contribute to their formation. The more complex compounds (lignin, polysaccharides, proteins) are probably degraded further into more simple molecules. Humic substances are considered to form from these simpler molecules through polycondensation reactions, largely involving phenols and quinones. Amino acid - phenol reactions and

amino acid - sugar reactions are also believed to occur. The amorphous nature of humic substances suggests that the formation reactions are essentially random, involving little or no biochemical control. A variety of mechanisms for the formation of humic substances in soils and sediments are likely to be active. Compounds resembling humic substances are also produced by fungi as secondary metabolites and released into soils and sediments (Kumada, 1987); synthetic organic compounds from human sources may also make a minor contribution in polluted environments (Bollag, 1983).

2.1.4 Practical Definitions of Humic Substances

Practical definitions of humic substances are largely operational in nature, and are a function of the extraction procedures (and any subsequent purification and fractionation procedures) used to isolate humic substances from the environment (Aiken *et al.*, 1985). Ideally, isolated humic substances should be truly representative of those which occur in the environment. In reality, different extraction, purification and fractionation procedures produce humic extracts with different properties (Swift and Posner, 1972; Hayes, 1985). Standardised methods have been devised by the International Humic Substances Society (Swift, 1989 (personal communication)). The IHSS method for extraction of humic substances from soils appears in Appendix 1. Humic substances from any source are conventionally divided into *operational* fractions (Figure 2.1): **fulvic acid**, which is soluble in aqueous systems below pH 1.0, and **humic acid**, which precipitates from aqueous solution at or below pH 1.0. A third fraction, **humin**, is insoluble in any aqueous solution and is therefore inaccessible to conventional extraction methods (Hayes and Swift, 1978; Aiken *et al.*, 1985). The fractions obtained are still extremely complex mixtures; differences in average bulk properties can, however, be observed.

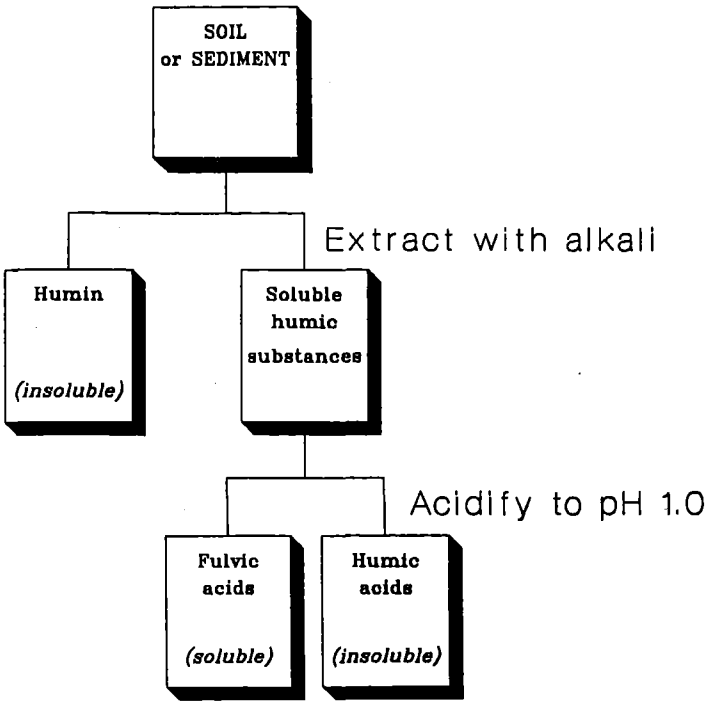

Figure 2.1 Relationships between commonly used fractions of soil humic substances.

2.2 Properties of Humic Substances Relevant to This Project

The definitive characterisation of humic substances is a problem which has eluded researchers for as long as humic substances have been studied. The heterogeneous nature of humic substances themselves may make this goal effectively unachievable; however, enough has been learned of the average properties of humic substances to provide a good qualitative description of their chemical and physical characteristics.

2.2.1 Elemental Composition

The microbial synthesis of humic substances from plant and animal detritus means that these substances are composed of organic molecules. This is reflected in their elemental composition; the main elements

present in humic substance molecules are carbon, hydrogen, oxygen, nitrogen and sulphur with other elements (for example, exchanged metal cations) present in smaller amounts. (It should be noted that elemental composition is conventionally measured using fully H^+-exchanged humic substances; in the natural environment, humic substances contain significant amounts of exchanged cations such as Na^+, Ca^{2+} and Al^{3+}.) The heterogeneous nature of humic substances has meant that a range of elemental compositions has been observed; average values for the major elements in soil humic substances are given in Table 2.1.

Table 2.1 Ranges of elemental composition values found for soil humic substances (condensed from Schnitzer and Khan, 1972; Stevenson, 1982; Steelink, 1985).

	Composition (% w/w)	
Element	Humic acids	Fulvic acids
Carbon	53.8-60.4	40.7-50.9
Hydrogen	3.2-6.2	3.3-7.0
Oxygen	31.9-38.3	39.7-50.0
Nitrogen	0.8-6.0	0.7-3.3
Sulphur	0.1-2.0	0.1-3.6

2.2.2 Chemical Structure

2.2.2.1 General considerations

As humic substances are composed of a range of organic macromolecules of indeterminate and variable geometry, it is impossible to define an exact structure. A range of important structural components can, however, be identified. Current concepts of the chemical structure of humic substances are based on the identification of degradation products, interpretation of infrared and ^{13}C nmr spectra, and inferences made from other characteristics such as elemental composition, reactive functional group analysis, acid-base/ion exchange properties, solubility in various solvents, and so forth.

When discussing the structure of humic substances, however, some conceptual problems arise. The biochemical origin of the materials from which humic substances are formed means that intact structures from biological sources, such as peptides and polysaccharides, may be incorporated into the humic substance structure. A conflict arises as to whether these intact, biologically derived and identifiable structures, which are released from humic substances on simple hydrolysis, should be considered intrinsic to humic substance structure or be regarded merely as impurities (Steelink, 1985). A similar situation exists for exchangeable metal ions; polyvalent metal ions such as Cu^{2+}, Al^{3+} and Fe^{3+} are bound very strongly to humic substances, and certainly form an integral part of humic substance structure under environmental conditions. It is the opinion of this author that reactivity is not a sufficient criterion in itself to exclude hydrolysable or exchangeable moieties from humic substance structure; a less operational method for distinguishing covalently bound from weakly associated structures would be preferable. This conflict is not trivial; structures such as amino acids may contribute significantly to complexation reactions between humic substances and metal ions.

2.2.2.2 Carbon-carbon bonding

Comprehensive reviews of chemical degradation studies of soil humic substances, and the structural inferences which may be made, have been compiled by Hayes and Swift (1978), Griffith and Schnitzer (1989), Hayes and O'Callaghan (1989), Parsons (1989), and Stevenson (1982, 1989). Identification of degradation products yields information on the carbon skeleton structure of humic substances. Shortcomings of any degradative method for structural determination include the possibility that the degradative procedure itself could give rise to compounds which were not present as structural components in the humic substance macromolecules. In addition, only a fraction of the carbon present in humic substances gives rise to identifiable degradation products. Unfortunately, since cleavage of the carbon bonds involves considerable energy, the reagents giving the highest proportion of degradation products are also the most likely to produce artefacts due to side-reactions (Hayes *et al.*, 1989a).

The main forms of carbon-carbon bonding which have been identified are single polysubstituted aromatic structures such as phenols and benzene carboxylic acids; condensed aromatic structures may also be present as minor structural components. Substituted and unsubstituted aliphatic and unsaturated chains, which may be branched or straight, have also been identified. Some of the more common types of degradation product are illustrated in Figure 2.2 for oxidative degradations and in Figure 2.3 for reductive degradations. No unambiguous information on how the structural 'units' implied from degradative studies of humic substances are interconnected is available. It is, however, likely that aromatic nuclei are connected by chains of carbon atoms of varying length; these carbon chains may also exist as non-connective substituents.

A technique which offers the possibility of non-destructive structural determination of unaltered humic substances is that of nuclear magnetic resonance (nmr) spectroscopy.

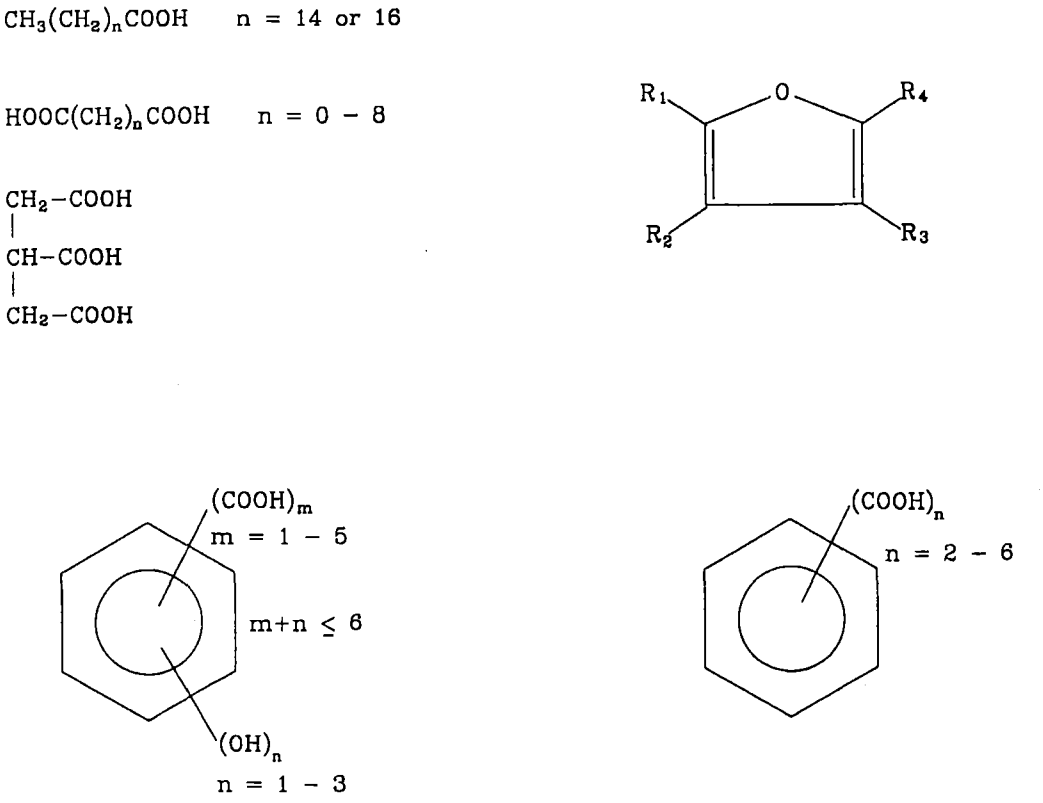

Figure 2.2 Generalised structures identified after oxidative degradations of humic substances (from Hayes and Swift, 1978; Schnitzer, 1989).

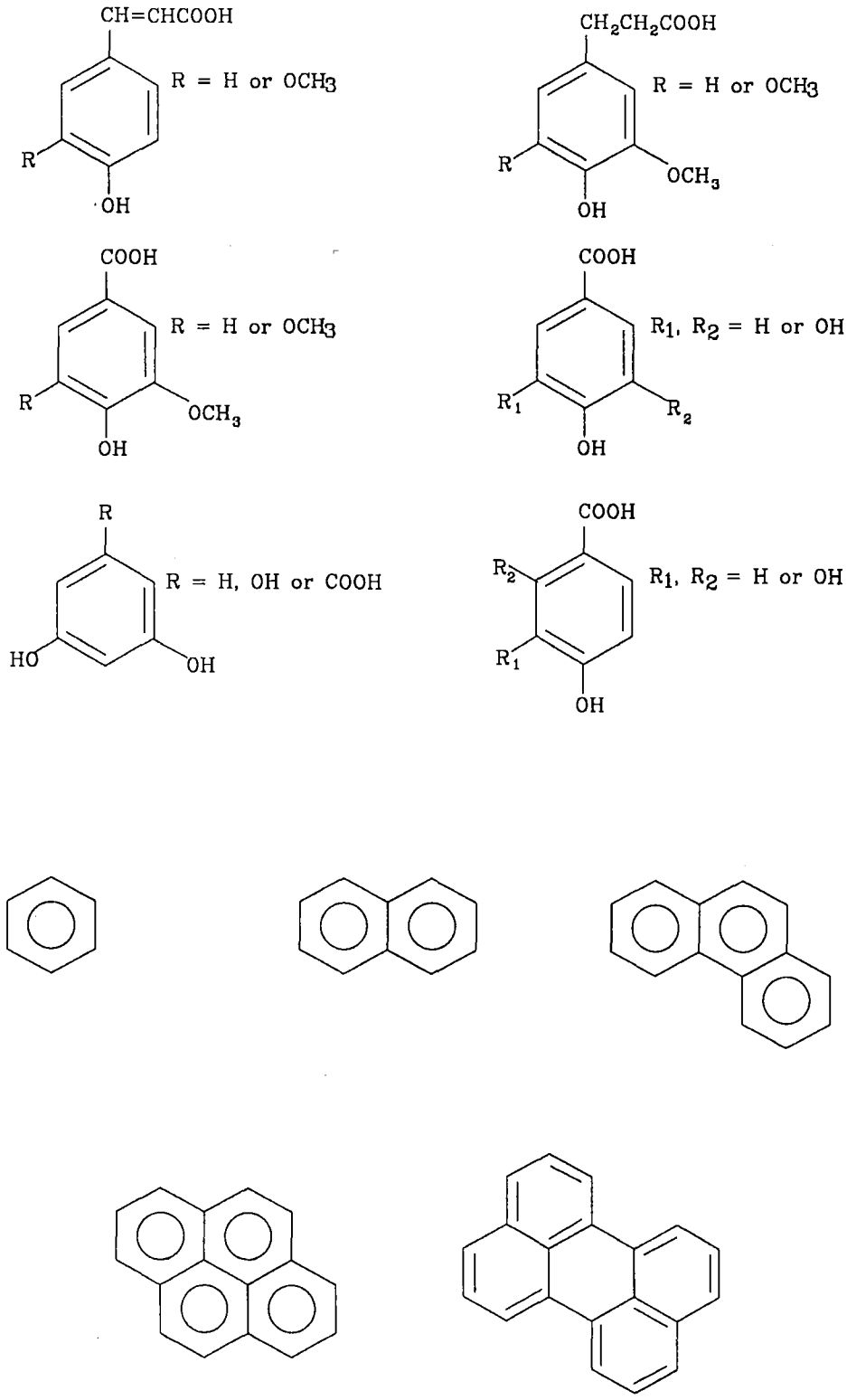

Figure 2.3 Generalised structures identified after reductive degradations of humic substances (from Hayes and Swift, 1978; Stevenson, 1989).

Considerable advances in instrumentation and techniques have been made in this technique in recent years, such as Fourier transform and solid state nmr using methods such as cross-polarisation and magic angle spinning (Wilson, 1989). In spite of this, nmr remains a semiquantitative tool for the determination of structure in humic substances (Malcolm, 1989). The nmr technique cannot yet identify specific structures in a complex mixture such as a humic substance; broad groupings of functionality may, however, be discerned. Quantitative analysis of the nmr spectra of humic substances is becoming more feasible. Perhaps the most important general result from nmr experiments is that the proportion of aromatic carbon is lower (c. 25-34% for soil humic acids) than was previously inferred from degradative experiments (Malcolm, 1989). A number of two-dimensional nmr techniques have been developed, and these show potential for greater resolution in the determination of humic substance structure (Wilson, 1989).

2.2.2.3 Reactive functional groups

Humic substance macromolecules contain a wide variety of reactive functional groups bonded to the essentially non-reactive carbon skeleton. The identity of these substituents has been inferred from degradative, spectroscopic and potentiometric studies; many functional groups may be quantified on the basis of their reaction with certain specific reagents. Oxygen containing functional groups include carboxyl (carboxylate) groups, hydroxyl groups (alcohols, phenols, enols, hydroquinones), carbonyl groups (aldehydes, ketones, quinones, keto-acids), esters, ethers, and anhydrides (Schnitzer and Khan, 1972; Hayes and Swift, 1978; Stevenson, 1982). Nitrogen containing functional groups are dominated by amino acids and amino sugars; primary and secondary amines, amides, imines, imino groups are also believed to occur (Hayes and Swift, 1978; Schnitzer, 1985; Anderson *et al.*, 1989). Heterocyclic and/or macrocyclic structures may also be minor components of humic substance structures (Goodman and Cheshire, 1976; Stevenson, 1982; Kumada, 1987).

Table 2.2 Abundances of oxygen-containing functional groups for soil humic substances (condensed from Schnitzer and Khan, 1972; Stevenson, 1982).

	Functional group content / meq g^{-1}	
Functional group	Humic acids	Fulvic acids
Total acidity	5.6-10.2	6.4-14.2
COOH	1.5-5.7	0.3-5.7
Weakly acidic or alcoholic OH	0.2-4.9	2.6-9.5
Carbonyl C=O	0.1-5.6	1.2-4.2
Methoxyl	0.3-0.8	0.3-1.2

2.2.2.4 Spatial arrangements

The tertiary structure of humic substance molecules is a topic receiving much debate; secondary structure, in the conventional polymer chemistry sense, is a concept which cannot be applied to humic substances. In contrast with other biologically synthesised macromolecules, such as proteins or polysaccharides, humic substances have no known repeating structural units or bond types, and so are in no sense polymeric. There are two important structural models: the randomly-coiled linear macromolecule model (Cameron *et al.*, 1972; Hayes and Swift, 1978), and the aggregate or membrane model (Wershaw *et al.*, 1977; Wershaw, 1986). At present the most widely accepted view of the tertiary structure of humic substances is that of an essentially linear macromolecule. The precise geometry assumed by this linear macromolecule depends on factors such as degree of ionisation, solvation or extent of polyvalent metal ion binding. These factors also determine whether the humic substances exist in the solution, gel or solid phase (Hayes and Swift, 1978). In aqueous solution, the linear molecule is thought to exist in an expanded random coil conformation when its acidic functional groups are

dissociated. Intramolecular hydrogen bonding and/or non-polar interactions serve to condense the expanded molecule when protonated; in the case of humic acids, the molecule is rendered insoluble. In this model, solid phase humic substance molecules are thought to be tightly condensed; when drying occurs, hydrophilic functional groups occupy the centre of the coil, with hydrophobic groups on the exterior of the collapsed coil (Hayes and Swift, 1978; Swift, 1989).

A growing body of evidence exists, however, which supports a small - molecule aggregate structure for humic substances (Chiou *et al.*, 1985; Wershaw, 1986). In this structural model, smaller molecules having polar and non-polar (which may include polar groups rendered effectively non-polar by hydrogen bonding) functional groups form a micelle - like aggregate, similar to a lipid membrane, with (effectively) non-polar groups on the interior of the aggregate. The smaller component molecules contain polar and/or ionisable functional groups, and non-polar, unionisable groups. The interior of the membrane structure contains effectively non-polar groups which associate by hydrogen bonding, non-polar attraction and attractive forces between induced dipoles in π-electron systems. The micelle structures themselves may aggregate, *via* hydrogen bonding in the protonated form, or bridging by polyvalent cations; these processes would form the basis for solution/solid phase changes. The same is true for linear macromolecules; these may also form intermolecular aggregates through the same processes. The fundamental difference between this model and the linear macromolecule model is that the macromolecular character of humic substance macromolecules is explained by physical, rather than chemical, bonding of smaller component molecules.

2.2.3 Molecular Weight and Size

Humic substances are macromolecular, polydisperse mixtures. In addition, individual macromolecules are known to form aggregates, both in the solution and solid phase, making molecular weight measurements difficult. Number average molecular weights for humic substances have been reported in the range 3×10^3 - 1×10^6 daltons for humic acids and 5×10^2 - 5×10^3 daltons for fulvic acids (Hayes and

Swift, 1978; Stevenson, 1982). Most measurements of the weight-average molecular weights of unfractionated soil humic acids have yielded values in the range 2×10^4 - 1×10^5 daltons (Hayes *et al.*, 1989b). Values for the radius of gyration (a time-averaged measure of molecular radius) for unfractionated soil humic acid have been measured in the range 3.6 - 13.7 nm (Hayes *et al.*, 1989b). A single average molecular weight, however, can be misleading as it does not give any indication of the range of molecular weights encountered in a humic substance sample. A single extracted humic substance may contain molecules of widely varying molecular weight.

A series of measurements made on a size-fractionated humic acid (Cameron *et al.*, 1972) yielded weight average molecular weights in the range 2.4×10^3 - 1.36×10^6 daltons, and corresponding radii of gyration in the range 1.5 - 25 nm.

2.2.4 Solubility Properties

The role of humic substances in the environment depends to a large extent on their solubility in aqueous systems. In addition, extraction and fractionation procedures for humic substances from soils and sediments rely on their solubility in a range of aqueous and non-aqueous solvents (Hayes, 1985). Humic substance solubility is affected by several important factors: the ability of the solvent to prevent intra- and intermolecular association of humic substances; whether the solvent allows humic substance molecules to dissociate; and the structural characteristics of humic substances molecules themselves (Hayes, 1985). Again it should be realised that, due to the heterogeneity inherent in humic substances, a range of solubility properties will always be observed for humic substances from any one particular source.

2.2.5 Ultraviolet-Visible Absorption and Fluorescence Spectra

2.2.5.1 UV-visible absorption spectra

Humic substances contain numerous types of structural moieties which can absorb UV and/or visible radiation *via* electronic transitions (Schnitzer and Khan, 1972; Flaig *et al.*, 1975). The nature of electronic transitions in organic compounds is such that transitions are more likely at shorter wavelength. Longer wavelength (visible) absorption is observed when the energy difference between bonding and antibonding orbitals is low, as in highly conjugated alkenic or aromatic systems, or if charge transfer processes occur, for example in metal:organic complexes or if free radicals are present. Since humic substance molecules contain such a wide variety of chromophoric groups, their observed UV-visible absorption spectra are distinctive in that they usually lack maxima, minima or pronounced inflections. Absorption is of low intensity at longer wavelength, and increases monotonically in intensity as the wavelength decreases (Kumada, 1987), as would be expected for a complex mixture of organic chromophores. Changes in the electronic environment of humic substance chromophores, for example in (de)protonation or metal complexation, may bring about small changes in the observed absorption spectra (Langford and Khan, 1975; Gamble *et al.*, 1980; Kumada, 1987).

2.2.5.2 UV-visible fluorescence spectra

Fluorescence occurs in organic compounds by radiative decay, to their ground state, of molecules excited by absorption of UV or visible radiation. Humic substances have been found to fluoresce (Schnitzer and Khan, 1972; MacCarthy and Rice, 1985). The specific fluorophores involved may include substituted alicyclic and aromatic moieties although some non-cyclic structures are also known to fluoresce (Schnitzer and Khan, 1972). Broad maxima are observed in both humic substance excitation and emission fluorescence spectra. Humic substance fluorescence intensity is not linearly dependent on concentration, due to self-absorbance of emitted radiation. Fluorescence intensity is

dependent on pH; unionised humic substances show only weak fluorescence (Saar and Weber, 1980). Complex forming metal ions, for example Cu^{2+} and Al^{3+}, either quench (suppress) (Saar and Weber, 1980) or enhance (Plankey and Patterson, 1987) humic substance fluorescence, depending on the particular metal ion and the excitation and emission wavelengths used.

2.3 Factors Influencing Complex Formation Reactions with Humic Substances

2.3.1 Introduction

Reactions in which humic substances form complexes with metal ions are important in many natural systems (Stevenson, 1982; Sposito, 1986; Buffle and Altmann, 1987). Through complexation reactions, humic substances are possibly the major determinants of trace metal ion speciation in soils and freshwater systems, and thus are involved in deficiency of essential trace metal ions and toxicity of pollutant metal ions. In conjunction with other variably charged natural colloids, such as metal oxides and clay minerals, humic substances are important in determining ambient pH levels in soils and sediments (Brady, 1974; Hayes *et al.*, 1989a). Humic substances affect major cation (Na^+, K^+, NH_4^+, etc.) speciation *via* cation exchange processes (Sposito, 1984). The ability of humic substances to form surface complexes with clay and metal (hydr)oxide particles is important for aggregate stability in soils and sediments (Brady, 1974; Hayes and Himes, 1986), and particulate mass transport in soils, sediments and aquatic environments (O'Melia, 1987).

Complexing equilibria are conveniently expressed in terms of proton and metal ion interaction with ligands. A *ligand* is defined as any molecular moiety which forms complexes with hydrogen ions or

metal ions (Cotton and Wilkinson, 1976). In this discussion, the definition can be more specific since the ligands in humic substances are the conjugate bases of (weak) organic acids (moieties such as protonated amine groups are considered to be acids). A *complex* is a new molecular association formed by chemical bonding between a ligand and a complexing ion (such as transition metal cations or the hydrogen ion). Associations which do not involve electron sharing or polarisation, such as ion-exchange processes, are usually excluded from this definition. These definitions include complexation reactions between aqueous phase ions and ligands in either the aqueous or solid/colloidal phases. (Complexation of ions by a solid or colloidal phase ligand is more commonly termed chemisorption, adsorption or simply sorption.) Two broad classes of complexes may be defined: *inner sphere* complexes, involving some degree of electron-sharing covalent bonding between the ligand and the complexed ion, and *outer sphere* complexes, involving attraction between the (negatively) charged ligand and induced dipoles in the H_2O molecules coordinated to the complexed cation. These definitions allow identical treatment of protonation and complex formation reactions (since protonation is just a special case of complexation), and emphasise the competitive process between protons and metal ions for binding sites on ligands in humic substances.

It is often convenient to treat reactions of ligands with hydrogen ions separately as protonation reactions. The extents of protonation equilibria are quantified by the protonation constants; Equations 2.1-2.3 define stepwise (K) and cumulative (β) protonation constants for a generalised ligand L. (Charges and phases are omitted for clarity; square brackets ([...]) denote concentrations). It should be noted that the constants defined here do not represent true thermodynamic equilibrium constants, which relate to equilibrium *activities* rather than concentrations and are independent of ionic strength. Equilibrium constants are of limited utility in many applications; ionic activities are only experimentally

accessible for some of the species in the equilibrium expression, for example H^+. Constants based on stoichiometric concentrations as defined here are dependent on, and vary with, solution ionic strength.

$$L + H \Leftrightarrow HL; \qquad K_{HL} = [HL]/[L][H] \tag{2.1}$$

.
.
.

$$H_{(n-1)}L + H \Leftrightarrow H_nL; \qquad K_{H_nL} = [H_nL]/[H_{(n-1)}L][H] \tag{2.2}$$

$$L + nH \Leftrightarrow H_nL; \qquad \beta_{H_nL} = [H_nL]/[L][H]^n \tag{2.3}$$

When metal cation - ligand complex formation reactions are considered, it is normal to simultaneously consider the relevant protonation reactions, since in aqueous systems hydrogen ions always compete with metal cations for weakly acidic complexing sites. For humic substances, it is convenient to consider only 1:1 complexes. In this way binding sites on the humic substance macromolecule, regardless of whether they are simple monodentate or polydentate chelating sites, are thus treated as discrete ligands. Formation constants for 1:1 metal:ligand complexes may be defined for reaction of metal ions with the free ligand (Equations 2.4a,b), proton displacements (Equations 2.5a,b) or conditional formation constants at fixed pH (Equations 2.6a-2.6c. Charges and phases are omitted for clarity; square brackets ([...]) denote concentrations.

$$M + L \Leftrightarrow ML; \tag{2.4a}$$

$$K_{ML} = [ML]/[M][L] \tag{2.4b}$$

$$M + H_nL \Leftrightarrow ML + nH; \tag{2.5a}$$

$$K_{ML} = [ML][H]^n/[M][H_nL] \tag{2.5b}$$

$$M + L' \Leftrightarrow ML, \text{ fixed } pH=10^{-[H]}; \tag{2.6a}$$

$$K_{ML}(pH=10^{-[H]}) = [ML]/[M][L'] \tag{2.6b}$$

and $[L'] = [L] + \Sigma_{i=1}^{n} [H_iL]$ (2.6c)

In the preceding discussion, it has been assumed that complexation reactions proceed in a single (aqueous) phase, facilitating easy description of reactant concentrations. In the common case of adsorption of an aqueous phase ion onto a solid or gel phase ligand, species in the solid phase are conveniently expressed in molalities (mol kg^{-1} in specified phase) or mole fractions (χ_i refers to the amount of species i bound to the solid phase ligand, as a fraction of total sites, on a mole basis); the general expressions for metal binding to a single solid phase ligand (L) then become:

$$\chi_{ML} = (\chi_{L'} K_{ML}[M]/(1 + K_{ML}[M])); \quad (2.7)$$

where $\chi_{L'} = \chi_{ML} + \chi_L + \Sigma_{i=1}^{n} (\chi_{H_nL})$ (2.8)

An experiment measuring binding by any complexing species (for example, H^+ or transition metal cations) to humic substances will invariably show a continuous decrease in apparent binding constant with increasing levels of bound cation (alternatively, increasing equilibrium levels of free ion, or in the case where the ion under consideration is H^+, decreasing pH). There are several factors which are involved simultaneously in giving rise to this type of observed behaviour. These will be discussed in turn in Sections 2.3.1 to 2.3.3.

2.3.2 Binding Site Heterogeneity

Metal cations form complexes with humic substances *via* the weakly acidic organic functional groups which are integral to the humic substance macromolecule. These acidic groups include, amongst others: carboxylic, phenolic, active methylene and protonated amine groups, in many different chemical environments (Perdue, 1985). Titration of the acidic groups on humic substances with strong base shows buffering over a wide pH range, inferring that these functional groups have a wide range of

effective dissociation constants. A wide range of protonation constants can be inferred from the nature of the acidic groups themselves. Weakly acidic organic functional groups exhibit a wide range of protonation constant values (Equations 2.1-2.3). Differences in proton affinity are largely due to the degree of charge stabilisation afforded to the anionic conjugate base by electron delocalisation and/or inductive effects. Some representative acids with their log K values are listed in Table 2.3.

Table 2.3 Protonation and 1:1 Cu^{2+}-complex stability constants (log K) for selected organic acids, 25 ° C, I=0.1 mol L^{-1} (from Sillen and Martell, 1971; Perrin, 1979; constants corrected where necessary to I=0.1 mol L^{-1} using activity coefficients from Kielland (1937)). ([a] 30 ° C, [b] 20 ° C, [c] I=0.15molL^{-1})

Organic ligand	log K_{HL}	log K_{H_2L}	log K_{H_3L}	log K_{CuL}
Formic acid (HL)	3.56	-	-	2.04[a]
Acetic acid (HL)	4.57	-	-	2.38[b]
Oxalic acid (H_2L)	3.83	1.25	-	4.85
Glycine (HL)	9.63	-	-	8.27
Malonic acid (H_2L)	5.28	2.64	-	5.04
Citric acid (H_3L)	5.74	4.36	2.86	5.90
Benzoic acid (HL)	4.02	-	-	-
Salicylic acid (H_2L)	13.2	2.80	-	10.8
Phthalic acid (H_2L)	5.03	2.77	-	3.14
Phenol (HL)	9.79	-	-	-
Catechol (H_2L)	13.00	9.32	-	13.96
Acetylacetone (L)	8.82	-	-	8.16
8-hydroxyquinoline (HL)	9.23	-	-	12.10
Pyridine (L)	5.33	-	-	2.54[c]
Aniline (L)	4.55	-	-	-

An equally wide range of affinities for transition metal and other complex-forming ions is observed for the conjugate bases of these simple organic acids (Perrin, 1979). Table 2.3 contains values for the stability constant of a 1:1 complex of Cu^{2+} with various organic ligands. The situation is complicated by competition with hydrogen ions which effectively changes free ligand concentration with pH; transition metal ions can displace protons from undissociated acidic sites, and also form complexes with non-acidic sites such as ether oxygen atoms which have non-bonding p-orbitals. Some possible

structures for metal ion binding sites in humic substances (Stevenson, 1982; Murray and Linder, 1983, 1984; Ephraim and Marinsky, 1986) are given in Figure 2.4. Formation of mixed-ligand complexes (for example, humate:metal:hydroxy) also complicates metal - humic substance complexation, as does the formation of chelate complexes. The formation of chelate complexes has never been demonstrated unequivocally, although it has been implicated in humic substance - metal ion complexation by many workers, for example Himes and Barber (1957); Cheam (1973); or Gamble *et al.* (1980). Chelation in humic substance - metal ion complexes is likely to occur at adjacent multifunctional sites such as phthalate or salicylate type functional groups (Gamble *et al.*, 1980). Chelation by separate groups remote on a linear humic substance macromolecule would be, due to entropy considerations, unfavourable because of loss of molecular flexibility; however, it may be a realistic possibility if the density of multifunctional groups is low. For humic substances, heterogeneity of functional groups with complex-formation ability means that at low levels of protonation (or metal ion loading), protons (or metal ions) will be bound preferentially to those sites having a high affinity for those ions. In terms of dissociative processes, the sites dissociating most readily on a thermodynamic basis will naturally be those with the lowest affinity for hydrogen ions (lowest protonation constant) or metal ions (lowest complex stability constant). Competition between protons and metal ions for humic substance ligands is expected , and has often been observed (for example, Kerndorff and Schnitzer, 1980) due to the weakly acidic nature of such ligands. Competition has also been observed (Kerndorff and Schnitzer, 1980; Susetyo *et al.*, 1990) between different transition-metal cations for binding sites on humic substances. Although alkaline-earth cations (for example, Ca^{2+}) have been observed to undergo significant complexation with humic substances (Dempsey and O'Melia, 1983; Hering and Morel, 1988a), research has indicated that Ca^{2+} does not compete with metal ions such as Cu^{2+} for humic substance ligands (Hering and Morel, 1988a). However, ionic strength effects (Section 2.3.2), for example in electrolyte solutions containing Ca^{2+}, may be observed (for example Hogg, 1989).

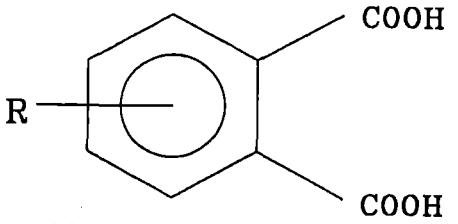

(i) Phthalic acid type

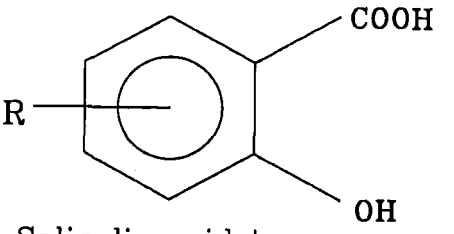

(ii) Salicylic acid type

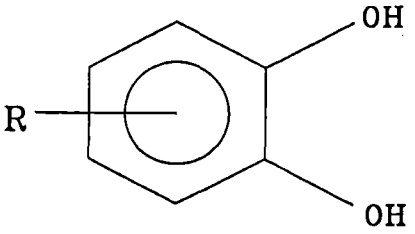

(iii) 1,2–dihydroxybenzenes

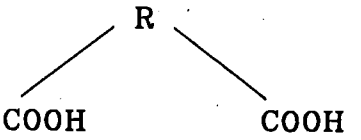

(iv) Non – aromatic dicarboxylic acids

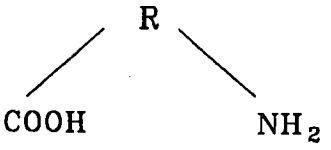

(v) α – amino acids

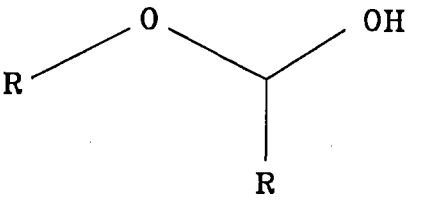

(vi) Alcoholic ethers/furans

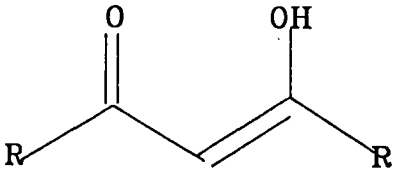

(vii) carbonyl/enol

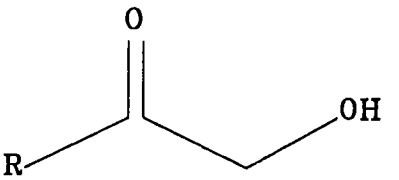

(viii) Hydroxyquinones/ hydroxyketones

R–COOH

(ix) Aromatic and aliphatic carboxylic acids

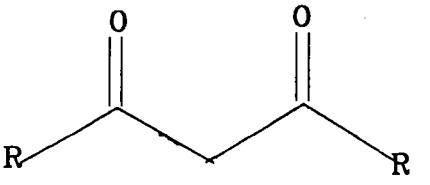

(x) β– diketones

Figure 2.4 Structures representative of potential metal ion binding sites on humic substances (**R** represents the remainder of a humic substance macromolecule). From Stevenson (1982), Murray and Linder (1983) and Ephraim and Marinsky (1986).

2.3.3 Polyelectrolyte Effects on Complex Formation Reactions of Humic Substances

For any polyprotic acid, differences are observed in protonation constants for successive protonation steps, even when the individual acidic groups involved are chemically identical. For example, for oxalic acid, a diprotic acid having two chemically equivalent carboxyl groups, the protonation constants are: $\log K_1 = 3.83$, $\log K_2 = 1.25$, (Perrin, 1979). This is a result of the electron-donating effect of deprotonated acidic groups, which tends to increase the affinity of the molecule for electropositive species such as hydrogen ions. As the acidic groups are successively protonated, the charge on the molecule decreases, and the electron-donating effect is diminished, leading to the observed sequence of protonation constants. The electrostatic attraction effect due to the high negative charge on the fully deprotonated molecule also contributes to the high value of the first protonation constant compared with successive protonation constants. Statistical factors are also involved; the fact that one site is protonated means that protonation of successive sites becomes less likely. Statistical effects are discussed in detail by Perdue (1985). Similar effects are observed for polyelectrolytes having many chemically equivalent acidic functional groups, such as poly(methacrylic acid) (Marinsky and Ephraim, 1986). The presence of high densities of various ionisable functional groups on humic substance macromolecules (electron-deficient groups such as carboxyl, phenolic, activated methylene or ammonium) gives humic substances macro-ionic characteristics analogous to polyelectrolytes (Posner, 1964; Dempsey and O'Melia, 1983; Ephraim *et al.*, 1986). For metal ion binding, however, binding sites are often assumed to be essentially independent at low to moderate metal loadings under constant protonation conditions, since (i) complexing sites are, on average, sufficiently distant on the macroion, and (ii) significant proton binding sites are more abundant than metal ion binding sites (Dzombak *et al.*, 1986). The macro-ionic behaviour of humic substances results in an observed dependence of binding affinity (for protons and/or

metal ions) on ionic strength (Posner, 1964; Ephraim *et al.*, 1986). Both protons and metal cations are found to bind more weakly to humic substances at higher ionic strength. This reflects the shielding of the electrostatic potential of the humic substance macro-ions by higher concentrations of counter-ions (ions of opposite charge) (Morawetz, 1975), rather than competition between monovalent cations (such as Na^+) and complex-forming cations for binding sites.

2.3.4 Effects of Molecular Conformation on Complex Formation by Humic Substances

It has been suggested (Hayes and Swift, 1978) that the complexation of hydrogen ions or polyvalent metal ions by humic substances induces conformational changes in humic substance macromolecules, leading ultimately to precipitation and aggregation. Such conformational changes are likely to affect subsequent humic substance - metal ion complexation reactions; binding of additional metal ions may either be facilitated (for example, by formation of pseudo-chelate sites through molecular contraction) or hindered (for example, as a result of steric inaccessibility). Aggregation processes have been implicated in metal ion-humic substance complexing processes by several authors (Rainville and Weber, 1982; Gamble *et al.*, 1985; Buffle and Altmann, 1987). Teasdale (1987) has shown that, in theory, the higher affinity of humic substances for copper(II) ions at low equilibrium copper concentrations may be partly accounted for if copper ions lead to association of humic substance macromolecules *via* cross-linking, or by allowing self-association by modification of the macromolecules. Cross-linking of macromolecules by bound cations leads to steric inaccessibility of some binding sites as the amount of bound ion increases. Conformational changes may also be responsible for the dependence of observed

complexation behaviour on humic substance concentration, aggregation being more likely at higher concentration (Saar and Weber, 1979).

2.4 Modelling Complexing Reactions of Humic Substances

The complicated nature of humic substance complexing equilibria has presented a challenge to researchers attempting to describe these reactions. Apart from purely academic reasons for attempting descriptions of the complexing reactions of humic substances, there is the possibility that an accurate mathematical description of the processes occurring may allow predictions to be made about chemical speciation in systems where humic substance complexing equilibria are important. For example, a reliable model of metal ion - humate complexing reactions in soils might allow more efficient application of trace-element fertilisers in agricultural situations; another pertinent consideration is the chemical fate of pollutant trace metal ions in soils and aquatic systems. Unfortunately, as described in Section 2.3, humic substances do not behave like simple ligands either in their protonation reactions or their complexation reactions with metal ions. Models which describe the heterogeneity inherent in any reactions of humic substances must, therefore, be used. According to Sposito (1986) an ideal model for description of humic substance - metal ion complexation reactions would include (1) chemical verisimilitude, (2) goodness of fit at environmentally significant levels of reactants, and (3) convenience of use for subsequent calculations. In reality these requirements have a degree of mutual exclusivity, and some form of compromise is found to be necessary.

Descriptions of heterogeneity in humic substance - metal ion complexation reactions fall into two broad classes. The first approach is result-oriented; models make no attempt to resolve heterogeneity in terms of chemical properties and rather the emphasis is on providing an accurate and facile model in terms of predictive capability. The second approach tends to be based on chemical thermodynamic properties; that is, a description of complexation heterogeneity in terms of the actual chemical and physical

processes occurring. For example, the effects of polyelectrolyte behaviour of humic substances is indistinguishable, in the first type of approach, from any other effects on metal ion binding heterogeneity. In the second type of approach, however, the contribution of polyelectrolyte behaviour and all other contributing factors to binding heterogeneity are considered separately.

2.4.1 Defining Ligand Concentrations for Humic Substances

The most convenient means of quantifying protonation or metal complexation reactions is to use the relevant stability constant(s) for the reactions involved. The equations which define these stability constants (Equations 2.1a - 2.6c) require knowledge of ligand concentrations. Several problems arise when attempting to define ligand concentrations for humic substances (Fish *et al.*, 1986; Turner *et al.*, 1986). The first problem is introduced by a lack of knowledge of the precise nature of complex-forming sites on humic substances molecules, and the fact that the abundances of these sites are unknown. The polydispersity of humic substances also presents difficulties; it is conceivable that smaller molecules present in the humic substance mixture have no metal ion binding sites, and that larger molecules have many. In addition, only an average molecular weight can be determined for humic substance preparations. Calculation of ligand concentration on the basis of numbers of humic substance molecules, therefore, introduces indeterminate error into any model embodying this assumption.

An alternative to calculating ligand concentrations on the basis of molecular weight is to define the number of ligands present as the number of binding sites present in the humic substance mixture. This forms the foundation for 'quasiparticle' (Sposito, 1986) or 'binding site' (Dzombak *et al.*, 1986) models of humic substance complexation reactions. This is convenient in that all complexes have a metal:ligand ratio of 1:1 by definition. This approach, however, is problematic. The number of binding sites in a ligand mixture can be estimated using an independently measured quantity, such as the total acidity (Stevenson, 1982). This procedure introduces assumptions that may not be correct; metal ions may bind to sites which do not bind protons (for example, β-diketones) or some proton binding sites

may not contribute significantly to metal ion binding (for example, isolated phenolic groups). Alternatively, binding site numbers can be measured directly, for example by saturating a humic substance with a complexing metal ion until all the binding sites are found to be occupied. This type of procedure is experimentally difficult (Perdue, 1989); dissolved humic substances may precipitate before their limiting metal loading is achieved (limiting steric accessibility of some sites), formation of insoluble metal (hydr)oxide(s) may occur, or such high amounts of metal ion may be required that the difference between free and total complexing ion is of the order of the experimental error (Buffle and Altmann, 1987). Usually metal - humate binding experiments do not extend to sufficiently high metal loadings, so that intrinsically inaccurate extrapolation procedures must be used.

It is clear, then, that some operational definition of ligand concentration must often be made for any measurement or modelling of humic substance complexation reactions.

2.4.1.1 Mixed ligand complexes

Another assumption intrinsic to most studies of humic substance - metal ion complexation reactions is that formation of mixed ligand complexes is ignored. Mixed ligand complexes may be important for any metal ion which undergoes significant hydrolysis, or when background electrolyte contains anions which are known to complex metal cations, such as chloride or (to a lesser extent) nitrate. In such experimental systems the formation of mixed ligand complexes is likely on a statistical basis (Sposito, 1986) or purely on mass-action considerations. Use of very weakly complexing anions in the background electrolyte, such as perchlorate, should minimise the risk of mixed-ligand complex formation.

2.4.2 Simple Empirical Models of Humic Substance Complexation Reactions

Conditional stability constants are most often found to be useful for humic substance complexing reactions. Equation 2.6a is often conveniently rearranged to express complex concentration as a function of free metal ion concentration. In many cases, a formation function $\bar{\nu}$ is defined, where:

$$\bar{\nu} = [ML]/C_L \tag{2.9}$$

$$C_L = [L] + \Sigma_{i=1}^{n}[HL_i] + \Sigma_{i=1}^{n}[ML_i] \tag{2.10}$$

C_L is the stoichiometric concentration of all forms of all ligands L_i (complexed and uncomplexed) or the concentration of *binding sites*. Use of formation function has been criticised by some researchers (for example, Dzombak *et al.*, 1986; Turner *et al.*, 1986) on the grounds that total ligand concentrations can seldom be measured or defined satisfactorily for humic substances. Using the mass balance equation for ligand species (Equation 2.10) and substituting this into the equilibrium expression for the formation of ML (Equation 2.4b), the following equations may be obtained:

$$[ML] = C_L K_{ML}[M]/(1 + K_{ML}[M]) \tag{2.11}$$

or

$$\bar{\nu} = K_{ML}[M]/(1 + K_{ML}[M]) \tag{2.12}$$

A similar treatment follows when a mixture of ligands L_i undergo complexation reactions with a metal ion M. In this case the following equations apply:

$$C_{ML} = \sum_{i=1}^{n}\left(C_i K_i [M]/(1 + K_i [M])\right) \tag{2.13}$$

where

$$C_{ML} = \sum_{i=1}^{n}[ML_i] \tag{2.14}$$

where C_{ML} is the stoichiometric concentration of complexed metal, L_i is the i^{th} ligand with metal complex stability constant K_i and stoichiometric concentration C_i.

Models used to describe general binding or sorption processes which make no attempt to account for humic substance heterogeneity have been used by many workers to describe complexing reactions of humic substances (for example, Himes and Barber, 1957; Schnitzer, 1969; Shuman and Cromer, 1979). Perhaps the simplest model founded on physical processes is based on ligands (or a single ligand) having identical and independent binding sites, that is, the single-component Langmuir or Scatchard model. The appropriate equation (Equation 2.11) is derived from the equilibrium expression for formation of a 1:1 complex.

The Langmuir model requires measurement of free metal (or H^+) ion concentrations and bound metal ion concentrations (or mole fractions for solid phase ligands). Simple graphical or linear regression methods may be used to extract the total ligand concentration, C_L, conditional stability constant, K_{ML}. In general, good agreement is not obtained between observed and predicted complexation behaviour when attempts to describe metal ion - humic substance binding using this model are made. Some authors, however, have found 'good' fits to the Langmuir Equation (for example Randle and Hartmann, 1980).

Another equation used to model humic substance - metal ion complexation is the Freundlich Equation. The form of the Freundlich Equation is as follows:

$$[ML] = A[M]^{\beta} \qquad (2.15)$$

where A and β are adjustable fitting parameters ($A > 0$, $0 < \beta \leq 1$). Unlike the Langmuir Equation, the Freundlich Equation has no derivation from simple equilibrium reactions. Although the Freundlich Equation was originally developed to provide an empirical model for adsorption phenomena, it is observed that in many cases this equation provides an excellent description of heterogeneous complexation (for example Sanders, 1980). Similar observations led Sips (1948) to propose that it had

some underlying physical meaning. Sips proposed that the Freundlich Equation was an approximation, valid for low values of [M], of the following equation:

$$[ML] = \frac{A[M]^{\beta}}{1 + (A/C_L)[M]^{\beta}} \qquad (2.16)$$

since as $[M] \rightarrow 0$, $(A/C_L)[M]^{\beta} \rightarrow 0$, and Equation 2.16 is approximated by Equation 2.15. The Sips Equation (Equation 2.16) is the analytical solution to an equation describing complexation by a continuous distribution of binding sites, which approximate a normal (Gaussian) distribution with respect to log K_{ML_i}. The mean log K_{ML_i} is defined by:

$$\log_{10} K_{\mu} = \ln(A/C_L)/(\ln 10)\beta \qquad (2.17)$$

The spread of the distribution depends on the value of β; low values of β imply a wide range of log K_{ML_i} values; conversely, high β values imply a narrower range. Sposito (1984) has shown that, in the upper limiting case that $\beta = 1$, the Sips equation reduces to the single site Langmuir Equation (Equation 2.11).

Other simple empirical equations have been used to model humic substance - metal ion binding behaviour (for example, McLaren *et al.*, 1973; Kerndorff and Schnitzer, 1980); these equations have not been used widely and were used for convenient comparison methods.

2.4.3 Discrete Multiple Binding Site Models

Discrete multiple binding site models are those assuming that humic substances contain a fixed, finite number of ligands (binding sites) L_i with conditional stability constant K_{ML_i} (Perdue and Lytle, 1983). Discrete ligands may be regarded as independent (usually the case for humic substance - metal ion

complexation models) or dependent (some models of humic substance protonation equilibria are based on polyelectrolyte properties, that is, ionisation of functional groups affects ionisation of other groups). Recently, a number of authors (Dzombak *et al.*, 1986; Buffle and Altmann, 1987) have commented on the operational nature of stability constants from humic substance - metal ion binding experiments. The point made is that calculated constants are dependent, to a large extent, on the analytical speciation techniques used. For example, in a mixture of ligands, the presence of binding sites with very high affinity can only be established if the analytical method used can detect very low levels of unbound metal ion. Similarly, binding sites having low affinity do not affect metal ion speciation significantly, and are subsequently unobservable in most humic substance - metal ion binding experiments. In all such experiments, therefore, there exists an *analytical window* (Buffle and Altmann, 1987) which determines upper and lower limits for experimentally measured conditional stability constants.

Discrete multiple binding site models are often used in response to the poor fit observed between experimental and calculated speciation using single-site models (Equation 2.11; Perdue and Lytle, 1983). Inclusion of terms for n independent ligands into Equation 2.12 results in Equation 2.18; use of only the first two terms gives the familiar two-site Langmuir (Scatchard) Equation. The equation (Equation 2.13) may also be expressed as:

$$C_{ML} = C_L \sum_{i=1}^{n} \left(\frac{C_i}{C_L} K_i [M] \Big/ \left(1 + K_i [M] \right) \right) \qquad (2.18)$$

Equation 2.13 (or Equation 2.18) has been used with n=2 by Tuschall and Brezonik (1983), Blaser and Sposito (1987) and Sikora and Stevenson (1988); with n=3 by Sposito *et al.* (1977) and Turner *et al.* (1986) and with n=4 by Gregor and Powell (1988b) to describe metal ion or proton binding to humic substances.

A different approach to implementation of a discrete binding site model for humic acid protonation has been proposed by Eberle and Feuerstein (1979). Their method of 'discrete pK spectrometry' involved

fixing a set of fixed, arbitrary K_i covering the expected binding constant range, and estimating the corresponding $[HL_i]$ values using linear regression.

An alternative to assuming formation of complexes with a multiligand mixture is to propose formation of higher order complexes, ML_n ($n > 1$). This type of reaction sequence also gives rise to an apparent decrease in conditional stability constant with increasing [M]. For the equilibrium represented by:

$$M + nL \Leftrightarrow ML_n \tag{2.19}$$

The cumulative stability constant is defined in Equation 2.20:

$$\beta_n = [ML_n]/[M][L]^n \tag{2.20}$$

For formation of an n^{th} order complex ML_n, the general equation is given by Equation 2.21.

$$C_{ML} = C_L \sum_{i=1}^{n} \left(\beta_i [M] / (1 + i\beta_i [M]) \right) \tag{2.21}$$

Modelling humic substance - metal ion complexation behaviour by invoking higher order complexes has been done for n=2 by Buffle *et al.* (1977), although according to Sposito (1986), this model is mathematically equivalent to one with n independent binding sites.

It is important to note at this stage that binding sites as described by (C_i, K_i) or (C_i, β_i) pairs are very unlikely to represent actual ligands in a mixture as complex as humic substances; nor do they represent *average* binding sites (Perdue and Lytle, 1983). A preferable terminology might be to call the K_i or β_i 'titration constants' (Gregor and Powell, 1988b) or 'conditional concentration quotients' (Perdue, 1989), terms which reflect the dependence on the analytical window. A number of authors (for example, Perdue and Lytle, 1983; Sposito, 1986) have stated that almost any function with several adjustable fitting parameters can be used to describe heterogeneous metal binding reactions, and have emphasised

the importance of formulating models that are chemically meaningful. If goodness of fit for a particular model is an important selection criterion, then it is important, where possible, to use the correct statistical tests (Turner *et al.*, 1986) so that unnecessary parameters are not used.

2.4.4 Polyelectrolyte Models

As discussed previously, the polyelectrolytic properties of humic substances exert the greatest effect on protonation reactions, since the charge on the humic substance macromolecule is caused by dissociation of acidic functional groups. From the definition of pH ($pH = -\log_{10}a_{H+}$), the definition of the degree of dissociation α ($\alpha = [L]/[L]+[HL]$) and the expression for the protonation constant of a monoprotic acid (Equation 2.1), the general Henderson-Hasselbalch equation can be derived (Equation 2.22).

$$pH = pK_a + \log(\alpha/1-\alpha) \qquad (2.22)$$

where $pK_a = -\log_{10}K_a$ (K_a is the dissociation constant) (2.23)

and $K_a = 1/K_{HL}$ (see Equation 2.1) (2.24)

For a polyelectrolyte with many identical acidic functional groups, a modified Henderson-Hasselbalch equation may be written (Equation 2.25), where η is a term describing the extent to which acidic groups interact electrostatically ($1 \leq \eta \leq 2$) (Dempsey and O'Melia, 1983) and pK_{HH} is the apparent dissociation constant at half neutralisation.

$$pH = pK_{HH} + \eta\log(\alpha/1-\alpha) \qquad (2.25)$$

An alternative to the modified Henderson-Hasselbalch equation is the Hermans-Overbeek equation (Equation 2.26), where pK_{app} is the apparent dissociation constant.

$$pK_{app} = pK_{int} - 0.868\omega n\alpha \qquad (2.26),$$

where $pK_{app} = pH - \log_{10}(\alpha/1-\alpha)$;

pK_{int} is an 'intrinsic' pK_a for a single, repeated acidic group;

ω is a composite electrostatic interaction term;

and n is the average number of acidic groups per macromolecule.

Polyelectrolyte models have been used by many authors to model protonation equilibria of humic substances (for example, Posner, 1964; Wilson and Kinney, 1977; Dempsey and O'Melia, 1983). It has been found, however, that the extent of variation in pK_{app} is greater than can be explained by polyelectrolyte behaviour alone, implying acidic functional group heterogeneity (Dempsey and O'Melia, 1983; Ephraim *et al.* , 1986). In addition, some authors (for example, Gregor and Powell, 1988b) have found no evidence of polyelectrolyte behaviour for fulvic acids (η=1 in Equation 2.25); such an observation is unusual.

For metal ion binding to humic substances at constant pH (constant α) and ionic strength, the charge on the macromolecules is often assumed to remain essentially constant until high metal loadings are reached, since only a small proportion of acidic sites are involved in metal complexing at low to moderate metal loadings. If this approximation is correct, the effect of changing potential at the humic substance macroion surface is important (that is, causes apparent variation in binding constants) only for complexation reactions observed under changing pH conditions. The theory for this situation has been developed thoroughly by Marinsky and co-workers (Ephraim *et al.*, 1986; Ephraim and Marinsky, 1986). Their model is based on the assumption that charged humic substance molecules, whether in solution or gel phase, behave as a charged surface, and concentrations of cations are enhanced in the diffuse double layer at this negatively charged surface relative to the bulk solution according to a Boltzmann-type distribution (Equation 2.27).

$$[M]_S = [M]_B \exp(-zF\psi/RT) \quad (2.27)$$

where $[M]_S$ is the concentration of M at the charged surface;

$[M]_B$ is the concentration of M in the bulk solution;

z is the charge on M;

ψ is the electrical potential at the charged surface;

and F is Faraday's constant, R is the gas constant and T is the absolute temperature. The Marinsky model assigns binding constants to specific sites, the identities of which are inferred from independent observations. Binding to these sites is modified by experimentally determined electrostatic terms, obtained by observing protonation in the assumed absence of electrostatic effects at very high ionic strength. Models of the type developed by Marinsky and coworkers have been successfully applied to humic substance - metal ion binding by Ephraim and Marinsky (1986) and Tipping *et al.* (1988).

2.4.5 Continuous Multiligand Models

Continuous multiligand models of humic substance - metal ion complexation reactions assume that the set of ligands present on humic substance macromolecules comprise a continuous distribution of binding sites with respect to binding strength (measured by K_{ML} or log K_{ML}). Sposito (1984, 1986) has presented a general equation describing complexation by a continuous distribution of ligands, as follows:

$$C_{ML} = \int_{-\infty}^{\infty} N(\kappa) \frac{\exp(\kappa)[M]}{(1 + \exp(\kappa)[M])} d\kappa \quad (2.28)$$

where $\kappa = \ln K_{ML}$ (or $\log_{10} K_{ML}$), and $N(\kappa)$ is a function describing the form of the distribution of sites with respect to ln K_{ML}, with the constraint that:

$$C_L = \int_{-\infty}^{+\infty} N(\kappa) d\kappa \quad (2.29)$$

The approach to data analysis based on a continuous multiligand model takes two paths; the form of the distribution $N(\kappa)$ may be assumed, or $N(\kappa)$ may be inferred from the experimental data. Models of humic substance complexation behaviour which assume a form for the distribution $N(\kappa)$ include the Sips distribution (Section 2.4.2) or the assumption that sites are normally distributed with respect to log K_{ML} (Perdue and Lytle, 1983). If log K_{ML} values are normally distributed, the function $N(\kappa)$ takes the form:

$$N(\kappa) = \frac{1}{\sigma_K\sqrt{2\pi}} \exp^{-\frac{1}{2}\left(\frac{\left(\ln K_{\mu} - \kappa\right)}{\sigma_K}\right)^2} \qquad (2.30)$$

where $\ln K_{\mu}$ and σ_K are the mean and standard deviation, respectively, of the normal distribution of log K_{ML} values. Experimental data are fitted to this model by optimizing $\ln K_{\mu}$ (or $\log_{10}K_{\mu}$) and σ_K values; the model has been used to successfully describe humic substance protonation (Perdue and Lytle, 1983) and complexation of metal ions (Perdue and Lytle, 1983; Turner *et al.*, 1986; Dobbs *et al.*, 1989a,1989b). An adaptation of this model involving a bimodal lognormal distribution has also been proposed and implemented (Perdue and Lytle ,1983).

In a series of recent articles (Dobbs *et al.*, 1989a,1989b; Susetyo *et al.*, 1990) the continuous lognormal binding model has been extended to incorporate competitive effects in systems containing humic substances, protons and two metal ions (Eu^{3+} and Al^{3+}). All cationic species are presumed to compete for the same sites; the model includes independent values of log K_{μ} for all three cations, but a single value of σ_K is assumed to apply to all binding reactions. In this form, the model successfully predicted competitive binding of H^+, Eu^{3+} and Al^{3+} to a humic substance (Susetyo *et al.*, 1990), an achievement not matched by any other model to date.

The determination of the form of the distribution of binding site affinities, $N(\kappa)$, from the experimental data itself at first appears to be an intractable problem, since an analytical solution of Equation 2.28 is,

in general, not possible (Thakur *et al.*, 1980). An approximate solution is, however, available using a numerical finite difference method developed by Ninomiya and Ferry (1959) to describe the relaxation of viscoelastic materials. Hunston and co-workers (Hunston, 1975; Thakur *et al.*, 1980), using the similarity between the equations of Ninomiya and Ferry (1959) and equations pertaining to binding of small substrates to proteins, developed a method for approximating the function $N(\kappa)$ from experimental data. The distribution $N(\kappa)$ may be approximated by Equation 2.31:

$$N(\kappa) = \left[\frac{f_1}{2 \log a} \left[f_1 - \frac{a}{(a-1)^2} \frac{(f_2 - 2f_1)}{2 \log a} \right] \right]_{[M]=1/K} \qquad (2.31)$$

where a is an empirical constant ($a > 1$);

$f_1 = B(a/K) - B(1/(aK))$;

$f_2 = B(a^2/K) - B(1/(a^2K))$, and;

$B(a/K) = C_{ML}$ when $[M] = a/k$;

$B(1/(aK)) = C_{ML}$ when $[M] = 1/(aK)$;

$B(a^2/K) = C_{ML}$ when $[M] = a^2/K$;

$B(1/(a^2K)) = C_{ML}$ when $[M] = 1/(a^2K)$.

B(a,K) values are interpolated from the (numerically smoothed) experimental binding isotherm ($\log C_{ML}$ vs. log[M]). Calculated this way, $N(\kappa)$ is a distribution or *affinity spectrum* with respect to logK such that the concentration of sites having log K in the interval (log K to (log K + dlog K)) is given by the area under the $N(\kappa)$ curve over this interval. This method requires appropriate smoothing of experimental data so that C_{ML} can be found for all measured values of [M]; the calculated form of the distribution is sensitive to factors such as experimental error and number of data used in the calculations (Thakur *et al.*, 1980). In addition, Thakur *et al.* (1980) showed that a continuous distribution of sites is inferred using this method, even if discrete site(s) are present.

An alternative method for finding the form of $N(\kappa)$ has been proposed by Leuenberger and Schindler (1986). They assume that the site distribution function may be approximated by a set of log K intervals; the width of these intervals determined the spectral resolution. Since the resulting affinity spectrum is defined by a set of adjacent rectangles, analytical integration is possible, and corresponding C_i values can be found by multiple linear regression.

Perhaps the most mathematically rigorous model for complexation by heterogeneous ligands has been presented by Gamble and coworkers (Gamble *et al.*, 1980). Gamble recognised that the the 'stability quotient' for humic substance - metal ion complexation (Equation 2.32)

$$\bar{K} = \frac{[ML]}{[M][L']} \qquad (2.32)$$

is not a constant, but varies with [ML] (or [M] or χ_{ML}), since:

$$\bar{K} = \frac{\Sigma_i K_i [L_i']}{\Sigma_i [L_i']} = \frac{\Sigma_i [ML_i]}{[M]\Sigma_i [L_i']} \qquad (2.33)$$

and thus at any point in a titration of humic substance with a metal (H^+) ion (or *vice versa*), $\bar{K}$ is only a weighted average of K_i values for all participating sites, and is dependent on the composition of the experimental system. Using $\bar{\nu} = C_{ML}/C_L$, a *differential equilibrium function* K' is related to the average equilibrium function $\bar{K}$ (Langford *et al.*, 1983) by:

$$K' = \frac{-d(\bar{K}(1-\bar{\nu}))}{d\bar{\nu}} \qquad (2.34)$$

This means that K' may be estimated from the slope of a plot of $\bar{K}(1 - \bar{\nu})$ *vs.* $\bar{\nu}$ at any point on the experimental curve. K' is thus a function of $\bar{\nu}$, such that:

$$K' = f(\bar{\nu}) = \frac{d[ML]}{[M]d[L']} \qquad (2.35)$$

and K' represents the 'instantaneous' binding constant defined for a certain value of $\bar{\nu}$ (that is, the binding constant relevant only to the infinitesimal fraction of sites d[L'] that M is binding to at the specified value of $\bar{\nu}$). The Gamble model may also be modified to allow for electrostatic concentration gradients (calculating [M] at the charged macromolecular surface from [M] in the bulk solution), essentially by incorporating Equation 2.27 into the initial binding equations.

It has been pointed out by some authors, however, that the Gamble model, being non-parametric, does not provide a succinct description of heterogeneous complexation reactions. Results derived from application of this model are usually presented in a tabular (for example Hansen *et al.*, 1990) or graphical (for example Cheam, 1973) format, expressing K or K' as a function of χ_{ML}.

2.5 Experimental Methods for Observing Humic Substance - Metal Ion Binding

In order to experimentally determine the extent of humic substance - metal ion binding, it is necessary to use some probe which distinguishes reactants and products of the complexation reaction; either bound and unbound metal, or bound and unbound ligand. Methods for achieving this rely on either a physical separation of the chemical species involved, or selective response on the basis of chemical speciation. In addition, the experimental design must allow calculation of the remaining components in the system, commonly by making certain assumptions of the stoichiometry of the complex(es) and using differences between total and measured species concentrations. Usually this is accomplished by a titration procedure; non-separative methods generally allow continuous titration, whereas separative methods are normally performed using a batch process.

In addition, methods for observing humic substance - metal ion complexation have been used which provide largely qualitative information, such as coordination symmetry of complexed metal ions, or nature of ligand donor atoms.

2.5.1 Separative Methods

Methods involving a physical separation of complexed and uncomplexed species are often based on either a phase separation (for measurements of binding to humic substances in the solid phase), separation on the basis of molecular size (exploiting the macromolecular nature of humic substances) or competitive equilibria (using a second ligand in the system for which complexation equilibria are well defined). An independent analysis method, such as atomic absorption spectroscopy, specific-ion potentiometry, anodic stripping voltammetry or use of radiolabelled metal ion, is required to determine free metal ion concentrations, and the detection limit of this method defines a lower limit for the titration window.

2.5.1.1 Phase separation

The preferred method of phase separation seems to be centrifugation (see for example McLaren *et al.*, 1981; Tipping *et al.*, 1988) often followed by a filtration step.

2.5.1.2 Molecular size separation

Physical separation of reactants and products may be achieved in the solution phase by exploiting the macromolecular properties of humic substances, for example using gel permeation (size exclusion)

chromatography (Mantoura and Riley, 1975) equilibrium dialysis (Rainville and Weber, 1982; Tipping *et al.*, 1988) or ultrafiltration (Tuschall and Brezonik, 1983).

2.5.1.3 Separation using competitive equilibria

While methods employing competitive equilibria do not always produce a true physical separation they are included here because they effectively separate a single component in a directly or indirectly identifiable form by disturbing humic substance - metal ion equilibria by a well defined amount. The main methods used have been ion exchange equilibrium (Schnitzer and Hansen, 1970) and competing-ligand differential spectrophotometry (Langford and Khan, 1975; Tuschall and Brezonik, 1983).

2.5.2 Non-separative methods

2.5.2.1 Potentiometric methods

The glass electrode has been used by many researchers (for example, Posner, 1964; Gamble, 1970; Wilson and Kinney, 1977; Perdue and Lytle, 1983; Ephraim *et al.*, 1986; Gregor and Powell, 1988b) to investigate protonation equilibria of humic substances. Determination of hydrogen ion activities using a glass electrode has been used to investigate humic substance - metal ion complexation by assuming the stoichiometry of proton displacement reactions (for example, Gamble *et al.*, 1970; Stevenson *et al.*, 1973; Ephraim *et al.*, 1986). Ion selective electrodes have been used to determine unbound metal ion for complexation reactions of humic substances with Cu^{2+} (for example Cheam, 1973; Buffle *et al.*, 1977; Ephraim and Marinsky, 1986), Cd^{2+} (Saar and Weber, 1979), Pb^{2+} (Buffle *et al.*, 1977), Ca^{2+} (Dempsey and O'Melia, 1983), and Ag^{+} (Sikora and Stevenson, 1988).

2.5.2.2 Amperometric methods

Anodic stripping voltammetry has been used by various researchers (Shuman and Cromer, 1979; Tuschall and Brezonik, 1983; Gregor and Powell, 1988a)to determine unbound metal ion in humic substance - metal ion binding experiments. Also used for this purpose has been the related technique of controlled potential amperometry (Waite and Morel, 1983; Hering and Morel, 1988a).

2.5.2.3 Spectrophotometric methods

Differences in the visible absorption spectrum of dissolved humic substances have been used to observe humic substance - metal ion complexation by some researchers (Langford and Khan, 1975; Gamble *et al.*, 1980) as has visible light scattering (Underdown *et al.*, 1985). A greater number of studies have used fluorescence quenching spectrometry to selectively determine bound humic substance binding sites (for example Saar and Weber, 1980; Cabaniss and Shuman, 1988).

2.5.2.4 Other spectroscopic methods

Electron spin resonance spectroscopy (ESR) has been used by several groups of researchers (for example Goodman and Cheshire, 1976; Bloom and McBride, 1979) to characterise humic substance - metal ion complexes. A few groups of researchers (for example Senesi *et al.*, 1977) have used Mössbauer spectroscopy to characterise Fe^{3+} - humic substance complexes. Recently Dobbs *et al.* (1989a) have described the use of lanthanide ion probe luminescence spectroscopy to quantify binding of Eu^{3+} to fulvic acids.

2.5.2.5 Other methods

The effect of metal ion binding on the molecular size, transport and ionic mobility properties of humic substances has been investigated by ultracentrifugation (Ritchie and Posner, 1982), light scattering (Underdown *et al.*, 1985) and gel chromatography (De Nobili *et al.*, 1989).

2.6 Studies of Complexing Reactions of Humic Substances

Studies of protonation and/or metal complexation reactions of humic substances are abundant in the literature of several disciplines including chemistry, biology, soil science, environmental science, geochemistry and marine/aquatic chemistry amongst others. The heterogeneity inherent in the systems under study, the variety of sources of humic substances, the different analytical methods and experimental conditions (pH, ionic strength, temperature, range of humic substance and metal concentrations) and the variety of chemical and mathematical models used all mean that comparisons between results from different researchers are of limited utility (Sposito, 1986; Turner *et al.*, 1986; Fish *et al.*, 1986).

2.6.1 General Complexation Behaviour

As far as complexation by different metal ions is concerned, complexation parameters seem to support an Irving-Williams series for complexes between humic substances and ions from the first transition series (Gamble *et al.*, 1983). Naturally enough, exceptions are found; the variability of humic substances undoubtedly contributes to this. A survey of review literature reveals that the range of metal ions studied in terms of humic substance complexation includes Al^{3+}, Fe^{2+} and Fe^{3+}, Pb^{2+}, Zn^{2+}, Cd^{2+}, Ni^{2+}, Co^{2+}, UO_2^{2+}, VO^{2+}, La^{3+}, Eu^{3+}, Mn^{2+}, Ag^{+}, Hg^{2+}, Cr^{3+}, Ca^{2+}, Mg^{2+}; in addition exchange reactions for alkali and alkaline earth cations have also been studied. The humic substances studied

have been isolated from a wide variety of sources, including: soils, fluvial systems, lakes, estuaries, littoral and pelagic marine environments, anthropogenic sources and 'synthetic' humic substances. In addition, the isolated humic substances studied with respect to metal/proton complexation have been fractionated in different ways (for example, peats, fulvic acids, humic acids, or more detailed fractionation procedures such as ultrafiltration). Most studies of humic substance - metal ion complexation have been done with fulvic acids as the ligand and Cu^{2+} as the metal ion; this reflects the wide range of aqueous solubility conditions available to fulvic acids, and the environmental relevance, strong complex formation and ease of analysis of divalent copper.

Many studies (see Sections 2.3.1 to 2.3.3) have illustrated the effect of changing pH, metal ion:humic substance ratio, competition between metal ions, and ionic strength on metal ion - humic substance complexation reactions.

A proportion of the literature is based on 'internal' comparisons, that is, comparisons between protonation/metal ion complexation properties of different metals or different humic substances by consistent methods within each publication. Often these properties are correlated with other properties of humic substances. An example of this type of approach is found in the study by Sikora and Stevenson (1988).

Comparison of methods of measurement for determining complexation parameters for humic substance - metal ion complexation has been the intention of other researchers (for example, Tuschall and Brezonik, 1983; Weber, 1988).

2.6.2 Comparisons of Mathematical Models

Since no definitive model for quantifying protonation and/or metal ion complexation equilibria exists, much of the literature to date has dealt with the development of suitable models. Recently a number of

reviews involving theoretical and experimental comparisons of models for humic substance - metal ion complexation have been published, for example by Perdue and Lytle (1983), Stevenson and Fitch (1984), Sposito (1986), Turner *et al.* (1986), Dzombak *et al.* (1986), Fish *et al.* (1986), Buffle and Altmann (1987), and Perdue (1989). From these comparisons a number of pertinent points emerge.

1. In instances where data from different researchers has enabled consistent comparisons to made, it appears that humic substances from various sources have remarkably similar properties with respect to complexation of protons and metal ions.

2. Models based on a set of discrete ligands, while providing good mathematical descriptions of humic substance - metal (hydrogen) ion complexation, do not necessarily have any chemical significance in terms of the molecular structure of humic substances and the processes which occur on the molecular level. Discrete multiligand models do, however, offer good predictive capability if extrapolations are not made outside the range of experimental measurement.

3. Estimates of complexation parameters are dependent on experimental restrictions such as detection limits and solubility considerations (as discussed in Section 2.5). Similarly, the operational nature of definitions of ligand concentrations (binding site numbers, complexation capacities) means that models which depend on measurement of this parameter may be intrinsically inaccurate.

4. Continuous multiligand models, although intuitively more realistic, may be more difficult to implement than simpler models and (with the exception of models with an assumed distribution) provide a less succinct description of binding.

5. Until very recently (Dobbs *et al.*, 1989a,b; Susetyo *et al.*, 1990), no models have been successful in predicting competitive equilibria in systems containing humic substances, protons, and more than one metal ion.

2.7 Kinetic Aspects of Humic Substance - Metal Ion Complexation

While it is well known that equilibrium speciation of protons and metal ions is critical in environmental systems, there has been less emphasis on the kinetic aspects of speciation. The rate of proton/metal ion uptake and/or release by complexing agents, including humic substances, is likely to be important if equilibria are disturbed for any reason, for example large concentration pulses of metal ions due to fertiliser applications or effluent discharges. In fact, in agricultural soils (Sparks, 1985), or natural waters (Pankow and Morgan, 1981) equilibrium situations are almost never achieved. It is also conceivable that release of bound metal ions may be rate limiting for micronutrient uptake by organisms (Shuman *et al.*, 1983), especially in soils and sediments where availability of metal ions is effectively controlled by solid or gel phase components.

2.7.1 Kinetic Concepts and Models

Rates of chemical reactions are described quantitatively by reaction order and the corresponding rate constant. For a simple first-order reaction (Equation 2.36):

$$R \rightarrow P;\ -d[R]/dt = k_F[R] \qquad (2.36),$$

where R refers to reactant, P to product and k_F is the first-order forward rate constant. For the reverse process, Equation 2.37 applies:

$$d[R]/dt = k_R[R] \qquad (2.37),$$

where k_R is the first-order reverse rate constant, which is related to the equilibrium constant K for the reaction (ignoring the effect of activity coefficients) by:

$$K = [P]/[R] = k_P / k_R \quad (2.38);$$

at equilibrium, $-d[R]/dt = d[R]/dt = 0$.

Data from studies of the time dependent behaviour of humic substance - metal ion complexation reactions have generally been analysed in terms of first order kinetics. This is true even when (as is most often the case) the experimental data is not described well by a single-component first-order kinetic model. This poor fit to a simple first-order model has always been interpreted in terms of humic substance heterogeneity, that is, simultaneous first-order reaction of kinetically different binding sites. There are several reasons for this: experiments are normally conducted using an isolation method (all reactants except one in excess), so that pseudo-first-order conditions should apply; in addition, the mechanisms of complex formation and dissociation are such that a reaction which is bimolecular in any one reactant is unlikely. First order behaviour for heterogeneous systems may be verified from superposition of $\ln([P]/[P]_0)$ vs t plots, in which the concentration scale is normalised to a common value for each experiment (Albery *et al.*, 1985). Kinetic heterogeneity has not always been assumed for the reactions of humic substances and metal ions; for example, Langford and Khan (1975) calculated rate constants by least-squares fit to a single component first order equation. When, however, kinetic heterogeneity has been recognised, it has been dealt with using mathematical models similar to those used to describe humic substance - metal ion complexation equilibria (Section 2.4). Kinetic heterogeneity has been interpreted for humic substance - metal ion complexation either in terms of sites having discrete rate constants, or as a continuous distribution of sites with respect to kinetic parameters.

For a mixture of n discrete sites L_i reacting simultaneously by first order processes, the relevant integrated rate equations take the form (for example, Lavigne *et al.*, 1987):

$$[ML]_t = \sum_{i=1}^{n} C_i(\exp(-k_i t)) \quad (2.39)$$

for association reactions, and (equivalently);

$$[ML]_t = \sum_{i=1}^{n} C_i(1 - \exp(-k_i t)) \qquad (2.40)$$

for dissociation reactions, where $[ML]_t$ is the concentration of bound metal ion at time t, C_i is the stoichiometric concentration of the i^{th} kinetically discrete site (as for binding equations), and k_i is the first order association (dissociation) rate constant for the i^{th} site. Such equations, usually with n = 2 to 4, have been used successfully to describe humic substance - metal ion association (Plankey and Patterson, 1987) or dissociation (Lavigne *et al.*, 1987; Cabaniss, 1990) kinetics. Discrete site kinetic models may be implemented in different ways. Cabaniss (1990) describes discrete kinetic spectra' in which values for the various k_i in Equation 2.40 are fixed at arbitrary values and the C_i terms are found by multiple linear regression. Cabaniss (1990) also implemented Equation 2.40 by fixing C_i terms at nominal, but realistic, values; the adjustable k_i were estimated using nonlinear regression. Both of these more restricted models were successful in describing Ni^{2+}- fulvic acid complex dissociation kinetics.

Recently, Harter (1989) has developed a model based on first order kinetics which invokes both association and dissociation reactions. In this model discrete sites are assigned both first order association and dissociation rate constants. During the course of a heterogeneous sorption reaction, metal ions initially adsorbed to quickly reacting sites may subsequently dissociate and bind to more slowly reacting sites with higher k_F/k_R (higher effective binding constant). The relevant equation effectively combines Equations 2.8 and 2.39, and may be written for n sites as (Harter, 1989):

$$\frac{[ML]_t}{[ML]_0} = \sum_{i=1}^{n} \left[(1/k_{Fi}) \left\{ (k_{Fi} - k_{Ri}A) \exp(-k_{Fi} t) + k_{Ri}A \right\} \right] \qquad (2.41)$$

where $A = (1 - [ML]_t / [ML]_0)$

k_{F_i} is the rate constant for the formation of a complex at the i^{th} site

k_{R_i} is the rate constant for dissociation of a complex at the i^{th} site.

The alternative to a discrete set of sites with respect to first order rate constants is a continuous distribution of sites with respect to (log)k. As is the case for humic substance - metal ion complexation equilibria, this distribution may be assumed *a priori* or estimated from the experimental data. The Elovich equation, originally developed to describe chemisorption of gases on solid surfaces, presumes a heterogeneous distribution of activation energy (E_a) such that E_a increases linearly with increasing surface coverage (Low, 1960 as quoted by Sparks, 1985). The form of the Elovich equation appears in Equation 2.42; an approximation to its integrated form has been derived by Chien *et al.* (1980) and appears in Equation 2.43.

$$d[ML]/dt = \alpha.\exp(-\beta[ML]) \qquad (2.42),$$

where α and β are constants

$$[M]_t = a - b.\ln t \qquad (2.43),$$

where a and b are constants such that:

$$a = [M]_0 - (1/\beta)\ln(\alpha\beta)$$

and $b = (1/\beta)$.

Equations describing kinetically heterogeneous sites with a Gaussian distribution with respect to ln k (corresponding to a Gaussian distribution with respect to activation energy) have been developed by Albery *et al.* (1985) to describe charge decay from photosensitive semiconductors. The model is summarised by:

$$\frac{C_t}{C_0} = \frac{\int_{-\infty}^{\infty} \exp(-x^2).\exp(-\tau\exp(\gamma x))\,dx}{\int_{-\infty}^{\infty} \exp(-x^2)\,dx} \qquad (2.44)$$

where $\exp(-x^2)$ defines the Gaussian distribution, τ is a dimensionless time parameter $\tau = \bar{k}t$, $\bar{k}$ being the mean rate constant, and γ is a parameter describing the spread of the distribution (reducing to a

single k value when $\gamma = 0$). A model of this type has, however, yet to be applied to humic substance - metal ion complexation kinetics.

Shuman and coworkers (Olson and Shuman, 1983; Shuman *et al.*, 1983) have presented a method by which the distribution of sites with respect to ln k can be estimated from experimental data. The method involves an approximate Laplace transform solution of an equation of the type:

$$C(k,t) = \int_0^{\infty} F(k,t)e^{-kt}.d(\ln k) \qquad (2.45)$$

where F(k,t) is a distribution function with respect to ln k such that:

$$\int_0^{\infty} F(k,t).d(\ln k) = \Sigma_{i=1}^{n} [ML_i]_0 \qquad (2.46)$$

The distribution function F(k,t) may be estimated using the following second-order approximation (Olson and Shuman, 1983):

$$F(k,t) = d^2[M]_t / d(\ln t)^2 - d[M]_t / d(\ln t) \qquad (2.47)$$

In effect, this method results in a non-parametric description of heterogeneous kinetics by transformation of ($[M]_t$,t) data into ($[M]_t$,k) space. This method gives a 'kinetic spectrum' with peaks at the most abundant values of ln k ($\equiv \ln(2/t)$); kinetic spectra have been used to estimate input parameters for least squares solution of Equation 2.40 (Lavigne *et al.*, 1987).

2.7.2 Factors Affecting Complexation Kinetics

2.7.2.1 Chemical considerations

The rates of both metal ion binding to, and dissociation from, a ligand are dependent on the chemical and physical nature of both the metal ion and ligand involved. The identity of the metal ion is especially important; for example, complexes of transition metal ions such as Cu^{2+} generally form quickly and are *labile* (quickly dissociating) (Wilkins, 1970), whereas complexes of Cr^{3+} or Co^{3+} tend, because of slow dissociation reactions, to be substitutionally inert (Cotton and Wilkinson, 1976). Association or ligand exchange reactions for *simple* ligands are found to be essentially independent of the identity of the incoming ligand; rates of ligand substitution depend rather on rates of exchange of coordinated H_2O (Cotton and Wilkinson, 1976), stressing the importance of the dissociative or S_N1 mechanism. For metal ion binding to macromolecular ligands such as humic substances, however, additional factors (including those described in Section 2.7.2.2) are likely to apply, especially for ligands in the gel or solid phase. Formation of chelate complexes may have chelate ring closure as the rate determining step, especially where a donor site is very weakly acidic or the chelate ring is large (Wilkins, 1970). In addition, dissociation of coordinated H_2O occurs more quickly if a ligand already bound to the metal ion is electron-donating (Wilkins, 1970). Electrostatic effects may also be important; dissociation may be slower from more highly charged ligands (Olson and Shuman, 1983). In addition, removal of ions from the effect of macro-ionic electrostatic potential may be rate determining for humic substances (Cabaniss, 1990).

2.7.2.2 Contribution of diffusive processes

The macromolecular nature of humic substances, and their tendency to reside in the gel or solid phase under environmental conditions, means that the processes of *film* and *intraparticle* diffusion are likely to be important (Sparks, 1985). Film diffusion is diffusion of reactant species (in this case protons or

metal ions) through the quiescent layer of solution surrounding solid or colloidal particles (in this case solid or gel phase humic substances, or perhaps even large dissolved humic substance molecules). Film diffusion will be dependent on the hydrodynamics of the reaction system. Mixing or flow processes tend to reduce the thickness of the hydrodynamic film, and film diffusion becomes less important. Intraparticle (or simply *particle*) diffusion refers to diffusion of small reactant species through the particle itself or, conceivably, the matrix of a single macromolecule. For a complexation process where some form of diffusion is the rate determining step, a simplified parabolic diffusion law is given by:

$$[M]_t / [M]_\infty = a + bt^{1/2} \qquad (2.48)$$

where a and b are constants (Salim and Cooksey, 1980); b may be considered to be an overall diffusion coefficient dependent on particle radius and ionic diffusion coefficients (Sparks, 1985). A linear dependence of reaction progress on $t^{1/2}$ may thus imply rate-limiting diffusion.

2.7.3 Methods for Measuring Kinetics in Complexation Reactions of Humic Substances

General kinetic methods fall into two main categories. Batch techniques involve either a series of identical samples allowed to react for different times, or a reaction system which is sampled periodically; samples must not react further after some method is used to quench the reaction (often a simple phase separation). Continuous techniques involve monitoring of the concentration of a reaction component continuously during the course of the reaction. Analytical methods for following reaction progress as a function of time for any continuous experiment must have response times which are short compared with the timescale of the observed reaction. This becomes especially important for experiments involving reactions with timescales of the order of seconds. Kinetics of humic substance -

metal ion association reactions may be initiated simply by mixing the necessary reactants; initiation of dissociation reactions requires some means of disturbing a system already at or near equilibrium.

2.7.3.1 Association Reactions

Batch methods. These methods have generally involved reaction of replicate solid humic substance or soil samples, in electrolyte solution, with a metal ion. Reactions are quenched at the desired time by phase separation using centrifugation. McLaren *et al.* (1981) followed the reaction of solid humic acids with Cu^{2+} by this type of method, using atomic absorption to determine free copper in the solution phase. Alternative detection methods used include anodic stripping voltammetry for Pb^{2+} (Salim and Cooksey, 1980).

Continuous methods. Bunzl *et al.* (1976) measured kinetics of the complex formation reactions between various metal ions and peat by following conductivity changes in the reaction solution; hydrogen ions displaced by metal ion exchange have higher molar conductivity than the metal ions themselves. Adsorption of Cu^{2+} and Cd^{2+} on whole soils has been followed using ion-selective electrodes by Cavallaro and McBride (1978). Faster reactions, especially those in the solution phase, have generally been followed using spectroscopic methods. Langford and Khan (1975) used stopped-flow UV-visible spectrophotometry to follow the reaction of Fe^{3+} and a fulvic acid, exploiting small absorbance changes in the fulvic acid on Fe complexation. Plankey and Patterson (1987) used UV-visible fluorescence spectrometry to monitor Al^{3+} - fulvic acid complexation.

2.7.3.2 Dissociation reactions

Continuous methods. Desorption of metal ions from peat was followed conductimetrically by Bunzl *et al.* (1976); metal ions were desorbed by adding H^+, which displaces metal ions from binding sites. If dissociation can be induced by introducing a competing metallochromic ligand to an equilibrated humic substance - metal ion complex, desorption can be followed spectrophotometrically or fluorimetrically. This method has been used by Langford and Khan (1975) using sulphosalicylic acid as the competing ligand in an Fe^{3+}-FA system; by Olson and Shuman (1983) and Shuman *et al.* (1983) for Cu^{2+}-FA systems using 4-(2-pyridylazo)resorcinol (PAR); Lavigne *et al.* (1987) and Cabaniss (1990) for Ni^{2+}-FA systems using PAR, and by Hering and Morel (1990) in Cu^{2+} - humic acid systems using calcein. A further method for measuring dissociation rates exploits the observation that a proportion of metal complexed by humic substances dissociates under the conditions of the anodic stripping voltammetry (ASV) experiment; the fraction dissociating depends on the flow characteristics of the experiment, that is, stirring or electrode rotation rates. Kinetic parameters for Cu^{2+} dissociation from humic and fulvic acids have been measured using ASV and rotating disk electrodes by Shuman and Michael (1978) and ASV and mercury drop electrodes by Shuman and Cromer (1979).

2.7.4 Studies of the Kinetics of Complexation Reactions of Humic Substances

In comparison with studies of equilibrium proton and metal ion binding to humic substances, studies of the kinetic behaviour of these reactions have been relatively few. To a certain extent, this reflects the emphasis placed on equilibrium processes in determining chemical speciation in the environment by many workers. There is an increasing awareness, however of the importance of nonequilibrium or

kinetic processes in many environmental situations. To the knowledge of this author, kinetics of proton binding processes have never been studied for humic substances; indeed, some studies involving metal ion binding (for example, Bunzl *et al.* (1976)) assume implicitly that (de)protonation reactions are never rate determining.

2.7.4.1 Kinetics involving solid phase humic substances

Slow rates of dissociation have been implicated by some workers (McLaren *et al.*, 1981; Hogg, 1989) as contributing to observed titration hysteresis in humic substance - metal ion complexation experiments. Most results (Bunzl *et al.*, 1976; Salim and Cooksey, 1980; McLaren *et al.*, 1981) suggest initial fast association reactions with slower reactions proceeding over much longer timescales. These results, however, are for whole soils although humic substances were implicated as a major metal ion binding component. The measured half lives for association ($t_{1/2}$ in the range 5 - 15 s; Bunzl *et al.* (1976)) appear to be largely a function of the initial fast reaction, and are perhaps misleading due to kinetic heterogeneity. Film diffusion has been found to be rate determining by Bunzl *et al.* (1976) and Salim and Cooksey (1980). Dissociation of metal ions from peat (Bunzl *et al.*, 1976) has been found to be similarly fast, but only half lives were measured. This gives less weighting to the effect of slowly dissociating components when describing kinetics with a single rate constant.

2.7.4.2 Kinetics involving aqueous phase humic substances

Most research on the kinetics of metal ion interaction with isolated humic substances has been performed with all reactants in aqueous solution. Of these studies, there has been more work observing complex dissociation than association reactions.

Association reactions. Complex formation kinetics has been studied by Langford and Khan (1975) for an Fe^{3+}-FA system and Plankey and Patterson (1987) for an Al^{3+}-FA system. Pseudo-first order association rate constants for Fe^{3+}-FA (with [Fe] = 0.2-1.25 x 10^{-2} mol L^{-1}, pH 1.65 and 25 ° C) were of the order of 0.5 s^{-1} (Langford and Khan, 1975). Plankey and Patterson (1987) found that two pseudo-first order rate constants were necessary and sufficient to describe their data, and related these to 'average' kinetically distinguishable sites on their fulvic acid sample. The faster site had pseudo first-order rate constants (for pH 3-4.5, [Al^{3+}] = 1.8-3.6 x 10^{-3} mol L^{-1} and 25 ° C) in the range 0.04-0.21; the slower site had constants in the range 0.004-0.03. Reaction rates were found to increase with increasing pH and temperature. Plankey and Patterson related their observed rate constants to a mechanistic scheme based on reaction of Al^{3+} with salicylic acid.

Dissociation reactions. Langford and Khan (1975) measured a half life of c. 10s for Fe^{3+}-FA complex dissociation at 25 ° C. First order dissociation rate constants were measured by Shuman and Cromer (1979) for Cu^{2+}-fulvate (k_1 = 2.7 s^{-1}) and Cu^{2+}-humate (k_1 = 0.1 s^{-1}) complexes. Shuman *et al.* (1983) observed Cu^{2+}-estuarine organic matter (EOM) complex dissociation (two first order rate constants; k_1 = 0.25-13.0 s^{-1}, k_2 = 0.02-0.25 s^{-1}, depending on salinity and size fraction) using ASV. The fraction of Cu^{2+} dissociating slowly enough to be observed, however, was only c.35-65%; the ASV technique can

measure dissociation rate constants in the range c. 10^{-3}-10^{2} s^{-1} (Shuman *et al.*, 1983). Cu^{2+}-EOM dissociation was also observed spectrophotometrically using the metallochromic ligand 4-(2-pyridylazo) resorcinol (PAR) to induce dissociation (25 ° C, I=0.1M) by Shuman *et al.* (1983). Data could be described by two or three first order rate constants in the range 0.01-34 s^{-1}, although c.77% of Cu^{2+} dissociated too fast to be observed ($k_1 \geq 50\ s^{-1}$). Reactions were observed to be faster at higher salinity and for smaller molecular size (as determined by ultrafiltration). Reaction rates observed spectrophotometrically were found to be independent of PAR concentration for $[PAR]/[Cu]_T$ in the range 2.9-140. A similar study by Lavigne *et al.* (1987), measuring dissociation of Ni^{2+} from a fulvic acid sample, showed that three first order rate constants (k_1=0.15 s^{-1}, k_2=0.021 s^{-1}, k_3=0.0026 s^{-1}; 25 ° C) were sufficient to describe Ni^{2+}-FA dissociation data over a range of initial FA concentrations. Nickel(II)-fulvic acid complex dissociation was also investigated by Cabaniss (1990) as a function of pH and ionic strength. An increase in solution ionic strength, or a decrease in pH, was found to cause substantial increases in Ni^{2+}-FA dissociation rate, especially at higher Ni:FA ratios. Results were expressed in terms of kinetic spectra and several implementations of a discrete multicomponent model.

In a recent study based on elucidation of reaction mechanisms, Hering and Morel (1990) proposed two possible pathways for the reaction of a competing ligand with Cu^{2+}-humic acid complexes. The first was the adjunctive mechanism (c.f. S_N2), where dissociation of a ternary humate-metal-ligand complex was rate determining, which was important at low Cu:humate ratio and low concentration of competing ligand. The second mechanism was termed *disjunctive* (c.f. S_N1) where dissociation of the initial Cu^{2+}-humate complex was rate determining. The disjunctive mechanism was considered to predominate at high Cu:humate ratio and high competing ligand concentration.

CHAPTER THREE

MATERIALS AND METHODS

3.1 General

All chemicals used in this work were AnalaR grade or equivalent unless otherwise specified. Glassware and plasticware was always cleaned before use by soaking in 10% HNO_3 for at least 24 hours and rinsing thoroughly with deionised water. All water used was purified in a Barnstead Nanopure reagent water system to a resistivity of 18.3 MΩ cm. Conventional volumetric equipment (such as pipettes, burettes or volumetric flasks) used was B-grade; uncertainties for the volumes measured were taken from Vogel (1979). Addition of small volumes of liquid was achieved using Finn micropipettes (0-20μl, 50-200μl, 200-1000μl); for accurate titration work, a Metrohm syringe burette was used.

Two centrifuges were used: a Sorvall RC-5B for analytical work and an IEC 6000B for preparative work.

3.2 Preparative Procedures

3.2.1 Humic Acid Samples

Humic acids were isolated from soils using the procedure adopted by the International Humic Substances Society (Appendix 1). These freeze-dried substances were stored in a desiccator at room

temperature in the fully H^+-exchanged form. For most experiments the humic acids were converted to the corresponding sodium or calcium humates.

3.2.2 Sodium and Calcium Humates

For experimental work, it was found to be most convenient to prepare sodium or calcium humates. Sodium humates are readily dissolved and thus are are suited to experiments involving aqueous phase humic substances. Conversely, calcium humates remain largely insoluble in aqueous solution and as such are suited to investigations involving humic substances in the solid phase. Both sodium and calcium humates facilitate maintenance of a steady pH in experimental systems; both contain acidic functional groups in associated and dissociated forms, thus providing a measure of buffering activity.

3.2.2.1 Sodium humates

Humic acid (5-10 g) was suspended in water (600-800 mL), and $NaOH_{(aq)}$ added under a steady stream of N_2, while stirring constantly, until a steady pH of 7.0 was attained. The resulting concentrated sodium humate solution was then centrifuged to remove insoluble residues, and freeze-dried. The dry sodium humate obtained was stored in a desiccator until used.

3.2.2.2 Calcium humates

These were prepared by adding $CaCl_2$ solution to the sodium humate solution above after the centrifugation step, so that the final $CaCl_2$ concentration was c. 1 mol L^{-1}. The pH of the resultant suspension of calcium humate was readjusted to pH 7 with $NaOH_{(aq)}$; the suspension was centrifuged and the supernatant solution discarded. The solid calcium humate was alternately washed/centrifuged 2-

3 times with 1.0 mol L^{-1} $CaCl_2$, then alternately washed/centrifuged (c.20 times) with 0.05 mol L^{-1} $CaCl_2$ until the level of humate in the supernatant (determined by UV absorption at 280 nm) had stabilised at a minimum (min. abs. 280 nm = 0.34 (Summit Hill); min. abs. 280 nm (Waimari Peat) = 0.47). The solid calcium humate was then alternately washed/centrifuged 2-3 times with water at 5 • C to remove excess salts; the solid remaining was freeze-dried and stored as the dry solid in a desiccator until used.

3.2.3 Humic Acid Solutions

Solutions of fully H^+-exchanged humic acids were prepared from sodium humates using a column of Dowex 50W-X8 ion exchange resin in H^+ form. An aliquot of sodium humate solution was eluted quantitatively through the column, and collected as a known (larger) volume of humic acid solution. The Dowex resin was treated to remove any organic impurities by (i) washing with methanol, and (ii) alternating washings with 0.1 mol L^{-1} NaOH and 0.1 mol L^{-1} HCl. This procedure was necessary as freeze-dried humic acids in the fully H^+-exchanged form were found to be significantly hydrophobic and difficult to dissolve directly.

3.2.4 Metal Ion Solutions

Stock $Cu(NO_3)_2$ and $Cd(NO_3)_2$ solutions (2000 mg L^{-1}) were prepared by dissolving the required weights of hydrated salt in the required volumes of water, and adding HNO_3 so that $[HNO_3] \simeq 0.010$ mol L^{-1}.

3.2.5 Standard Acid and Alkali Solutions

Standard NaOH solutions were prepared in CO_2-free water according to Vogel (1979), and standardised using a potentiometric titration/Gran plot method (Gran, 1952) against known weights of potassium hydrogen phthalate ($C_6H_4(COOH)(COOK)$). Standard HNO_3 and HCl solutions were similarly standardised against known weights of disodium tetraborate ($Na_2B_4O_7.10H_2O$).

3.2.6 Buffer Solutions

The NBS standard buffer solutions described in Table 3.1 were prepared according to Vogel (1979).

Table 3.1 pH values for selected NBS buffer solutions as a function of temperature.

	Buffer		
Temperature/°C	KHphthalate (0.05M)	KH_2PO_4/Na_2HPO_4 (0.025M/0.025M)	$Na_2B_4O_7$ (0.01M)
0	4.003	6.982	9.460
10	3.996	6.921	9.331
20	3.999	6.878	9.227
25	4.008	6.865	9.183
30	4.011	6.851	9.143
40	4.030	6.836	9.074
50	4.055	6.831	9.017

3.3 Instrumental Methods

3.3.1 Measurement of pH

Measurement of solution and suspension pH was achieved using an Orion 91-02 or 91-56 combination glass-Ag/AgCl reference electrode in conjunction with an Orion 701A or a Radiometer PHM26 or

PHM84 pH/mV meter. Electrodes were conditioned regularly by soaking in 0.1 mol L^{-1} HCl for 5 minutes, followed by soaking in pH 7 buffer for at least 1 hour. Glass/reference electrodes were stored in 0.05 mol L^{-1} KHphthalate/0.05 mol L^{-1} KCl when not in use. Electrode calibration was performed using one or more of the NBS standard KH phthalate, phosphate or borate buffers, depending on the accuracy required and the pH range to be measured.

3.3.2 Ion Selective Electrode (ISE) Measurements

Measurements of free Cu^{2+} and Cd^{2+} were made using Orion 9429 (Cu) and Orion 9448 (Cd) electrodes and Orion 9002 double-junction reference electrodes in conjunction with an Orion 701A or a Radiometer PHM26 or PHM84 pH/mV meter. The solid state ISEs were polished regularly, and filling solutions for reference electrodes were renewed as recommended. The response of the ISEs is sensitive to ambient light levels; in variable lighting conditions, constant light levels were maintained by enclosing the entire measurement solution and electrode assembly in a light-proof box. The outer filling solution for the double-junction reference electrode was filled with a solution containing the same inert electrolyte (at a higher concentration to ensure correct function of the liquid junction) as the analyte solution. The ISE-reference electrode pairs were calibrated in titration-generated Cu^{2+} (Cd^{2+}) standard solutions at the same ionic strength as the analyte solution.

As expected, calibrations in the absence of a complexing ligand were non-Nernstian at low ($\leq 10^{-6}$ mol L^{-1}) levels of Cu^{2+} and Cd^{2+}. Electrode response was Nernstian for both Cd^{2+} and Cu^{2+} when metal ion concentrations were $\geq 10^{-6}$ mol L^{-1}. The response of the Cu^{2+} electrode was observed at pCu levels in the range 7-10 (where $pCu \equiv -\log_{10}[Cu^{2+}]$), by varying the pH of solutions of Cu^{2+} and 1,2-diaminoethane (en) between c.3.5 and 6.0. Cu^{2+} concentrations were calculated from total Cu and en concentrations using the protonation and Cu-complex stability constants for 1,2-diaminoethane (Perrin, 1979). Linear or near-linear response was observed with a sensitivity slightly less than calculated by the Nernst equation (observed: 24.5 mV/decade [Cu]; calculated: 29.1 mV/decade [Cu] at

20° C). Linearity of electrode response was maintained at total solution Cu concentrations below 1×10^{-6} mol L^{-1}. This is in contrast to Sanders (1982), whose calibration method assumed that electrode slope was dependent only on total Cu concentration, and was independent of the presence or absence of complexing ligands. Midgley (1976) also found linear, Nernstian response for Cu^{2+} ion selective electrodes when complexation by nitrilotriacetic acid produced pCu values in the range 6-9, and when total Cu concentrations were above 1×10^{-6} mol L^{-1}. Linear, Nernstian response for a Cu^{2+} ISE has been observed to pCu = 19 when $[Cu]_{total}$ was > 10^{-6} mol L^{-1} (Avdeef *et al.*, 1983). Avdeef *et al.* (1983) also found electrode response was linear with respect to $\log[Cu^{2+}]$ when total [Cu] was less than 10^{-6} mol L^{-1}, although calibration slope was less than Nernstian. In light of these observations, only the portion of the calibration curve showing a linear relationship between potential and $\log[Cu^{2+}]$ was used, and a linear extrapolation was used whenever measured potentials were outside this calibration range.

3.3.3 Voltammetric Measurements

An anodic stripping voltammetry (ASV) procedure was used to measure total Cu and Cd concentrations; analyses were performed using a Princeton Applied Research Model 303 Static Mercury Drop Electrode in conjunction with a Princeton Applied Research 174A polarographic analyser and RE0089 X-Y recorder. Voltammetric parameters for analysis of Cu and Cd are contained in Table 3.2.; triple-distilled mercury was used throughout. Analyte solutions were acidified with HNO_3 (to $[HNO_3] \simeq$ 0.010 mol L^{-1}) to dissociate any complexes; calibrations were made *in situ* using a standard addition procedure. The porous frit and filling solution (0.7 mol L^{-1} KCl/sat. AgCl) for the Ag/AgCl reference electrode were renewed when necessary.

Table 3.2 Differential pulse-ASV parameters for determination of total solution Cu^{2+} and Cd^{2+}; potentials are relative to the Ag/AgCl half-cell.

	Analyte metal ion	
Parameter	Cu^{2+}	Cd^{2+}
Deposition potential	-0.4 V	-1.0 V
Voltage ramp	+5 mV s^{-1}	+5 mV s^{-1}
Pulse frequency	2 s^{-1}	2 s^{-1}
Pulse modulation amplitude	50 mV	50 mV
$M_{(Hg)}$ oxidation potential	-0.03 V	-0.67 V

3.3.4 Electrothermal Atomic Absorption

Electrothermal atomic absorption spectroscopy (ETAAS) was performed using a Pye-Unicam PU9000 Atomic Absorption Spectrophotometer with PU9095 graphite furnace head/furnace programmer and SP9 autosampler. The furnace heating program for Cu determination is contained in Table 3.3; oxygen-free nitrogen was used as the sheathing gas throughout the heating cycle. Sample injection volumes were 5 μl.

Table 3.3 Heating program for Cu determination by ETAAS.

Heating function	Final temperature/°C	Ramp speed/ °C s^{-1}	Hold time/s
Dry	120	10	30
Ash	800	100	5
Atomise	2600	>2000	5
Tube clean	2900	>2000	5

3.3.5 Ultraviolet-Visible Spectrophotometry

Absorbance scan, fixed wavelength and change in absorbance *versus* time spectrophotometric measurements were performed on a Philips PU8700 Fixed-Bandwidth UV-Visible spectrophotometer equipped with PU8732 Cell programmer/cell temperature controller, and dedicated Philips P3105 PC with 8086 processor. Absorbance scan and fixed wavelength measurements used conventional 1 cm quartz cells; kinetic measurements (see Section 3.5) were made using a semi-micro flow cell with 1 cm pathlength.

3.4 Proton and Metal Binding Experiments

3.4.1 Binding to Solid Calcium Humates

The method used to measure metal ion binding on solid phase calcium humates was an adaptation of that described by McLaren *et al.* (1981). Portions of calcium humate (Section 3.2.2) (50-100 mg) were weighed into 40 mL polypropylene centrifuge tubes. Calcium nitrate solution (0.05 mol L^{-1}, 20 mL) was added to each tube; the resulting suspensions were spiked with varying amounts of metal ion (Cu^{2+} or Cd^{2+}) solution so that two replicate series of additions were made. The pH of the suspensions was adjusted with HNO_3 or $Ca(OH)_2$ under N_2. Attainment of steady pH readings was very slow (c. 3-4 hours per sample) so adjustments with explicit pH measurement were made only for the suspensions with the lowest and highest Cu(Cd) additions. The volumes of acid or base required for pH adjustment of the remaining solutions were calculated by interpolation using these two previously measured values. The pH-adjusted suspensions were equilibrated at the desired temperature in an incubator on an end over end shaker for ≥48 hours. After this equilibration period, the suspensions were centrifuged and the supernatant solutions filtered (0.45 μm membrane) and stored in polyethylene vials until metal ion determinations were made. Free metal ion concentrations were determined by ISE potentiometry

(Section 3.3.2); total metal ion concentrations, when measured, were determined by ASV (Section 3.4) or ETAAS (Section 3.5).

The choice of 0.05 mol L^{-1} $Ca(NO_3)_2$ as the supporting electrolyte was based on the following reasoning. Firstly, the amount of soluble calcium humates in solution were kept to a minimum by the presence of excess Ca^{2+} ions. Separate experiments showed that lower or higher concentration of $Ca(NO_3)_2$ increased the concentrations of soluble humates. In the case of higher $Ca(NO_3)_2$ concentrations, this was tentatively attributed to the formation of a positively-charged Ca^{2+}-humate complex as site saturation increased due to mass-action effects. (A similar effect was observed when preparing calcium humates; a substantial amount of dissolved humate was present in solutions containing 1 mol L^{-1} $CaCl_2$.) Secondly, the presence of large amount of Cl^- can interfere with the determination of Cu^{2+} by stabilising the Cu^{+1} oxidation state; such an effect is not found with NO_3^-.

3.4.2 Binding by Sodium Humates (Aqueous Phase)

Solution metal binding experiments were performed at constant temperature, pH and ionic strength in a jacketed titration cell. Metal ion concentrations and pH were monitored using the appropriate metal ISE and glass electrode respectively. Sodium humate solution, at the desired concentration and ionic strength ($NaNO_3$), was introduced into the titration cell and the pH adjusted to the desired value with HNO_3 or NaOH. This solution was titrated with incremental additions of metal ion solution, and the pH of the solution readjusted after each addition with NaOH. After each addition, the potential measured by the ion-selective electrode was allowed to reach a steady value, and the steady potential and the volume of NaOH solution required for pH adjustment were recorded. Approximately twenty additions of metal ion solution were made in a typical titration. The temperature of the cell contents was maintained at a constant level during the titration by circulating water from a thermostatically controlled bath at the desired temperature through the cell jacket. Carbon dioxide uptake by the titration solution was suppressed by continuously bubbling a stream of nitrogen through the constantly stirred solution.

Calibrations of the glass and ion-selective electrodes were performed prior to titration at the measurement temperature under nitrogen as described in Sections 3.3.1 and 3.3.2. After titration the ion selective electrode was recalibrated. For Cd^{2+} titrations, this calibration was performed *in situ*, as follows. HNO_3 was added to the titration solution after the final Cd addition to suppress complexation (pH ≈ 2.7). The measured ISE potential of this solution and the potential after further Cd additions formed the basis for the calibration; the response of the Cd ISE was always found to be Nernstian. This procedure was not successful for Cu^{2+} titrations; *in situ* calibrations were consistently non-Nernstian with greater than Nernstian slopes. This was attributed to (i) the pH being insufficiently low to dissociate the more stable Cu-humate complexes, and (ii) interferences caused by the observed precipitate formation at these levels of humate, Cu^{2+} and H^+ concentration.

Experiments were performed in duplicate for each set of experimental conditions.

3.4.3 Humic Acid Protonation Experiments (Aqueous Phase)

Fully H^+-exchanged humic acid was prepared as described in Section 3.2.3. From this, a solution of humic acid at the desired concentration and ionic strength ($NaNO_3$) was prepared and titrated (25 °C, under N_2) with standardised NaOH (Section 3.2.5) using a Metrohm piston burette. The pH/reference electrode was calibrated beforehand using NBS buffers and standard HNO_3 as described in Sections 3.2.6 and 3.3.1; approximately 50 pH - titre volume data were collected in the range bracketed by the buffers listed in Table 3.1.

3.5 Kinetic Measurements

3.5.1 Dissociation of Cu^{2+} from Dissolved Sodium Humates

The experimental technique used to observe dissociation of Cu-sodium humate complexes was an adaptation of that used by Shuman *et al.* (1983). Pre-equilibrated solutions of sodium humate and copper ions were allowed to react with solutions of the metallochromic reagent 4-(2-pyridylazo) resorcinol (PAR) (Figure 3.1), at constant pH and ionic strength, and the formation of the intensely coloured CuPAR complex followed spectrophotometrically (510 nm) as a function of time.

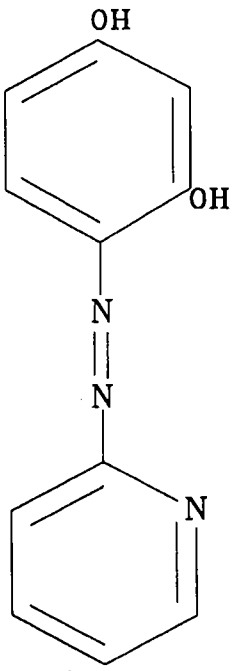

Figure 3.1 Structural formula of 4-(2-pyridylazo) resorcinol (PAR).

Copper/sodium humate and PAR solutions were prepared with the desired concentration of $NaNO_3$, and the pH of these solutions adjusted with HNO_3 or NaOH solution to the pH required for measurement. The copper/sodium humate solutions were allowed to equilibrate for at least 18 hours before reaction with PAR; reactions were also followed when the solutions had equilibrated for at least 48 hours. Reactions were initiated by injecting Cu/sodium humate and PAR solutions, using two identical

syringes, directly into the spectrophotometer flow cell; data collection began when the reagent flow was stopped.

3.5.2 Solid Phase Kinetics Experiments

The technique used to follow Cu dissociation from solid phase calcium humates was based on the method of Harter and Lehmann (1984) who measured Cu dissociation from whole soils. A suspension of calcium humate (0.05g) in 0.05 mol L^{-1} $Ca(NO_3)_2$ solution (600 mL) was prepared and spiked with Cu^{2+} to the desired level. This suspension was adjusted to the desired pH under N_2 using HNO_3 (0.01 mol L^{-1}) or $Ca(OH)_2$ (sat.), and equilibrated for a predetermined length of time at 20° C.

Desorption of Cu^{2+} from the suspended calcium humate was achieved by adding a 5 mL spike of 0.10 mol L^{-1} Na_2HNTA (NTA = nitrilotriacetate). Just prior to addition of the NTA spike the suspension was sampled to obtain $[Cu^{2+}]$ at t=0. After NTA addition, 5 mL samples were withdrawn through a fixed sampling tube with a syringe and the dissociation reaction quenched by phase separation using a 0.45 μm membrane filter. During the course of the experiment the temperature of the suspension was maintained at 20° C using a thermostatically controlled water bath; the suspension was stirred constantly and was purged by a continuous stream of N_2 to suppress CO_2 uptake.

Cu analysis in the collected samples was achieved using a Cu^{2+}-ion selective electrode/double junction reference electrode combination using the method of standard additions (Bauer *et al.*, 1978). For the calculation of [Cu] using the standard addition method, Nernstian electrode response was assumed; this was not unreasonable given that measured copper concentrations were generally greater than 1×10^{-6} mol L^{-1}. A separate electrode calibration under similar solution conditions indicated that Nernstian response could be achieved at this level of copper concentration. Samples were spiked with 0.3 mL 1.0 mol L^{-1} HNO_3 before analysis to dissociate any Cu-NTA or Cu-humate complexes; a correction was made for the dilution involved in this step.

3.6 Numerical and Computational Methods

3.6.1 Hardware/Operating Systems

Programs were run on either:

(i) a MicroVAX cluster operating under VAX/VMS, or;

(ii) a network of IBM compatible PCs sharing a common fileserver, and operating under Novell Netware 2.15 and MS-DOS 3.3.

3.6.2 Data Transformation

All datasets were submitted to statistical or nonlinear regression programs in ASCII format. Kinetic data was generated by the Philips spectrophotometer (Sections 3.3.5, 3.5.1) as percent-transmission in a binary format. Conversion to absorbance *versus* time data in ASCII format was achieved using a simple BASIC program (Appendix 4) running under MS-DOS; the resulting data pairs occurred in approximately equal log time intervals. Arithmetic transformations of data were achieved using general purpose statistical or spreadsheet software packages under either operating system.

3.6.3 Nonlinear Optimisation Program Development

3.6.3.1 Proprietary software

Data was fit to simple models using GENSTAT 5 (Genstat, 1987). More complicated models, for example those involving a larger number of adjustable parameters or those involving a numerical integration routine were unable to be fitted to data using proprietary software. Models with many ($\geq$ 5)

adjustable parameters were generally found not to converge using GENSTAT 5, and this program has no facility for iterative solution of equations or numerical integration, as was necessary for many of the modelling applications in this work.

3.6.3.2 Choice of minimisation algorithm

The problems referred to in Section 3.6.3.1 made necessary the development of a purpose-written nonlinear optimisation program. This program had the following requirements:

(i) the capability to fit data to a model, perhaps having 5 or more nonlinear adjustable parameters and/or requiring iterative solutions to modelling equations, by minimising a residual sum of squares;

(ii) the option of systematically weighting regressions;

(iii) relative insensitivity to starting estimates of the adjustable parameters;

(iv) it should include calculation of some reliable tests of significance and/or goodness of fit;

(v) it should be relatively easy to get running, due to constraints on development time.

The optimisation algorithm selected was the downhill simplex method in multidimensions, first developed by Nelder and Mead (1965) and described in detail by Press *et al.* (1986) and Bunday (1984). The downhill simplex algorithm is a direct search method which does not require knowledge of, or approximations to, function derivatives. Although less efficient (in terms of number of function evaluations required) than other algorithms (for example: Powell's, Fletcher-Marquadt) (Press *et al.*, 1986), this algorithm will always converge to an at least local minimum given sufficient iterations. Essentially, if n is the number of adjustable parameters, the algorithm creates a simplex or geometrical figure with n + 1 vertices in n-dimensional space, by stepping fractions of a unit vector in each dimension from the starting-guess vector. The simplex is then subjected to geometrical transformations in n-dimensional space; if the function value (residual sum of squares) is improved (decreased) at the transformed simplex point(s) then the transformed simplex becomes the base simplex and is subject to

further transformation. Geometrical transformations mostly involve the worst (highest) point of the simplex and the *centroid* or vector average of all points except the highest; the simplex may be: *reflected* away from the high point through the centroid; *reflected and expanded* away from the high point through the centroid; *contracted* in one dimension away from the high point toward the centroid, or *reduced* in all dimensions towards the low (best) point of the simplex. Convergence is achieved when all points of the simplex have the same function value within some fractional tolerance range, or when the variance of the function values at the simplex vertices falls below some predetermined value. The program written for this work (Appendix 5) used the fractional range convergence condition as suggested by Press *et al.* (1986); calculation of the variance of function values of simplex vertices, recommended by Nelder and Mead (1965) was found to be too coarse a convergence test for the applications in this work, terminating the algorithm before true convergence was attained.

3.6.3.3 Model formulation

The optimisation process may be carried out with respect to different variables. For example, the equations for metal binding models may be written so that either bound metal or free metal is the dependent variable. Often the modelling equation could be solved analytically, but in some cases a numerical solution was necessary, for example when expressing free metal concentration as a function of bound metal in a three discrete site binding model. The resulting (in this case, cubic) model function was solved by writing the equation in the form f(bound metal)=0 and finding roots numerically using a combined bisection/Newton-Raphson method (Turner *et al.*, 1986; Press *et al.*, 1986).

Iterative Solution of Polynomial Equations In order to evaluate the effect that changing the dependent variable to log[M] had on fitting binding data to modelling equations (see Chapter Four), those equations written *in terms of* [M] were rearranged to *solve* for [M]. In the case of discrete multiple binding site models, the rearranged equations were polynomials of order n, where n is the number of discrete sites. For example, a three discrete binding site model may be expressed in terms of [M] by:

$$C_{ML} = \Sigma_{i=1}^{3} (C_i K_i [M] / (1 + K_i [M])) \qquad (3.1)$$

When rearranged to solve for [M], the resultant cubic equation is:

$$[M] = a + b(C_{ML}) + c(C_{ML})^2 + d(C_{ML})^3 \qquad (3.2);$$

where $a = C_{ML}$;

$b = C_{ML}(K_1 + K_2 + K_3) - (C_1K_1 + C_2K_2 + C_3K_3)$;

$c = K_1K_2(C_{ML} - (C_1 + C_2)) + K_1K_3(C_{ML} - (C_1 + C_3)) + K_2K_3(C_{ML} - (C_2 + C_3))$;

and $d = K_1K_2K_3(C_{ML} - (C_1 + C_2 + C_3))$.

Since analytical solution of polynomials of higher order than two is not possible, equations such as Equation 3.2 were solved using a combined Newton-Raphson/bisection iterative algorithm adapted from Press *et al.* (1986). Convergence to the solution of the polynomial was initially by Newton-Raphson, defaulting to the less efficient bisection method if interim solutions moved outside of their logical bounds. Logical bounds for [M] in Equation 3.2 are zero and C_{ML}; any solutions outside these bounds are not physically meaningful. The relevant routines for incorporation into the nonlinear optimisation program appear in Appendix 7.

Numerical Integration When metal-humate binding was fitted to a model incorporating a log-normal distribution of binding constants, a numerical integration routine was required, since a normal distribution cannot be integrated analytically. The technique of Romberg integration (Press *et al.*, 1986) was chosen to achieve this. The Romberg method of numerical integration is an extension of the trapezium method; the integrand is divided into trapezoidal segments and the segment width is progressively halved, with the calculated value of the integrand saved after each halving. After a predetermined number of trapezoid-width halvings, a polynomial function is fit to the (trapezium width, integrand solution) data pairs and extrapolated to zero width. Romberg integration typically requires far fewer function evaluations than other methods (Press *et al.*, 1986). As such, it is well suited to this

application, where function evaluations (involving summations of large numbers of data) are time-consuming.

3.6.4 Program Structure

The program was designed, for conceptual simplicity, in three modules:

(i) a 'driver' routine which input experimental data and adjustable parameter estimates, initiated optimisation, and produced output;

(ii) the multidimensional simplex optimisation routine, and;

(iii) a routine which formulated the required modelling equation, and calculated the residual sum of squares to be minimised by module (ii).

The driver routine made calls to the modelling routine to generate the initial simplex on the n-dimensional residual sum of squares surface. This initial simplex was passed to the optimisation routine and transformed until minimisation to the required convergence tolerance was achieved. Transformations of the simplex required evaluation of the residual sum of squares at every new vertex; this was accomplished by calls to the modeling subroutine. After convergence the final simplex, containing the refined parameter estimates, was passed back to the driver routine which output the desired information.

Representative examples of source code (Vax-11 FORTRAN) for driver, and modelling routines for models with analytical solutions, are listed in Appendices 5 and 7 respectively. The optimisation routine was common to all applications and is listed in Appendix 6. Modified modelling routines are also listed for models requiring iterative polynomial solution (Appendix 8) and numerical integration (Appendix 9).

3.6.5 Statistical Considerations

3.6.5.1 Optimisation criteria

The FORTRAN program written read data to be fitted and initial estimates of parameters from external files and used an adaptation of the downhill multidimensional simplex algorithm given by Press *et al.* (1986) to minimise a residual sum of squares which could be weighted by slightly modifying one of the subroutines. The residual or error sum of squares (SS_E) is given by:

$$SS_E = \Sigma_{i=1}^{\theta}((Y_{obs_i} - Y_{calc_i}).w)^2 \qquad (3.3)$$

where Y_{obs_i} are the observed (experimental) values of the dependent variable;

Y_{calc_i} are the calculated values of the dependent variable, being a function of the independent variable and the adjustable modelling parameters;

θ is the number of data;

w is the weighting factor applied (w=1 for unweighted data).

The simplex is thus transformed in as many dimensions as there are adjustable parameters until SS_E converges to a minimum.

Data Weighting Ideally (Brook and Arnold, 1985) data should be weighted by dividing by the variance of the dependent variable in the error sum of squares calculation. By this means the most reliable data have most influence on the regression. For many experimental systems, however, an accurate estimate of the variance is not available; furthermore, for model fitting there are often considerations other than reliability of data. If the dependent variable shows a wide range, then an unweighted regression will emphasise the contribution of data of greater magnitude; residuals will be relatively larger for smaller values of the dependent variable, indicating a poorer fit. This problem may be overcome by use of various weighting schemes. Perdue and Lytle (1983) advocate fitting of metal binding data to models

by minimising relative residuals, that is, the weighting factor w in Equation 3.3 is equal to $1/Y_{calc_i}$. Turner *et al.* (1986) used nonlinear regression to fit data to models using log-transformed data. Not only does this method remove large differences in magnitude of the dependent variable, it also relates the fitted data back to the original potentiometric measurements, which are (not unrealistically) assumed to have equal variance.

3.6.5.2 Estimates of goodness-of-fit

The program was also written to calculate R^2 and perform a simple analysis of variance as measures of goodness and significance of fit. R^2 measures the percentage of variance in the experimental data explained by the model being fitted, and is calculated by:

$$R^2 = 100(1 - SS_E/SS_R) \tag{3.4}$$

where SS_R is the sum of squares for the regression model such that:

$$SS_R = SS_T - SS_E \tag{3.5}$$

$$SS_T = \Sigma_{i=1}^{\theta} (Y_{obs_i} - \bar{Y})^2 \tag{3.6}$$

where SS_T is the total sum of squares.

The analysis of variance involves calculation of the mean square terms by dividing sum of square terms by their corresponding degree of freedom, where:

degrees of freedom (regression), $DF_R = n-1$;

degrees of freedom (residual), $DF_E = \theta - n$;

degrees of freedom (total), $DF_T = \theta\text{-}1$ $(= DF_M + DF_R)$

The error mean square may be used as an unbiased estimate of the variance of experimental values from values calculated by the model (Brook and Arnold, 1985). This is because the degrees of freedom divisor incorporates corrections for both number of parameters and number of data. More commonly used for this purpose, however, is the variance or F-ratio, where:

$$F = MS_E / MS_R \tag{3.7}$$

and $MS_E = SS_E/DF_E$,

$MS_M = SS_R/DF_R$,

which allows tests for significance of fit to be made, along with tests as to whether addition of further adjustable parameters into the model significantly improve fit to the experimental data (Brook and Arnold, 1985).

3.6.5.3 Analysis of residuals

For the ideal situation, where the model chosen is the 'correct' one for the experimental data, residuals should reflect random experimental errors (Brook and Arnold, 1985). If the observed residuals show systematic (for example, cyclic) patterns, then it is likely that there is some trend to the data that is not explained either by random errors or the modelling parameters. Correlations amongst residuals may be described by an autocorrelation function (Brook and Arnold, 1985). Tests to determine whether residual autocorrelations are significant may be carried out using the autocorrelation coefficient.

The singly lagged residual autocorrelation, r_1, is given by (Bhattacharyya and Johnson, 1977):

$$r_1 = \frac{\Sigma_{i=2}^{\theta}\left(\left(E_{i-1} - \bar{E}\right)\left(E_i - \bar{E}\right)\right)}{\Sigma_{i=1}^{\theta}\left(E_i - \bar{E}\right)^2} \qquad (3.8)$$

where E_i is the i^{th} residual ($E_i = Y_{obs_i} - Y_{calc_i}$), and;

$\bar{E}$ is the mean residual ($\bar{E} = \Sigma_i(E_i/\theta)$).

The significance of the singly lagged residual autocorrelation may be tested, using the approximation that $r_1\sqrt{\theta}$ is approximately normally distributed (μ=0, σ=1), against the null hypothesis that the population analogue of r_1 is zero (Bhattacharyya and Johnson, 1977). The value of r_1 thus approximates a Z-score which may be compared with tables of the standard normal distribution.

3.6.6 Comparison of models

For purely predictive purposes (within the range of data observed in experiments) the most simple measure of goodness of fit is the proportion of experimental variance explained by the model, give by R^2 (Brook and Arnold, 1985). A model which consistently gives a higher R^2 when applied to data will be most suitable for predictive purposes.

Goodness of fit will generally be improved, to some extent, by inclusion of further adjustable parameters in a model. R^2 values provide no information regarding the appropriateness of the model, or whether inclusion of additional parameters is justified. Comparison of error (residual) mean square values or F ratios from analysis of variance (Section 3.6.5.2) provide unbiased estimates of the degree to which a model explains experimental variance (Brook and Arnold, 1985). For related families of models, for example discrete multiligand binding models (Section 2.4.3), a more rigorous test is based on the use of a null hypothesis that some parameter(s) (in the more complex model) equal zero (Ratkowsky, 1983). Consider two models, M_1 and M_2, where M_2 is derived from M_1 by addition of additional adjustable parameters (such as an extra ($[C_i]$,K_i) pair in a discrete multiligand binding model). If experimental data

is fitted to both models, and error sum of squares (SS_E) and error mean square (MS_E) can be calculated in both instances. An F-statistic to test the null hypothesis is given by:

$$F_{calc} = \frac{\left[SS_E(M_1) - SS_E(M_2)\right] / \left[DF_T(M_1) - DF_T(M_2)\right]}{MS_E(M_2)} \qquad (3.9)$$

which has a F-distribution with ($DF_T(M_1)$ - $DF_T(M_2)$) and $DF_T(M_2)$ degrees of freedom, and may be compared with tabulated F-distribution values. That is, the extra parameters are justified (significantly different from zero) with the desired level of confidence if $F_{calc} \geq F_{table}$.

CHAPTER FOUR

COMPUTER PROGRAM DEVELOPMENT AND TESTING

4.1 INTRODUCTION

The nonlinear least-squares regression program described in Chapter 3 was tested for correct functioning and its ability to handle realistic data using a thorough testing regime based on the use of simulated data. The testing strategy allowed semiquantitative evaluation of the effects of:

(i) varying levels of random experimental error;

(ii) restricted data ranges;

(iii) spacing of experimental data;

(iv) choice of dependent variable and/or weighting in regressions, and;

(v) initial estimates of adjustable parameters.

4.2 METHODS

4.2.1 Testing for Correct Program Functioning

The regression program was tested for correct formulation of modelling equations and performance of the optimisation routine. This was achieved by generating ideal (error-free) simulated data according to the particular model being used, and generating parameter estimates for the same model by least-squares optimisation using the regression program. Where possible, ideal simulated data was generated

independently using spreadsheet software. In addition, for binding or kinetics models involving a continuous distribution of sites (Chapter 2, Section 2.4.5; Chapter 7, Section 7.3.1.2) approximations to ideal simulated data were generated using a large number (≥ 20) of discrete sites, such that the combination of discrete sites mimicked the continuous distribution (Figure 4.1).

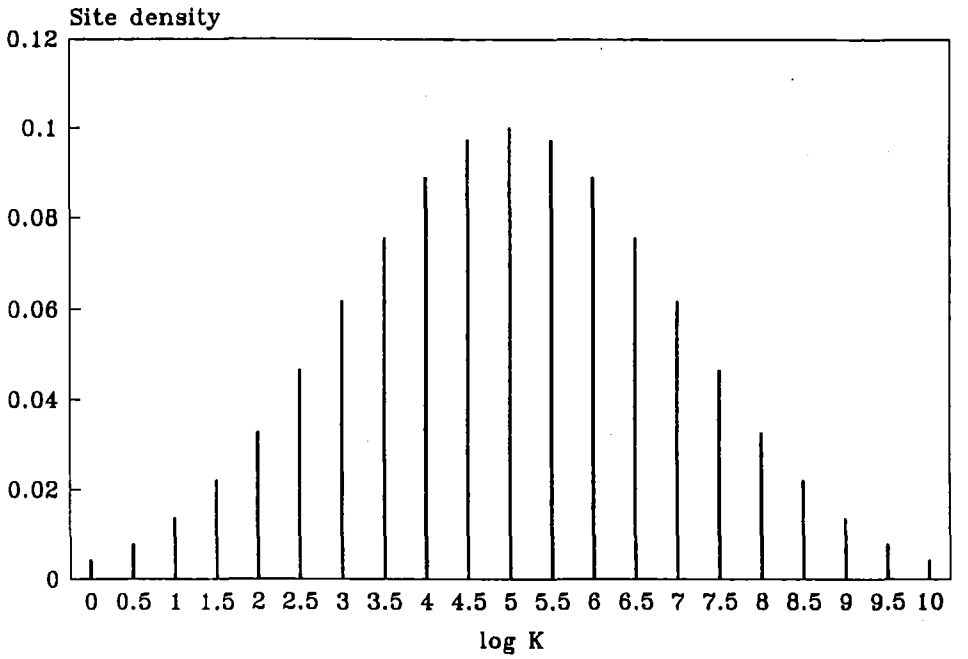

Figure 4.1 Set of discrete sites used to mimic sites with a lognormal distribution of metal-complex formation constants.

4.2.2 Non-Ideal Simulated Data

The strategy for testing the effects of non-ideal data on least-squares parameter optimisation was as follows. A discrete site-binding model with three sites was selected to both generate and model simulated data. This model has six adjustable parameters (C_1, K_1, C_2, K_2, C_3, K_3) and as such is considered to have sufficient degrees of freedom to be sensitive to data which is non-ideal with respect to different criteria. The modelling equation is given by:

$$C_{ML} = \Sigma_{i=1}^{3} \left(C_i K_i [M] / (1 + K_i [M]) \right) \qquad (4.1)$$

and the values of adjustable parameters used to generate simulated data are given in Table 4.1.

Table 4.1 Values of adjustable parameters used to generate simulated binding data.

Binding site	Parameter	Value	log (value)
Ligand 1	C_1	0.03	-1.529
	K_1	1.0×10^{10}	10.00
Ligand 2	C_2	0.15	-0.8239
	K_2	1.0×10^{8}	8.000
Ligand 3	C_3	0.50	-0.3010
	K_3	2.0×10^{6}	6.301

An array of j [M] values (in the range $-10.6 \leq \log [M] \leq -5.6$), equally spaced with respect to $\log [M]_j$, were used to generate a corresponding C_{ML} array. Using this ideal set of simulated data as a starting point, several non-ideal 'treatments' were generated, each with five replicates.

4.2.2.1 Simulated experimental error

In any real experimental situation, data will contain random, and possibly systematic, experimental errors. While the effects of systematic error on data modelling are reasonably straightforward to predict, the effects of random error are less obvious.

An array **e** of j simulated random deviations was generated using:

$$\mathbf{e}_j = 10^{(\delta_j \rho \log [M]_j)} \qquad (4.2)$$

where e_j is the j^{th} deviation

δ_j is the j^{th} normally distributed ($\mu = 0$, $\sigma = 1$) random number

and ρ is the level of error (for example, $\rho = 0.01$ for 1% error).

A set of simulated binding data with the desired level of experimental error was comprised of a two-dimensional ([M] + e, C_{ML}) array; C_{ML_j} values remained error-free. Five 'replicates' were prepared in two 'treatments', one with 1% error ($\rho = 0.01$) and one with 5% error ($\rho = 0.05$). A different δ (random number) array was used for each replicate.

4.2.2.2 Restriction of data ranges

For real metal ion-humate binding or kinetic data, it is often the case that experimental measurements cannot be made in ranges where certain components of the mixture make an important contribution to the reaction. For example, detection limits in metal ion determination fix an upper observable limit for the effective stability constant of binding sites. Similarly, for kinetic data, sites having large rate constants require measurements to be made of the order of microseconds after initiation, timescales which are inaccessible to many monitoring techniques.

Truncated sets of simulated binding data were prepared such that the range -log [M] values did not include either or both of the log K_i extremes (log K_1 and log K_3). This resulted in three 'treatments' (all having 1% simulated error). The first having $-9.0 \leq \log [M] \leq -5.6$; the second $-10.6 \leq \log [M] \leq 7.4$; and the third $-9.0 \leq \log [M] \leq -7.4$. Five 'replicates' of each treatment were prepared, in addition to error-free examples, at each level of truncation.

4.2.3 Spacing of Data

It was considered that data obtained using increasing, rather than fixed, titration increments would produce more reliable estimates of adjustable parameters. The reasoning behind this assumption was that data obtained by increasing titration increments (in this work) contained a higher proportion of data

in the region of metal-humate titrations where the greatest changes in metal ion speciation were occurring.

The effect of the increments between adjacent data was investigated by comparing the effects. on predicted parameters in the three site binding model, of:

(i) data which was equally spaced with respect to log [M], and;

(ii) data which was equally spaced with respect to [M].

Both error-free, and data with 1% normally distributed random error, was generated in the range $-10.6 \leq \log [M] \leq -5.6$ for both data spacing treatments.

4.2.4 Effects of Dependent Variable and Weighting in Regressions

The optimised value for the residual sum of squares (SS_E) (and therefore any parameter estimates) is obviously dependent on which experimental measurement the regression model is formulated to calculate. In addition, a systematically weighted residual sum of squares may be calculated. In testing the regression program, three combinations of dependent variable and/or systematic weighting were considered. Firstly, a formulation of the regression models to minimise SS_E (Equation 3.1; w=1) with respect to C_{ML} by calculating bound metal (C_{ML}) from experimental [M] values. Second, minimisation of SS_E (Equation 3.1; w=1) with respect to log [M], or formulation of regression models to calculate log [M] values from experimental C_{ML} values (Turner *et al.*, 1986). Thirdly, a combination of formulating models to calculate C_{ML} and systematically weighting regressions by minimising a sum of squares of relative residuals (Equation 3.1, $w=(1/Y_{calc})$; Perdue and Lytle, 1983). All three regression procedures were tested with ideal simulated data and the combinations of data with simulated random error and/or restricted data ranges described in Sections 4.2.2.1 and 4.2.2.2.

4.2.5 Effect of Initial Parameter Estimates

The effect of inaccuracy in initial estimates for adjustable parameters was evaluated by setting initial values for all three C_i values at 0.15 and for all three log K_i values at 8.0. This was done both for ideal simulated data, and untruncated data with 1% simulated random error.

4.3 RESULTS AND DISCUSSION

4.3.1 Tests for Correct Program Functioning

The combination of various modelling subroutines and residual sum of squares minimisation using the multidimensional simplex algorithm (Press *et al.*, 1986; Chapter 3) was found to function correctly using ideal simulated data. That is, if any one model was used to generate simulated data, then fitting that data to the same model using the regression program always produced parameter estimates that were within 0.1% of the original values used. This was true regardless of the combination of dependent variable and/or systematic weighting used in the model formulation and regression procedures. In fact, if a particular implementation of the fitting program did not perform in this manner, the program code was revised until this criterion was fulfilled. Where the models involved a continuous (log)normal distribution of sites, fitting approximations to ideal simulated data (derived from discrete approximations to the continuous distribution) also resulted in optimised parameters that were effectively identical to those used to generate data.

In terms of program efficiency, all combinations of dependent variable in model formulation and systematic regression weighting required similar numbers of simplex iterations (depending on the number of adjustable parameters in the particular modelling equation; see Nelder and Mead, 1965) to converge to a least-squares solution. Regression with log [M] as the dependent variable, however, required significantly greater amounts of processing time due to the iterative nature of the Newton-

Raphson/Bisection routine used to solve rearranged modelling equations (Chapter 3, Section 3.6.3.3). In addition, for this particular application, the Newton-Raphson routine appeared to be prone to numerical instability in the form of floating-point (real number) overflow, due to very high values for the function and derivative near the solution to the function. This problem was overcome by compiling source programs so that an extended floating-point format was specified; on some computer systems this may further retard program execution.

4.3.2 Effect of Initial Parameter Estimates on Regression Procedures

One of the features of multidimensional simplex optimisation algorithms is their ability to converge to a function minimum or maximum from virtually any vector of initial parameter estimates. In addition the generation of the initial n-dimensional simplex from the input parameters means that this algorithm effectively starts with n + 1 sets of parameter estimates, where n is the number of adjustable parameters in the model being fitted. This capability was confirmed for the Nelder-Mead algorithm used in this work; for error free simulated data, and using inaccurate parameter estimates (as in Section 4.2.4), correct solutions were always found, using any of the three combinations of model formulation and systematic weighting. Optimisation was slow, however, and efficient use of the program required that an independent estimate of adjustable parameters (for example, from a Scatchard plot or from previous fitting of similar data) be made.

For data with 1% simulated random error, acceptable values for optimised adjustable parameters were also returned in most cases, from inaccurate parameter estimates. This was ensured by restarting the algorithm from the first convergence point, as suggested by Press *et al.*, 1986, a procedure which was also used with real data (Chapters 5, 6 and 7).

4.3.3 Effect of Simulated Random Error

Results from fitting simulated binding data with either 1% or 5% simulated random error are presented for the three combinations of model formulation and systematic weighting in Tables 4.2 to 4.4. It is evident from these results that the mean parameter values (five replicates) for the 1% error treatment are not significantly different (based on the finding that 95% confidence intervals for the means include the true parameter values) from the true parameter values, regardless of the combination of dependent variable and systematic weighting used in the regression. Unweighted regression with C_{ML} as the dependent variable produced more variable mean parameter estimates (relative standard deviation (rsd) 4-15%) than the other two regression strategies (regression with respect to log [M]; relative residual sum of squares minimisation with respect to C_{ML}) which had rsd for mean parameter estimates in the range 1-8%.

Table 4.2 Effects of random error in simulated binding data on means (5 replicates) of estimates of modelling parameters; fitting by minimising SS_E in C_{ML}. ([a]Significance level (Student's t) for difference of treatment mean and true parameter value.)

1. Data range -10.6 ≤ log [M] ≤ -5.6; 1% simulated random error.

Parameter	Mean	Standard deviation	Significance level[a]
log C_1	-1.480	0.217	ns
log K_1	9.903	0.472	ns
log C_2	-0.814	0.070	ns
log K_2	7.917	0.359	ns
log C_3	-0.307	0.030	ns
log K_3	6.271	0.112	ns

2. Data range -10.6 ≤ log [M] ≤ -5.6; 5% simulated random error.

Parameter	Mean	Standard deviation	Significance level[a]
log C_1	-1.454	0.245	ns
log K_1	10.403	0.685	ns
log C_2	-0.621	0.135	95%
log K_2	7.558	0.319	95%
log C_3	0.853	2.82	ns
log K_3	4.70	2.98	ns

Table 4.3 Effects of random error in simulated binding data on means (5 replicates) of estimates of modelling parameters; fitting by minimising relative SS_E in C_{ML}. ([a]Significance level (Student's t) for difference of treatment mean and true parameter value.)

1. Data range $-10.6 \leq \log [M] \leq -5.6$; 1% simulated random error.

Parameter	Mean	Standard deviation	Significance level[a]
$\log C_1$	-1.539	0.074	ns
$\log K_1$	10.033	0.174	ns
$\log C_2$	-0.834	0.064	ns
$\log K_2$	8.044	0.173	ns
$\log C_3$	-0.297	0.018	ns
$\log K_3$	6.304	0.099	ns

2. Data range $-10.6 \leq \log [M] \leq -5.6$; 5% simulated random error.

Parameter	Mean	Standard deviation	Significance level[a]
$\log C_1$	-1.554	0.204	ns
$\log K_1$	10.946	0.637	95%
$\log C_2$	-0.723	0.272	ns
$\log K_2$	8.013	0.769	ns
$\log C_3$	-0.391	0.099	ns
$\log K_3$	6.278	0.489	ns

Table 4.4 Effects of random error in simulated binding data on means (5 replicates) of estimates of modelling parameters; fitting by minimising SS_E in log [M]. ([a]Significance level (Student's t) for difference of treatment mean and true parameter value.)

1. Data range -10.6 ≤ log [M] ≤ -5.6; 1% simulated random error.

Parameter	Mean	Standard deviation	Significance level[a]
$\log C_1$	-1.554	0.059	ns
$\log K_1$	10.019	0.112	ns
$\log C_2$	-0.834	0.065	ns
$\log K_2$	8.074	0.170	ns
$\log C_3$	-0.303	0.020	ns
$\log K_3$	6.346	0.087	ns

2. Data range -10.6 ≤ log [M] ≤ -5.6; 5% simulated random error.

Parameter	Mean	Standard deviation	Significance level[a]
$\log C_1$	-6.08	2.68	95%
$\log K_1$	11.08	3.56	ns
$\log C_2$	-3.69	3.2	ns
$\log K_2$	11.05	3.66	ns
$\log C_3$	0.98	1.90	ns
$\log K_3$	6.68	1.62	ns

For simulated data containing 5% random error, none of the three regression strategies produced acceptable sets of mean parameter estimates from five 'replicates'. The lack of significant difference from actual parameters implied, for most cases, in Table 4.2 - 4.4 is due to the large degree of variability between replicates rather than the ability of the regression strategies to provide accurate parameter estimates from poor data.

In most cases, however, real data (Chapters 5, 6 and 7) appeared to contain far less *random* error in log [M] than simulated data with wither 5% or even 1% associated random error. The possibility of significant *systematic* errors cannot, however, be discounted. It may be inferred from this observation that fits of real data to any hypothetical 'ideal model' should not be biased as a result of either the observed (low) levels of random error, or the regression strategy used.

4.3.4 Effects of Restricting the Range of Data

For error-free simulated data with a restricted log [M] range, fits to the three site model using any regression strategy most often produced acceptable (within 0.05%) parameter estimates. The single exception was for the most severely restricted simulate data ($-9.0 \leq \log [M] \leq -7.4$) when fitted by minimising the SS_E in C_{ML}. In this case, refined parameter estimates differed from the actual parameters by 0.2 - 14%, the greatest differences being in estimates of C_3 and $\log K_3$.

Means of five replicates for the three data range restriction treatments, all with 1% random error with respect to log [M], are shown in Tables 4.5 to 4.7 for all regression strategies. In all cases, estimates of adjustable parameters from data with a restricted range were more variable and further from the actual values than from data with the same level of random error but with a more inclusive range in log [M].

Table 4.5 Effects of restricting ranges of simulated binding data on means (5 replicates) of estimates of modelling parameters; fitting by minimising SS_E in C_{ML}. ([a]Significance level (Student's t) for difference of treatment mean and true parameter value.)

1. Data range -9.0 ≤ log [M] ≤ -5.6; 1% simulated random error.

Parameter	Mean	Standard deviation	Significance level[a]
$\log C_1$	-1.623	0.267	ns
$\log K_1$	12.830	4.335	ns
$\log C_2$	-0.841	0.057	ns
$\log K_2$	8.069	0.149	ns
$\log C_3$	-0.283	0.013	95%
$\log K_3$	6.292	0.085	ns

2. Data range -10.6 ≤ log [M] ≤ -7.4; 1% simulated random error.

Parameter	Mean	Standard deviation	Significance level[a]
$\log C_1$	-1.581	0.158	ns
$\log K_1$	10.112	0.310	ns
$\log C_2$	-0.859	0.153	ns
$\log K_2$	8.106	0.371	ns
$\log C_3$	2.625	4.411	ns
$\log K_3$	2.135	1.772	ns

3. Data range -9.0 ≤ log [M] ≤ -7.4; 1% simulated random error.

Parameter	Mean	Standard deviation	Significance level[a]
$\log C_1$	-1.481	0.170	ns
$\log K_1$	29.6	32.3	ns
$\log C_2$	-0.701	0.035	99%
$\log K_2$	7.850	0.146	ns
$\log C_3$	-0.928	2.547	ns
$\log K_3$	2.059	0.241	99%

Table 4.6 Effects of restricting ranges of simulated binding data on means (5 replicates) of estimates of modelling parameters; fitting by minimising relative SS_E in C_{ML}. ([a]Significance level (Student's t) for difference of treatment mean and true parameter value.)

1. Data range -9.0 ≤ log [M] ≤ -5.6; 1% simulated random error.

Parameter	Mean	Standard deviation	Significance level[a]
log C_1	-1.558	0.137	ns
log K_1	13.785	3.764	ns
log C_2	-0.828	0.08	ns
log K_2	8.033	0.076	ns
log C_3	-0.280	0.015	95%
log K_3	6.259	0.145	ns

2. Data range -10.6 ≤ log [M] ≤ -7.4; 1% simulated random error.

Parameter	Mean	Standard deviation	Significance level[a]
log C_1	-1.623	0.295	ns
log K_1	10..201	0.580	ns
log C_2	-0.895	0.327	ns
log K_2	8.194	0.717	ns
log C_3	6.5	14.7	ns
log K_3	-1.6	14.1	ns

3. Data range -9.0 ≤ log [M] ≤ -7.4; 1% simulated random error.

Parameter	Mean	Standard deviation	Significance level[a]
log C_1	-1.405	0.214	ns
log K_1	32.4	26.0	ns
log C_2	-0.877	0.434	ns
log K_2	7.753	0.189	95%
log C_3	-0.82	1.09	ns
log K_3	2.63	2.88	95%

Table 4.7 Effects of restricting ranges of simulated binding data on means (5 replicates) of estimates of modelling parameters; fitting by minimising SS_E in log [M]. ([a]Significance level (Student's t) for difference of treatment mean and true parameter value.)

1. Data range -9.0 ≤ log [M] ≤ -5.6; 1% simulated random error.

Parameter	Mean	Standard deviation	Significance level[a]
$\log C_1$	-1.562	0.265	ns
$\log K_1$	14.06	4.48	ns
$\log C_2$	-0.829	0.073	ns
$\log K_2$	8.013	0.169	ns
$\log C_3$	-0.290	0.018	ns
$\log K_3$	6.308	0.125	ns

2. Data range -10.6 ≤ log [M] ≤ -7.4; 1% simulated random error.

Parameter	Mean	Standard deviation	Significance level[a]
$\log C_1$	-1.642	0.335	ns
$\log K_1$	10.234	0.706	ns
$\log C_2$	-2.75	2.92	ns
$\log K_2$	9.01	1.02	ns
$\log C_3$	-0.981	0.374	ns
$\log K_3$	6.134	3.505	ns

3. Data range -9.0 ≤ log [M] ≤ -7.4; 1% simulated random error.

Parameter	Mean	Standard deviation	Significance level[a]
$\log C_1$	-1.634	0.329	ns
$\log K_1$	13.4	7.9	ns
$\log C_2$	-0.959	0.427	ns
$\log K_2$	8.276	0.511	ns
$\log C_3$	-0.962	0.924	ns
$\log K_3$	6.14	3.36	ns

For simulated data which excluded only low values of log [M], all regression strategies predicted log K_i and C_i values for the two weaker sites which were not significantly different from the actual values. Estimates of C_3 were low using all regression strategies; the difference was significant where regressions minimised either absolute or relative residual sums of squares in C_{ML}. The parameters for the strongest site (C_1, log K_1) were not estimated accurately; C_1 was underestimated by all regression strategies and log K_1 was overestimated, with rsd values in the range 8 - 34%. This poor resolution for this site was expected given the level of random error and the absence of data in the region where this 'site' makes an important contribution to the simulated binding reactions. A similar situation was found for simulated data where the range excluded values at high [M]. The weakest site (defined by C_3, log K_3) was expected to be most sensitive to their restriction in data, and this was observed to be the case. For all regression strategies, mean values for (log) C_3 and log K_3 had rsd $\geq$ 57% and, with the exception of regressions which minimised a residual sum of squares in log [M] mean parameter estimates for C_3 and log K_3 differed substantially from actual values. A significant difference in the parameters for sites 1 and 2 was found only for the estimate of log K_2 obtained by SS_E minimisation in log [M].

Finally, for simulated data which excluded values at high and low [M] ($-9.0 \leq \log [M] \leq -7.4$), none of the regression strategies resolved any of the sites satisfactorily. Only for log K_2 did all regression strategies produce mean binding constant estimates within an order of magnitude of true values; however, minimisation of SS_E in log [M] did produce a reasonably close estimate of log K_3. Estimates of site densities (log C_i) were closer to true values, but invariably showed high associated variability (rsd 5 - 300%).

4.3.5 Effect of Data Spacing

For error-free data which was equally spaced with respect to log [M], parameter estimates, using all methods for SS_E calculation, were almost identical to actual parameters (Section 4.3.1; Table 4.1). For ideal simulated data which was equally spaced in terms of [M], minimisation of SS_E in log [M] or

relative SS_E in C_{ML} also produced precise parameter estimates. Minimisation of SS_E in C_{ML} (unweighted), however, underestimated C_1 and overestimated log K_1.

With simulated binding data containing 1% random error and equal [M] increments, mean estimates of adjustable parameters (Table 4.8) were never significantly different from actual values (Section 4.3.3; Table 4.2). For simulated data with 1% error and equal [M] increments, all methods for SS_E minimisation gave significantly low estimates for (log) C_1, compared with the true value. In addition, parameter estimates showed more variability between replicates than for data with equal log [M] increments. In general, fitting data with equal [M] increments resulted in underestimation of both concentration and affinity for the strongest site. Minimisation of SS_E with respect to log [M] produced the most accurate and precise parameter estimates.

Table 4.8 Effects of equal [M] increments in simulated binding data on means of estimates of modelling parameters (5 replicates). ([a]Significance level (Student's t) for difference of treatment mean and true parameter value.)

1. Minimising residual sum of squares in C_{ML}.

Parameter	Mean	Standard deviation	Significance level[a]
log C_1	-1.841	0.236	95%
log K_1	9.285	1.795	ns
log C_2	-0.829	0.100	ns
log K_2	8.594	0.933	ns
log C_3	-0.294	0.021	ns
log K_3	6.343	0.055	ns

2. Minimising relative residual sum of squares in C_{ML}.

Parameter	Mean	Standard deviation	Significance level[a]
log C_1	-1.862	0.266	95%
log K_1	9.968	0.588	ns
log C_2	-0.725	0.185	ns
log K_2	8.363	1.129	ns
log C_3	-0.337	0.072	ns
log K_3	6.264	0.122	ns

3. Minimising residual sum of squares in log [M].

Parameter	Mean	Standard deviation	Significance level[a]
log C_1	-1.685	0.164	95%
log K_1	9.937	0.331	ns
log C_2	-0.845	0.074	ns
log K_2	8.268	0.834	ns
log C_3	-0.296	0.023	ns
log K_3	6.379	0.044	95%

4.4 SUMMARY

The program-testing regime described in this Chapter indicates that none of the three methods used to calculate the residual sum of squares in regressions has any distinct advantage in terms of ability to estimate parameters in binding equations from simulated data. The decision as to which calculation method is most suitable must, therefore, be based on other criteria. Although calculation of SS_E in log [M] is more acceptable in that the dependent variable for regression is also the actual experimental variable, formulation of models to achieve this requires iterative solution of the fundamental equations, which is inefficient in terms of processing time.

Calculation of SS_E with respect to C_{ML} allows analytical solution of binding equations, and as such produces a more efficient fitting program. Systematic weighting by calculating a relative SS_E was not found, in this work, to provide significantly more accurate parameter estimates under any conditions. This is considered to be a function of the spacing of the simulated data, which resembles that resulting from conventional titration procedures, that is, increasing increments in [M] as a titration progresses. Over-emphasis of data at higher levels of metal ion addition, inferred by Perdue and Lytle (1983) is likely to be a problem only for metal ion-humate binding data which is approximately equally spaced with respect to [M].

The critical effect of the experimental observation window on modelling the behaviour of complex mixtures is illustrated by the effects of excluding values in certain ranges for simulated multiligand binding data. Observations of this type emphasise the operational character of model parameters for a complex mixture such as humic substances, and suggest that extrapolations outside the range of data used in experiments should be made with much caution.

The effects of random error on model parameters derived from fitting simulated binding data suggest that commonly observed levels of random error are unlikely to adversely affect values found for

adjustable parameters when modelling reactions of humic substances, providing that the amount of replication is sufficient.

CHAPTER FIVE

PROTONATION BEHAVIOUR OF WAIMARI PEAT AND WHOLE AND SIZE - FRACTIONATED SUMMIT HILL HUMIC ACIDS

5.1 Introduction

As discussed in Chapter Two, the predominant reactive functional groups on humic substance macromolecules are weakly acidic in nature. The protonation reactions of humic substances, therefore, affect any property or subsequent reaction of humic substances which involves these functional groups, such as: dissolution, molecular conformation, and metal binding reactions.

A description of the protonation reactions of humic substances which provides an accurate representation of the actual chemical and physical processes occurring is not available. Much useful information, however, can be obtained from experiments designed to observe the proton binding (or dissociation) behaviour of humic substances.

Perhaps the most fundamental measurable property of humic substances with respect to their acidic groups is the total titratable acidity under aqueous conditions. The measured quantity offers information on the density of ionisable functional groups and can also serve as an operational estimate of maximum metal ion binding capacity in the absence of more reliable data. Measurement of total acidity also defines the cation exchange capacity. Total acidity may be subdivided on the basis of 'classes' of exchange sites, for example, those dissociating below a predetermined pH value, or 'carboxyl acidity'.

Determination of carboxyl acidity involves either: detection of intermediate inflections in experimental titration curves; or reaction with a functional - group specific reagent such as calcium acetate.

A further step towards quantification of humic substance protonation behaviour is to attempt to calculate proton binding parameters, that is, to define the strength(s) and/or abundance(s) of the acidic group(s). This necessitates the adoption of a model for proton binding behaviour; various models describing humic substance protonation are outlined in Chapter Two (Section 2.4).

The protonation behaviour of macromolecules such as humic substances is also dependent, to some extent, on the conformation assumed by the macromolecules. Experiments observing the effect of ionic strength on humic substance protonation can yield conformational information regarding permeability to simple electrolytes and molecular flexibility (Marinsky & Ephraim, 1986).

5.2 Experimental

5.2.1 Acidimetric Measurements

Measurements of the amounts of titratable protons in Summit Hill humic acid (SHHA) and Waimari Peat humic acid (WPHA) were made using several methods.

5.2.1.1 $Ba(OH)_2$ Displacement Method

The first method used was the '$Ba(OH)_2$' method described by Schnitzer and Khan (1972) and Perdue (1985). This method measures all acidic groups neutralised by c. 0.1 mol L^{-1} $Ba(OH)_2$ solution and as such should measure all acidic groups able to dissociate in an aqueous system at pH $\leq$ 13. Accurately weighed samples of humic acid (c. 0.1g) were suspended in 20 mL of 0.05 mol L^{-1} $Ba(OH)_{2\,(aq)}$. The resulting suspension was allowed to equilibrate under N_2 and was then filtered (0.45 μm membrane) and

the residual $Ba(OH)_2$ titrated to pH 8.4 with standardised HCl. Blank titrations were performed on 20 mL $Ba(OH)_2$ (0.05 mol L^{-1}) aliquots which had been allowed to equilibrate for a similar period. Experiments were performed in duplicate.

5.2.1.2 NaOH Dissolution/HCl Titration

A measure of the amount of titratable acidity present on the humic acids at selected fixed pH values was available by the following method. An accurately weighed sample of humic acid was dissolved in sufficient CO_2 - free NaOH solution to dissociate all acidic functional groups. The resulting sodium humate solution was then titrated, under N_2, with standard HCl. Comparison with a titration of NaOH containing no dissolved humic acid yielded (by difference) amounts of humic substance acidic groups dissociated at fixed pH values.

5.2.1.3 Direct Titration of Humic Acids

The reaction of solid humic acid with alkali was found to be too slow to conveniently implement a direct titration procedure that measured titratable acidity. Solutions of fully H^+ - exchanged humic acid were prepared using an ion exchange resin column as described in Section 3.2.3. These solutions were titrated with standard NaOH at constant temperature, under $N_{2(g)}$. These experiments yielded the titratable acidity, at selected fixed pH values, over the pH range 4 - 9, and gave an estimate of total carboxyl acidity from the first inflection observable in the titration curve. Duplicate titrations, consisting of 30 - 60 pH *versus* volume of titre data pairs, were performed for both SHHA and WPHA.

The humic acid solutions titrated in this way were prepared from known weights of sodium humate (Section 3.2.3). So that calculated quantities could be expressed with respect to weight of humic acid, a correction had to be made to account for the difference in equivalent weights of sodium humate and humic acid. The calculation requires knowledge of the pH to which the original humic acid was

adjusted to prepare the sodium humate, and the NaOH titre (meq g^{-1}) required to attain that pH. The mass of humic acid, m_H, which is isoequivalent with a known weight, m_{Na}, of sodium humate is given by:

$$m_H = m_{Na} - (nNa^+.A_R(Na)) + (nH^+.A_R(H)) \quad (5.1)$$

where nNa^+ (equal to nH^+ to maintain electroneutrality) is the number of moles of Na^+ associated with mass m_{Na} of sodium humate, and $A_R(Na)$ and $A_R(H)$ refer to the respective relative atomic masses of Na and H. A correction may be made (for example, for COOH content) according to:

$$COOH_H = COOH_{Na}.m_{Na}/m_H \quad (5.2)$$

where $COOH_H$ and $COOH_{Na}$ are the COOH contents of humic acid and sodium humate on an equivalent per mass basis respectively.

5.2.2 Potentiometric Titration of Humic Acids at Varying Ionic Strength

5.2.2.1 Titration Procedures

Solutions of SHHA and WPHA were prepared as described in Section 3.2.3. Aliquots of these solutions were diluted with $NaNO_3$ solutions of appropriate concentration and titrated with standardised NaOH solution as described in Section 3.4.3. Both SHHA and WPHA were titrated at $[NaNO_3]$ = 0.005, 0.01 and 0.05 mol L^{-1}; WPHA was also titrated at $[NaNO_3]$ = 0.10 mol L^{-1}.

5.2.2.2 Calculation Procedures

The standardised pH value at each point in the titration was found by fitting the actual and measured pH values for the three NBS buffers to a line by linear regression, and interpolating using this line. Hydrogen and hydroxide ion concentrations were found using the activities calculated from the standard pH and the single - ion activity coefficients, at the appropriate ionic strength and temperature, listed by Kielland (1937). A value of the ion product of water (K_W) corrected for ionic strength was also used in this calculation. A similar calculation was used to calculate sodium ion activity using the known sodium ion concentration.

The degree of dissociation (α) for the humic acid molecule may be calculated (provided the initial concentration of acidic sites, L_0, is defined) as follows:

$$\alpha = ([H^+] + [Na^+]_{titre} - [OH^-])/(L_0.V/(V + v)) \quad (5.3)$$

where v is the titre volume,

V is the initial volume, and

$[Na^+]_{titre}$ is the concentration of sodium ions added by the NaOH titrant, such that:

$$[Na^+]_{titre} = [NaOH].V/(V + v) \quad (5.4)$$

The concentration of bound H^+ may be found using:

$$[H^+]_{bound} = C_L.(1 - \alpha) \quad (5.5)$$

where C_L ($= L_0.(V/(V + v))$) is the total concentration of acidic sites.

An apparent dissociation constant ($pK_{app} = -\log_{10}K_{app}$) at every titration point can be calculated as follows:

$$pK_{app} = pH - \log_{10}(\alpha/(1 - \alpha)) \qquad (5.6)$$

5.2.3 Acidimetric Titration of Size Exclusion Chromatographic Fractions of Summit Hill Humic Acid

Size exclusion (gel permeation) chromatography (SEC) differs from conventional adsorptive chromatographic processes in that separations are based on differences in effective molecular size. The chromatographic medium for SEC consists of a flexible or rigid gel which is crosslinked in such a way that its macromolecular structure is porous. Consider a solution containing molecules of different molecular size which is passed through a column prepared using this porous gel. Large molecules are unable to enter the pores because of their size and so are not retarded in their progress through the column. Smaller molecules, however, can enter gel pores and their progress through the SEC column will be retarded as a consequence. In fact, there are two limiting elution volumes for SEC columns. The first, corresponding to the volume of solution in the column which is external to the gel pores, is the column void volume (V_0). Large molecules which are totally excluded from the gel pores will elute at V_0. The second limiting volume is the total volume of solution in the column, V_t, which includes the volume of solution within the gel pores. Small molecules which are able to enter the gel pores readily will elute at V_t. Molecules of intermediate size elute between V_0 and V_t. Log (molecular weight) is inversely proportional to elution volume (V_e) for molecules having similar solution conformation (De Nobili *et al.*, 1989). A useful parameter for characterising SEC behaviour of a molecule on a particular type of gel is the relative elution volume, K_{av}, defined by:

$$K_{av} = \frac{V_e - V_0}{V_t - V_0} \qquad (5.7)$$

5.2.3.1 Fractionation Procedures

The actual size exclusion chromatography (SEC) fractionation of the Summit Hill humic acid was carried out by Dr R. L. Leonard of the Department of Soil Science, Lincoln University. Humic acid extracted by the IHSS method (Appendix 1) from the Summit Hill soil (Appendix 2) was dissolved (1% w/w) in 0.01 mol L^{-1} $Na_2B_4O_7$. This solution was eluted through a column of Sephadex G-150 and collected as fractions; the elution profile and subsequent fractionation scheme (R.L. Leonard, personal communication) is shown in Figure 5.1. Fractions from five areas under the curve were pooled and refractionated separately on Sepharose 6B, Sephadex G-150 or Sephadex G-75 columns depending on their elution volume in the first fractionation. The second elutions were divided into three to four operational subfractions; the subfractions containing the highest concentration of humic substance were used in this work. These subfractions are considered to have greatly reduced polydispersity relative to the unfractionated humic acid (R.L. Leonard, personal communication). Mean K_{av} values for the subfractionations and for the isolated fractions on Sephadex G-150 are listed in Table 5.1.

Table 5.1 Size - exclusion chromatographic data for fractionation of Summit Hill humic acid. Humic acid applied to columns as 1% w/w solution in 0.01 mol L^{-1} $Na_2B_4O_7$.

Fraction	Subfractionation K_{av}			Isolated fraction
	6B	G-150	G-75	K_{av} (Sephadex G-150)
1-3	0.503	-	-	0.0
2-2	-	0.430	-	0.286
3-2	-	0.639	-	0.552
4-2	-	-	0.614	0.756

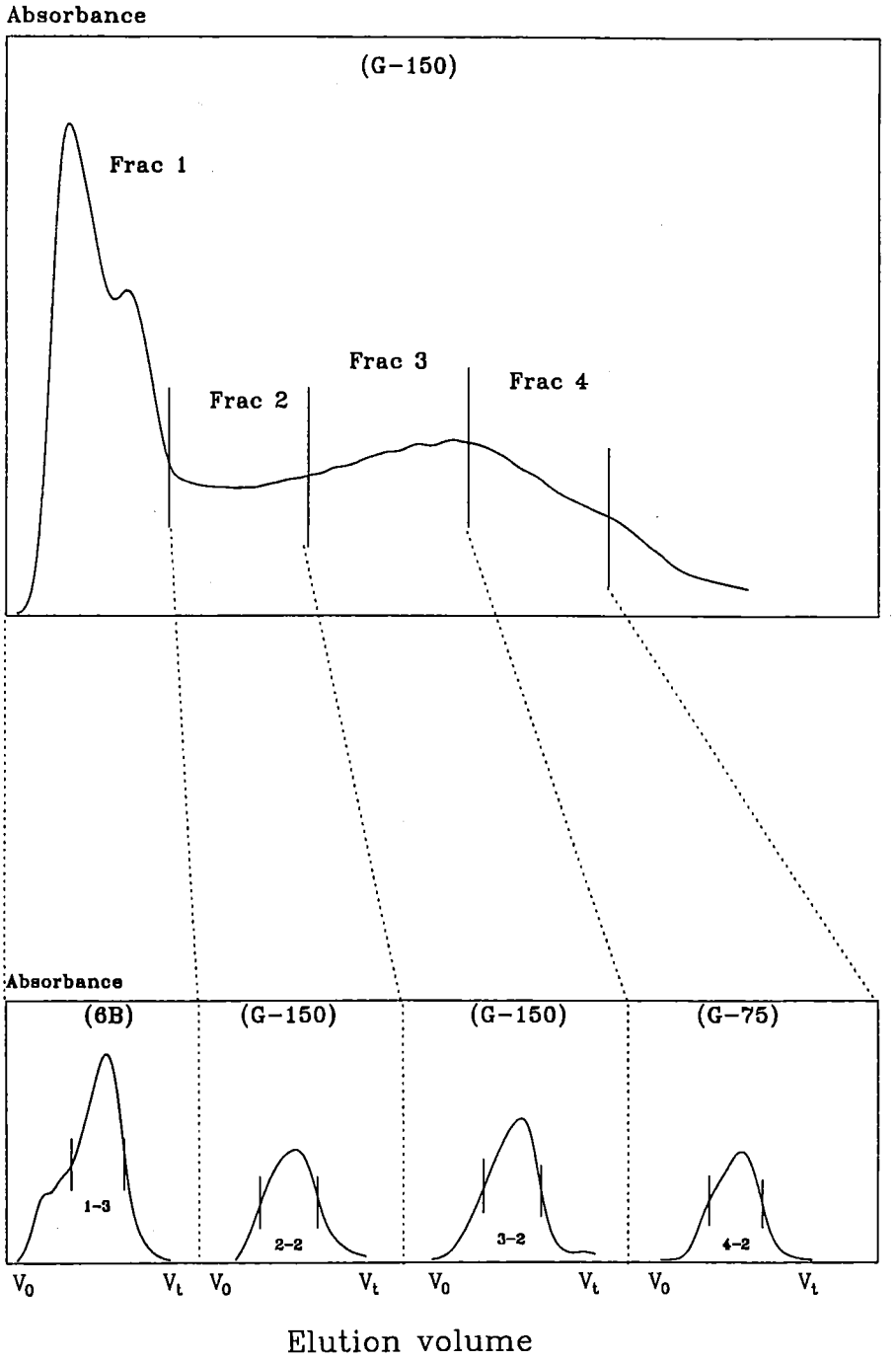

Figure 5.1 Size-exclusion chromatography fractionation scheme for Summit Hill humic acid: (a) initial fractionation of whole Summit Hill humic acid (1% w/w in 0.01 mol L^{-1} $Na_2B_4O_7$) on Sephadex G-150; (b) sub-fractionations.

5.2.3.2 Titration Procedures

Samples of the SHHA molecular size fractions obtained by size-exclusion chromatography were prepared as stable solutions of the fully H^+ - exchanged humic acid as detailed in Section 3.2.3. Aliquots of these solutions were diluted with $NaNO_3$ solution to give a final $NaNO_3$ concentration of 0.01 mol L^{-1} and titrated with standardised NaOH solution as described in Section 3.4.3. Calculated COOH contents were corrected for differences in equivalent weights of sodium humates and humic acids using the procedure outlined in Section 5.2.1.3.

5.2.4 Modelling the Protonation Behaviour of Humic Acids

The protonation reactions of the carboxylic acid functional groups on unfractionated SHHA and WPHA, and SEC fractions of SHHA were modelled by fitting the data from pH - potentiometric titrations to various theoretical equations.

The first model fitted was the polyelectrolyte or modified Henderson - Hasselbalch model which assumes a single type of acidic site, the behaviour of which is modified by the changing electrical potential of the humic substance macromolecule as successive acidic groups dissociate. The Henderson - Hasselbalch model may be expressed as:

$$pH = pK_{HH} + \eta \log(\alpha/(1 - \alpha)) \qquad (5.8)$$

where pK_{HH} is the apparent pK_a at half neutralisation, and;

η is a composite electrostatic interaction term.

The parameter relating to the changing electrical potential is η, the slope of a plot of pH *versus* $\log(\alpha/(1 - \alpha))$. It has a maximum value of 2 for a macromolecule containing a single type of site (Dempsey and O'Melia, 1983). Potentiometric data were fitted to the equation by simple linear

regression of pH *versus* $\log(\alpha/(1 - \alpha))$ with $\log(\alpha/(1 - \alpha)) \leq 1$. Calculation was as described in Section 5.2.2. The regression was not weighted in any way; pH values are directly proportional to experimental electrode potentials and may be assumed to have equal variance (Turner *et al.*, 1986).

The protonation reactions of humic acids can also be described in terms of polyelectrolyte behaviour by the Hermans - Overbeek equation (Wilson and Kinney, 1977; Perdue, 1985):

$$pK_{app} = pK_{int} - 0.868\omega n\alpha \qquad (5.9)$$

where pK_{app} is the apparent dissociation constant;

pK_{int} is the 'intrinsic' pK_a of the single type of acidic group present on the macromolecule;

ω is a composite electrostatic interaction term;

and n is the average number of acidic groups per macromolecule.

The procedures used to fit protonation data to this equation were similar to those used with the modified Henderson - Hasselbalch equation. Values of pK_{app} and α were calculated as described in Section 5.2.2.2 for each point in a titration. Simple, unweighted linear regression of pK_{app} against α was then used to estimate pK_{int} and $(-0.868\omega n)$, for $0 \leq \alpha \leq 0.95$.

A family of site - binding models were also fitted to titration data. These models describe humic acid protonation in terms of a hypothetical set of n independent monoprotic acids as follows:

$$C_L(1 - \alpha) = \Sigma_{i=1}^{n} (C_i K_i [H^+]/(1 + K_i [H^+])) \qquad (5.10)$$

where C_L is the total concentration of acidic groups;
C_i is the concentration of the i^{th} monoprotic acid;
and K_i is the protonation constant for the i^{th} acid.

Potentiometric data were fitted to equations of this type with n = 1, 2 and 3. Parameter optimisation was performed using the program described in Chapter Three with an appropriate modelling subroutine such

that log[H+] was the dependent variable; this necessitated rearrangement of the forms of Equation 5.10 as outlined in Chapter Three. The resulting equations were solved analytically where possible (n = 1,2) and by Newton Raphson/Bisection (Chapter Three; Appendix 7) where the rearrangement of Equation 5.10 resulted in a cubic function of ($C_L(1 - \alpha)$).

Potentiometric data were also fit to a model that described humic acid protonation in terms of acidic functional groups having a lognormal distribution of protonation constants. This model may be written as:

$$C_L(1 - \alpha) = \frac{C_L}{\sigma_K\sqrt{2\pi}} \int_{-5\sigma}^{+5\sigma} -\frac{1}{2}\left(\frac{\log K_\mu - \log K}{\sigma_K}\right)^2 \frac{10^{\log K}[H^+]}{1 + 10^{\log K}[H^+]}\, d(\log K) \qquad (5.11)$$

where $\log K_\mu$ and σ_K are the mean and standard deviation, respectively, of the normal distribution in $\log_{10}K$.

Parameter optimisation was carried out using the program described in Chapter Three (Section 3.6.4) with the modelling routine written so that ($C_L(1 - \alpha)$) was the dependent variable. Optimisations were performed by minimising both absolute and relative residual sums of squares to evaluate the effects of systematic weighting in regressions.

Finally, an aggregation model, based on modification/self - association processes, and developed by Teasdale (1987) was evaluated in terms of its ability to describe humic acid protonation data. This model assumes a single type of acidic site; proton binding to a humate macromolecule modifies the macromolecule so that reversible self - association is possible. The model may be expressed as:

$$C_L(1 - \alpha) = \frac{C_L K[H]}{K[H] + (1 - P_C)^f} \qquad (5.12)$$

where K is the protonation constant, P_c is the probability that a self - association site on L has reacted with an equivalent site on another L molecule, and f is the number of self - association sites per L molecule. Since P_c will be dependent on the amount of self association sites which are already linked, a self association binding constant, K_s, may be defined as (Teasdale, 1987):

$$K_s = \frac{P_c}{f[HL](C_L(1-\alpha))(1 - P_c)^2} \qquad (5.13)$$

If, for example, f is assigned a nominal but realistic value of 2 (resulting in the formation of linear aggregates), this equation may be rearranged to give (Teasdale, 1987):

$$C_L(1 - \alpha) = \frac{C_L K[H]}{K[H] + \{1 - K_s[H]([HL] + [M])\}^2} \qquad (5.14)$$

where $[HL] = C_L(1 - \alpha)$ as before. This equation may itself be rearranged to give a cubic function in $C_L(1 - \alpha)$, and solved by bisection/Newton - Raphson as outlined for rearranged site - binding models earlier in this Section. The model was fitted in this form, by optimising C_L, K and K_s values, to protonation data.

5.3 Results

5.3.1 Acidimetric Measurements

5.3.1.1 Determination of Total Acidity; $Ba(OH)_2$ Method

The results presented in Table 5.2 indicate that total acidity measured by the $Ba(OH)_2$ method shows moderate but acceptable variability. It is apparent that the Waimari Peat humic acid has a higher acidic functional group content than Summit Hill humic acid. A comparison with values in the literature (Stevenson, 1985; Mathur and Farnham, 1985) revealed that this is not a general result for soil- and peat-derived humic acids, which tend to have similar total acidities. Both values, however, fall within the ranges presented in the the literature, with the value for SHHA being slightly lower than expected for a temperate climate soil humic acid (Stevenson, 1985).

Table 5.2 Total acidity values for Summit Hill and Waimari Peat humic acids determined by $Ba(OH)_2$ displacement. *[HCl] = 0.181 mol L^{-1}.

Humic acid	Replicate	Titre/ml*	Wt HA/g	Total acidity/ meq g^{-1}
Summit Hill	1	4.99	0.1040	3.95
Summit Hill	2	5.16	0.1047	3.63
Summit Hill	3	4.87	0.1067	4.05
	mean±sd			3.9±0.2
Waimari Peat	1	4.23	0.1010	5.43
Waimari Peat	2	4.47	0.1002	5.04
Waimari Peat	3	4.42	0.1025	5.01
	mean±sd			5.2±0.2
	blank	7.26	0	

5.3.1.2 NaOH Dissolution/Acid Titration Method

This method gave results which were much more reproducible than those from the $Ba(OH)_2$ method (Table 5.2). Results were consistently higher than those obtained by the direct titration method; Table 5.3 shows a comparison of amounts of protons measured by each method at selected fixed pH values.

Table 5.3 Acidimetric titres (mean±sd) for Summit Hill (SH) and Waimari Peat (WP) humic acids measured by HCl and NaOH titration; 25 °C, $[NaNO_3] = 0.01$ mol L^{-1}.

	Titre / meq g^{-1}			
	NaOH dissolution/ HCl titration		Direct titration	
pH	SH	WP	SH	WP
4.0	0.94±0.04	1.68±0.03	-	0.04±0.01
4.5	1.29±0.04	2.07±0.03	0.61±0.03	1.21±0.05
5.0	1.62±0.04	2.41±0.02	1.15±0.01	1.82±0.06
5.5	1.93±0.03	2.73±0.01	1.53±0.01	2.27±0.07
6.0	2.21±0.04	3.03±0.01	1.83±0.01	2.64±0.07
6.5	2.46±0.04	3.31±0.01	2.11±0.01	2.94±0.08
7.0	2.68±0.04	3.53±0.01	2.33±0.01	3.18±0.08
7.5	2.85±0.04	3.71±0.01	2.50±0.01	3.38±0.08
8.0	3.01±0.04	3.86±0.01	2.67±0.01	3.56±0.08

5.3.1.3 Direct Titration Method

Titration curves for both humic acids showed a single inflection in the pH range 7.5-7.8. Titration curves representative of those for both humic acids are shown in Figures 5.2 and 5.3. Table 5.3 shows experimentally observed NaOH titre values at selected fixed pH values. The titre value at which the inflection occurred was taken as indicating complete titration of humic acid carboxylic acid groups. Table 5.4 lists calculated COOH contents and inflection pH values for both SHHA and WPHA. These values for carboxyl acidity are within the ranges listed for soil (Stevenson, 1985) and peat (Mathur and Farnham, 1985) humic acids, the value for SHHA again being at the lower end of the range.

The difference between total acidity and carboxylic acid content is coomonly used as an estimate of the phenolic group content for humic substances (Perdue, 1985). The phenolic hydroxyl group contents were calculated in this way for SHHA and WPHA, and are listed in Table 5.4.

Table 5.4 Inflection pH and carboxyl and phenolic hydroxyl group contents for Summit Hill and Waimari Peat humic acids inferred from NaOH titration.

Humic acid	pH at inflection[a]	COOH content /meq g(HA)$^{-1}$[b]	Phenolic OH content /meq g(HA)$^{-1}$[c]
Summit Hill	7.62	2.66±0.04	1.2±0.2
Waimari Peat	7.76	3.54±0.06	1.7±0.3

[a][$NaNO_3$]=0.01 mol L^{-1}; [b]mean for all titrations; [c]difference between $Ba(OH)_2$ and COOH acidity.

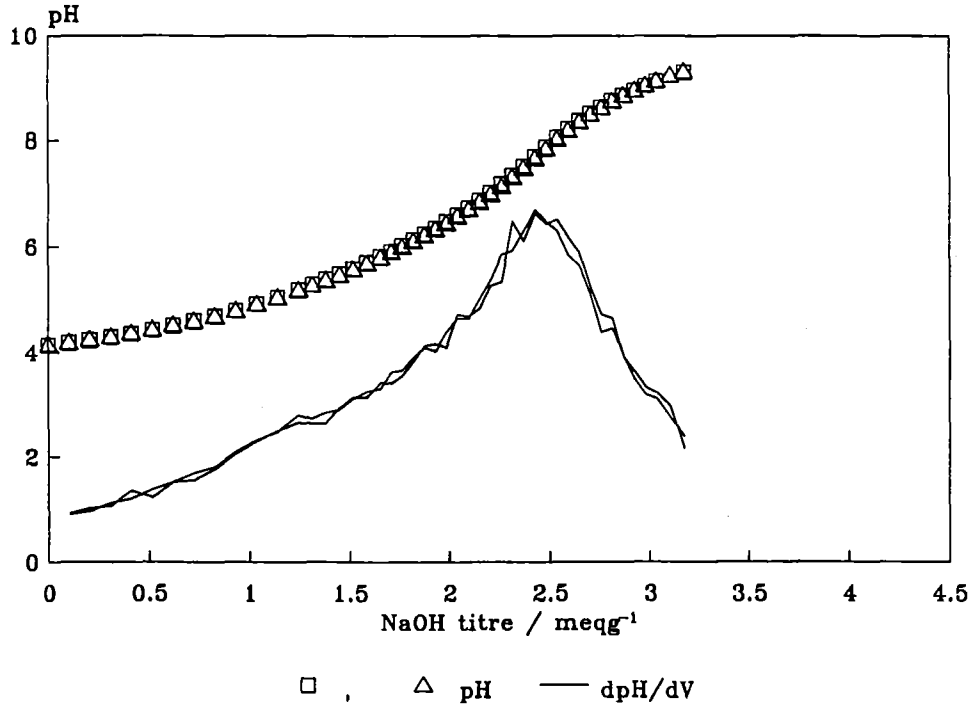

Figure 5.2 Titration curves (pH *versus* titre; ΔpH/Δtitre *versus* titre) for duplicate titrations of SHHA. [$NaNO_3$] = 0.01 mol L^{-1}; 25 ° C.

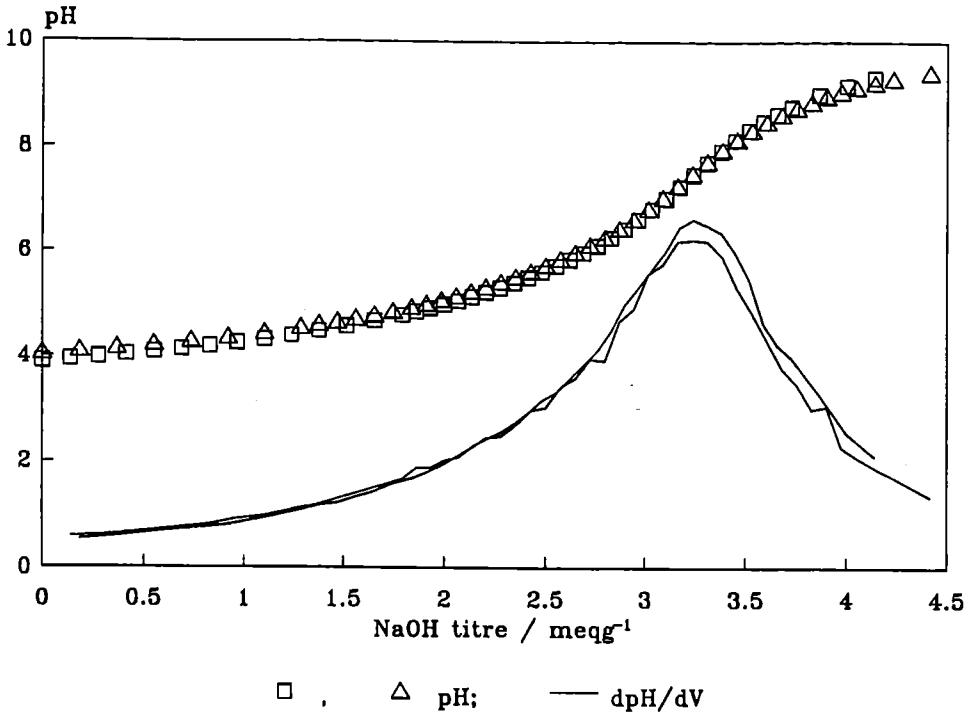

Figure 5.3 Titration curves (pH *versus* titre; ΔpH/Δtitre *versus* titre) for duplicate titrations of WPHA. $[NaNO_3] = 0.10 mol\ L^{-1}$; 25 °C.

5.3.2 Effect of ionic strength on humic acid protonation behaviour

Titration of SHHA and WPHA in solutions at any ionic strength resulted in titration curves which were superficially similar to those in Figures 5.2 and 5.3. A single inflection was observed in all titration curves for both humic acids; for either humic acid the position of this inflection did not vary significantly with varying ionic strength. The titration data are presented in plots of: pK_{app} (apparent dissociation constant) *versus* degree of dissociation (α) (Figures 5.4 and 5.5); pK_{app} *versus* pH (Figures 5.6 and 5.7) and pK_{app} *versus* (pH + pNO_3) (Figures 5.8 and 5.9). Figures 5.10 and 5.11 present titration data in plots of (pH - pNO_3) *versus* α. The significance of such plots is discussed later, in Section 5.4.2. Calculations were made on the basis of humic acid carboxylic acid groups only, assuming that the observed titration curve inflection represented an end point for complete titration of these acidic groups.

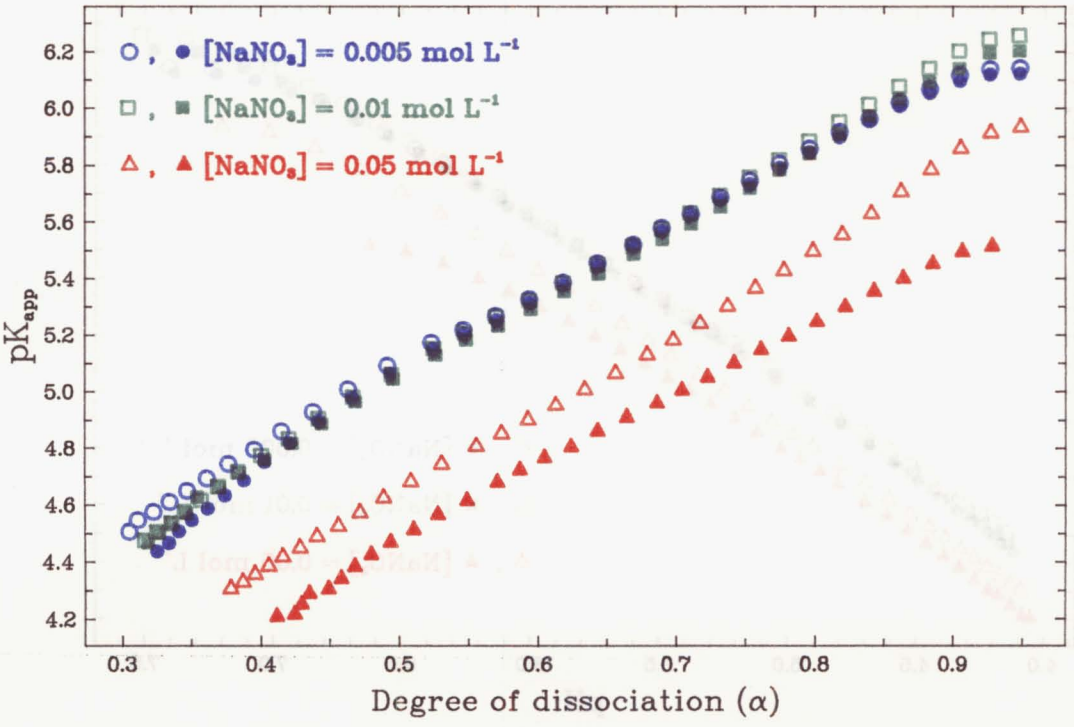

Figure 5.4 Apparent dissociation constant (pK_{app}) versus degree of dissociation (α), at varying $NaNO_3$ concentrations, during titrations of SHHA with NaOH.

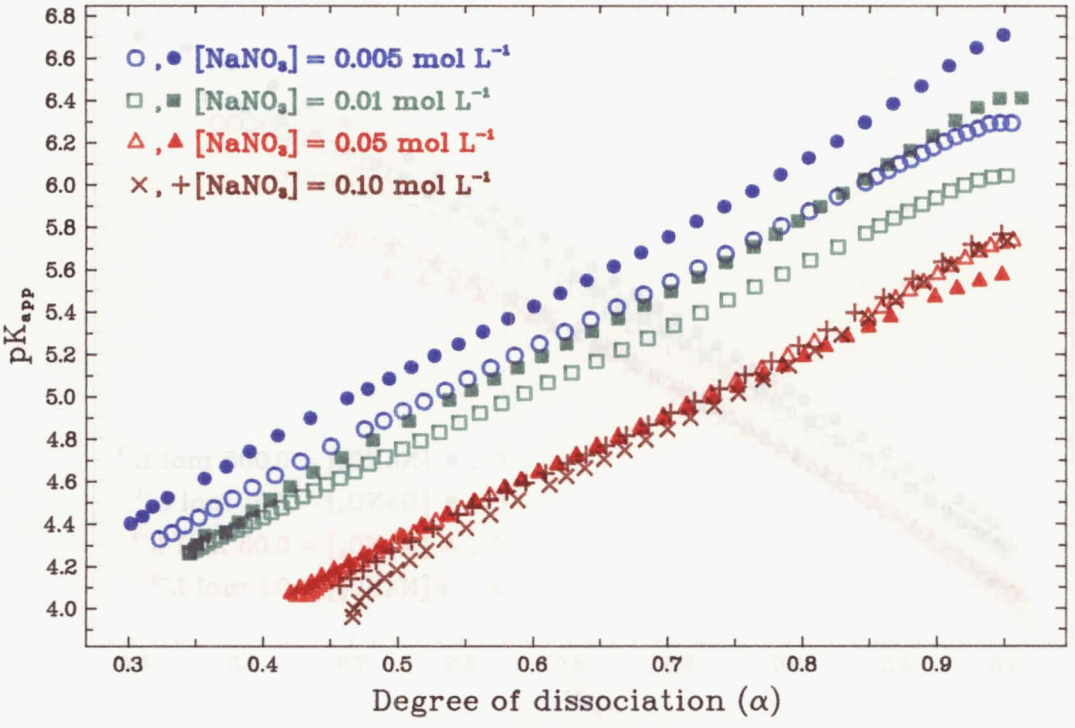

Figure 5.5 Apparent dissociation constant (pK_{app}) versus degree of dissociation (α), at varying $NaNO_3$ concentrations, during titrations of WPHA with NaOH.

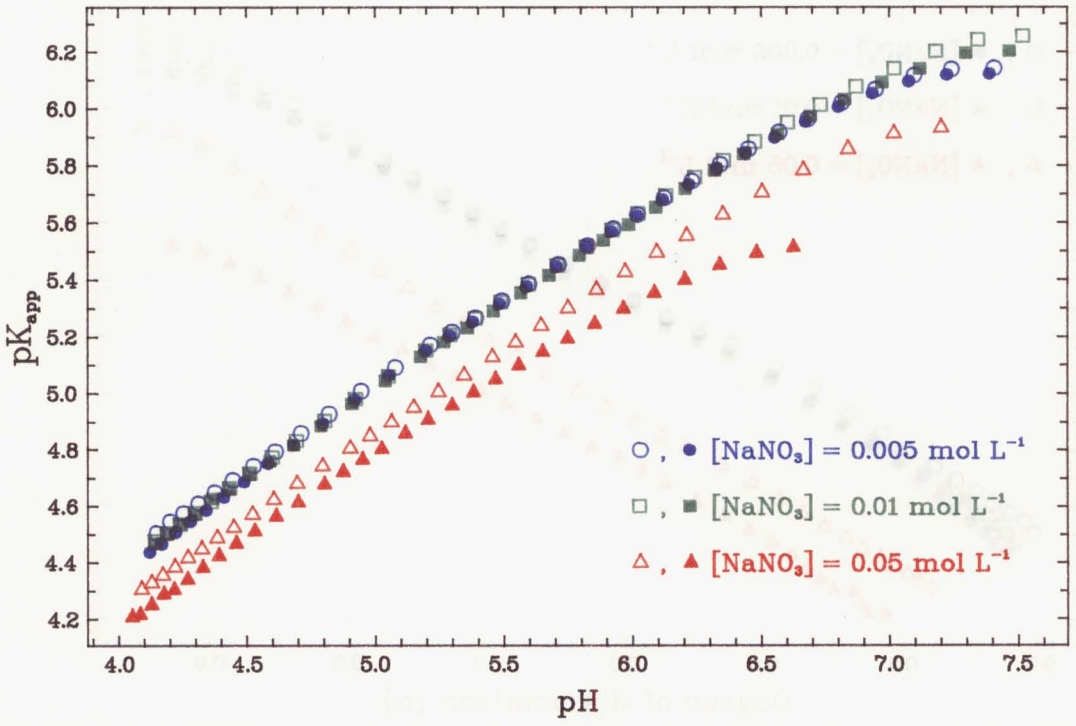

Figure 5.6 Apparent dissociation constant (pK_{app}) versus pH, at varying $NaNO_3$ concentrations, during titrations of SHHA with NaOH.

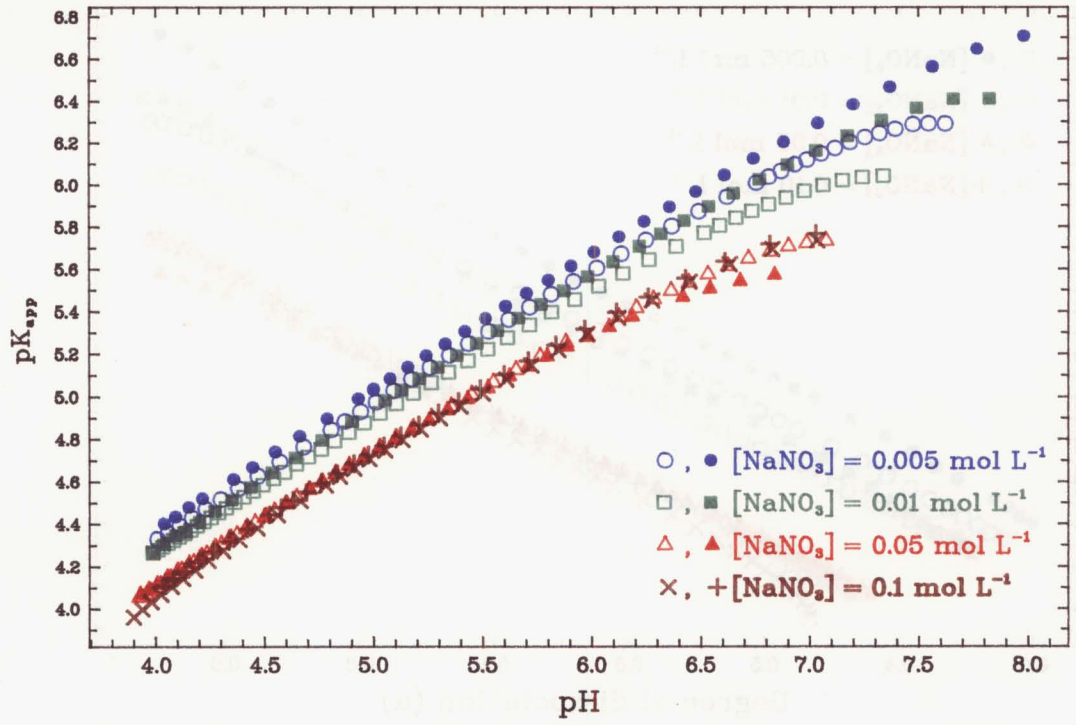

Figure 5.7 Apparent dissociation constant (pK_{app}) versus pH, at varying $NaNO_3$ concentrations, during titrations of WPHA with NaOH.

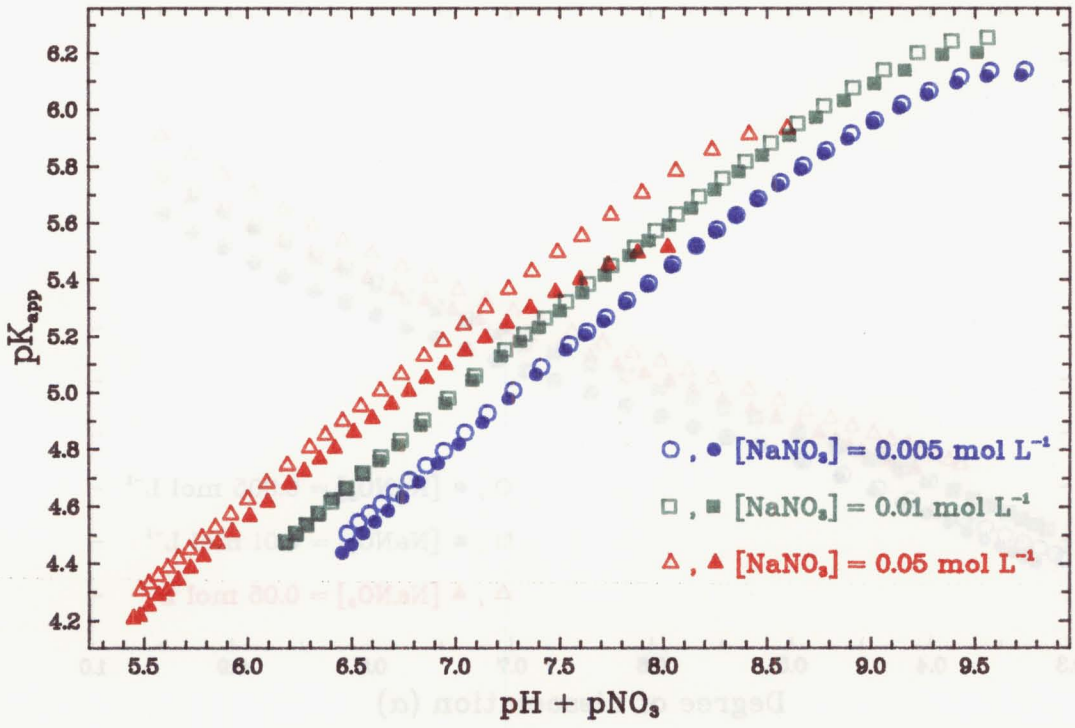

Figure 5.8 Apparent dissociation constant (pK_{app}) versus (pH + pNO_3), at varying $NaNO_3$ concentrations, during titrations of SHHA with NaOH.

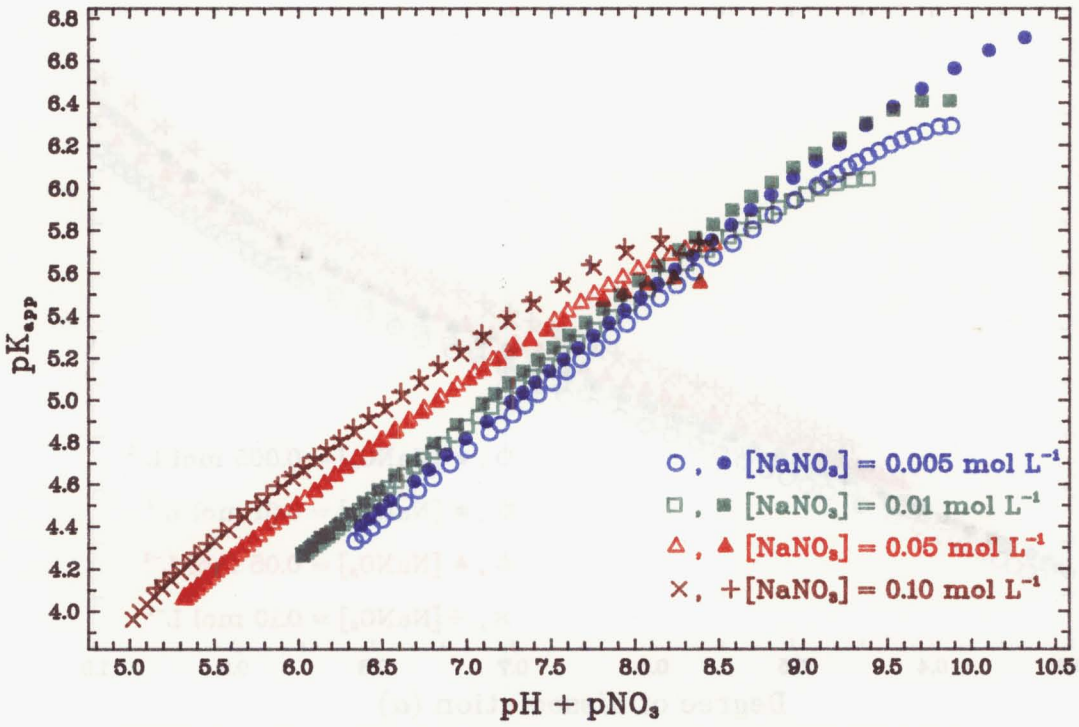

Figure 5.9 Apparent dissociation constant (pK_{app}) versus (pH + pNO_3), at varying $NaNO_3$ concentrations, during titrations of WPHA with NaOH.

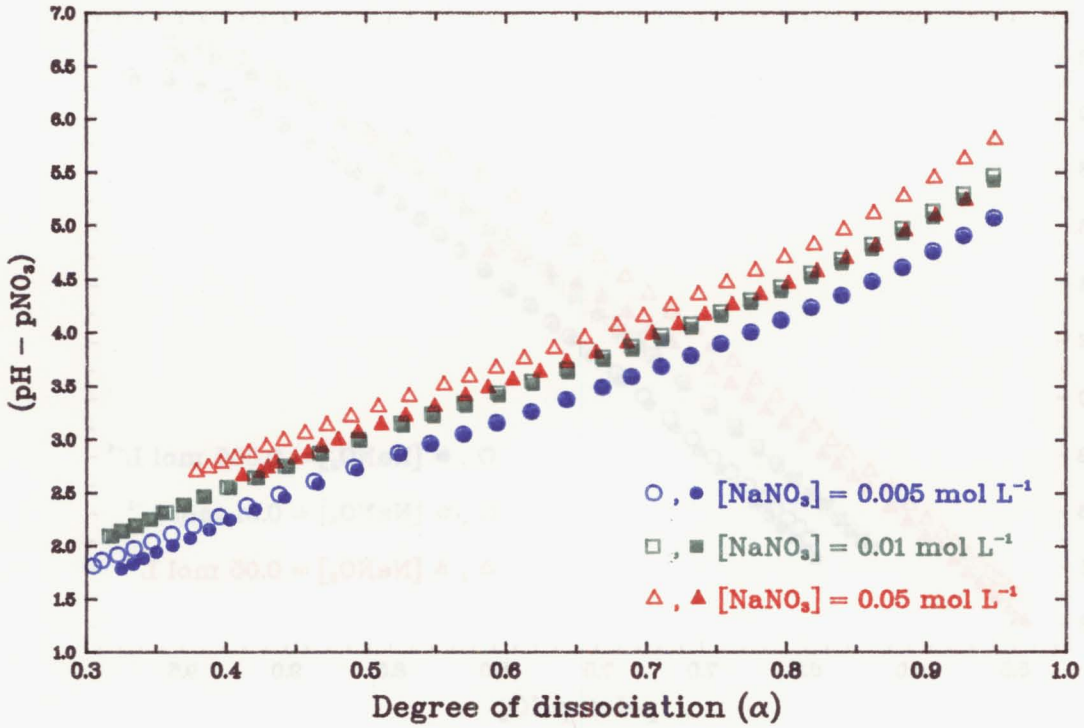

Figure 5.10 (pH – pNO_3) versus degree of dissociation (α), at varying $NaNO_3$ concentrations, during titrations of SHHA with NaOH.

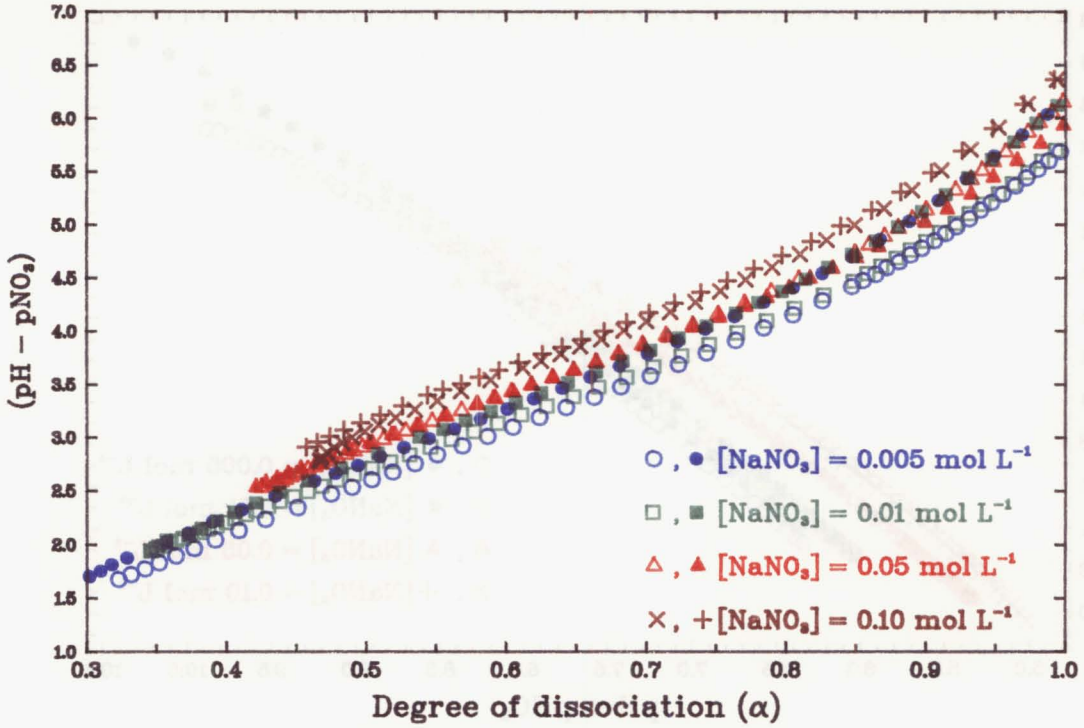

Figure 5.11 (pH – pNO_3) versus degree of dissociation (α), at varying $NaNO_3$ concentrations, during titrations of SHHA with NaOH.

5.3.3 Protonation Behaviour of Summit Hill Humic Acid Fractionated by Size-Exclusion Chromatography

5.3.3.1 Variation in Carboxyl Acidity

Experimentally determined values for the carboxyl acidity of the molecular size fractions of SHHA appear in Table 5.5. Titration curves used to generate these values appear in Figure 5.12.

Table 5.5. Carboxyl acidities for SEC fractions of SHHA determined by NaOH titration. ([a]Mean of duplicates; uncertainties based on estimate of total cumulative experimental error.)

Fraction	COOH content / meq g(HA)$^{-1}$[a]
1-3	2.62±0.04
2-2	2.21±0.03
3-2	2.95±0.04
4-2	4.00±0.06
Unfractionated	2.66±0.04

5.3.4 Modelling Humic Acid Protonation Data

Results derived from fitting the models described in Section 5.2.4 are listed for data from different titrations in Tables 5.6 - 5.10. Fitting of protonation data to the modified Henderson - Hasselbalch equation was achieved using datasets truncated so that all ($\log(\alpha/(1 - \alpha))$,pH) data pairs fulfilled the condition that $\log(\alpha/(1 - \alpha)) < 1$ (corresponding to $\alpha <$ c. 0.91).

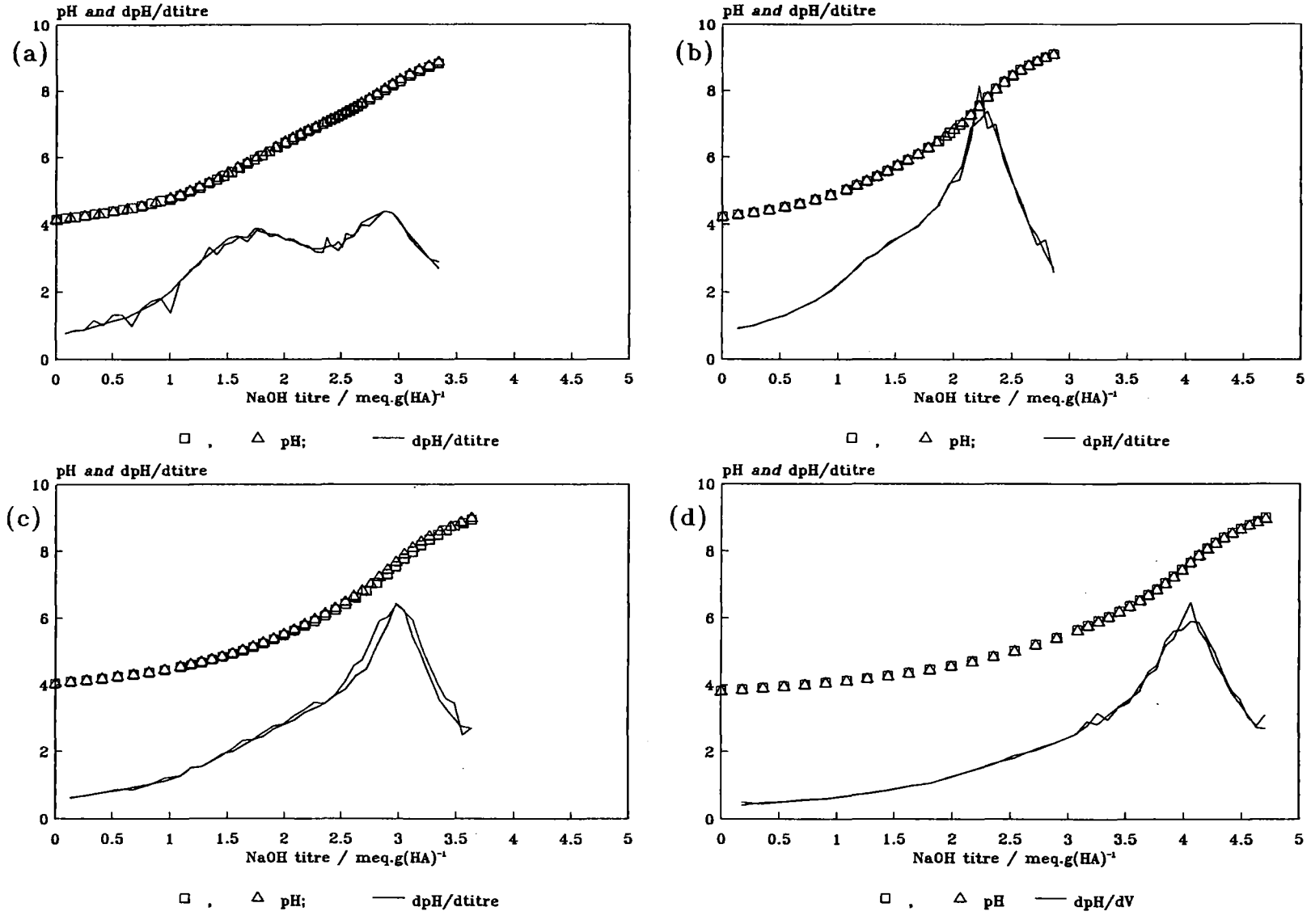

Figure 5.12 Titration curves (pH *versus* titre; ΔpH/Δtitre *versus* titre) from duplicate titrations of SEC fractions of SHHA with NaOH. [$NaNO_3$] = 0.01 mol L^{-1}; 25 ° C.

Protonation data was truncated in this way to reduce the effects on the regressions of severe curvature of plots of pH *versus* $\log(\alpha/(1 - \alpha))$ at higher degrees of dissociation. This curvature may have been due, in part, to the observation that the actual degree of dissociation was still increasing at the point in the titration (characterised by a $\Delta pH/\Delta V$ *versus* V maximum) that was used to operationally define the concentration of acidic groups, and thus to calculate α. In other words, very weakly acidic functional groups were probably still being titrated at this point in the titration.

Results are not tabulated for description of humic acid proton binding behaviour in terms of a single monoprotic acid, as this model provided a poor description of protonation data for all titrations, even when C_L was treated as an adjustable parameter in regressions. Figure 5.13(a) shows observed and predicted proton binding using the one-site model; R^2 values were between 44 and 70% for data from all titrations.

Where the total concentration of acidic groups (C_L) was a fixed parameter in regressions (for example: discrete monoprotic acid models; lognormal distribution of protonation constants; Sips binding equation) the value used for the unfractionated humic acids was a pooled mean from titrations at all ionic strengths. For the SEC fractions of SHHA means from duplicate titrations were used. A fixed value of C_L, apart from adjustments for dilution during the titration, remained unaltered throughout a parameter optimisation procedure.

It was found, when fitting protonation data to the Teasdale modification / self - association model, that the goodness of fit was nearly independent of the value of log K_s. The summary of refined parameter estimates and statistical tests shown in Table 5.13 are those found for an initial estimate for log K_s of 1.0.

(For Tables 5.6 - 5.13, the general nomenclature SHFx-x refers to Summit Hill humic acid SEC fraction x-x.)

Results derived from fitting the various models to a representative dataset (SHHA, [$NaNO_3$] = 0.01 mol L^{-1}) are presented graphically in Figures 5.13 - 5.15. Results using data from other titrations were similar to those presented for this dataset. Obvious exceptions to this generalisation are discussed in greater detail in Section 5.4.4. Such comparisons of observed and fitted values are a convenient and useful qualitative tool for assessment of various models. In addition, areas where the agreement between observed data and predicted values is especially poor may be identified from these plots.

(a)

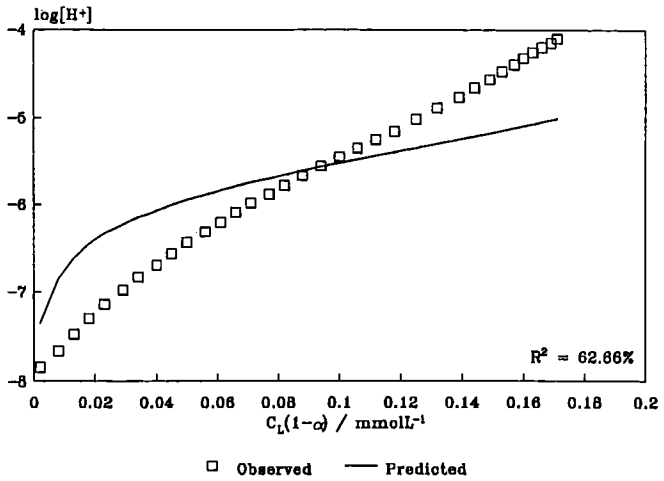

(b)

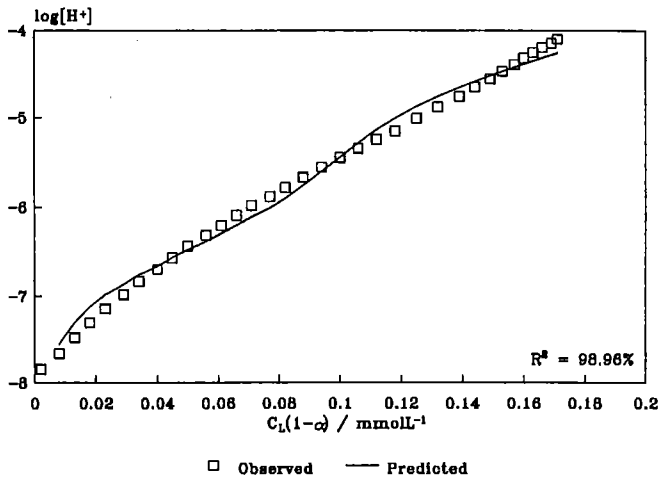

(c)

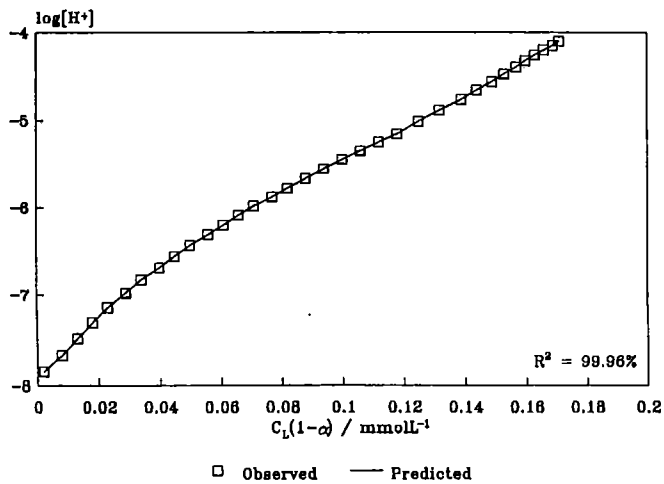

Figure 5.13 Relationship between observed protonation data and values predicted using: (a) one-acid; (b) two-acid, and; (c) three-acid models.

(a)

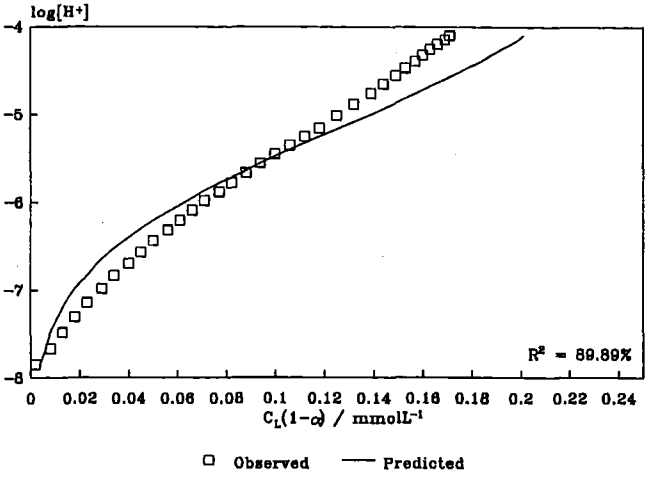

(b)

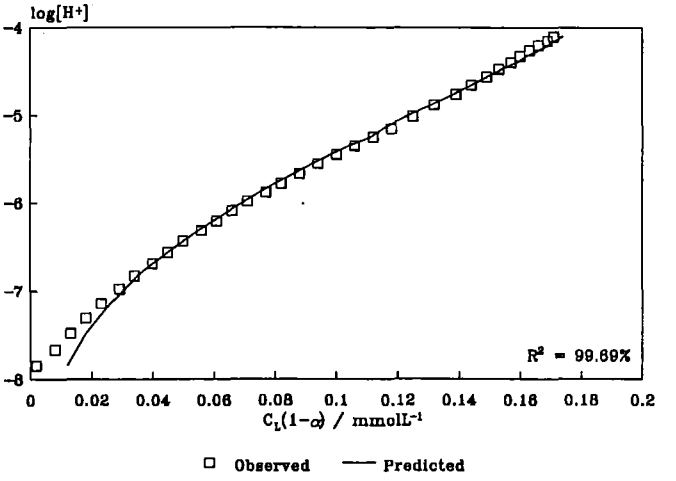

(c)

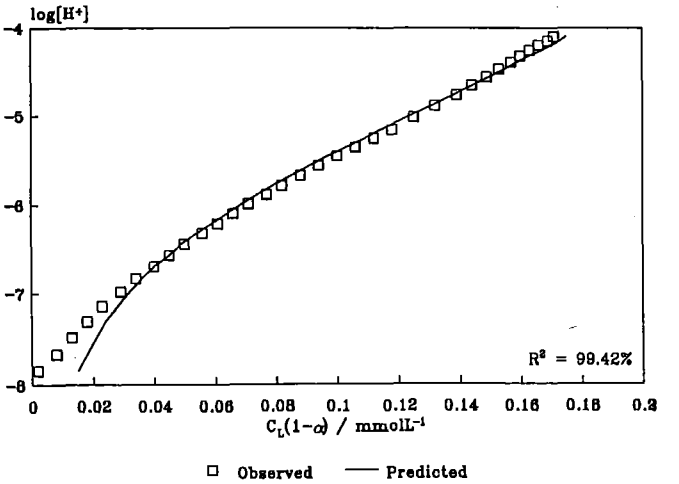

Figure 5.14 Relationship between observed protonation data and values predicted using: (a) lognormal (weighted regression); (b) lognormal (unweighted regression), and; (c) Sips binding models.

(a)

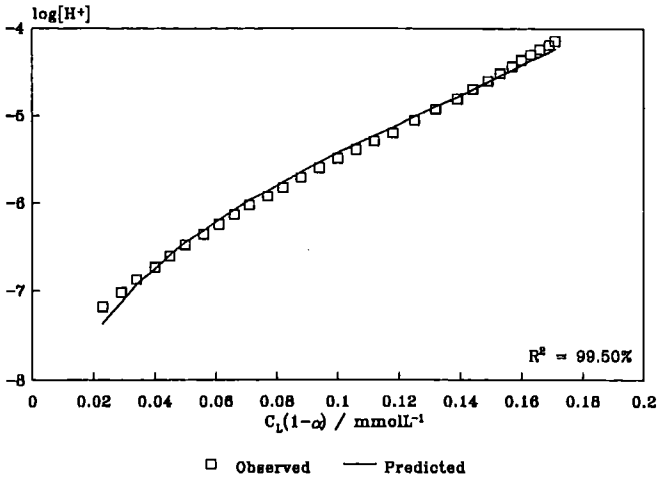

(b)

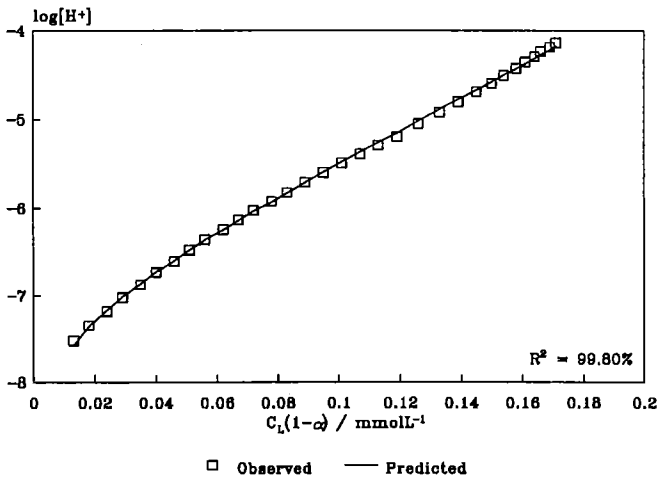

(c)

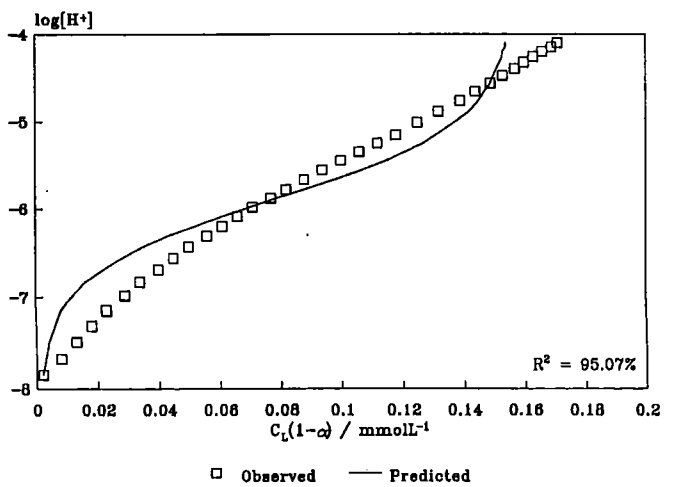

Figure 5.15 Relationship between observed protonation data and values predicted using: (a) modified Henderson-Hasselbalch; (b) Hermans-Overbeek, and; (c) Teasdale modification-self association models.

Table 5.6 Summary of fits of protonation data for SHHA and WPHA to the modified Henderson - Hasselbalch equation. [a]Fitted parameters (Equation 5.7); [b]singly lagged residual autocorrelation coefficient (* $p<0.05$).

Humic acid	$[NaNO_3]$/ mol L^{-1}	Number of data	$pK_{HH} \pm sd^a$	$\eta \pm sd^a$	R^2 (%)	F	$r_1{}^b$ (all *)
SHHA	0.005	30	5.06±0.02	2.29±0.03	99.4	4777	0.761
SHHA	0.005	30	5.01±0.02	2.37±0.05	99.0	2698	0.798
SHHA	0.01	30	5.03±0.02	2.39±0.03	99.5	5473	0.777
SHHA	0.01	30	5.01±0.02	2.35±0.03	99.5	5673	0.737
SHHA	0.05	30	4.65±0.01	2.36±0.02	99.8	11358	0.734
SHHA	0.05	30	4.48±0.02	2.21±0.04	99.2	3386	0.784
SHF1-3	0.01	39	5.16±0.03	2.72±0.07	97.7	1585	0.888
SHF1-3	0.01	29	5.21±0.03	2.83±0.08	97.8	1185	0.808
SHF2-2	0.01	20	4.90±0.02	2.42±0.05	99.1	2044	0.659
SHF2-2	0.01	21	4.92±0.02	2.37±0.05	99.2	2494	0.705
SHF3-2	0.01	26	4.44±0.03	2.61±0.08	97.8	1073	0.773
SHF3-2	0.01	26	4.50±0.02	2.64±0.07	98.5	1603	0.789
SHF4-2	0.01	24	3.95±0.05	3.0±0.1	97.0	707	0.804
SHF4-2	0.01	24	3.91±0.05	3.0±0.1	96.6	621	0.822
WPHA	0.005	38	4.90±0.02	2.49±0.03	99.5	7463	0.883
WPHA	0.005	33	5.09±0.01	2.65±0.03	99.7	10379	0.759
WPHA	0.01	46	4.72±0.01	2.44±0.02	99.6	12345	0.876
WPHA	0.01	33	4.82±0.01	2.66±0.03	99.6	8548	0.801
WPHA	0.05	45	4.31±0.01	2.46±0.03	99.5	8820	0.896
WPHA	0.05	32	4.34±0.01	2.37±0.03	99.4	5298	0.739
WPHA	0.10	30	4.20±0.02	2.62±0.04	99.3	4025	0.790
WPHA	0.10	29	4.32±0.02	2.50±0.03	99.5	5674	0.734

Table 5.7 Summary of fits of protonation data to the Hermans - Overbeek equation for $0 < \alpha < 0.95$. [a]Fitted parameters (Equation 5.8); [b]singly lagged residual autocorrelation coefficient (* $p<0.05$).

Humic acid	$[NaNO_3]$/ mol L^{-1}	Number of data	pK_{int}[a] ± sd	$-0.868\omega n$[a] ± sd	R^2 (%)	F	r_1[b]
SHHA	0.005	32	3.77±0.02	2.61±0.03	99.7	10234	0.645*
SHHA	0.005	32	3.63±0.03	2.76±0.05	99.2	3547	0.791*
SHHA	0.01	32	3.62±0.01	2.85±0.02	99.8	18539	0.721*
SHHA	0.01	32	3.64±0.01	2.77±0.02	99.9	20045	0.616*
SHHA	0.05	32	3.21±0.02	2.87±0.02	99.8	19553	0.242
SHHA	0.05	32	3.20±0.02	2.54±0.03	99.5	5943	0.654*
SHF1-3	0.01	42	3.44±0.06	3.46±0.09	97.4	1514	0.895*
SHF1-3	0.01	31	3.45±0.07	3.5±0.1	97.1	979	0.834*
SHF2-2	0.01	21	3.44±0.02	2.92±0.04	99.7	5779	0.691*
SHF2-2	0.01	22	3.50±0.02	2.86±0.03	99.8	13101	0.757*
SHF3-2	0.01	27	2.73±0.06	3.4±0.1	97.9	1179	0.798*
SHF3-2	0.01	28	2.81±0.04	3.36±0.07	99.0	2543	0.818*
SHF4-2	0.01	26	1.7±0.1	4.4±0.2	97.2	831	0.812*
SHF4-2	0.01	26	1.6±0.1	4.5±0.2	96.6	692	0.846*
WPHA	0.005	43	3.33±0.01	3.17±0.01	100.0	156732	0.722*
WPHA	0.005	35	3.37±0.02	3.46±0.02	99.8	18652	0.866*
WPHA	0.01	50	3.24±0.01	2.99±0.01	100.0	306018	0.814*
WPHA	0.01	36	3.10±0.01	3.46±0.02	99.9	23606	0.859*
WPHA	0.05	50	2.72±0.01	3.16±0.01	99.9	56166	0.927*
WPHA	0.05	35	2.90±0.01	2.86±0.01	99.9	42939	0.739*
WPHA	0.10	32	2.42±0.03	3.48±0.04	99.6	8340	0.790*
WPHA	0.10	31	2.61±0.02	3.32±0.02	99.9	22720	0.867*

Table 5.8 Summary of fits of protonation data for humic acids to a two - independent monoprotic acid/fixed concentration of acid groups model; [b]singly lagged residual autocorrelation coefficient ([*] $p<0.05$).

Humic acid	$[NaNO_3]$ /mol L^{-1}	Number of data	Fixed C_1/ meq g^{-1}	C_1/C_L	log K_1	log K_2	R^2 (%)	F	r_1[b]
SHHA	0.005	34	2.66	0.4324	6.356	4.204	99.1	1648	0.586*
SHHA	0.005	34	2.66	0.4448	6.319	4.104	99.0	1496	0.632*
SHHA	0.01	34	2.66	0.4079	6.457	4.215	99.0	1494	0.728*
SHHA	0.01	34	2.66	0.4084	6.408	4.203	99.0	1539	0.685*
SHHA	0.05	34	2.66	0.4013	6.184	4.013	99.1	1654	0.608*
SHHA	0.05	34	2.66	0.4055	5.741	3.725	98.8	1276	0.325*
SHF1-3	0.01	44	2.62	0.4658	6.678	4.061	99.3	3129	0.755*
SHF1-3	0.01	33	2.62	0.4756	6.678	4.06	99.3	2077	0.742*
SHF2-2	0.01	23	2.21	0.4228	6.281	4.065	98.8	813	0.231
SHF2-2	0.01	24	2.21	0.4178	6.307	4.108	98.8	878	0.266
SHF3-2	0.01	29	2.95	0.4172	5.964	3.609	99.2	1578	0.719*
SHF3-2	0.01	30	2.95	0.3942	6.109	3.763	99.2	1781	0.779*
SHF4-2	0.01	29	4.00	0.3582	6.007	3.360	98.6	932	0.839*
SHF4-2	0.01	29	4.00	0.3611	5.987	3.312	98.6	902	0.848*
WPHA	0.005	49	3.54	0.3832	6.545	4.153	98.8	1873	0.741*
WPHA	0.005	37	3.54	0.3707	6.857	4.343	98.2	945	0.897*
WPHA	0.01	55	3.54	0.3814	6.297	3.995	99.2	3223	0.800*
WPHA	0.01	39	3.54	0.3630	6.592	4.115	98.5	1189	0.815*
WPHA	0.05	56	3.54	0.3464	5.976	3.715	98.7	1972	0.553*
WPHA	0.05	38	3.54	0.3851	5.736	3.635	97.2	625	0.208*
WPHA	0.10	35	3.54	0.3304	5.959	3.653	98.7	1243	0.655*
WPHA	0.10	33	3.54	0.3191	6.044	3.812	99.0	1493	0.617*

Table 5.9 Summary of fits of SHHA and WPHA protonation data to a model incorporating three noninteracting acidic sites. Unweighted regressions with respect to $C_L(1 - \alpha)$. [a]Adjustable parameters, Equation 5.9. §See discussion, Section 5.4.4.2; [b]singly lagged residual autocorrelation coefficient (* $p<0.05$).

Humic acid	$[NaNO_3]$ /mol L^{-1}	Number of data	Fixed C_L /meq g^{-1}	C_1/C_L[a]	C_2/C_L[a]	log K_1[a]	log K_2[a]	log K_3[a]	R^2 (%)	F	r_1[b]
SHHA	0.005	34	2.66	0.2640	0.3484	6.720	5.321	3.702	99.97	22235	0.374*
SHHA	0.005	34	2.66	0.2700	0.3509	6.691	5.288	3.491	99.97	20839	0.390*
SHHA	0.01	34	2.66	0.2404	0.3573	6.858	5.374	3.659	99.98	25449	0.384*
SHHA	0.01	34	2.66	0.2442	0.3606	6.796	5.320	3.633	99.97	20587	0.414*
SHHA	0.05	34	2.66	0.2105	0.3303	6.569	5.101	3.512	99.97	21677	0.364*
SHHA	0.05	34	2.66	0.2466	0.3222	6.086	4.823	3.186	99.95	11770	0.366*
SHF1-3	0.01	44	2.62	0.3658	0.2347	6.882	5.287	3.559	99.95	14181	0.575*
SHF1-3	0.01	33	2.62	0.3616	0.2278	6.922	5.397	3.626	99.95	11784	0.524*
SHF2-2	0.01	23	2.21	0.2524	0.3096	6.680	5.327	3.628	99.97	11026	0.137
SHF2-2	0.01	24	2.21	0.2459	0.3076	6.706	5.370	3.717	99.97	11499	0.221
SHF3-2	0.01	29	2.95	0.2628	0.2951	6.306	4.951	2.629	99.97	16553	0.289
SHF3-2	0.01	30	2.95	0.2445	0.2915	6.447	5.074	3.133	99.97	19143	0.314*
SHF4-2§	0.01	29	4.00	0.1913	0.2999	6.451	4.965	-5.517	99.98	19018	0.295
SHF4-2§	0.01	29	4.00	0.1873	0.2961	6.450	4.987	-4.618	99.96	12163	0.603*
WPHA	0.005	49	3.54	0.2305	0.3291	6.906	5.370	3.623	99.97	25800	0.768*
WPHA	0.005	37	3.54	0.2173	0.3442	7.298	5.587	3.747	99.94	11412	0.750*
WPHA	0.01	55	3.54	0.2254	0.3259	6.661	5.187	3.530	99.98	52729	0.684*
WPHA	0.01	39	3.54	0.2112	0.3441	7.030	5.357	3.506	99.96	15791	0.652*
WPHA	0.05	56	3.54	0.1913	0.3120	6.388	4.930	3.199	99.98	41779	0.701*
WPHA	0.05	38	3.54	0.2156	0.3132	6.175	4.839	3.190	99.97	20436	0.451*
WPHA	0.10	35	3.54	0.1907	0.3359	6.387	4.822	2.815	99.97	17798	0.447*
WPHA	0.10	33	3.54	0.1950	0.3121	6.416	4.914	3.168	99.97	19635	0.341*

Table 5.10a Summary of fits of protonation data for humic acids to model incorporating a lognormal distribution of protonation constants and fixed concentration of acidic groups. [a]Adjustable parameters, Equation 5.10; [b]singly lagged residual autocorrelation coefficient (* $p<0.05$). Optimisation by minimising relative residuals with respect to $C_L(1 - \alpha)$.

Humic acid	$[NaNO_3]$ /mol L^{-1}	No. of data	Fixed C_L /meq g^{-1}	log K_μ[a]	σ_K[a]	R^2 (%)	F	r_1[b] (all *)
SH	0.005	33	2.66	5.118	0.8970	89.7	300	0.982
SH	0.005	32	2.66	5.268	0.8533	83.2	197	0.982
SH	0.01	33	2.66	5.083	0.8866	86.3	226	0.983
SH	0.01	33	2.66	5.053	0.9974	92.1	393	0.982
SH	0.05	34	2.66	4.733	0.6373	74.9	127	0.983
SH	0.05	34	2.66	4.597	0.7475	83.2	190	0.983
SHF1-3	0.01	44	2.62	5.309	1.133	84.2	266	0.964
SHF1-3	0.01	33	2.62	5.359	1.096	80.5	159	0.964
SHF2-2	0.01	23	2.21	4.613	0.6750	79.0	129	0.966
SHF2-2	0.01	24	2.21	5.072	1.162	95.4	1002	0.967
SHF3-2	0.01	29	2.95	4.572	1.187	89.6	261	0.968
SHF3-2	0.01	30	2.95	4.623	1.137	89.7	271	0.970
SHF4-2	0.01	29	4.00	4.130	1.432	89.3	252	0.970
SHF4-2	0.01	29	4.00	4.102	1.440	88.5	235	0.972
WP	0.005	51	3.54	5.166	1.292	96.4	1351	0.982
WP	0.005	37	3.54	5.195	1.326	95.8	838	0.952
WP	0.01	56	3.54	4.870	0.9026	87.5	434	0.980
WP	0.01	39	3.54	4.982	1.314	95.1	752	0.975
WP	0.05	59	3.54	4.542	1.072	91.8	694	0.977
WP	0.05	39	3.54	4.538	1.125	94.5	670	0.979
WP	0.10	36	3.54	4.395	1.330	94.9	667	0.980
WP	0.10	34	3.54	3.964	1.488	92.8	447	0.981

Table 5.10b Summary of fits of HA protonation data to a lognormal distribution of protonation constants/fixed C_L model. Optimisation by minimising absolute residuals with respect to $C_L(1 - \alpha)$ (no systematic data weighting). [a]Adjustable parameters, Equation 5.10; [b]singly lagged residual autocorrelation coefficient (* $p<0.05$).

Humic acid	$[NaNO_3]$/ mol L^{-1}	Number of data	Fixed C_L /meq g^{-1}	log K_μ	σ_K	R^2 (%)	F	r_1[b] (all *)
SHHA	0.005	34	2.66	5.022	1.445	99.6	4278	0.820
SHHA	0.005	34	2.66	4.968	1.518	99.4	2475	0.859
SHHA	0.01	34	2.66	4.981	1.535	99.7	5231	0.796
SHHA	0.01	34	2.66	4.960	1.499	99.7	5304	0.791
SHHA	0.05	34	2.66	4.568	1.503	99.8	8846	0.709
SHHA	0.05	34	2.66	4.396	1.401	99.4	2867	0.819
SHF1-3	0.01	44	2.62	5.104	1.831	98.4	1346	0.901
SHF1-3	0.01	33	2.62	5.153	1.853	98.2	858	0.883
SHF2-2	0.01	23	2.21	4.850	1.558	98.4	1846	0.777
SHF2-2	0.01	24	2.21	4.874	1.527	99.5	2364	0.771
SHF3-2	0.01	29	2.95	4.375	1.748	98.4	847	0.834
SHF3-2	0.01	30	2.95	4.440	1.722	99.0	1411	0.840
SHF4-2	0.01	29	4.00	3.850	2.064	97.9	648	0.858
SHF4-2	0.01	29	4.00	3.813	2.093	97.6	573	0.868
WPHA	0.005	49	3.54	4.855	1.600	99.7	6873	0.913
WPHA	0.005	37	3.54	5.036	1.732	99.9	13513	0.727
WPHA	0.01	55	3.54	4.665	1.552	99.8	12053	0.891
WPHA	0.01	39	3.54	4.765	1.730	99.8	8221	0.807
WPHA	0.05	56	3.54	4.225	1.577	99.7	10382	0.897
WPHA	0.05	38	3.54	4.257	1.494	99.6	4366	0.841
WPHA	0.10	35	3.54	4.090	1.710	99.5	3641	0.787
WPHA	0.10	33	3.54	4.211	1.631	99.7	5206	0.737

Table 5.11 Summary of fits of protonation data for humic acids to the Sips binding equation. Unweighted regression with respect to $C_L(1 - \alpha)$. [a]Adjustable parameters, Equation 2.16); [b]singly lagged residual autocorrelation coefficient (* $p<0.05$).

Humic acid	$[NaNO_3]$ /mol L^{-1}	Number of data	Fixed C_L/ meq g^{-1}	A[a]	β[a]	log K_μ	R^2 (%)	F	r_1[b] (all *)
SHHA	0.005	34	2.66	0.03937	0.4374	5.024	99.3	4755	0.842
SHHA	0.005	34	2.66	0.03074	0.4204	4.971	99.0	3116	0.867
SHHA	0.01	34	2.66	0.03046	0.4186	4.983	99.4	5357	0.837
SHHA	0.01	34	2.66	0.03232	0.4254	4.963	99.4	5479	0.825
SHHA	0.05	34	2.66	0.02228	0.4264	4.573	99.6	7381	0.786
SHHA	0.05	34	2.66	0.02403	0.4504	4.402	99.0	3235	0.841
SHF1-3	0.01	44	2.62	0.01609	0.3594	5.106	97.9	2042	0.908
SHF1-3	0.01	33	2.62	0.01578	0.3543	5.156	97.7	1335	0.882
SHF2-2	0.01	23	2.21	0.01776	0.4126	4.851	99.0	2138	0.793
SHF2-2	0.01	24	2.21	0.01974	0.4198	4.877	99.2	2602	0.801
SHF3-2	0.01	29	2.95	0.00981	0.3746	4.382	97.8	1202	0.835
SHF3-2	0.01	30	2.95	0.01101	0.3805	4.446	98.5	1821	0.846
SHF4-2	0.01	29	4.00	0.00580	0.3296	3.869	97.1	937	0.864
SHF4-2	0.01	29	4.00	0.00545	0.3257	3.832	96.8	843	0.871
WPHA	0.005	49	3.54	0.03163	0.4088	4.861	99.3	6719	0.927
WPHA	0.005	37	3.54	0.02616	0.3774	5.046	99.7	10079	0.823
WPHA	0.01	55	3.54	0.02854	0.4161	4.667	99.5	10903	0.913
WPHA	0.01	39	3.54	0.02120	0.3796	4.772	99.5	7115	0.853
WPHA	0.05	56	3.54	0.01868	0.4152	4.235	99.4	8920	0.924
WPHA	0.05	38	3.54	0.02229	0.4300	4.267	99.2	4286	0.866
WPHA	0.10	35	3.54	0.01246	0.3855	4.104	99.1	3689	0.821
WPHA	0.10	33	3.54	0.01223	0.4021	4.225	99.3	4612	0.792

Table 5.12 Summary of fits of protonation data for humic acids to the Freundlich binding equation. Unweighted regression with respect to $C_L(1 - \alpha)$. [a]Adjustable parameters, Equation 2.15); [b]singly lagged residual autocorrelation coefficient (* $p<0.05$).

Humic acid	$[NaNO_3]$ /mol L^{-1}	Number of data	Fixed C_L/ meq g^{-1}	$A^a/10^3$	β^a	log K_μ	R^2 (%)	F	r_1^b (all *)
SHHA	0.005	34	2.66	1.836	0.2397	3.612	96.0	792	0.891
SHHA	0.005	34	2.66	1.643	0.2322	3.521	95.2	662	0.897
SHHA	0.01	34	2.66	1.666	0.2327	3.540	96.2	849	0.893
SHHA	0.01	34	2.66	1.732	0.2370	3.547	96.3	860	0.887
SHHA	0.05	34	2.66	1.805	0.2579	3.329	97.4	1254	0.875
SHHA	0.05	34	2.66	2.026	0.2782	3.267	96.4	885	0.882
SHF1-3	0.01	44	2.62	1.141	0.2006	3.421	94.0	701	0.922
SHF1-3	0.01	33	2.62	1.085	0.1941	3.422	93.3	464	0.895
SHF2-2	0.01	23	2.21	1.228	0.2406	3.496	95.9	512	0.838
SHF2-2	0.01	24	2.21	1.310	0.2454	3.542	96.2	580	0.851
SHF3-2	0.01	29	2.95	1.119	0.2304	3.031	94.2	469	0.853
SHF3-2	0.01	30	2.95	1.203	0.2346	3.111	95.4	604	0.869
SHF4-2	0.01	29	4.00	1.121	0.2219	2.531	94.3	472	0.878
SHF4-2	0.01	29	4.00	1.086	0.2201	2.489	93.9	441	0.883
WPHA	0.005	49	3.54	2.175	0.2393	3.295	96.0	1174	0.941
WPHA	0.005	37	3.54	1.667	0.2068	3.255	96.5	1010	0.896
WPHA	0.01	55	3.54	2.120	0.2450	3.173	97.1	1836	0.943
WPHA	0.01	39	3.54	1.725	0.2210	3.111	96.7	1116	0.906
WPHA	0.05	56	3.54	2.127	0.2662	2.926	97.4	2068	0.946
WPHA	0.05	38	3.54	2.243	0.2699	2.972	96.7	1095	0.899
WPHA	0.10	35	3.54	1.682	0.2482	2.728	96.8	1042	0.871
WPHA	0.10	33	3.54	1.530	0.2602	3.061	97.2	1116	0.854

Table 5.13 Summary of fitted parameters and statistical tests for fits of protonation data to Teasdale modification/self-association binding model. [a]Adjustable parameters, Equation 5.13; [b]singly lagged residual autocorrelation coefficient (* $p<0.05$).

Humic acid	$[NaNO_3]$ /mol L^{-1}	Number of data	C_L[a]/ mmol L^{-1}	log K_{ML}[a]	log K_S[a]	R^2 (%)	F	r_1[b] (all *)
SHHA	0.005	34	0.1595	5.889	0.2633	95.6	349	0.943
SHHA	0.005	34	0.1540	5.918	7.421	96.1	393	0.943
SHHA	0.01	34	0.1546	5.913	7.427	95.1	318	0.946
SHHA	0.01	34	0.1547	5.875	7.426	95.3	330	0.949
SHHA	0.05	34	0.1416	5.591	7.376	95.5	341	0.947
SHHA	0.05	34	0.1366	5.427	7.342	97.4	602	0.932
SHF1-3	0.01	44	0.1399	6.387	7.471	95.0	408	0.957
SHF1-3	0.01	33	0.1396	6.416	7.469	94.7	285	0.927
SHF2-2	0.01	23	0.1027	5.876	7.666	96.3	267	0.895
SHF2-2	0.01	24	0.1033	5.893	7.676	96.0	260	0.896
SHF3-2	0.01	29	0.1168	5.679	-2.204	97.2	462	0.931
SHF3-2	0.01	30	0.1186	5.715	-2.386	96.5	386	0.937
SHF4-2	0.01	29	0.1392	5.675	7.189	97.5	527	0.943
SHF4-2	0.01	29	0.1374	5.680	7.098	97.6	553	0.943
WPHA	0.005	49	0.1919	5.944	7.225	94.4	411	0.956
WPHA	0.005	37	0.1978	6.060	7.222	91.8	207	0.948
WPHA	0.01	50	0.1940	5.671	7.158	94.3	416	0.972
WPHA	0.01	39	0.1898	5.889	7.204	93.4	273	0.959
WPHA	0.05	50	0.1733	5.390	7.106	95.6	537	0.971
WPHA	0.05	38	0.1735	5.373	7.128	96.7	525	0.947
WPHA	0.10	35	0.1630	5.401	7.125	95.9	389	0.958
WPHA	0.10	33	0.1237	5.464	-33.27	95.3	319	0.938

5.4 Discussion

5.4.1 Acidimetric measurements

5.4.1.1 $Ba(OH)_2$ Displacement

It is unlikely that the variability observed in total acidity measured by this method (Table 5.1) is due to physical differences between replicates. A more realistic explanation may be with the nature of the filtration step. Perdue (1985) stated that potential for error in detection of end points may exist when substantial dissolved or colloidal humic substance remains in the filtrate that is titrated. Since filtration in these determinations was through a 0.45 μm membrane, it is probable that soluble or finely colloidal humic substances were not removed by filtration.

As well as providing an estimate of the total amount of acidic sites on humic acids, it is possible that the quantity measured by the $Ba(OH)_2$ method has some further utility. Its usefulness as an estimate for metal binding capacity is possibly questionable, since it is unlikely that all proton binding sites are significant binding sites for metal ions, especially at pH values which are environmentally relevant. Considering the difficulty in obtaining meaningful estimates of metal binding capacity, however (Perdue, 1989), $Ba(OH)_2$ acidity is possibly the most suitable operational estimate of this quantity available.

5.4.1.2 NaOH dissolution/HCl titration

A potential problem with this method is the strong possibility of CO_2 uptake by the NaOH/sodium humate solution in the early stages of the titration. End points are, however, steeper than for direct titration, since residual NaOH is titrated with strong acid. In addition, the procedure used to remove inorganic contaminants from the humic acids (washing with HCl/HF mixtures) is a potential source of

error. Residual HCl or HF may remain in the humic acids (possibly as humic - hydrochlorides or hydrofluorides) despite the subsequent dialysis procedures used. Such residual acid would obviously cause spuriously high results. A further explanation for the observed discrepancy may be that titration of these humic acids shows considerable hysteresis on back - titration with acid. Such behaviour has been observed previously (Flaig *et al.*, 1975; Sposito and Holtzclaw, 1977).

Overall, although this method gives good estimates of the numbers of protons titrated at fixed pH values, no information on intermediate inflections in the titration curve is available (since only unreacted base is titrated). Thus, this method only offers information about amounts of acidic groups titrated as a function of pH over a restricted range.

5.4.1.3 Direct titration

This method makes the assumption that the ion - exchange resin used to prepare the humic acid solutions does not interact in any way with humic substances. Unfortunately the red - brown colour of DOWEX resin precluded visual inspection of columns for humic substance adsorption. The fact that both the resin matrix and dissociated humic substances have an overall negative charge tends to suggest that adsorption or ion exchange processes are unlikely. If this assumption is correct, the humic acid solution produced will be a representative, unfractionated sample of the original humic acid. It should be mentioned that strong cation exchange resins have been used in the hydrolysis of humic substances (Parsons, 1989). The short contact times ($\leq$ 30 minutes) and low (ambient) temperatures used should, however, reduce the risk of hydrolysis, especially for humic acid preparations such as these where HCl/HF pretreatment has been performed.

Titre values at selected fixed pH values are consistently lower using this method than those determined by NaOH dissolution/HCl titration (Table 5.3). Possible explanations for this are outlined in Section 5.4.1.2 above. A further possibility is that the humic acids are not fully exchanged with hydrogen ions

by elution through a column of Dowex 50W-X8 cation exchange resin. This possibility, however, is considered to be unlikely for the following reasons. Firstly, the acid groups on the polystyrene sulphonic acid Dowex resin are strong; benzene sulphonic acid has a pK_a of 0.70 (Weast *et al.*, 1983). As a result, only acidic groups with a similarly small protonation constant would remain incompletely exchanged after elution. Secondly, the Dowex resin column always contained a large excess of hydrogen ions on an equivalent basis with respect to the aliquots of sodium humate solution applied. Finally, a check was performed by eluting some humic acid samples twice through the column and measuring their pH values. No significant pH difference was found between singly and doubly resin-treated humic acid solutions, suggesting that no further humic acid protonation was occurred during the second resin treatment.

The observation that a solution (or extremely stable sol) of a fully proton - exchanged humic acid may be prepared in this way is of some interest. Humic acids are operationally defined as being insoluble in acid aqueous solution. Separation of humic acids from crude humic substances, however, is generally achieved with an excess of hydrogen ions at a pH of 1 or 2. Humic acid solutions prepared using ion - exchange resin only contain sufficient hydrogen ions to satisfy the charge balance of dissociated acidic groups, and have a pH of approximately 4.2 - 4.4 in the absence of added electrolyte. In addition, the degree of dissociation of a humic acid (with respect to -COOH groups) in such solutions was typically in the range 0.3 - 0.45, and the corresponding charge on the macromolecules should be sufficient to ensure aqueous solubility. Even if moderate concentrations of electrolyte are added, the humic acid solution remains stable. This may be due, in part, to electrolyte counterions (cations) displacing hydrogen ions in the immediate vicinity of the macromolecule, allowing further dissociation. This macro-ionic effect is observed for both SHHA and WPHA; for both humic substances the degree of dissociation at any level of NaOH addition increases with increasing ionic strength. In other words, the acidic groups on the humic acid macromolecules are effectively stronger (have smaller protonation constants) at higher ionic strength. This effect is illustrated more fully by comparing plots of apparent pK_a *versus* degree of dissociation at varying ionic strength; such plots for both humic acids appear in Figures 5.4 and 5.5.

The position of the inflection observed in the pH range 7.5-7.8 suggests that it corresponds to an end point for titration of humic acid carboxylic acid groups. The relatively low slope of this inflection suggests that buffering from a small proportion of acidic groups is occurring in this region, but most naturally occurring carboxylic acid moieties should be titrated below pH 7.5, even when polyelectrolyte behaviour causes enhancement of proton binding. Phenolic groups in many chemical environments expected for humic substances (for example, with activating substituents such as -OH, para-COOH or in condensed aromatic structures) have pK_a values in the range 9.3-9.9 (Weast *et al*, 1983) and thus would make only a small contribution to measurable acidity at pH 7.8. Clearly, the decision to assign the observed titration curve inflection to complete titration of humic acid carboxylic acid groups is an operational one (Perdue, 1985); it is conceivable that some COOH groups remain protonated, while some weaker acidic groups such as phenols are partially dissociated. It is considered that defining the titration end point for humic acid carboxylic acid functional groups in terms of an observable inflection, is no less arbitrary, and has greater physicochemical significance, than defining an arbitrary pH value to define the same end point.

This end point has been used a basis for calculating the degree of dissociation of the the titrated humic acids, and thus in calculating parameters for subsequent data analysis such as apparent dissociation constants. It follows, then, that such calculated quantities are also operational, and do not necessarily correspond to the physical state of the humic substance macromolecules. The very presence of a titration curve inflection, however, means also that the degree of ionisation of the macromolecule does not change appreciably over a certain pH range. Thus, quantities such as degree of dissociation (with the assumption that this inflection is an end point) can be taken to represent a hypothetical macromolecule containing only the (carboxylic) acid groups titrated before the observed inflection. This hypothetical representation of humic substance macromolecules is not unreasonable; carboxylic acid groups form the major proportion of humic substance acidic groups. The range of effective protonation constants shown by humic acid COOH groups means that they are the major controllers of humic acid potentiometric properties in the environmentally significant pH range.

5.4.2 Protonation Behaviour of SHHA and WPHA as a Function of Ionic Strength

In Section 5.1 it was mentioned that analysis of protonation data for humic acids obtained over a range of ionic strengths could yield information regarding the conformation of the macro-ions in solution. The relevant analyses of protonation data are those proposed by Marinsky and coworkers (Marinsky *et al.*, 1982; Merle and Marinsky, 1984; Marinsky and Ephraim, 1986; Marinsky, 1987). Their reasoning is based on the use of a Donnan equilibrium model, which assumes that humic substance macromolecules can be described by a separate (gel) phase, in which the prevailing conditions in the bulk solution are not necessarily operative. The analysis of the theory of Donnan equilibria by Marinsky and coworkers yielded several conclusions (Marinsky and Ephraim, 1986); these are outlined below.

(i) If, for humic acid protonation data obtained at different ionic strengths, plots of pK_{app} *versus* (pH + pX) are coincident at all ionic strengths, then the separate phase defined by the humic substance must be *rigid* and *permeable* to the diffusible components of the system. (pX is $-\log[X^-]$, where X is the electrolyte anion, for example NO_3^-.)

(ii) Similarly, if plots are made of pK_{app} *versus* pH, then coincidence of these plots for experiments at different ionic strengths indicates that the separate (gel) phase must be *rigid* and *impermeable* to the diffusible components of the system.

The definition of *rigidity* used here is that the volume of the gel matrix is independent of ionic strength, but may vary due to changes in other conditions (such as degree of dissociation).

Recently, however, the conclusions of Marinsky and coworkers have been criticised by Cabaniss and Morel (1989). These authors state that coincidence of pK_{app} *versus* (pH + pX) plots for data obtained at different ionic strengths will not necessarily occur for a rigid and permeable polyelectrolyte, especially

if more than one type of acidic site is present. A more rigorous test for rigidity/permeability of polyanions such as humic substances (Cabaniss and Morel, 1989) is by checking for coincidence of plots of (pH - pX) *versus* degree of dissociation (α).

In addition, Cabaniss and Morel (1989) state that coincidence of plots of pK_{app} *versus* pH at different ionic strengths do not imply rigidity and impermeability, since such plots are also coincident for small acids. Rather, the uniqueness of such plots implies the absence of a separate Donnan phase.

5.4.2.1 Plots of apparent dissociation constant *versus* degree of dissociation

Inspection of plots of pK_{app} *versus* α (Figures 5.4 and 5.5) shows that the curves obtained from experiments at different ionic strength are not coincident for either SHHA or WPHA. This implies that both humic acids behave as polyelectrolytes having variably charged surfaces (Ephraim *et al.*, 1986). In addition, the change in pK_{app} observed over the range of α is larger than that observed for a polyelectrolyte with a single type of acidic site, and thus implies acidic functional group heterogeneity (Ephraim *et al.*, 1986). A further indication that these humic acids contain more than one type of acid functional group was obtained by fitting the data to the modified Henderson - Hasselbalch equation (Equation 5.8). Table 5.6 summarises fits to this equation for SHHA and WPHA. Without exception, the magnitude of the composite electrostatic interaction term, η, is greater than 2 which is the maximum possible value for a polyelectrolyte with a single type of acidic functional group (Dempsey and O'Melia, 1983).

5.4.2.2 Plots of apparent dissociation constant *versus* pH

Inspection of plots of pK_{app} *versus* pH (Figures 5.6 and 5.7) offers further information. For SHHA (Figure 5.6), these plots appear to coincide (within experimental error) where [$NaNO_3$] is 0.005 and 0.01

mol L^{-1}. According to Cabaniss and Morel (1989) this may imply that SHHA does not exist as a separate Donnan phase in this ionic strength range. The plot of pK_{app} *versus* pH for SHHA at [$NaNO_3$] = 0.05 mol L^{-1} does not coincide with those at lower ionic strength, however, making any conclusions ambiguous. For WPHA, plots of pK_{app} *versus* pH (Figure 5.7) are more closely spaced, tending to coincide for [$NaNO_3$] $\geq$ 0.05 mol L^{-1}. The implication of such coincident plots is that WPHA does not exist as a separate Donnan phase at higher inert electrolyte concentrations (Cabaniss and Morel, 1989); it is conceivable that electrostatic effects of the macromolecule are masked at higher ionic strength. At higher neutral salt concentrations, the difference in counterion activity between that in the bulk solution and that in the domain of the macromolecule may become negligible, even for quite highly charged macro-ions (Tanford, 1961). The result of this is that there is effectively no longer a separate phase defined by the domain of the macro-ion.

5.4.2.3 Plots of apparent dissociation constant *versus* (pH + pNO_3)

For SHHA, these plots (Figure 5.8) are not inconsistent with behaviour expected for a rigid and permeable Donnan phase macro-ion with acidic functional group heterogeneity (Cabaniss and Morel, 1989). The observation that these plots do not coincide, however, makes this deduction of solution conformation rather ambiguous. A similar situation exists for WPHA (Figure 5.9). Plots of pK_{app} *versus* (pH + pNO_3) cannot be interpreted to discount the possibility that WPHA exists in solution as a rigid, permeable Donnan phase, but again the situation cannot be resolved unequivocally due to acidic functional group heterogeneity.

For both humic acids, the slope of these plots is close to 0.5, a property expected (Marinsky, 1989) for rigid gels. The observation that this slope is maintained to high degree of dissociation, however, means that the humic acid macro-ions must *decrease in volume* with increasing dissociation (Marinsky, 1989). This seems unlikely for humic acids if a flexible, linear macromolecular structure (Cameron *et al.*, 1972; Hayes and Swift, 1978) is assumed to be correct.

5.4.2.4 Plots of (pH - pNO_3) *versus* degree of dissociation

Coincidence of these plots at different ionic strength implies a rigid, permeable conformation for a Donnan phase polyanion (Cabaniss and Morel, 1989). For SHHA (Figure 5.10), such plots are not coincident for experiments at different ionic strength, and this implies that SHHA does not exist as a rigid and permeable Donnan phase under these solution conditions.

The situation for WPHA is less clear-cut; there is less separation of (pH - pNO_3) *versus* α plots (Figure 5.11) at different ionic strength, and plots for $[NaNO_3]$ = 0.005, 0.01 and 0.05 mol L^{-1} may be interpreted as being coincident, within experimental error. It is possible, then, that WPHA exists in solution as a rigid and permeable Donnan phase over the ionic strength range 0.005 - 0.05. The observation that this behaviour does not extend to $[NaNO_3]$ = 0.10 mol L^{-1} may result from masking of electrostatic effects at this higher ionic strength, and the corresponding loss of a separate macro-ionic Donnan phase.

Overall, the results for WPHA from this section of work seem to indicate noticeable changes in conformation with ionic strength, observations consistent with a flexible macromolecular structure. Plots of both pK_{app} *versus* α (Figure 5.5), and pK_{app} *versus* pH (Figure 5.7), are essentially coincident at $[NaNO_3]$ = 0.05 and 0.10 mol L^{-1}, but are not at lower ionic strength. These two results suggest (Ephraim *et al.*, 1986; Cabaniss and Morel, 1989) a rigid and permeable conformation for WPHA in this higher ionic strength range. This is not, however, in agreement with conclusions suggested by coincidence of (pH - pNO_3) *versus* α plots, that is, a rigid and impermeable conformation especially at lower ionic strength.

The variation in degree of expansion (or volume) of flexible macro-ions with changing ionic strength and/or degree of dissociation is well documented (Tanford, 1961; Morawetz, 1975). If a flexible, linear macro-ionic structure proposed for humic acids is correct, then it would be unlikely that the average volume occupied by solvated humate macro-ions would remain constant with changing ionic strength as

implied by Marinsky's definition of rigidity. The results from this investigation tend to support a non-rigid or flexible, variable-volume solution conformation for humate macro-ions.

5.4.3 Protonation Behaviour of Summit Hill Humic Acid Molecular Size Fractions

5.4.3.1 Carboxyl acidity as a function of molecular size

It is clear from inspection of Table 5.5 that carboxyl acidity measured by this method is not simply related to elution volume on Sephadex carboxymethyldextran gels. This implies that -COOH content is not simply related to molecular weight in a mixture of humic acid macromolecules. The results do, however, show a general increase in -COOH content with increasing elution volume on Sephadex. This result is not unexpected; it is well established (for example, Stevenson (1982)) that smaller humic substance molecules (for example, fulvic acids) tend to be more substituted by oxygen containing functional groups than humic substance macromolecules having higher molecular weight. These results fit in well with the concept that 'humic' and 'fulvic' acids are not distinct entities but members of a continuous series of substances with globally similar properties.

5.4.3.2 Titration Curve Inflections

It is evident from inspection of Figure 5.12 that the proton buffering behaviour of the SEC fractions of SHHA shows substantial variability between fractions. The most obvious difference is the presence of two inflections in the titration curve of Fraction 1-3, the fraction with the lowest SEC elution volume and thus highest effective molecular size. On closer inspection, it is possible to interpret the $\Delta pH/\Delta V$ *versus* NaOH titre of Fractions 2-2 and 3-2 as indicating a less obvious inflection in the same pH range, apparent as shoulders before the main peak in the curves.

The most conventional explanation for two titration curve inflections would be that they are caused by a mixture of at least two independent, monoprotic weak acids. (The possibility of a simple *diprotic* acid may be discounted, since the second inflection occurs at less than twice the titre of the first.) Two of these acids must have pK_a values sufficiently different to produce distinguishable buffering zones in the observed titration curve. The first observed buffering zone (and thus approximate pK_a value) is centered in the pH range 4.6 - 4.7, and covers a wider titre volume range than the second, buffering in the pH range 6.7 - 6.9. The pK_a value implied by the position of the first buffering zone is consistent with a hypothesis that isolated carboxylic acid groups are responsible for this buffering behaviour. It was found that data from titration of this fraction was described very well by a model incorporating two noninteracting acidic groups ($R^2 = 0.993$; Table 5.8). The positions of the observed zones of maximum buffering and the refined values of the two protonation constants ($\log K_1 = 6.68$; $\log K_2 = 4.07$; means from duplicate titrations), however, are not in perfect agreement, although this model predicts a value for the position of the intermediate inflection which is similar to that shown in the titration curve ($C_1/C_L = 0.534$). These results suggest that a two site model does not contain sufficient heterogeneity to explain the protonation behaviour. It was found that a three - acid model (Table 5.9) implied the existence of a third less abundant (c. 23% of C_L) site, with a log K value ($\log K_2 = 5.34$; mean from duplicate titrations) between the two implied by the observed zones of buffering.

Two other explanations are possible for the observed buffering zones and associated inflections in the titration curve of SHHA fraction 1-3. The first presumes that the first inflection is non-humic in origin (since this inflection is absent from all other humic acid titration curves in this work) and assigns the observed buffering behaviour to an inorganic or 'ash' component present as an impurity. Higher molecular weight humic acid fractions are often observed to have high ash contents (R.S. Swift, personal communication). It is unlikely, however, that the acidic component which is fully titrated by the first inflection is entirely due to an impurity, since this inflection occurs at >50% of the COOH titre.

In addition, both the HCl/HF pretreatment and the preparation of humic acid solutions using a cation exchange resin should have greatly reduced the levels of inorganic contaminants.

The second possibility is on the observation (Marinsky, 1987) that some weakly acidic polyelectrolytes undergo substantial conformational change on dissociation, resulting in titration curve discontinuities. Since humic acids are also considered to alter conformation during the dissociation process (Hayes and Swift, 1978), then it may not be unreasonable to suspect such a process to explain the behaviour observed for fraction 1-3 of the Summit Hill humic acid.

5.4.4 Modelling of the Protonation Behaviour of Humic Acids

5.4.4.1 Polyelectrolyte models

Both the modified Henderson - Hasselbalch equation, and the Hermans - Overbeek equation provided good empirical descriptions of proton binding data for all humic acid titration experiments. The modified Henderson - Hasselbalch equation, in general, modelled protonation data reasonably accurately (R^2 in the range 96.6 - 99.8%). The assumptions behind this equation, however, mean that it is unlikely that the fitted parameters have any physical meaning. As mentioned previously, however, the magnitude of the electrostatic interaction parameter (>2 for all humic acids) implies a degree of acidic functional group heterogeneity (Dempsey and O'Melia, 1983). The other fitted parameter for this equation (pK_{HH}), for the apparent dissociation constant at half neutralisation, is again useful for predictive purposes but has little physical significance.

The Hermans - Overbeek equation provided a slightly better fit of humic acid protonation data (R^2 in the range 99.6 - 100.0) than the modified Henderson - Hasselbalch equation. The fitted parameters are, again, of limited physical significance due to functional group heterogeneity. The first, the intrinsic dissociation constant (pK_{int}) would be of value in assigning a structure to acidic functionality in the

situation where only a single type of acidic group was present. The values for the composite electrostatic interaction term (-0.868ωn) again, however, imply functional heterogeneity and therefore values of pK_{int} should be interpreted with some caution, even though their fitted values seem to be physically realistic (pK_{int} in the range 1.8 - 3.86). In addition, with no data collected in the range $\alpha = 0$ to c. 0.4, the determination of pK_{int} involves an extrapolation outside the measurement range to $\alpha = 0$. As a result, the fitted estimates for pK_{int} may be less reliable than if data in the acid titration range ($\alpha = 0$ - 0.4) were available.

It should be remembered that the two polyelectrolyte models were not used to fit the entire range of titration data. Their main advantages are:

(i) ease of fitting data; (no sophisticated software is required) and;

(ii) good empirical description of humic acid protonation data in the pH range 4 - 7 (that is, they offer good predictive capability).

The good fit of both these models is achieved using only three parameters: the (fixed) total concentration of -COOH groups (C_L) which is determined independently from titration inflections, and the two (adjustable) linear regression parameters (pK_{HH} and η for the modified Henderson - Hasselbalch equation; pK_{int} and -0.868ωn for the Hermans - Overbeek equation).

5.4.4.2 Discrete site proton binding models

It was not expected that the protonation reaction of the humic acids studied would be described well in terms of a single, noninteracting acid. That this was the case was confirmed by the poor fits obtained when data were fitted to single acid models (Figure 5.13(a)); even when the total acid group

concentration was allowed to vary, agreement of observed and predicted values was poor. This is a general result with investigations of humic acid protonation (Perdue, 1985).

A much better description of humic acid protonation was obtained for all experiments by using models incorporating a hypothetical mixture of two or three noninteracting monoprotic acids. The slightly better fit obtained when C_L was allowed to vary is not unexpected, due to the greater degree of freedom in the regression. In these cases, however, the value of C_L predicted by the model was always lower than determined independently from titration inflections. This was probably due to the lack of titration data at higher levels of humic acid protonation, and emphasises the importance of making full use of independently determined parameters when formulating a model.

It is, however, unlikely that the discrete sites implied by the optimised parameters for these site binding models correspond to actual sites on the humic acid macromolecules. The very good fits observed are most likely to have resulted from the relatively high numbers of adjustable parameters in these models. Sposito (1982) shows that binding at a heterogeneous mixture of sites can always be described adequately by a two site binding model with four adjustable parameters. Gregor and Powell (1988b) suggested that the binding constants (log K_i) obtained by fitting discrete multisite models to fulvic acid titration data should be called 'titration constants' to avoid the implication that they are true thermodynamic constants. It would also be incorrect to consider the fitted parameters as being indicative of average thermodynamic constants for 'classes' of sites, as shown by Perdue and Lytle (1983).

When data from NaOH titration SHHA SEC fraction 4-2 was fitted to a three acid model, the final refined parameters (Table 5.9) implied that the third site was unnecessary for adequate description of protonation. In this case the value found for log K_3 (mean from two titrations = -5.07) implies a site which would never contribute significantly to proton binding. In fact, if the third site is ignored, the remaining two sites are described by parameters which very closely match the refined parameters from a two acid model where the total concentration of acid groups is allowed to vary. This observation further

reinforces the hypothesis that a two acid model is the most suitable discrete site binding model to describe the protonation reactions of SHHA fraction 4-2, even though the fit is improved markedly when a third site is included in the model (F(2 site) = 917; F(3 site) = 15591).

For all other protonation data, a three acid model was a better predictor of protonation behaviour than was a two acid model. F-tests (Section 3.6.6) indicated significantly better fits for titration data using the three acid model when compared with the two acid model, taking into account the greater degree of freedom in the regression model.

The poor agreement between refined estimates of binding site parameters for titration data of WPHA is most probably a function of the spacing of titration data. Titrations containing more data have a large amount of data collected near the titration inflection, that is, at low levels of $C_L(1 - \alpha)$. As a result, the regression may be somewhat biased towards binding at stronger sites (larger log K). This is found by inspection of Tables 5.8 and 5.9. Refined parameters for WPHA titrations comprised of closely spaced data tend to indicate stronger and more abundant proton binding sites than those with less data. This observation suggests an important point: that these site binding models are *empirical* in nature, and are dependent to a significant extent on the nature of the data.

As expected, refined parameters from the site binding models showed a systematic dependence on the ionic strength at which titration data were collected. For both the two and three acid models, optimised values of the binding parameters implied an increase in both the abundance and strength of the site with the lowest log K_i value (the strongest acid) with increasing ionic strength. Although the abundance of sites would not change with changing ionic strength (this is a result of the empirical nature of this binding model), this trend reflects the expected effect of ionic strength on apparent dissociation constants as a function of the macro-ionic characteristics of the humic acid macromolecules.

5.4.4.3 Continuous distribution multiligand models

The lack of weighting in the regression is in contrast to the recommendation made by Perdue and Lytle (1983) that a sum of squares of *relative* residuals should be minimised. Weighting of residuals in this way was found to result in rather poor descriptions of humic acid proton binding behaviour (Table 5.10a). Although under some circumstances unweighted regressions may cause inappropriate weighting of data obtained at higher values of ($C_L(1 - \alpha)$), these regressions were considered to be most appropriate for these sets of experimental data. This is partly due to the spacing of titre volume increments in the experiments. At lower levels of ($C_L(1 - \alpha)$) data are more closely spaced and thus the greater abundance of data in this area of the titration affords a certain degree of weighting in the regression. In addition, since only base titrations were performed, data at very high values of ($C_L(1 - \alpha)$) are absent. Finally, although predicted and observed values showed greater disagreement at low values of ($C_L(1 - \alpha)$) (high pH), these data occur in a pH range (7 - 8) which is unlikely to be encountered in the natural environment of either of the humic acids studied. Ambient pH values for the Summit Hill and Waimari Peat soils are c. 5.4 and 5.0 respectively (Appendices 2 and 3).

The observation that protonation data were generally described well by a model incorporating proton binding sites with a lognormal distribution of protonation constants (Table 5.10b) is in agreement with other authors (Perdue and Lytle, 1983). Protonation data was described better by this model than by the two acid model, with the exception of data from titration of SHHA fraction 1-3. This is not surprising in view of the fact that this humic acid fraction showed two distinct regions of buffering during titration (Section 5.4.3.2).

The refined values of log K_μ (Table 5.10b) are in the range expected for carboxylic acid functional groups. These values can not, however, be used to identify the 'most abundant' proton binding sites on the basis of a comparison of pK_a values. This is because the lognormal distribution model makes no distinction as to the source of the variation in protonation constants, and thus it is impossible to state

whether the observed protonation constants result from functional group heterogeneity or macro-ionic effects.

The general trend of optimised log K_{μ} values, for titrations of the same humic acid, is a decrease with decreasing ionic strength. Ionic strength has no effect, however, on optimised σ_K values. This trend is expected; at higher concentration of neutral salt, the electrical potential due to the charge of the humic acid macromolecule is masked, and as a result protons (or any ions) should be held less strongly.

One of the features of the lognormal distribution model is that it predicts a small number of very strong proton binding sites (very weak acidic functional groups) at the upper 'tail' of the distribution. This means that at higher degree of dissociation, predicted pH values are higher than actually observed and, in fact, this is the region of titration data which are most poorly described by this model.

If the lognormal distribution model is formulated such that C_L is an adjustable parameter, the refined value of C_L is always lower than that implied by titration inflections, as found for the discrete site binding models. The reason for this is the same as that described for the discrete binding models in Section 5.4.4.2.

Optimised values for log K_{μ} were also found to decrease with decreasing molecular size (inferred by increasing SEC elution volumes). This implies that the smaller humic acid molecules may contain a higher density of more strongly acidic sites. The standard deviations of the distributions show a general increase with decreasing molecular size, reinforcing the hypothesis that the smaller molecules are more strongly acidic. The trend for protonation constants to decrease (stronger acidic groups) with decreasing molecular size is supported by the binding parameters generated by the two and three acid models; both show a general decrease in both protonation constants and density of the strongest 'binding site' with decreasing molecular size. These observations imply differences in the chemical, rather than physical, nature of the acidic sites with changing molecular size. If the acidic sites on humic acid molecules were

chemically similar, then the higher charge density of the smaller molecules (Table 5.5) would be expected to enhance proton binding, giving effectively weaker acids.

The observation that the lognormal distribution model provides a good description of the protonation reactions of these humic acids suggests that the Freundlich and Sips equations should also model these data well. If the Freundlich equation is assumed to approximate the Sips equation, both these equations imply a distribution of protonation constants closely resembling a lognormal distribution. Good fits are indeed observed (Tables 5.11 and 5.12) indicating that these equations, which are much simpler to implement than the lognormal distribution model, could provide a convenient empirical model for humic acid protonation for predictive purposes. A further indication of the degree to which the Sips equation can approximate the lognormal distribution model may be obtained by inspection of refined values for log K_{μ} (Tables 5.10b and 5.11; Figure 5.16). Good agreement between log K_{μ} values for both these models is achieved for all sets of titration data. The lognormal distribution parameter σ_K perhaps provides a more logical measure of the spread of the distribution. A comparison of lognormal σ_K and Sips β values (Figure 5.16), however, shows that these parameters are approximately inversely proportional.

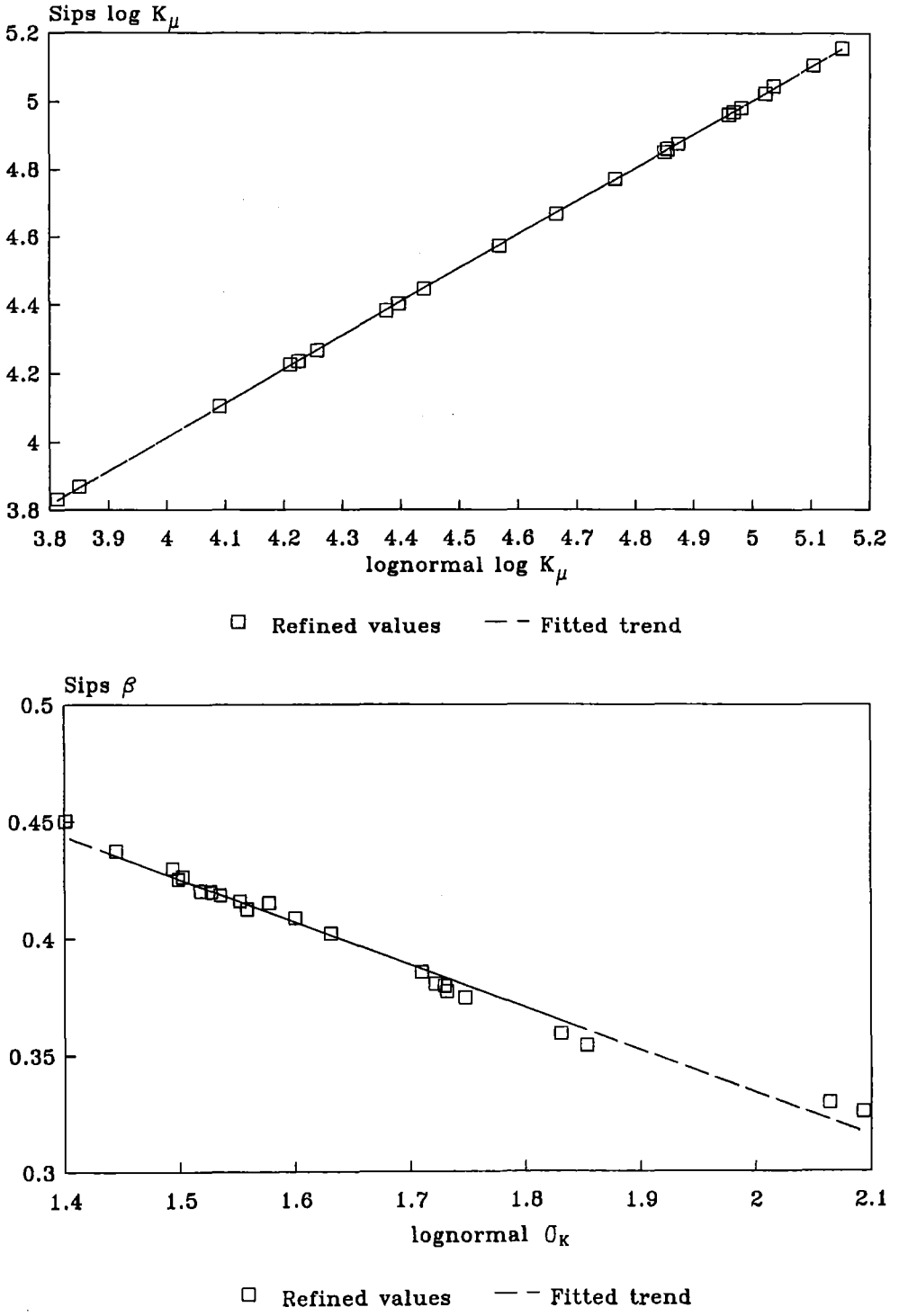

Figure 5.16 Relationship between parameters defining Sips and lognormal distribution models for humic acid protonation data.

5.4.4.4 Modification - self association model.

Of the two theoretical models based on aggregation processes presented by Teasdale (1987), this model is the only one which may be applicable to humic substance protonation. Teasdale's models were developed to explore the possibility that binding by polyvalent metal ions could involve self association or crosslinking processes. It is considered unlikely that univalent hydrogen ions would be involved in the type of crosslinking reaction suggested by Teasdale (1987). It is probable, however, that protonation of ionised humates could lead to aggregation through processes such as hydrogen bonding or nonpolar interactions.

Fixing f (Equations 5.12 and 5.13) at a value of 2 restricts the modification/self - association model to describing formation of linear aggregates only. It is probable, however, that 3-dimensional aggregates form as well. Chen and Schnitzer (1989), however, state that linear aggregates are commonly observed in electron microscopy studies of humic substances, especially from solutions at lower ionic strength.

The refined estimates for the parameter log K_s for this model (Table 5.13) showed substantial variability, and were possibly unrealistic in some cases. A value for log K_s of c. 7 was obtained in many cases; this is indicative of substantial aggregation under these experimental conditions. Physically improbable values for log K_s may result from the shortcomings of this model (which does not consider functional group heterogeneity) rather than indicating actual aggregation processes.

5.4.4.5 Comparison of models

All models used except the 'one acid' model modelled the protonation behaviour of SHHA and WPHA well enough to be used for predictive purposes in an environmentally significant pH range. The best fit was achieved by the three acid model. None of the models used, however, invoked an accurate description of the actual chemical and physical processes involved. Analysis of residuals in terms of a

singly lagged residual autocorrelation (Tables 5.6 - 5.12) often indicated that residuals were significantly autocorrelated. This indicated systematic trends in the data which were unexplained by the models, or a periodic character in the modelling equation which was not present in the data. Even for regressions where the combination of data and model gave poorly correlated residuals, plots of residual *versus* predicted values showed periodic trends in the residuals. If the model was correct, and all errors were random experimental deviations, the residuals should show no discernible trend over the range of data (Brook and Arnold, 1985). These observations further reinforce the deduction that none of the models fitted provide an accurate explanation of humic acid protonation reactions.

It is important to recognise that the models used only describe humic acid protonation over the range of conditions used in the titration experiments. This is especially relevant for the Henderson - Hasselbalch and Hermans - Overbeek models, where the limited range of titration data available was further reduced by truncating data close to the end point. It is likely that if a greater range of titration data was available, for example at lower degree of dissociation (lower pH), then the apparent heterogeneity would be greater and the less complicated models would become less appropriate.

As far as use of these models for predictive purposes is concerned, ease of implementation is as important as simple goodness of fit. In this respect, the discrete site binding models, specifically the three acid model, are favourable. These models may be formulated so that predictive calculations may be made conveniently using readily available software such as spreadsheet programs.

The Henderson - Hasselbalch and Hermans - Overbeek equations, while providing a good empirical description of protonation, are not so amenable to calculation. Quantities required by the model, such as the degree of dissociation, require knowledge of parameter(s) (that is, C_L) which are not explicitly contained in the fitted parameters.

Modelling the protonation reactions of humic acids in terms of a lognormal distribution of protonation constants provided a good (and intuitively acceptable) description of humic acid protonation.

Unfortunately, however, this model requires complex numerical calculations to be carried out and as such is not a convenient predictive model. As mentioned previously, the more empirical Freundlich or Sips equations imply a similar continuous distribution, and are more easily implemented. The heterogeneity parameter (β) in both of these models is, however, less comprehensible than the more commonly understood standard deviation in the lognormal model.

5.5 Summary

Humic acid solutions, prepared using a strong acid ion exchange resin, were titrated with standard alkali. For all humic acid preparations, a titration curve inflection was consistently observed in the pH range 7.5 - 7.8, which was attributed to complete titration of carboxylic acid functional groups.

The protonation behaviour of the humic acid carboxylate functional groups implied a degree of functional group heterogeneity which was found, by modelling studies, to be too large to be explained by macro-ionic, aggregational or statistical effects alone. It was thus inferred that a proportion of the heterogeneity in proton affinity was due to structural heterogeneity, a conclusion consistent with what is known of humic substance structure in general. All models, regardless of whether or not they had any physicochemical basis, were found to give essentially empirical descriptions of humic acid protonation reactions, even where models allowed close prediction of protonation behaviour.

Analysis of the ionic strength dependence of the humic acid protonation reactions confirmed the importance of macro-ionic effects. The behaviour of the humate macro-ions at different ionic strengths was consistent with a flexible, permeable solution conformation under the experimental conditions used.

The protonation behaviour of molecular size fractions of the Summit Hill reference humic acid showed differences in both the amounts and strengths of carboxylic acid functional groups. These differences

were considered to be due to chemical or structural differences rather than to physical differences such as charge characteristics.

CHAPTER SIX

COPPER AND CADMIUM BINDING BY SUMMIT HILL AND WAIMARI PEAT HUMIC ACIDS

6.1 Introduction

Measurements of the amounts of copper(II) and cadmium(II) bound to solid phase calcium humates and solution phase sodium humates, as a function of unbound metal ion, have been made using batch and continuous potentiometric titration techniques. The effect of temperature on the extent of metal binding was also studied.

The complexation reactions between soil humic substances and polyvalent metal ions are important determinants of metal speciation in soils (Stevenson, 1982, 1985; Sposito, 1984) and natural waters (Steinberg and Muenster, 1985; Malcolm, 1985). An understanding of these reactions is important to many applications, for example: trace element nutrition of plants (Ennis and Brogan, 1985); environmental response to input of pollutants, such as from industrial sources (de Haan and Zwerman, 1976) or sewage sludge application (Sposito *et al.*, 1979); and the effect of changes in soil acidity (Schnitzer, 1980). A reliable model for these reactions would contribute greatly to the ability to make predictions about (equilibrium) speciation of trace metal ions in soil systems.

In addition, the response of humic substance - metal ion complexation reactions to changes in temperature is important when considering seasonal temperature changes in soils, and in light of contemporary research into anthropogenic energy inputs into many environments (Schneider, 1989).

6.2 Materials and Methods

6.2.1 Copper(II) and Cadmium(II) Binding to Calcium Humates

Samples of SHHA and WPHA were converted to the corresponding calcium humates using the procedures outlined in Section 3.2.2. The relationships between bound and unbound Cu^{2+}, and bound and unbound Cd^{2+}, on Summit Hill calcium humate (SHCa) and Waimari Peat calcium humate (WPCa) were determined by batch titration/ion selective electrode potentiometry as outlined in Sections 3.4.1 and 3.3.2. All experiments were performed at pH 6.00 and 0.05 mol L^{-1} $Ca(NO_3)_2$. Generally, 10 - 12 additions of metal ion were made, in the ranges 0 - 0.10 mmol g(humate)$^{-1}$ for Cu^{2+} and 0 - 0.06 mmol g(humate)$^{-1}$ for Cd^{2+}. Uncomplexed Cu^{2+} or Cd^{2+} was determined in the solution phases of the reaction systems using ion selective electrodes (Section 3.3.2) after phase separation by centrifugation/membrane filtration. The amount of metal ion bound to the solid phase calcium humate was determined by difference between total added and free metal ion, assuming zero Cu or Cd content for either calcium humate. This calculation method assumed, not unrealistically, that the contribution to binding by any dissolved humates present (Chapter 3, Section 3.4.1) was negligible. In fact, for Cd^{2+} binding to calcium humates, the total amount of Cd in the solution phase (measured by ASV) was found to be approximately equal to unbound solution phase Cd^{2+} (determined by ISE potentiometry). Similar measurements for Cu^{2+}-calcium humate binding revealed that total solution phase Cu concentration (ETAAS or ASV) was between 1.6 to 25 times greater than unbound copper concentration (ISE). It was considered, however, that the relatively poor quality of Cu^{2+}-calcium humate binding data did not justify more detailed analysis on the basis of these observations.

Duplicate experiments for all combinations of humate and metal ion were performed at each of three temperatures: 5 ° C, 20 ° C and 40 ° C.

6.2.2 Copper(II) and Cadmium(II) Binding to Sodium Humates

Samples of Summit Hill and Waimari Peat humic acids were converted to the corresponding sodium humates using the procedure described in Section 3.2.2.

The extents of binding of Cu^{2+} and Cd^{2+} to Summit Hill sodium humate (SHNa) and Waimari Peat sodium humate (WPNa) were determined by continuous titration/ion selective electrode potentiometry as described in Section 3.4.2 and 3.3.2. All experiments were performed at pH 6.00 and 0.10 mol L^{-1} $NaNO_3$. Titrations involved 12 - 25 additions of Cu^{2+} or Cd^{2+} in the approximate ranges 0 - 0.65 mmol g(humate)$^{-1}$ for Cu^{2+} titrations and 0 - 0.45 mmol g(humate)$^{-1}$ for Cd^{2+} titrations. Uncomplexed Cu^{2+} or Cd^{2+} was determined in the titration solution after each addition using the appropriate (Cu or Cd) ion-selective electrode (Section 3.3.2). The amount of metal ion bound to the solution phase sodium humate was determined at each point in the titration by difference, assuming zero initial metal ion content for either SHNa or WPNa. Since pH was maintained by addition of standard alkali and acid following metal ion additions, it was also possible to estimate proton release as a function of bound metal ion (allowing for the HNO_3 present in the metal ion titrant solutions).

Duplicate experiments for all combinations of sodium humate and metal ion were performed at 20° C and 40° C.

6.2.3 Effect of Temperature Reduction on Copper(II) Binding to Waimari Peat Calcium Humate

An experiment was designed to check whether a reduction in temperature in a Cu^{2+}-WPCa system would result in an increase in the concentration of unbound copper. Copper(II) (0.25 mmol g(humate)$^{-1}$) was added to duplicate suspensions of WPCa (0.100g) in 500 mL 0.05mol L^{-1} $Ca(NO_3)_2$ and the suspensions adjusted to pH 6.0. These suspensions were equilibrated at 40° C for c.

50 hours, at 20 ° C for a further c. 50 hours, and at 5 ° C for a final c. 50 hours. At the end of each 50-hour equilibration period (immediately prior to a temperature change) the suspensions were sampled. Unbound Cu^{2+} was determined in the filtered (0.45 μm membrane) samples by ion-selective electrode potentiometry as described in Sections 3.3.2 and 3.4.1.

6.2.4 Modelling Complexation Reactions

The nonlinear optimisation program described in Section 3.6 was used with appropriate subroutines to fit metal-humate binding data to various model equations as described in Section 2.4. When C_L was a fixed parameter in regressions for any model, the value used was equal, on an equivalent basis, to the total titratable acidity of the corresponding humic acid (Chapter 5, Table 5.2).

As with protonation data (Chapter 5) data derived from the titration procedures described in Section 6.2.1 and 6.2.2 were initially fitted to a family of discrete site-binding models. The general form of the site-binding equation used for Cu^{2+} and Cd^{2+} binding to calcium humates was:

$$C_{ML} = C_L \sum_{i=1}^{n} \frac{\chi_i K_i [M]}{(1 + K_i [M])} \qquad (6.1)$$

where n is the number of discrete sites (n = 1, 2 or 3);

C_{ML} is the sum over all forms of bound M (M = Cu^{2+} or Cd^{2+});

C_L is the total amount of available sites;

χ_i is the mole fraction of the i^{th} site with respect to C_L;

and K_i is the conditional M-complex formation constant for the i^{th} site.

For Cu^{2+} and Cd^{2+} binding to sodium humates, the site binding equation used was:

$$C_{ML} = C_L \sum_{i=1}^{n} \frac{C_i}{C_L} \frac{K_i[M]}{(1 + K_i[M])} \qquad (6.1b)$$

where C_i is the concentration of the i^{th} site.

For either of these equations, the total amount of binding sites, C_L, could be treated as an adjustable parameter and refined implicitly in regressions as the sum over all C_i. Alternatively, C_L could be fixed at a predetermined value, allowing one of the C_i to be omitted from the regression since it is defined by the difference between C_L and the remaining C_i values.

Binding data were also fitted to a model incorporating a lognormal distribution of pH and ionic strength dependent binding constants. The relevant binding equation is given by:

$$C_{ML} = C_L \frac{1}{\sigma_K\sqrt{2\pi}} \int_{-5\sigma_K}^{+5\sigma_K} \left[\frac{10^{\kappa}[M]}{1 + 10^{\kappa}[M]} . \exp\left[-\frac{1}{2} \left[\frac{\log K_\mu - \kappa}{\sigma_K} \right]^2 \right] \right] d\kappa \qquad (6.2)$$

where $\kappa = \log K$;

$\log K_\mu$ is the mean of the normal distribution in log K;

and σ_K is the standard deviation of the normal distribution in log K.

The lognormal distribution model was formulated such that C_L could be treated as either an adjustable or fixed parameter in the regression analysis.

Metal-humate binding data were also modelled in terms of the Sips binding equation (Equation 2.16), where C_L was either a fixed or adjustable parameter in the regression analysis.

Models based on aggregation phenomena, as developed by Teasdale (1987), were also evaluated for their ability to provide a description of metal binding to solution-phase sodium humates. These models

were not applied to metal-calcium humate binding data, since it was considered unlikely that further aggregation processes would have been important in these systems.

The first of the aggregation models used was the modification/reversible self association model (Teasdale, 1987) discussed in Section 5.2.4. The second aggregation model was the crosslinking model (Teasdale, 1987) which assumes a single intrinsic binding constant, K_x, for the crosslinking reaction shown in Figure 6.1(a). Every humate macromolecule, L, is assumed to have f sites available for crosslinking, allowing the formation of large crosslinked structures shown in Figure 6.1(b).

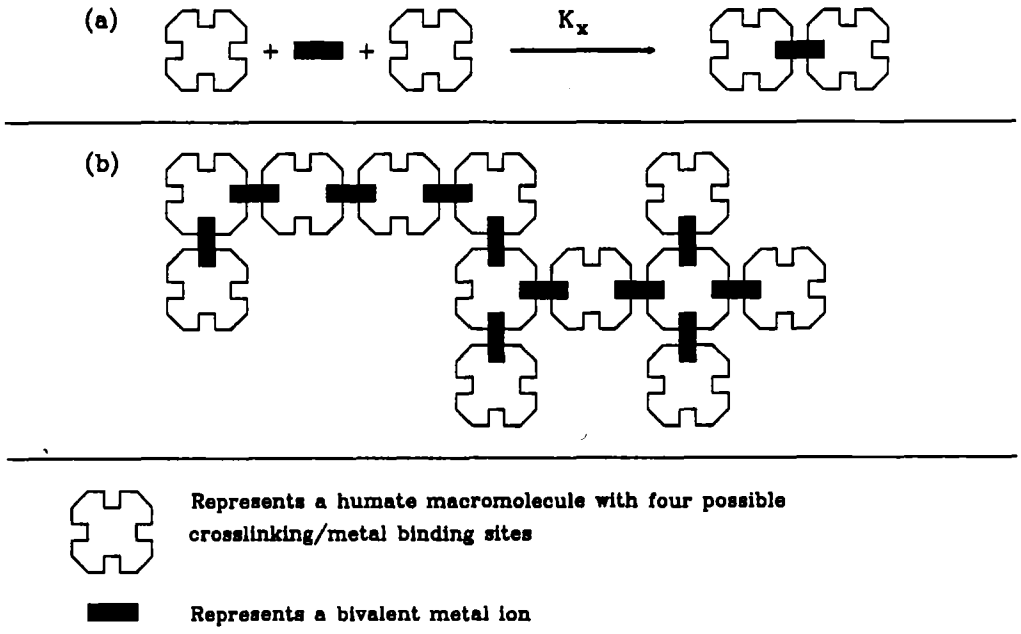

Figure 6.1 (a) Generalised crosslinking reaction between a bivalent metal ion and macromolecular ligand, and; (b) hypothetical cross-linked aggregate structure. Adapted from Teasdale (1987).

The modelling equation expresses the concentration of bound metal, C_{ML}, in terms of the free metal concentration, [M], as follows (Teasdale, 1987):

$$C_{ML} = C_L \left(\frac{2fK_x[M]}{1 + 2K_x[M]} + \Omega \right) \qquad (6.3a)$$

$$\Omega = \frac{1 - 4K_x^2[M]^2}{8K_x^2C_L[M]}\left\{1 + \frac{4fK_x^2C_L[M]}{(1 + 2K_x[M])^2} - \left[1 + \frac{8fK_x^2C_L[M]}{(1 + 2K_x[M])^2}\right]^{\frac{1}{2}}\right\} \qquad (6.3b)$$

6.2.4.1 Metal complexing by electrolyte anions

Since experiments always used $NaNO_3$ or $Ca(NO_3)_2$ as a background electrolyte, nitrate complexes of Cd^{2+} and Cu^{2+} were always accounted for when modelling binding data. This was achieved by using stability constants for the relevant complexes derived from Lindsay (1979) to correct measured free metal concentrations to actual free metal concentrations. Since the ion selective electrode calibration/measurement procedure measured a sum of free and NO_3^--complexed metal ion, a corrected value for free metal ion could be found using:

$$[M] = [M]_{cal}/(1 + \beta_{MNO_3}[NO_3^-] + \beta_{M(NO_3)_2}[NO_3^-]^2 \qquad (6.5)$$

where $[M]_{cal}$ is [M] derived from the electrode calibration, and β_{MNO_3} and $\beta_{M(NO_3)_2}$ are cumulative formation constants for the species $M(NO_3)^+$ and $M(NO_3)_2^0$ respectively (M = Cu or Cd).

6.2.4.2 Metal ion hydrolysis

The contribution of Cd^{2+} and Cu^{2+} hydrolysis reactions to observed metal ion binding were accounted for, in all models, by including terms in the binding equations derived from the equilibrium constants presented by Lindsay (1979). Hydrolysis equilibrium constants were converted to mixed concentration/activity constants, with equations written to include hydrogen ion activity which was calculated directly from solution pH.

Preliminary calculations indicated that only the species listed in Table 6.1 would have a significant effect on Cd^{2+} and Cu^{2+} speciation under the experimental conditions used. Single ion activity coefficients used to adjust the equilibrium constants for ionic strength were taken from Kielland (1937).

Table 6.1 Formation reactions and log K^0 values for Cd^{2+} and Cu^{2+} complexes with nitrate and hydroxide. Log K^0 refers to zero ionic strength and 25° C; from Lindsay (1979).

Formation reaction	log K^0
$Cd^{2+} + NO_3^- \Leftrightarrow Cd(NO_3)^+$	0.31
$Cd^{2+} + 2NO_3^- \Leftrightarrow Cd(NO_3)_2^0$	0.00
$Cd^{2+} + H_2O \Leftrightarrow Cd(OH)^+ + H^+$	-10.10
$Cd^{2+} + 2H_2O \Leftrightarrow Cd(OH)_2^0 + 2H^+$	-20.30
$2Cd^{2+} + H_2O \Leftrightarrow Cd_2(OH)^{3+} + H^+$	-6.40
$Cu^{2+} + NO_3^- \Leftrightarrow Cu(NO_3)^+$	0.50
$Cu^{2+} + 2NO_3^- \Leftrightarrow Cu(NO_3)_2^0$	-0.40
$Cu^{2+} + H_2O \Leftrightarrow Cu(OH)^+ + H^+$	-7.70
$Cu^{2+} + 2H_2O \Leftrightarrow Cu(OH)_2^0 + 2H^+$	-13.78
$2Cu^{2+} + 2H_2O \Leftrightarrow Cu_2(OH)_2^{2+} + 2H^+$	-10.68

6.3 Results

6.3.1 Cadmium(II) Binding by Summit Hill and Waimari Peat Calcium Humates

Results of experiments measuring binding of Cd^{2+} to SHCa and WPCa at 5°, 20° and 40° C are presented as plots of log[Cd^{2+}] *versus* bound Cd^{2+} in Figures 6.2 and 6.3 respectively. Cadmium(II) binding to both calcium humates showed good internal consistency within experiments and good reproducibility between replicates. Levels of unbound Cd^{2+} show a consistent decrease with increasing temperature at equivalent levels of bound Cd^{2+}.

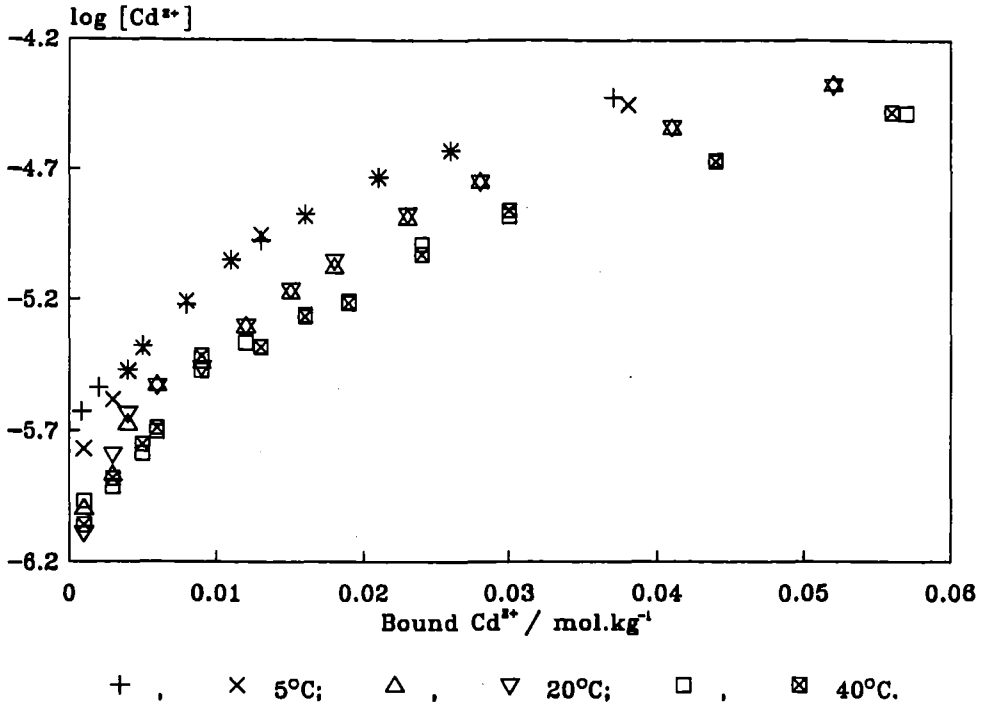

Figure 6.2 Effect of temperature on binding of Cd^{2+} by SHCa. $[Ca(NO_3)_2]$ = 0.05 mol L^{-1}; mass SHCa = 0.05 g; pH 6.0.

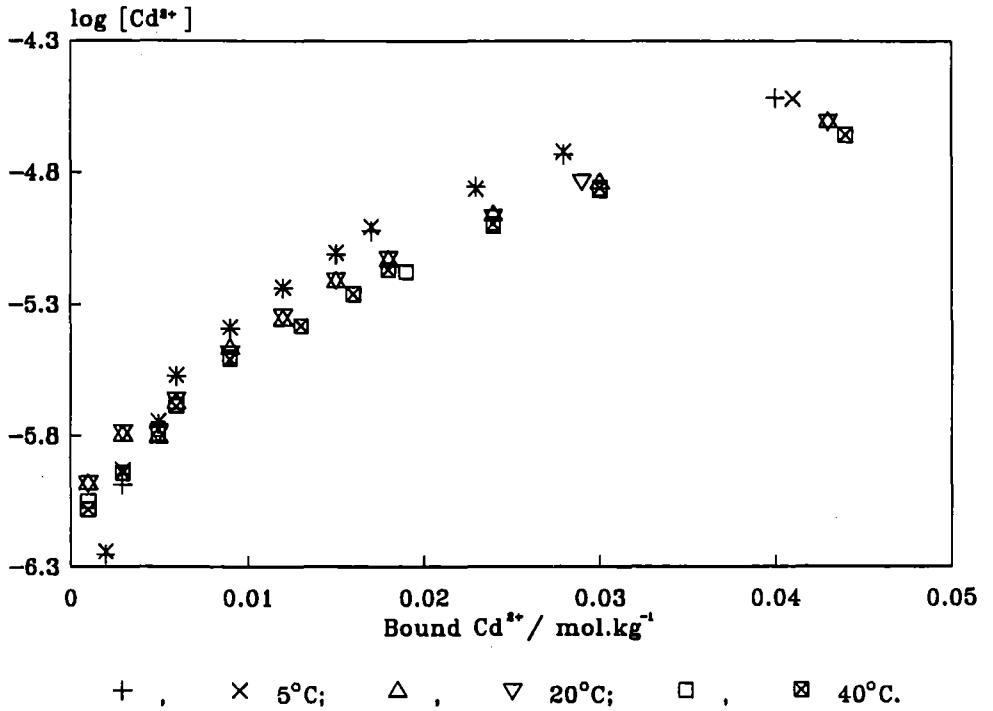

Figure 6.3 Effect of temperature on binding of Cd^{2+} by WPCa. $[Ca(NO_3)_2]$ = 0.05 mol L^{-1}; mass WPCa = 0.05 g; pH 6.0.

6.3.2 Copper(II) Binding by Summit Hill and Waimari Peat Calcium Humates

Results from experiments measuring binding of Cu^{2+} to SHCa and WPCa at 5°, 20° and 40° C are presented as plots of log[Cu^{2+}] *versus* bound Cu^{2+} in Figures 6.4 and 6.5 respectively. The results obtained for copper(II) binding were not, in general, internally consistent or reproducible for either SHCa or WPCa at any measurement temperature. There was a discernible trend, however, for unbound Cu^{2+} concentrations to decrease with increasing temperatures for equivalent levels of bound Cu^{2+}. Conversely (and equivalently), for equal free Cu^{2+} concentrations, bound Cu^{2+} increased with increasing temperature.

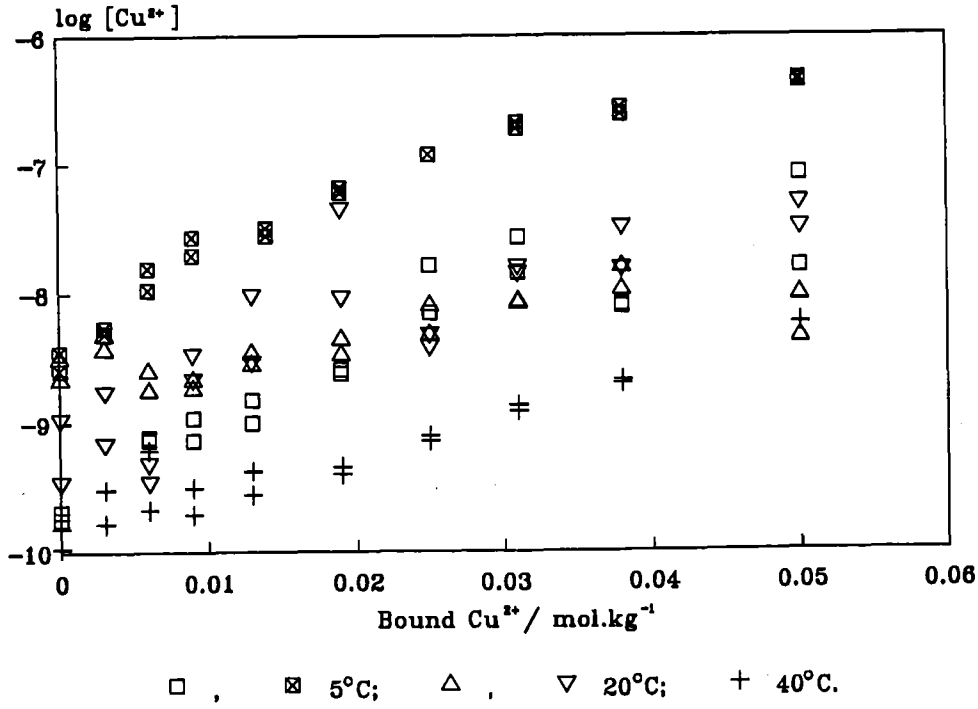

Figure 6.4 Effect of temperature on binding of Cu^{2+} by SHCa. [$Ca(NO_3)_2$] = 0.05 mol L^{-1}; mass SHCa = 0.05 g; pH 6.0.

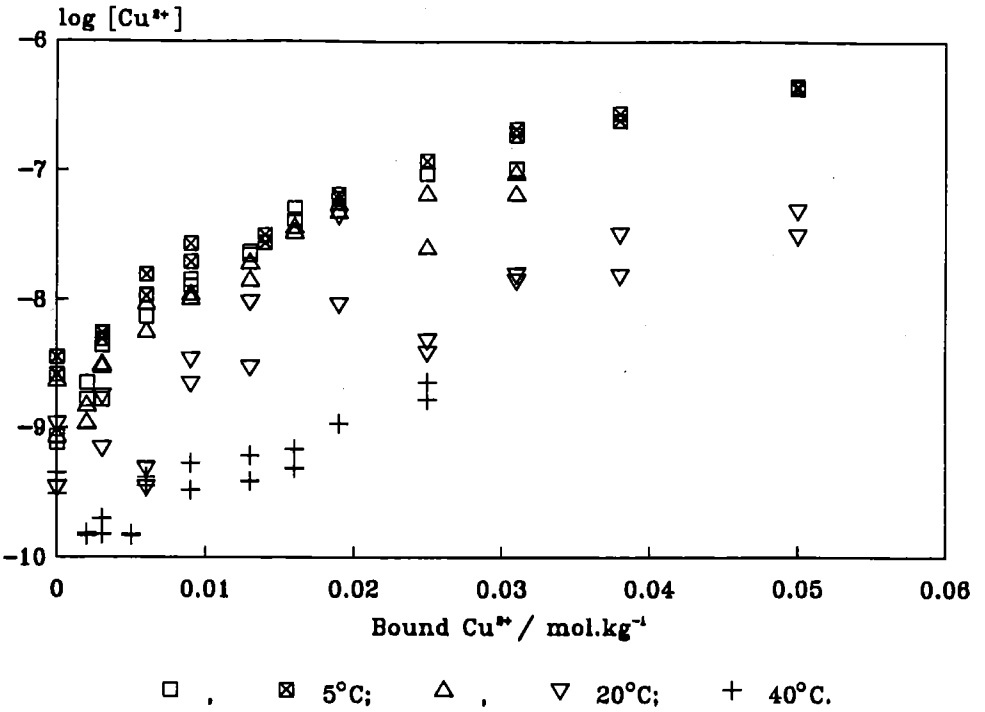

Figure 6.5 Effect of temperature on binding of Cu^{2+} by WPCa. $[Ca(NO_3)_2]$ = 0.05 mol L^{-1}; mass WPCa = 0.05 g; pH 6.0.

6.3.3 Cadmium(II) Binding to Summit Hill and Waimari Peat Sodium Humates

Results from experiments observing the binding of Cd^{2+} to SHNa and WPNa at 20° and 40° C are summarised as plots of log[Cd^{2+}] *versus* bound Cd^{2+} (C_{CdL}) in Figures 6.6 and 6.7 respectively. Binding data from these experiments showed good internal consistency, and reproducibility between replicates. Levels of free Cd^{2+} in the Cd^{2+}-SHNa system, for any constant level of bound Cd^{2+}, were virtually unaffected by temperature. A similar situation was observed for the Cd^{2+}-WPNa system (Figure 6.7), although unbound Cd^{2+} concentrations were very slightly lower at higher temperature for equivalent levels of bound Cd^{2+}.

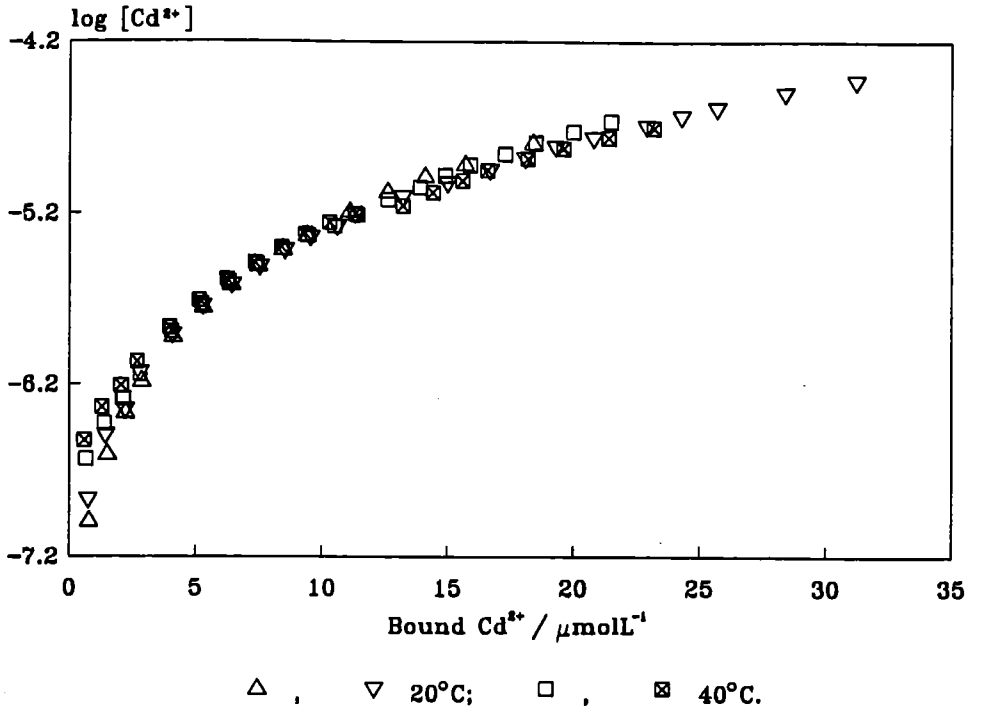

Figure 6.6 Effect of temperature on binding of Cd^{2+} by SHNa. $[NaNO_3] = 0.10$ mol L^{-1}; initial SHNa concentration = 0.10 g L^{-1}; pH 6.0.

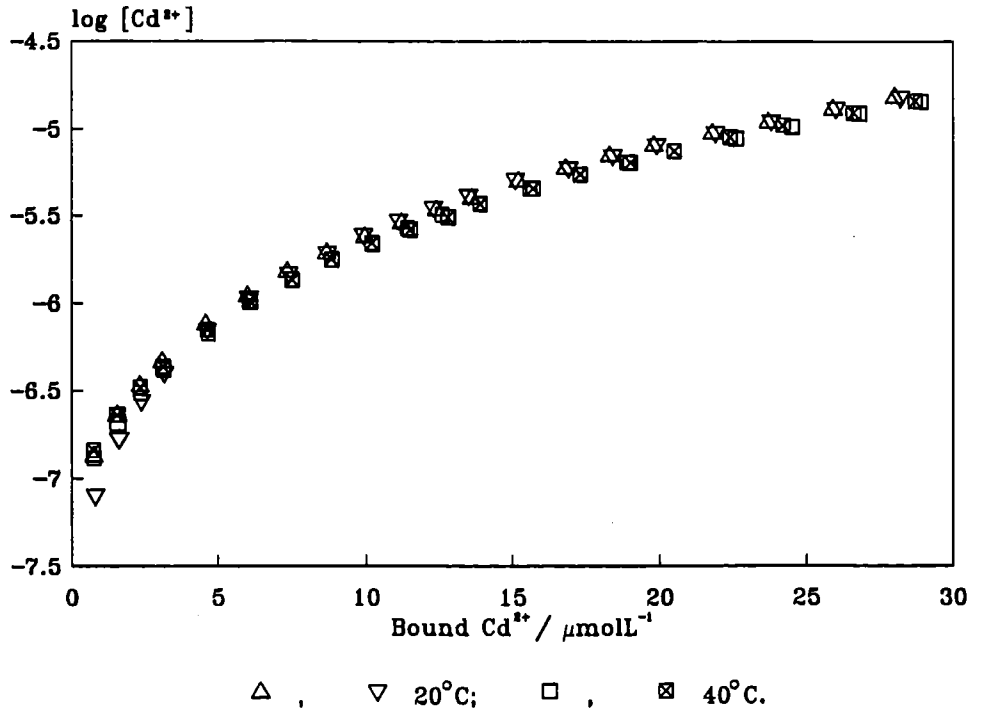

Figure 6.7 Effect of temperature on binding of Cd^{2+} by WPNa. $[NaNO_3] = 0.10$ mol L^{-1}; initial WPNa concentration = 0.10 g L^{-1}; pH 6.0.

Calculations using the volumes of standard alkali and acid required to maintain solution pH at 6.0 show that for each mole of Cd^{2+} bound, approximately 0.6-0.8 moles of H^+ were released, from both SHNa and WPNa. The amount of H^+ released showed a slight decrease with increasing Cd^{2+} addition over the course of titrations.

6.3.4 Copper(II) Binding to Summit Hill and Waimari Peat Sodium Humates

Results from experiments observing the binding of Cu^{2+} to SHNa and WPNa at 20° and 40°C are presented graphically as plots of $\log[Cu^{2+}]$ *versus* bound Cu^{2+} (C_{CdL}) in Figures 6.8 and 6.9 respectively. Binding data from these experiments showed good internal consistency within experiments. Reproducibility between replicates was poor, however, compared with cadmium binding experiments. For Cu^{2+} binding to SHNa and WPNa the concentration of unbound Cu^{2+} showed an obvious temperature dependence. For equivalent levels of bound Cu^{2+}; the concentration of unbound Cu^{2+} decreased with increasing temperature under the conditions of these experiments.

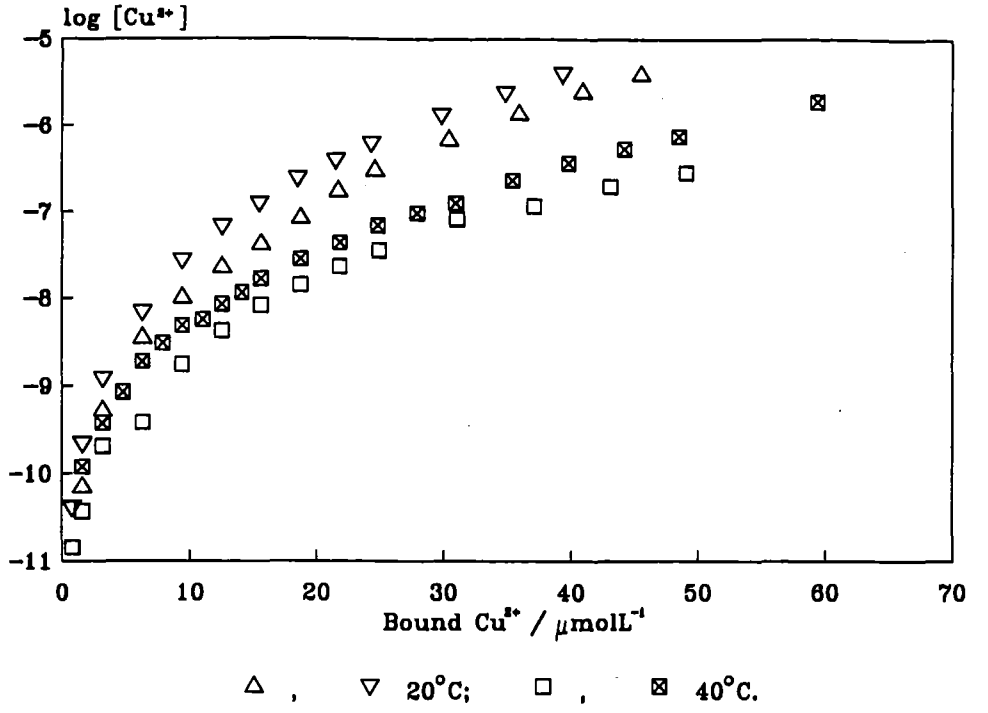

Figure 6.8 Effect of temperature on binding of Cu^{2+} by SHNa. $[NaNO_3]$ = 0.10 mol L^{-1}; initial SHNa concentration = 0.10 g L^{-1}; pH 6.0.

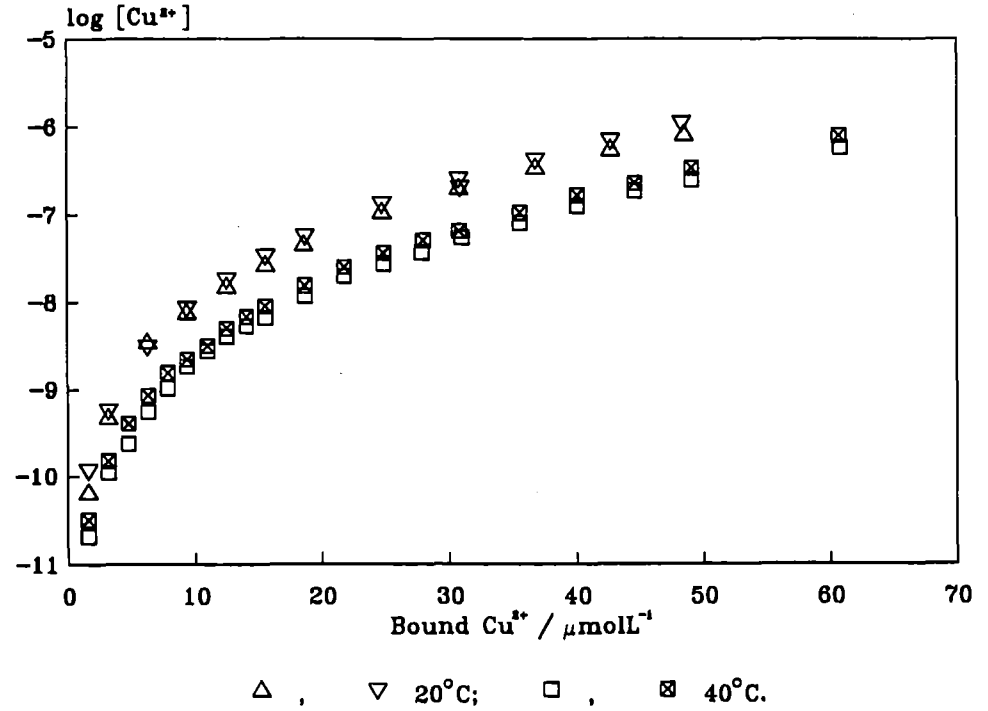

Figure 6.9 Effect of temperature on binding of Cu^{2+} by WPNa. $[NaNO_3]$ = 0.10 mol L^{-1}; initial WPNa concentration = 0.10 g L^{-1}; pH 6.0.

Proton release in Cu^{2+} titrations of both SHNa and WPNa at pH 6.0 was approximately 1.4 mol H^+ released per mole of Cu^{2+} bound. Proton release from both sodium humates consistently showed and initial increase, and a subsequent gradual decrease, with increasing bound Cu^{2+}.

6.3.5 Effect of Temperature Decrease on Copper(II) Binding to Waimari Peat Calcium Humate

Under the conditions of this experiment, levels of unbound copper decreased with decreasing temperature (decreased with increasing equilibration time). Results are presented graphically in Figure 6.10.

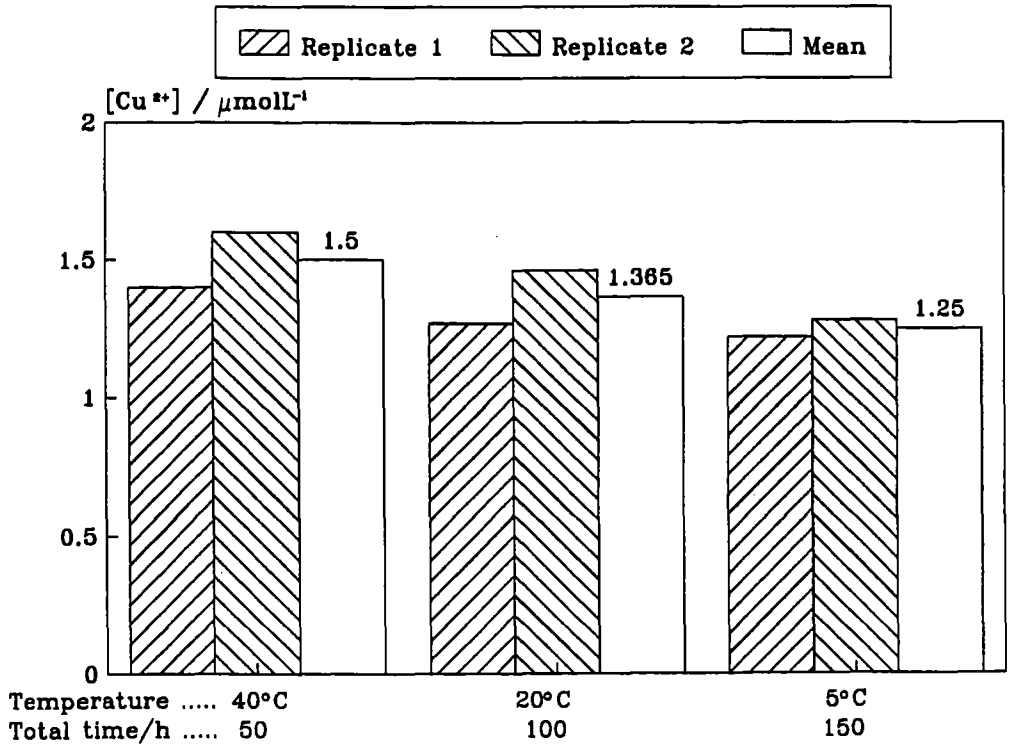

Figure 6.10 Effect of stepwise temperature decreases on binding of Cu^{2+} to WPCa. $[Ca(NO_3)_2]$ = 0.05 mol L^{-1}; mass (WPCa) = 0.05 g; pH 6.0.

6.3.6 Descriptions of Metal Binding Data Using Modelling Equations

Summaries of refined fitting parameters, and statistical tests, for the fitting of the various models to experimental binding data are contained in Tables 6.2 - 6.13.

With the possible exception of the single discrete site models, the small number of poor fits (implied by low R^2 values or F ratios) found for any model are likely to be a reflection of the quality of titration data rather than a shortcoming of the model involved. For example, for copper(II) binding to SHCa at 20° C, R^2 values are consistently low regardless of the equation used to model the data.

6.3.6.1 Discrete binding site models

The single site/variable C_L (Langmuir) model provided a good description of Cd^{2+} binding data (R^2 in the range 98.6 - 99.7%; see Table 6.3). In contrast, the single site/fixed C_L model produced noticeably poorer descriptions of Cd^{2+}-humate binding, with R^2 in the range 81.0 - 99.4%. Models incorporating a single type of site with no interaction and fixed C_L did not, in general provide an adequate description of Cu^{2+} binding data from any experiment ($R^2 \leq 80\%$; Table 6.3). For models having C_L as an adjustable fitting parameter (Langmuir adsorption isotherm), better descriptions of Cu^{2+} binding were obtained (R^2 in the range 11 - 96.9%; Table 6.4).

A model incorporating two discrete, noninteracting binding sites, with the total site concentration a fixed parameter in regressions, without exception provided a better empirical description of Cd^{2+} and Cu^{2+} binding to sodium and calcium humates than a single discrete site model. Fits were particularly good for Cd^{2+} binding data (R^2 in the range 99.1 - 99.96%; Table 6.4). Fits were improved slightly by allowing C_L to vary; cadmium binding data gave R^2 in the range 93.1 - 100.0%, and copper binding data gave $R^2 \leq 99.3\%$ (Table 6.5).

A three discrete binding site model was used to describe selected sets of metal-humate binding data. For these selected datasets (see Discussion, Section 6.4.3.1), a three site model resulted in significantly better agreement between observed and predicted values (Tables 6.6 and 6.7) than was achieved with the two discrete site model.

6.3.6.2 Continuous multiligand models

Data from experiments measuring Cd^{2+} and Cu^{2+} binding data to sodium and calcium humates were generally described well by a model incorporating a lognormal distribution of binding constants (Tables 6.8 and 6.9). As described in Chapter 5, the regression minimised an unweighted sum of squares of residuals, with C_{ML} being the dependent variable. For Cd^{2+} binding data, this model, with C_L a fixed parameter in regressions, achieved R^2 values in the range 99.17 - 99.96%; for Cu^{2+} binding data, R^2 for the fixed C_L model was in the range 5.00 - 99.96%. Fits were improved slightly by allowing C_L to vary (R^2 in the range 99.55 - 99.98% for Cd^{2+} binding data; R^2 in the range 5 - 99.99% for Cu^{2+} binding data). In general, the spread of the distributions (measured by the standard deviation term, σ_K) was narrower for Cd^{2+} binding data than for Cu^{2+} binding data.

The Sips binding equation, with C_L a fixed parameter in regressions, was also found to provide a good description of Cd^{2+} and Cu^{2+} binding to sodium and calcium humates. For Cd^{2+} binding data, R^2 was in the range 98.81 - 99.97%; for Cu^{2+} binding data, R^2 was in the range 3 - 99.96% (Table 6.10). If C_L was treated as an adjustable parameter in regressions, fits were improved slightly (R^2 in the range 99.42 - 99.98% for Cd^{2+} binding data and R^2 in the range 18 - 99.98% for Cu^{2+} binding data; see Table 6.11 for details). Refined values of the parameter β (Equation 2.17) generally indicated a narrower distribution of effective binding constants for Cd^{2+} binding than for Cu^{2+} binding. The Sips equation consistently returned a higher value for log K_μ than the lognormal binding model for metal-humate binding.

6.3.6.3 Models based on aggregation phenomena

A model incorporating a single type of metal ion binding site, which modified sodium humate molecules to allow reversible self association, was able to provide a reasonable description of the binding of Cd^{2+} to SHNa and WPNa (R^2 in the range 99.3 - 99.6%; Table 6.12). This model provided a less accurate description of Cu^{2+}-SHNa (WPNa) binding (R^2 in the range 90.0 - 94.8%; Table 6.12).

A model based on the formation of crosslinked aggregates of humate macromolecules, induced by polyvalent metal ion binding (Equation 6.4) was able to provide a good description of Cd^{2+} binding to SHNa and WPNa. (R^2 in the range 98.6 - 99.7%; Table 6.13). This model described Cu^{2+} binding to SHNa and WPNa less accurately (R^2 in the range 90.1 - 94.2%; Table 6.13). When all three parameters in the model (C_L, log K, f) were allowed to vary during the regression procedure, the optimised value of f implied a very large number of sites available for crosslinking per humate macromolecule, often giving values which appeared to be physically unrealistic (for example, $f = 7.4 \times 10^5$ for Cu^{2+}-WPNa binding at 40° C). In these cases, the refined values of C_L were correspondingly small, although the product $C_L.f$ (Table 6.13), corresponding to the total number of 'binding sites' available, gave values in a range similar to that predicted by the discrete and continuous binding site models with adjustable C_L (Tables 6.3, 6.5, 6.7, 6.9 and 6.11). Consequently, the model was also evaluated in a form where f was fixed at selected values (f = 2, 4, 8) which were considered to be physically feasible. These restricted crosslinking models tended to result in poorer fits to binding data (Table 6.14). At a higher fixed value of f (f = 8), however, agreement between observed and predicted binding was quite close for the Cd^{2+}-sodium humate systems (R^2 in the range 98.4 to 99.6%; Table 6.14).

Table 6.2 Summary of refined parameters and statistical tests for fits of Cd and Cu - humate binding data to a one discrete site/fixed C_L model. Unweighted regressions with respect to C_{ML}; hydrolysis products and NO_3^- complexes are included. [a]Adjustable parameter, Equation 6.1a,b. [b]Singly lagged residual autocorrelation (*P≤0.05).

Ligand	Metal ion	Temp. /° C	Number of data	Fixed C_L /mmol g^{-1}	log K_1[a]	R^2 (%)	F	r_1[b]
SHCa	Cd	5	11	1.95	2.77	97.9	472	0.337
SHCa	Cd	5	11	1.95	2.79	99.4	1618	0.536*
SHCa	Cd	20	12	1.95	2.90	92.7	151	0.415
SHCa	Cd	20	12	1.95	2.90	93.7	173	0.459
SHCa	Cd	40	12	1.95	3.05	94.3	194	0.273
SHCa	Cd	40	12	1.95	3.04	93.4	162	0.249
SHCa	Cu	5	16	1.95	5.74	-	-6	-0.065
SHCa	Cu	5	18	1.95	4.90	69.6	56	0.692*
SHCa	Cu	20	18	1.95	6.32	-	13	0.342
SHCa	Cu	20	18	1.95	5.82	-	5	-0.120
SHCa	Cu	40	18	1.95	6.82	-	10	0.596*
SHNa	Cd	20	15	1.95	3.93	81.0	74	0.649*
SHNa	Cd	20	23	1.95	3.85	87.2	171	0.777*
SHNa	Cd	40	20	1.95	3.89	81.8	104	0.769*
SHNa	Cd	40	20	1.95	3.95	91.3	218	0.754*
SHNa	Cu	20	13	1.95	5.11	-	3	0.562*
SHNa	Cu	20	13	1.95	5.02	-	6	0.538*
SHNa	Cu	40	14	1.95	6.27	29.9	19	0.621*
SHNa	Cu	40	20	1.95	5.71	-	6	0.459*
WPCa	Cd	5	11	2.60	2.80	94.6	184	0.330
WPCa	Cd	5	11	2.60	2.80	95.4	219	0.409
WPCa	Cd	20	11	2.60	2.92	94.3	176	0.276
WPCa	Cd	20	11	2.60	2.91	94.5	181	0.330
WPCa	Cd	40	11	2.60	2.97	95.8	239	0.416
WPCa	Cd	40	11	2.60	2.97	96.1	257	0.484
WPCa	Cu	5	18	2.60	5.13	85.7	119	0.519*
WPCa	Cu	5	18	2.60	4.78	69.1	55	0.691*
WPCa	Cu	20	18	2.60	5.26	59.8	42	-0.186
WPCa	Cu	20	18	2.60	5.69	-	5	-0.119
WPCa	Cu	40	17	2.60	6.82	57.6	38	0.387
WPNa	Cd	20	20	2.60	4.03	85.6	132	0.740*
WPNa	Cd	20	20	2.60	4.04	86.5	141	0.756*
WPNa	Cd	40	20	2.60	4.08	85.4	130	0.736*
WPNa	Cd	40	20	2.60	4.07	84.1	119	0.751*
WPNa	Cu	20	12	2.60	5.64	23.2	14	0.544*
WPNa	Cu	20	13	2.60	5.54	-	10	0.489*
WPNa	Cu	40	20	2.60	6.02	-	8	0.430*
WPNa	Cu	40	20	2.60	5.89	-	7	0.427*

Table 6.3 Summary of refined parameters and statistical tests for fits of Cd and Cu - humate binding data to Langmuir binding model. Model accounts for metal hydrolysis and complexation by NO_3^-. Unweighted regressions with respect to C_{ML}. [a]Adjustable parameters, Equation 6.1a,b. [b]Singly lagged residual autocorrelation (*P≤0.05).

Ligand	Metal ion	Temp. /° C	Number of data	C_L[a]/ mmol g^{-1}	log K_1[a]	R^2 (%)	F	r_1[b]
SHCa	Cd	5	11	0.147	3.98	99.3	1378	0.430
SHCa	Cd	5	11	0.256	3.72	99.7	3369	0.296
SHCa	Cd	20	12	0.105	4.39	99.5	1856	0.413
SHCa	Cd	20	12	0.110	4.35	99.4	1796	0.528*
SHCa	Cd	40	12	0.129	4.42	99.6	2756	0.075
SHCa	Cd	40	12	0.121	4.45	99.4	1713	-0.028
SHCa	Cu	5	16	0.0457	8.50	77.8	63	0.491*
SHCa	Cu	5	18	0.0642	6.84	96.9	522	0.512*
SHCa	Cu	20	18	0.0887	7.86	11.1	18	0.485*
SHCa	Cu	20	18	0.0486	8.15	57.4	38	0.175
SHCa	Cu	40	18	0.0642	8.88	91.2	183	0.461*
SHNa	Cd	20	15	0.259	5.15	98.6	925	0.695*
SHNa	Cd	20	23	0.457	4.77	99.1	2214	0.796*
SHNa	Cd	40	20	0.311	5.02	99.5	3398	0.728*
SHNa	Cd	40	20	0.404	4.86	99.6	4964	0.557*
SHNa	Cu	20	13	0.404	7.05	90.0	110	0.719*
SHNa	Cu	20	13	0.372	6.74	93.3	163	0.719*
SHNa	Cu	40	14	0.475	7.69	93.2	177	0.708*
SHNa	Cu	40	20	0.511	7.32	91.0	200	0.711*
WPCa	Cd	5	11	0.0944	4.41	99.6	2549	0.416
WPCa	Cd	5	11	0.102	4.37	99.6	2220	0.175
WPCa	Cd	20	11	0.104	4.48	99.6	2103	0.330
WPCa	Cd	20	11	0.105	4.47	99.6	2011	0.375
WPCa	Cd	40	11	0.116	4.47	99.7	2767	0.150
WPCa	Cd	40	11	0.119	4.45	99.6	2178	0.181
WPCa	Cu	5	18	0.0487	7.17	95.2	334	0.417*
WPCa	Cu	5	18	0.0642	6.84	96.9	522	0.512*
WPCa	Cu	20	18	0.0411	7.46	86.4	118	0.066
WPCa	Cu	20	18	0.0468	8.15	57.4	38	0.175
WPCa	Cu	40	17	0.0445	8.88	90.0	149	0.353
WPNa	Cd	20	20	0.421	5.13	99.3	2661	0.825*
WPNa	Cd	20	20	0.430	5.11	99.0	1801	0.849*
WPNa	Cd	40	20	0.435	5.16	99.4	2859	0.823*
WPNa	Cd	40	20	0.423	5.18	99.5	3287	0.755*
WPNa	Cu	20	12	0.479	7.22	94.7	190	0.677*
WPNa	Cu	20	13	0.476	7.10	94.4	197	0.713*
WPNa	Cu	40	20	0.543	7.63	91.2	205	0.729*
WPNa	Cu	40	20	0.542	7.51	91.4	208	0.736*

Table 6.4 Refined parameters and statistical summaries from fitting metal-humate binding data to a two discrete site/fixed C_L model also including NO_3^- and OH^- complexes. Unweighted regressions with respect to log $[M^{2+}]$; [a]adjustable parameters, Equation 6.1a,b. [b]Singly lagged residual autocorrelation (*P≤0.05).

Ligand	Metal ion	Temp. /°C	Number of data	Fixed C_L /mmol g^{-1}	C_1/C_L	log K_1	log K_2	R^2 (%)	F	r_1[b]
SHCa	Cd	5	11	1.95	0.0756	3.98	-3.00	99.35	613	0.430
SHCa	Cd	5	11	1.95	0.00537	4.61	2.70	99.75	1618	0.346
SHCa	Cd	20	12	1.95	0.0151	4.88	2.61	99.67	1357	0.297
SHCa	Cd	20	12	1.95	0.0132	4.91	2.64	99.67	1381	0.540*
SHCa	Cd	40	12	1.95	0.0402	4.58	2.43	99.65	1274	0.034
SHCa	Cd	40	12	1.95	0.0550	4.49	1.86	99.42	772	-0.037
SHCa	Cu	5	16	1.95	0.0205	8.61	4.86	79.51	32	0.412
SHCa	Cu	5	18	1.95	0.0115	7.51	4.60	99.44	1329	-0.299
SHCa	Cu	20	18	1.95	0.0455	7.86	0.335	11.01	8	0.486*
SHCa	Cu	20	18	1.95	0.0240	8.15	-0.828	57.42	18	0.176
SHCa	Cu	40	18	1.95	0.0330	8.88	-0.262	91.24	86	0.461*
SHNa	Cd	20	15	1.95	0.0385	5.88	3.65	99.94	9437	0.595*
SHNa	Cd	20	23	1.95	0.0681	5.43	3.57	99.92	11904	0.633*
SHNa	Cd	40	20	1.95	0.0682	5.45	3.49	99.93	11628	0.517*
SHNa	Cd	40	20	1.95	0.0786	5.26	3.58	99.81	4410	0.474*
SHNa	Cu	20	13	1.95	0.129	7.70	4.65	98.31	296	0.554*
SHNa	Cu	20	13	1.95	0.111	7.43	4.56	98.30	293	0.523*
SHNa	Cu	40	14	1.95	0.110	8.63	5.92	98.95	523	0.410
SHNa	Cu	40	20	1.95	0.167	7.86	5.16	98.09	444	0.613*
WPCa	Cd	5	11	2.60	0.0052	5.20	2.61	99.97	15112	-0.134
WPCa	Cd	5	11	2.60	0.0046	5.24	2.64	99.95	7309	-0.560*
WPCa	Cd	20	11	2.60	0.0265	4.61	2.22	99.58	947	0.343
WPCa	Cd	20	11	2.60	0.0268	4.60	2.21	99.56	905	0.404
WPCa	Cd	40	11	2.60	0.0138	4.85	2.64	99.73	1467	0.292
WPCa	Cd	40	11	2.60	0.0093	4.99	2.73	99.70	1351	0.354
WPCa	Cu	5	18	2.60	0.0187	7.17	-26.2	95.20	156	0.417*
WPCa	Cu	5	18	2.60	0.0086	7.51	4.47	99.44	1329	-0.300
WPCa	Cu	20	18	2.60	0.0158	7.46	-284	86.40	55	0.066
WPCa	Cu	20	18	2.60	0.0180	8.15	0.228	57.42	18	0.176
WPCa	Cu	40	17	2.60	0.0171	8.88	-0.528	89.95	70	0.353
WPNa	Cd	20	20	2.60	0.0543	5.69	3.71	99.98	36187	0.236
WPNa	Cd	20	20	2.60	0.0426	5.87	3.78	99.94	14320	0.617*
WPNa	Cd	40	20	2.60	0.0578	5.70	3.75	99.97	28962	0.390
WPNa	Cd	40	20	2.60	0.0642	5.64	3.71	99.98	41213	0.155
WPNa	Cu	20	12	2.60	0.0974	7.85	5.24	99.22	579	0.563*
WPNa	Cu	20	13	2.60	0.105	7.69	5.07	98.65	371	0.627*
WPNa	Cu	40	20	2.60	0.122	8.23	5.53	97.88	402	0.665*
WPNa	Cu	40	20	2.60	0.124	8.11	5.39	97.78	383	0.689*

Table 6.5 Refined parameters and statistical summaries for fits of metal-humate binding data to a two discrete site model also including NO_3^- and OH^- complexes. Unweighted regressions with respect to C_{ML}; [a]adjustable parameters, Equation 6.1a,b. [b]Singly lagged residual autocorrelation (*P≤0.05).

Ligand	Metal ion	Temp. /°C	Number of data	C_1[a]/ mmol g^{-1}	log K_1[a]	C_2[a]/	log K_2[a]/ mmol g^{-1}	R^2(%)	F	r_1[b]
SHCa	Cd	5	11	0.147	3.98	34.0	-4.26	99.35	357	0.430
SHCa	Cd	5	11	0.0115	4.59	3.92	2.39	99.75	946	0.348
SHCa	Cd	20	12	0.0295	4.88	2.38	2.52	99.67	804	0.297
SHCa	Cd	20	12	0.0261	4.91	2.90	2.46	99.68	819	0.539*
SHCa	Cd	40	12	0.0649	4.61	0.156	3.71	99.65	756	0.039
SHCa	Cd	40	12	0.107	4.49	3.99	1.53	99.42	457	-0.037
SHCa	Cu	5	16	0.0399	8.61	1.79	4.89	79.51	20	0.413*
SHCa	Cu	5	18	0.0226	7.51	4.14	4.26	99.44	828	-0.302
SHCa	Cu	20	18	0.0106	7.86	0.0782	7.86	11.10	5	0.485*
SHCa	Cu	20	18	0.00214	15.1	0.0463	8.06	57.97	11	0.178
SHCa	Cu	40	18	0.0642	8.88	0.695	1.37	91.24	53	0.461*
SHNa	Cd	20	15	0.0593	6.01	0.596	4.27	99.95	7185	0.563*
SHNa	Cd	20	23	0.0670	5.81	0.664	4.27	99.96	15860	0.187
SHNa	Cd	40	20	0.0847	5.63	0.437	4.38	99.94	8236	0.398*
SHNa	Cd	40	20	0.0516	5.64	0.501	4.52	99.82	2888	0.402*
SHNa	Cu	20	13	0.177	8.13	0.366	5.96	99.58	713	0.521*
SHNa	Cu	20	13	0.116	8.29	0.344	6.05	99.62	795	0.403
SHNa	Cu	40	14	0.145	9.16	0.542	6.85	99.63	903	-0.055
SHNa	Cu	40	20	0.205	8.31	0.506	6.33	99.62	1390	0.655*
WPCa	Cd	5	11	0.0922	4.42	0.0149	2.90	99.65	663	0.403
WPCa	Cd	5	11	0.0978	4.37	0.182	2.48	99.60	584	0.233
WPCa	Cd	20	11	0.104	4.48	0.857	-1.85	99.57	545	0.330
WPCa	Cd	20	11	0.105	4.47	0.423	-2.00	99.55	521	0.375
WPCa	Cd	40	11	0.117	4.47	0.0137	2.47	99.68	718	0.160
WPCa	Cd	40	11	0.119	4.45	0.454	-2.96	99.59	565	0.181
WPCa	Cu	5	18	0.0087	8.22	34.8	3.82	97.67	200	0.042
WPCa	Cu	5	18	0.0226	7.51	8.55	3.95	99.44	828	-0.302
WPCa	Cu	20	18	0.0168	7.95	6.11	4.51	87.84	38	-0.040
WPCa	Cu	20	18	0.0468	8.15	14.6	-0.702	57.42	11	0.176
WPCa	Cu	40	17	0.0445	8.88	7.39	-1.34	89.95	43	0.353
WPNa	Cd	20	20	0.111	5.79	0.8656	4.30	99.98	31503	0.248
WPNa	Cd	20	20	0.0627	6.18	0.686	4.56	99.99	66997	-0.332
WPNa	Cd	40	20	0.0989	5.88	0.705	4.50	99.99	39468	0.165
WPNa	Cd	40	20	0.165	5.65	2.17	3.76	99.98	25868	0.156
WPNa	Cu	20	12	0.154	8.32	0.524	6.40	99.76	1115	0.402
WPNa	Cu	20	13	0.125	8.54	0.479	6.49	99.70	982	-0.151
WPNa	Cu	40	20	0.161	8.97	0.567	6.87	99.53	1141	0.650*
WPNa	Cu	40	20	0.166	8.80	0.555	6.76	99.65	1505	0.542*

Table 6.6 Refined parameters and statistical summaries for fits of selected metal-humate binding data to a three discrete site/fixed C_L model also including NO_3^- and OH^- complexes. Unweighted regressions with respect to C_{ML}; [a]adjustable parameters, Equation 6.1a,b. [b]Singly lagged residual autocorrelation (*P≤0.05).

Ligand	Metal ion	Temp. /°C	Number of data	Fixed C_L /mmol g^{-1}	C_1/C_L[a]	C_2/C_L[a]	log K_1[a]	log K_2[a]	log K_3[a]	R^2 (%)	F	r_1[b]
SHCa	Cd	5	11	1.95	0.0756	0.462	3.98	-4.17	-16.1	99.35	230	0.430
SHCa	Cd	5	11	1.95	0.0537	0.300	4.61	2.70	2.71	99.75	607	0.346
SHCa	Cd	20	12	1.95	0.0150	0.233	4.88	2.71	2.58	99.67	528	0.297
SHCa	Cd	20	12	1.95	0.0132	0.750	4.91	2.65	2.64	99.67	537	0.540*
SHCa	Cd	40	12	1.95	0.0398	0.460	4.58	2.76	-97.5	99.65	495	0.034
SHCa	Cd	40	12	1.95	0.0550	0.411	4.49	2.23	-57.2	99.42	300	-0.037
SHCa	Cu	5	16	1.95	0.0205	0.106	8.61	4.86	4.86	79.51	13	0.412*
SHCa	Cu	5	18	1.95	0.0125	1.60	7.46	5.01	5.32	99.44	579	-0.323
SHNa	Cd	20	15	1.95	0.0044	0.0420	7.05	5.56	3.61	99.98	11591	0.329
SHNa	Cd	20	23	1.95	0.0133	0.0890	6.27	5.00	3.48	99.98	18915	-0.043
SHNa	Cd	40	20	1.95	0.0112	0.0770	6.05	5.18	3.40	99.95	6787	0.335
SHNa	Cd	40	20	1.95	0.0129	0.119	5.83	4.90	3.40	99.82	2068	0.410*
SHNa	Cu	20	13	1.95	0.0685	0.111	8.43	6.60	4.40	99.72	713	0.375
SHNa	Cu	20	13	1.95	0.0401	0.109	8.78	6.64	4.35	99.89	1813	0.215
SHNa	Cu	40	14	1.95	0.0480	0.105	9.57	7.73	5.78	99.86	1565	-0.521*
SHNa	Cu	40	20	1.95	0.0625	0.165	8.78	7.03	4.92	99.87	2931	0.283
WPCa	Cd	5	11	2.60	0.0466	0.234	5.25	3.23	-0.620	99.97	5707	-0.157
WPCa	Cd	5	11	2.60	0.0458	0.0473	5.24	2.64	2.64	99.95	2741	-0.560*
WPCa	Cd	20	11	2.60	0.0263	0.203	4.61	2.91	0.465	99.58	355	0.343
WPCa	Cd	20	11	2.60	0.0269	0.285	4.60	2.71	1.25	99.56	339	0.403
WPCa	Cd	40	11	2.60	0.0138	2.231	4.85	2.68	2.63	99.73	550	0.292
WPCa	Cd	40	11	2.60	0.00931	0.323	4.99	2.73	99.70	506	0.353	
WPNa	Cd	20	20	2.60	0.0425	0.333	5.79	4.30	-15.1	99.98	22150	0.248
WPNa	Cd	20	20	2.60	0.0241	0.264	6.18	4.56	-81.0	99.99	47107	-0.332
WPNa	Cd	40	20	2.60	0.0376	0.192	5.88	4.60	3.15	99.99	27311	0.164
WPNa	Cd	40	20	2.60	0.0636	0.837	5.65	3.76	-157	99.98	18188	0.156
WPNa	Cu	20	12	2.60	0.0232	0.0968	9.40	7.35	5.13	99.88	1513	0.105
WPNa	Cu	20	13	2.60	0.0323	0.113	8.99	6.99	4.85	99.83	1186	0.004
WPNa	Cu	40	20	2.60	0.0388	0.133	9.52	7.45	5.31	99.89	3449	0.374*
WPNa	Cu	40	20	2.60	0.0430	0.138	9.22	7.27	5.12	99.91	4017	0.446*

Table 6.7 Refined parameters and statistical summaries for fits of selected metal-humate binding data to a three discrete site model incorporating NO_3^- and OH^- complexes. Unweighted regressions with respect to C_{ML}; [a]adjustable parameters, Equation 6.1a,b. [b]Singly lagged residual autocorrelation (*P≤0.05).

Ligand	Metal ion	Temp. /°C	Number of data	C_1[a]/ mmol g^{-1}	log K_1[a]	C_2[a]/ mmol g^{-1}	log K_2	C_3[a]/ mmol g^{-1}	log K_3[a]	R^2(%)	F	r_1[b]
SHCa	Cd	5	11	3.1×10^{-15}	4.30	0.147	3.98	7.4×10^{-4}	-0.7638	99.35	153	0.430
SHCa	Cd	5	11	0.0113	4.59	1.77	2.60	1.85	2.15	99.75	405	0.345
SHCa	Cd	20	12	0.0292	4.88	0.102	2.81	2.62	2.44	99.67	362	0.297
SHCa	Cd	20	12	0.0262	4.91	3.48	2.35	0.348	2.16	99.68	369	0.539*
SHCa	Cd	40	12	0.0506	4.66	0.133	3.93	1.77	-0.0581	99.65	340	0.041
SHCa	Cd	40	12	0.0855	4.52	0.0469	4.09	2.64	-11.3	99.42	206	-0.034
SHCa	Cu	5	16	0.0399	8.61	3.28×10^{5}	0.621	2.39×10^{7}	7.20×10^{-17}	79.52	10	0.412
SHCa	Cu	5	18	0.0224	7.51	2.49	4.49	505	-6435.	99.44	425	-0.300
SHNa	Cd	20	15	0.00822	7.09	0.0831	5.63	2.23	3.52	99.98	11540	0.309
SHNa	Cd	20	23	0.0603	5.85	0.282	4.54	0.704	3.74	99.97	9747	0.154
SHNa	Cd	40	20	0.0252	6.01	0.153	5.15	2.13	3.30	99.95	5074	0.334
SHNa	Cd	40	20	0.0384	5.71	0.243	4.79	0.575	3.89	99.82	1534	0.408*
SHNa	Cu	20	13	0.0385	9.92	0.169	7.70	0.369	5.79	99.97	4525	-0.355
SHNa	Cu	20	13	0.0559	9.13	0.138	7.14	0.342	5.63	99.96	3671	-0.095
SHNa	Cu	40	14	0.0809	9.67	0.154	8.02	0.694	6.40	99.87	1263	-0.666*
SHNa	Cu	40	20	0.0748	9.20	0.218	7.58	0.491	6.04	99.94	4870	0.318
WPCa	Cd	5	11	0.0119	5.25	0.166	3.53	0.852	2.83	99.97	3805	-0.161
WPCa	Cd	5	11	0.0118	5.24	0.730	2.88	2.26	2.40	99.95	1823	-0.561*
WPCa	Cd	20	11	0.0584	5.61	0.0102	4.61	0.874	2.69	99.58	237	0.343
WPCa	Cd	20	11	0.0270	4.62	0.0411	4.59	0.373	3.08	99.56	226	0.405
WPCa	Cd	40	11	0.0347	4.88	0.0914	3.09	0.905	3.09	99.73	366	0.290
WPCa	Cd	40	11	0.0238	4.50	1.79	2.89	0.231	1.92	99.70	337	0.354
WPNa	Cd	20	20	0.0225	5.79	0.0881	5.79	0.866	4.30	99.98	16539	0.248
WPNa	Cd	20	20	0.0474	6.30	0.104	5.22	0.872	4.25	99.99	41080	-0.445*
WPNa	Cd	40	20	0.0164	5.88	0.0825	5.88	0.705	4.50	99.99	20721	0.165
WPNa	Cd	40	20	0.165	5.65	2.16	3.76	0.00365	1.84	99.98	13581	0.156
WPNa	Cu	20	12	0.0294	10.3	0.163	7.90	0.542	6.24	99.99	10876	-0.329
WPNa	Cu	20	13	0.0560	9.38	0.157	7.55	0.462	6.20	99.86	1006	-0.207
WPNa	Cu	40	20	0.0682	9.93	0.202	8.00	0.562	6.53	99.96	6940	0.056
WPNa	Cu	40	20	0.0749	9.62	0.200	7.84	0.531	6.44	99.94	4641	0.250

Table 6.8 Summary of refined parameters and statistical tests from fitting metal ion binding data to a model incorporating a lognormal distribution of binding constants with C_L fixed and including NO_3^- and OH^- complexes. Unweighted regressions with respect to C_{ML}; [a]adjustable parameters, Equation 6.2. [b]Singly lagged residual autocorrelation (*P≤0.05).

Ligand	Metal ion	Temp. /°C	Number of data	Fixed C_L /mmol g^{-1}	log K_μ	σ_K	R^2 (%)	F	r_1[b]
SHCa	Cd	5	11	1.95	1.95	0.908	99.24	1177	0.464
SHCa	Cd	5	11	1.95	2.21	0.746	99.75	3526	0.315
SHCa	Cd	20	12	1.95	1.56	1.25	99.57	2342	0.451
SHCa	Cd	20	12	1.95	1.60	1.22	99.60	2506	0.620*
SHCa	Cd	40	12	1.95	1.91	1.14	99.50	2010	0.180
SHCa	Cd	40	12	1.95	1.85	1.17	99.17	1203	0.136
SHCa	Cu	5	16	1.95	0.509	3.38	68.38	44	0.310
SHCa	Cu	5	18	1.95	2.35	1.92	99.18	1943	0.060
SHCa	Cu	20	18	1.95	4.86	1.29	5.51	17	0.479*
SHCa	Cu	20	18	1.95	1.81	2.65	52.70	34	0.202
SHCa	Cu	40	18	1.95	4.05	2.07	86.29	117	0.700*
SHNa	Cd	20	15	1.95	2.76	1.36	99.89	11870	0.433
SHNa	Cd	20	23	1.95	3.15	1.10	99.92	27580	0.426*
SHNa	Cd	40	20	1.95	2.91	1.26	99.90	17634	0.542*
SHNa	Cd	40	20	1.95	3.26	1.00	99.80	9037	0.455*
SHNa	Cu	20	13	1.95	3.43	2.68	99.90	11428	0.483*
SHNa	Cu	20	13	1.95	3.28	2.49	99.96	26305	0.405
SHNa	Cu	40	14	1.95	5.13	1.20	99.46	2218	0.346
SHNa	Cu	40	20	1.95	4.67	2.12	99.95	34130	0.196
WPCa	Cd	5	11	2.60	1.26	1.30	99.95	19723	-0.121
WPCa	Cd	5	11	2.60	1.33	1.26	99.90	8559	-0.466
WPCa	Cd	20	11	2.60	1.56	1.21	99.37	1421	0.474
WPCa	Cd	20	11	2.60	1.57	1.20	99.35	1373	0.555*
WPCa	Cd	40	11	2.60	1.73	1.15	99.63	2427	0.497*
WPCa	Cd	40	11	2.60	1.72	1.15	99.63	2435	0.447
WPCa	Cu	5	18	2.60	2.53	1.80	96.98	529	0.216
WPCa	Cu	5	18	2.60	1.94	2.00	99.18	1951	0.061
WPCa	Cu	20	18	2.60	2.27	1.98	87.25	126	-0.062
WPCa	Cu	20	18	2.60	1.25	2.76	52.62	34	0.203
WPCa	Cu	40	17	2.60	4.46	1.66	87.06	116	0.465*
WPNa	Cd	20	20	2.60	3.09	1.21	99.95	34966	0.630*
WPNa	Cd	20	20	2.60	3.09	1.22	99.92	23598	0.691*
WPNa	Cd	40	20	2.60	3.16	1.20	99.96	48308	0.517*
WPNa	Cd	40	20	2.60	3.14	1.21	99.91	21003	0.675*
WPNa	Cu	20	12	2.60	4.19	2.06	99.91	10645	0.384
WPNa	Cu	20	13	2.60	4.00	2.14	99.85	7426	0.134
WPNa	Cu	40	20	2.60	4.65	2.16	99.91	20717	0.583*
WPNa	Cu	40	20	2.60	4.51	2.18	99.95	35596	0.476*

Table 6.9 Refined parameters and statistical summaries for fits of metal-humate binding data to a model incorporating a lognormal distribution of metal-humate binding constants and including NO_3^- and OH^- complexes. Unweighted regressions with respect to C_{ML}; [a]adjustable parameters, Equation 6.2. [b]Singly lagged residual autocorrelation (*P≤0.05).

Ligand	Metal ion	Temp. /°C	Number of data	C_L[a]/ mmol g^{-1}	log K_μ[a]	σ_K[a]	R^2 (%)	F	r_1[b]
SHCa	Cd	5	11	1.73	2.04	0.886	99.24	528	0.464
SHCa	Cd	5	11	3.59	1.74	0.860	99.74	1565	0.330
SHCa	Cd	20	12	1.26	1.98	1.16	99.59	1090	0.433
SHCa	Cd	20	12	1.75	1.70	1.20	99.60	1135	0.617*
SHCa	Cd	40	12	1.09	2.47	0.997	99.54	969	0.159
SHCa	Cd	40	12	1.34	4.36	0.204	99.42	772	-0.033
SHCa	Cu	5	16	0.0472	8.46	0.249	77.84	29	0.469*
SHCa	Cu	5	18	3.04	1.71	2.05	99.19	920	0.056
SHCa	Cu	20	18	2.12	4.79	1.30	5.52	8	0.476*
SHCa	Cu	20	18	2.02	1.70	2.68	52.69	16	0.208
SHCa	Cu	40	18	1.36	4.61	1.94	86.45	55	0.697*
SHNa	Cd	20	15	5.99	1.28	1.72	99.93	9083	0.395
SHNa	Cd	20	23	6.66	1.61	1.53	99.97	33384	0.019
SHNa	Cd	40	20	0.857	3.91	0.915	99.93	12542	0.320
SHNa	Cd	40	20	2.18	3.14	1.04	99.80	4176	0.464*
SHNa	Cu	20	13	2.34	2.94	2.83	99.91	5278	0.518*
SHNa	Cu	20	13	4.55	1.13	3.09	99.99	44258	-0.457*
SHNa	Cu	40	14	3.86	3.65	2.45	99.63	1488	0.192
SHNa	Cu	40	20	1.83	4.81	2.07	99.95	16673	0.173
WPCa	Cd	5	11	2.59	1.26	1.30	99.96	8801	-0.158
WPCa	Cd	5	11	2.71	1.31	1.26	99.90	3846	-0.426
WPCa	Cd	20	11	1.17	4.39	0.205	99.57	939	0.339
WPCa	Cd	20	11	1.31	4.29	0.291	99.55	894	0.410
WPCa	Cd	40	11	2.12	3.98	0.472	99.70	1346	0.239
WPCa	Cd	40	11	3.02	1.59	1.17	99.63	1073	0.468
WPCa	Cu	5	18	2.70	2.49	1.80	96.98	248	0.217
WPCa	Cu	5	18	3.70	1.42	2.11	99.18	917	0.063
WPCa	Cu	20	18	2.66	2.23	1.98	87.27	59	-0.062
WPCa	Cu	20	18	2.53	1.29	2.76	52.66	16	0.206
WPCa	Cu	40	17	2.83	4.35	1.69	87.05	54	0.467*
WPNa	Cd	20	20	2.86	2.98	1.24	99.95	16376	0.630*
WPNa	Cd	20	20	12.0	1.16	1.69	99.98	35910	0.416*
WPNa	Cd	40	20	2.13	3.40	1.13	99.96	23760	0.511*
WPNa	Cd	40	20	1.25	4.01	0.924	99.93	12921	0.526*
WPNa	Cu	20	12	10.2	1.29	2.82	99.97	13802	0.038
WPNa	Cu	20	13	4.19	2.98	2.44	99.87	3375	0.026
WPNa	Cu	40	20	6.05	2.73	2.71	99.96	23414	0.108
WPNa	Cu	40	20	3.65	3.75	2.41	99.96	22018	0.297

Table 6.10 Refined parameters and statistical summaries for fits of metal-humate binding data to the Sips/fixed C_L binding model incorporating NO_3^- and OH^- complexes. Unweighted regressions with respect to C_{ML}; [a]adjustable parameters, Equation 2.17; [b]calculated using Equation 2.17. [c]Singly lagged residual autocorrelation (*P≤0.05).

Ligand	Metal ion	Temp. /°C	Number of data	Fixed C_L/ mmol g^{-1}	A[a]	β[a]	log K_μ[b]	R^2 (%)	F	r_1[c]
SHCa	Cd	5	11	1.95	332	0.883	2.53	99.01	907	0.492
SHCa	Cd	5	11	1.95	570	0.930	2.65	99.71	3151	0.443
SHCa	Cd	20	12	1.95	94.7	0.735	2.29	99.37	1577	0.539*
SHCa	Cd	20	12	1.95	107	0.747	2.33	99.44	1784	0.687*
SHCa	Cd	40	12	1.95	183	0.771	2.56	99.21	1270	0.328
SHCa	Cd	40	12	1.95	162	0.761	2.52	98.81	842	0.279
SHCa	Cu	5	16	1.95	10.3	0.316	2.28	66.30	42	0.327
SHCa	Cu	5	18	1.95	153	0.542	3.50	99.14	1851	0.140
SHCa	Cu	20	18	1.95	2.14×10^5	0.719	5.62	3.15	17	0.480
SHCa	Cu	20	18	1.95	44.7	0.407	3.34	51.43	33	0.213
SHCa	Cu	40	18	1.95	712	0.496	5.17	84.92	106	0.728*
SHNa	Cd	20	15	1.95	0.0142	0.591	3.15	99.93	18422	0.635*
SHNa	Cd	20	23	1.95	0.0239	0.628	3.35	99.94	36674	0.495*
SHNa	Cd	40	20	1.95	0.0169	0.604	3.21	99.62	4783	0.763*
SHNa	Cd	40	20	1.95	0.0495	0.690	3.48	99.60	4514	0.649*
SHNa	Cu	20	13	1.95	0.00237	0.293	3.70	99.76	4612	0.742*
SHNa	Cu	20	13	1.95	0.00280	0.321	3.61	99.93	16547	0.551*
SHNa	Cu	40	14	1.95	0.0210	0.381	5.33	99.71	4157	0.075
SHNa	Cu	40	20	1.95	0.00949	0.351	4.81	99.70	6012	0.659*
WPCa	Cd	5	11	2.60	112	0.755	2.16	99.95	18169	0.170
WPCa	Cd	5	11	2.60	134	0.771	2.22	99.91	9952	-0.202
WPCa	Cd	20	11	2.60	193	0.784	2.39	99.05	948	0.528*
WPCa	Cd	20	11	2.60	199	0.787	2.39	99.03	925	0.597*
WPCa	Cd	40	11	2.60	263	0.802	2.50	99.42	1548	0.618*
WPCa	Cd	40	11	2.60	271	0.805	2.51	99.47	1711	0.621*
WPCa	Cu	5	18	2.60	724	0.625	3.91	97.16	563	0.175
WPCa	Cu	5	18	2.60	148	0.540	3.25	99.13	1847	0.143
WPCa	Cu	20	18	2.60	368	0.574	3.75	86.99	123	-0.073
WPCa	Cu	20	18	2.60	43.4	0.406	3.01	51.39	33	0.214
WPCa	Cu	40	17	2.60	1.55×10^5	0.659	5.73	85.99	107	0.497*
WPNa	Cd	20	20	2.60	0.0344	0.625	3.39	99.79	8618	0.759*
WPNa	Cd	20	20	2.60	0.0334	0.622	3.39	99.97	54579	0.484*
WPNa	Cd	40	20	2.60	0.0369	0.624	3.45	99.79	8548	0.745*
WPNa	Cd	40	20	2.60	0.0342	0.618	3.43	99.64	4937	0.806*
WPNa	Cu	20	12	2.60	0.0138	0.385	4.49	99.96	22680	0.408
WPNa	Cu	20	13	2.60	0.0103	0.371	4.31	99.81	5767	0.160
WPNa	Cu	40	20	2.60	0.0149	0.359	4.89	99.93	24455	0.315
WPNa	Cu	40	20	2.60	0.0130	0.357	4.76	99.86	13262	0.528*

Table 6.11 Refined parameters and statistical summaries for fits of metal-humate binding data to the Sips binding model incorporating NO_3^- and OH^- complexes. Unweighted regressions with respect to C_{ML}; [a]adjustable parameters, Equation 2.17; [b]calculated using Equation 2.18. [c]Singly lagged residual autocorrelation (*P≤0.05).

Ligand	Metal ion	Temp. /°C	Number of data	C_L[a]/ mmol g^{-1}	A[a]	β[a]	log K_μ[b]	R^2 (%)	F	r_1[c]
SHCa	Cd	5	11	0.0869	7700	1.14	4.34	99.47	756	0.331
SHCa	Cd	5	11	0.303	1130	0.986	3.62	99.63	1504	0.316
SHCa	Cd	20	12	0.155	605	0.883	4.07	99.57	1045	0.430
SHCa	Cd	20	12	0.180	494	0.869	3.96	99.57	1057	0.598*
SHCa	Cd	40	12	0.131	308	0.993	4.40	99.64	1241	0.076
SHCa	Cd	40	12	0.113	4950	1.03	4.51	99.42	779	-0.045
SHCa	Cu	5	16	0.0471	4.15×10^{6}	0.939	8.46	77.85	29	0.473*
SHCa	Cu	5	18	0.419	260	0.572	4.89	99.15	882	0.112
SHCa	Cu	20	18	0.0453	9.44×10^{15}	1.95	8.36	19.49	9	0.449*
SHCa	Cu	20	18	0.0489	1.70×10^{7}	0.931	8.10	57.49	18	0.180
SHCa	Cu	40	18	0.0579	1.76×10^{10}	1.17	8.99	91.58	89	0.354
SHNa	Cd	20	15	1.15	0.0199	0.615	3.64	99.94	9468	0.510*
SHNa	Cd	20	23	1.19	0.0424	0.672	3.78	99.97	29219	0.092
SHNa	Cd	40	20	0.488	0.148	0.764	4.56	99.91	9148	0.358
SHNa	Cd	40	20	0.574	0.373	0.842	4.53	99.81	4367	0.385*
SHNa	Cu	20	13	1.87	0.00531	0.336	5.04	99.86	3452	0.580*
SHNa	Cu	20	13	1.14	0.00520	0.355	4.673	99.98	26521	-0.049
SHNa	Cu	40	14	5.38	0.0102	0.346	3.697	99.76	2243	0.016
SHNa	Cu	40	20	1.14	0.0290	0.410	5.865	99.90	8679	0.433*
WPCa	Cd	5	11	0.401	178.6	0.791	3.35	99.96	10584	-0.156
WPCa	Cd	5	11	0.725	167.4	0.788	3.00	99.91	4549	-0.327
WPCa	Cd	20	11	0.0955	4674	1.03	4.548	99.58	951	0.301
WPCa	Cd	20	11	0.0942	5050	1.04	4.55	99.56	916	0.327
WPCa	Cd	40	11	0.124	273	0.982	4.42	99.68	1238	0.185
WPCa	Cd	40	11	0.157	1510	0.937	4.25	99.61	1036	0.283
WPCa	Cu	5	18	0.102	673	0.621	-1.90	97.17	265	0.172
WPCa	Cu	5	18	0.419	260	0.572	4.88	99.15	882	0.112
WPCa	Cu	20	18	0.0878	453	0.7040	6.70	87.22	59	-0.037
WPCa	Cu	20	18	0.0488	1.72×10^{7}	0.931	8.105	57.49	18	0.180
WPCa	Cu	40	17	1.87	1.47×10^{5}	0.657	5.930	85.97	50	0.515*
WPNa	Cd	20	20	0.821	0.147	0.730	4.46	99.91	9920	0.679*
WPNa	Cd	20	20	1.55	0.0502	0.651	3.854	99.98	36403	0.331
WPNa	Cd	40	20	0.808	0.178	0.7366	4.538	99.93	12827	0.601*
WPNa	Cd	40	20	0.676	0.277	0.7682	4.703	99.89	7652	0.592*
WPNa	Cu	20	12	1.86	0.0198	0.4037	5.018	99.97	13175	0.193
WPNa	Cu	20	13	1.35	0.0249	0.4186	5.414	99.88	4265	-0.126
WPNa	Cu	40	20	1.69	0.0279	0.3912	5.670	99.98	36700	-0.137
WPNa	Cu	40	20	1.47	0.0322	0.4037	5.801	99.98	36913	0.061

Table 6.12 Summary of fits of Cd^{2+} and Cu^{2+} - SHNa and WPNa binding data to Teasdale modification/self-association model; f (Equation 5.12) is assumed to be 2. Unweighted regressions with respect to C_{ML}; [a]adjustable parameters, Equation 5.12. [b]Singly lagged residual autocorrelation (*P≤0.05).

Ligand	Metal ion	Temp. /°C	Number of data	C_L[a]/ mol $L^{-1}\times10^{-5}$	log K_{ML}[a]	log K_S[a]	R^2 (%)	F	r_1[b] (all *)
SHNa	Cd	20	15	0.263	5.13	7.47	98.96	576	0.579
SHNa	Cd	20	23	0.475	4.73	2.04	99.17	1209	0.755
SHNa	Cd	40	20	0.306	5.03	7.47	99.58	2014	0.645
SHNa	Cd	40	20	0.409	4.85	1.87	99.54	1859	0.488
SHNa	Cu	20	13	0.403	7.06	1.36	90.06	50	0.717
SHNa	Cu	20	13	0.372	6.64	2.32	93.34	75	0.714
SHNa	Cu	40	14	0.474	7.70	1.44	93.57	86	0.695
SHNa	Cu	40	20	0.510	7.32	1.44	91.18	96	0.704
WPNa	Cd	20	20	0.425	5.12	1.45	99.30	1208	0.753
WPNa	Cd	20	20	0.431	5.11	1.62	99.06	906	0.813
WPNa	Cd	40	20	0.438	5.15	0.924	99.34	1284	0.747
WPNa	Cd	40	20	0.425	5.18	1.21	99.41	1441	0.674
WPNa	Cu	20	12	0.479	7.22	1.56	94.82	87	0.671
WPNa	Cu	20	13	0.475	7.10	1.38	94.50	91	0.707
WPNa	Cu	40	20	0.555	7.58	0.860	91.47	100	0.744
WPNa	Cu	40	20	0.542	7.51	0.795	91.50	100	0.731

Table 6.13 Summary of fits of Cd^{2+}- and Cu^{2+}- sodium humate binding data to Teasdale crosslinking model with f treated as an adjustable parameter. Unweighted regressions with respect to C_{ML}; [a]adjustable parameters, Equation 6.4. [b]Singly lagged residual autocorrelation (*P≤0.05).

Ligand	Metal ion	Temp. /°C	Number of data	C_L[a]/ mol $L^{-1}\times10^{-8}$	log K_X[a]	f[a]	$C_L.f$/ mol $L^{-1}\times10^{-5}$	R^2(%)	F	r_1[b] (all *)
SHNa	Cd	20	15	7.24	4.80	402	2.91	98.65	443	0.696
SHNa	Cd	20	23	21.1	4.43	238	5.03	99.08	1091	0.795
SHNa	Cd	40	20	18.1	4.66	193	3.49	99.50	1689	0.730
SHNa	Cd	40	20	35.5	4.50	127	4.52	99.63	2312	0.567
SHNa	Cu	20	13	0.0425	6.61	1.48×10^5	6.30	91.60	60	0.735
SHNa	Cu	20	13	0.0868	6.29	6.47×10^4	5.61	93.94	83	0.733
SHNa	Cu	40	14	0.0371	7.09	2.24×10^5	8.30	92.18	70	0.707
SHNa	Cu	40	20	0.0317	6.78	2.70×10^5	8.54	90.84	93	0.745
WPNa	Cd	20	20	11.0	4.75	451	4.95	99.34	1279	0.828
WPNa	Cd	20	20	8.69	4.74	580	5.04	99.01	854	0.848
WPNa	Cd	40	20	11.2	4.78	461	5.15	99.38	1366	0.826
WPNa	Cd	40	20	11.2	4.80	447	5.02	99.47	1604	0.753
WPNa	Cu	20	12	0.0625	6.66	1.28×10^5	8.02	94.10	76	0.675
WPNa	Cu	20	13	0.104	6.55	7.54×10^4	7.86	93.87	82	0.715
WPNa	Cu	40	20	0.0272	7.04	3.47×10^5	9.44	89.98	85	0.736
WPNa	Cu	40	20	0.0253	6.93	3.69×10^5	9.33	90.31	88	0.744

Table 6.14 Representative fits, using Cd^{2+}-SHNa binding data, to the Teasdale crosslinking model with f fixed at different values. Unweighted regressions with respect to C_{ML}; [a]adjustable parameters, Equation 6.4. [b]Singly lagged residual autocorrelation (*P≤0.05).

Ligand	Metal ion	Temp. /° C	Number of data	C_L[a]/ μmol L^{-1}	log K_X[a]	Fixed f	$C_L \cdot f$/ μmol L^{-1}	R^2(%)	F	r_1[b] (all *)
SHNa	Cd	20	15	13.5	4.73	2	27.0	97.85	605	0.724
SHNa	Cd	20	23	23.9	4.38	2	47.9	98.63	1529	0.820
SHNa	Cd	40	20	16.3	4.61	2	32.6	99.07	1944	0.785
SHNa	Cd	40	20	20.5	4.48	2	40.9	99.41	3068	0.654
SHNa	Cd	20	15	7.00	4.75	4	28.0	98.19	717	0.717
SHNa	Cd	20	23	12.3	4.40	4	49.1	98.83	1799	0.812
SHNa	Cd	40	20	8.41	4.63	4	33.7	99.26	2446	0.768
SHNa	Cd	40	20	10.7	4.49	4	42.8	99.516	3720	0.621
SHNa	Cd	20	15	3.57	4.77	8	28.6	98.40	810	0.709
SHNa	Cd	20	23	6.22	4.41	8	49.7	98.95	2005	0.806
SHNa	Cd	40	20	4.28	4.64	8	34.3	99.38	2882	0.753
SHNa	Cd	40	20	5.50	4.50	8	44.0	99.57	4223	0.596

6.4 Discussion

6.4.1 Experimental Methods

The confidence placed in measurements of humic substance-metal ion binding is directly dependent on the reliability of the experimental technique. The ideal technique would be able to determine uncomplexed metal ion with good selectivity, accuracy and precision. Selectivity in an analytical method may be considered as the degree of freedom from interference, or whether the measurement variable (for example, electrode potential) is affected only by the analyte species. Accuracy refers to the closeness of the analytical result to the true level of analyte; precision is related to reproducibility and is a measure of the variability in experimental measurement (Bauer *et al.*, 1978).

6.4.1.1 Selectivity in metal ion determinations

Methods used for determining speciation in humic substance-metal ion systems are discussed in Section 2.5. Potential interferences when determining free metal ion concentrations, as applied to this work, are: (i) the electrode calibration procedure results in a measured response to a sum of free and NO_3^--complexed metal ion, and; (ii) possible interference due to surface activity of humic substances on the electrode surface.

Problem (i) above is accounted for using the correction procedure outlined in Section 6.2.4. As nitrate is a rather weakly complexing ligand, the effect on total metal binding is small, especially in competition with stronger ligands such as those present on humic substances. Problem (ii) above is impossible to avoid when working with humic substances, and difficult to correct for. The *in-situ* calibration technique used for cadmium/sodium humate titrations (Section 3.4.2) may allow for any effects of humic substances on electrode surfaces. Since the charge on humic substance macromolecules changes with pH, however, it is unlikely that humic substance surface activity remains constant with pH.

Certainly, at the pH of measurement, it is not possible to distinguish between effects on electrode potentials due to reduction in metal ion activity by complexation, or effects on potentials due to surface processes such as humic substance adsorption on electrodes.

6.4.1.2 Accuracy of metal ion determinations

The procedure used to calibrate ion selective electrode response is the single most important factor influencing the accuracy of free metal ion determination. In this work, extrapolations from the region of calibration curves where electrode response is linear and close to Nernstian, have been made to infer metal ion concentrations outside (that is, below) the calibration range. Justification for this procedure depends on the work of Midgley (1976) and Avdeef *et al.* (1983) who tested the response of copper(II) ion-selective electrodes at very low levels of free copper in the presence of complexing ligands. Both sets of workers found Nernstian electrode response was maintained under these conditions (see Chapter 3, Section 3.3.2).

Other problems with accuracy of calibrations have been minimised by ensuring that calibration and measurement conditions were, as far as possible, identical (Chapter 3; Sections 3.3.2, 3.4.1 and 3.4.2).

6.4.1.3 Precision in metal ion determinations

Since no independent measurements were made to estimate the degree of reproducibility in metal ion determinations, the precision of metal ion determinations is inferred from reproducibility between individual titrations.

A titration experiment for which four replicates were performed enabled the pattern in variability to be examined with respect to either (log)metal concentration, or amount of metal bound. Replicates were

compared in terms of $[Cd^{2+}]$ and amount of bound Cd^{2+} at equivalent levels of total Cd^{2+}. Results are presented as plots of standard deviations and relative standard deviations *versus* mean values in Figure 6.11. These results show that relative errors cannot be considered to be constant for either bound Cd^{2+} or free Cd^{2+} concentration. It appears from these limited results that variance is approximately equal for measurements of bound Cd^{2+} or $[Cd^{2+}]$. Since constant absolute variance with respect to log [M] requires, by definition, constant relative variance with respect to [M], then variance can not, in this case, have been constant with respect to the log of metal ion concentration, as has been assumed by other authors (for example, Turner *et al.*, 1986). The observation that the variance with respect to bound metal was found to be approximately constant lends further justification to the combination of model formulation and/or systematic weighting used in regressions (Chapters 3 and 4). It is assumed that these trends in variability of titration data are also true for other titrations.

In qualitative terms, it is apparent from Figures 6.2 - 6.9 that there is much greater variability in measurements of $[Cu^{2+}]$ than in measurements of $[Cd^{2+}]$. This is most likely to be a result of the much lower copper ion concentrations being measured. Comparison of experiments involving copper binding show that substantially more variability is observed for experiments involving calcium humates than for those involving sodium humates. This may indicate possible interferences from colloidal humic substances in the analyte solutions. Alternatively, large amounts of random variability could result from the binding reactions themselves. For reactions involving calcium humates, the need for metal ions to diffuse through non-uniform macromolecular aggregates may have resulted in high variability due to heterogeneity in diffusion rates. The greater degree of internal consistency observed, in titrations of sodium humates with Cu^{2+}, may have been a function of the continuous titration technique. Any systematic errors were likely to affect all measurements similarly, since all measurements were made on a single titration solution.

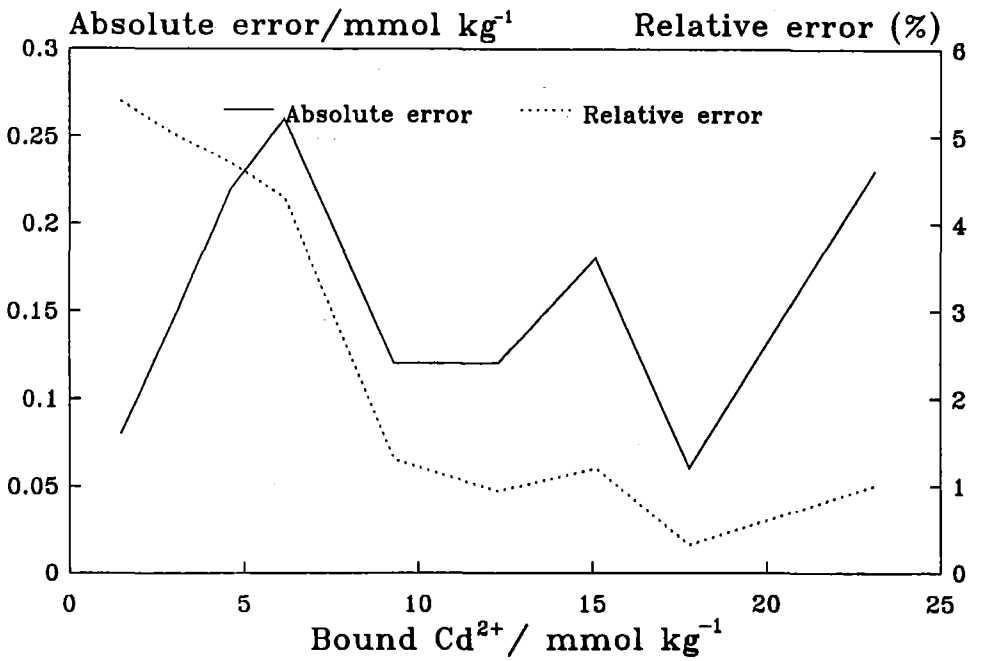

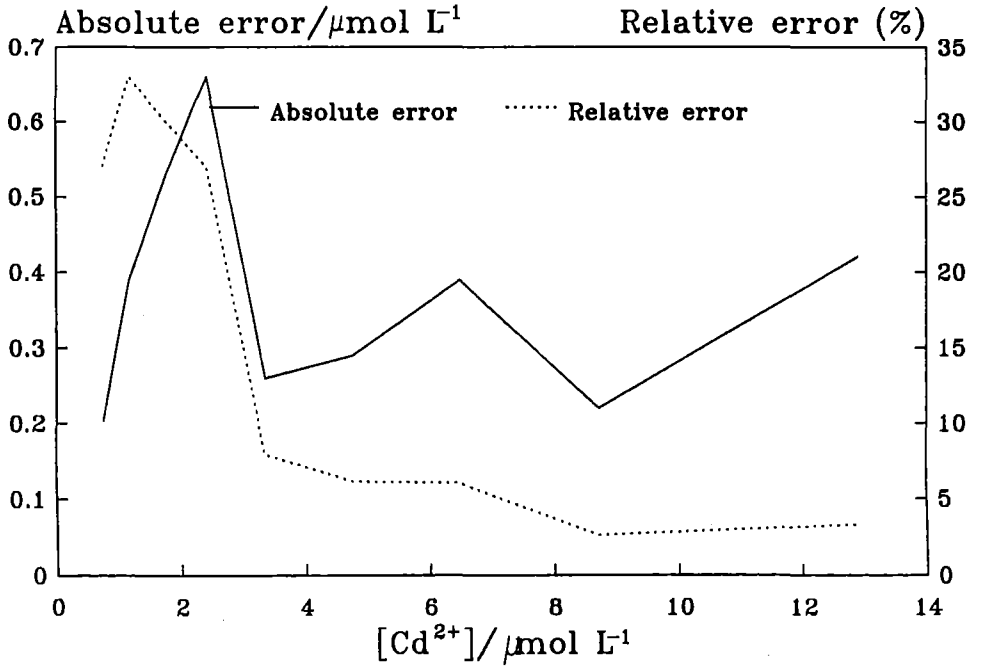

Figure 6.11 Trends in variability for experiments measuring binding of Cd^{2+} to SHCa: (a) with respect to humate-bound Cd; (b) with respect to $[Cd^{2+}]$.

6.4.2 Complexation Reactions

Waimari Peat humates (WPCa, WPNa) were able to bind Cd^{2+} and Cu^{2+} slightly more strongly than Summit Hill humates (SHCa, SHNa) (Figures 6.2 - 6.9). For example, for equivalent levels of bound metal ion, free metal ion concentrations were 0.1-0.4 log[M] units lower in WPNa systems than in SHNa systems, given identical experimental conditions. This effect is considered to be a result of the higher charge, at pH 6.0., for WPHA (2.46 mmol g^{-1}; Table 5.3) compared with SHHA (1.83 mmol g^{-1}; Table 5.3). Effects due to other chemical differences cannot, however, be discounted.

Comparison of Figures 6.2 - 6.9 also shows that Cu^{2+} is bound much more strongly than Cd^{2+} by all humate ligands in this work. For equivalent levels of bound metal, free metal ion concentrations were approximately two orders of magnitude lower for Cu^{2+} than for Cd^{2+}, given the same humate ligand and experimental conditions. This observation is consistent with the expected complexation behaviour for these two metal cations.

Additional information on the difference in Cu^{2+}- and Cd^{2+}-humate complexation behaviour is obtained from proton release data from metal ion - sodium humate titration experiments (Sections 6.3.3 and 6.3.4). Both metal ions are able to displace H^+ from ligands on humic substances at pH 6.0; however, Cu^{2+} binding, on average, liberates approximately twice as many protons as Cd^{2+} binding.

The nature or stoichiometry of the metal humate complexes is not accessible, in this case, from proton release data. The values obtained from alkali consumption in titrations (1.4 mol H^+/mol bound Cu^{2+}; 0.6 - 0.8 mol H^+/ mol bound Cd^{2+}) are averages over many sites, and there is no requirement that individual sites are electrically neutral. In addition, the amount of carboxylic acid groups remaining protonated at pH 6.0 can be estimated from titration data for the appropriate humic acid (Chapter 5, Tables 5.3 and 5.4). For both sodium humates, the amounts of undissociated carboxylic acid groups (0.83 mmol g^{-1} for SHNa, 0.90 mmol g^{-1} for WPNa) are sufficient to account for all proton release in titrations, meaning that it is unnecessary to invoke complexation by more weakly acidic ligands to

explain the observed release of H^+. This does not mean that functional groups such as phenols are not involved in complexation reactions, but merely illustrates the ambiguity that remains when attempting to assign structure or stoichiometry to metal-humate complexes.

That proton release does occur is interesting, however, as it provides evidence for inner sphere complexation for both Cu^{2+} and Cd^{2+}, especially since hydrolysis reactions were found to be unimportant (Section 6.4.2). As levels of metal ion addition were low in all titrations, the possibility that proton release is due to a Donnan effect can also be discounted.

It is considered that changes in the electrostatic potential of the humate macro-ions may have contributed to the observed binding heterogeneity observed in these experiments. The presence of inert electrolyte (0.1 mol L^{-1} $NaNO_3$ or 0.05 mol L^{-1} $Ca(NO_3)_2$), in both titrant and humate solutions, would have made any changes in ionic strength during titrations negligible. The maximum levels of metal ion addition used ($\leq$0.15 meq g^{-1} for calcium humates; $\leq$1.3 meq g^{-1} for sodium humates) were, however, significant compared with the total numbers of dissociated acidic functional groups (1.83 meq g^{-1} for SHHA, 2.64 meq g^{-1} for WPHA, at pH 6.0; Table 5.3), and thus charge neutralisation by complexing metal ions may have occurred.

6.4.3 Description of Humate-Metal Binding using Modelling Equations

The binding reactions of copper(II) and cadmium(II) with calcium and sodium humates are described well, in terms of goodness of fit in an empirical manner, by several of the equations used. All of the equations used to model the binding data have some theoretical basis (see Chapter 2). Whether the particular theory involved applies to metal-humic substance binding reactions, however, is questionable in some cases. As far as the value of the various models for predictive purposes is concerned, the observation that so many of the models would allow predictions to be made with confidence means that choice of a suitable predictive model will be based on ease of implementation, rather in terms of an

accurate description of the processes involved. If this is the case, the lack of requirement for an accurate physicochemical description would justify the use of more conceptually simple models.

Inclusion of Cd^{2+} and Cu^{2+} hydrolysis products and nitrate complexes in the models allowed calculation of the proportions of bound metal accounted for by these solution species. For both cadmium and copper, the mono-nitrate complex was found to be an important species, accounting for c. 0.8 - 4.5% of bound Cd^{2+} and c. 0.003 - 0.4% of bound Cu^{2+} at higher levels of metal addition in titrations of sodium humates. The only other species ever exceeding 0.1% of total metal speciation was $Cd(NO_3)_2^0$. The contribution of such complexes to metal ion speciation emphasises that they should not be ignored when formulating models for metal complexing behaviour in systems such as those observed in this work. Figure 6.12 shows a hypothetical distribution of humate-bound Cd^{2+} species and Cd^{2+}-nitrate complexes, derived from parameter estimates from the application of a three discrete ligand model to Cd^{2+}-SHNa binding data.

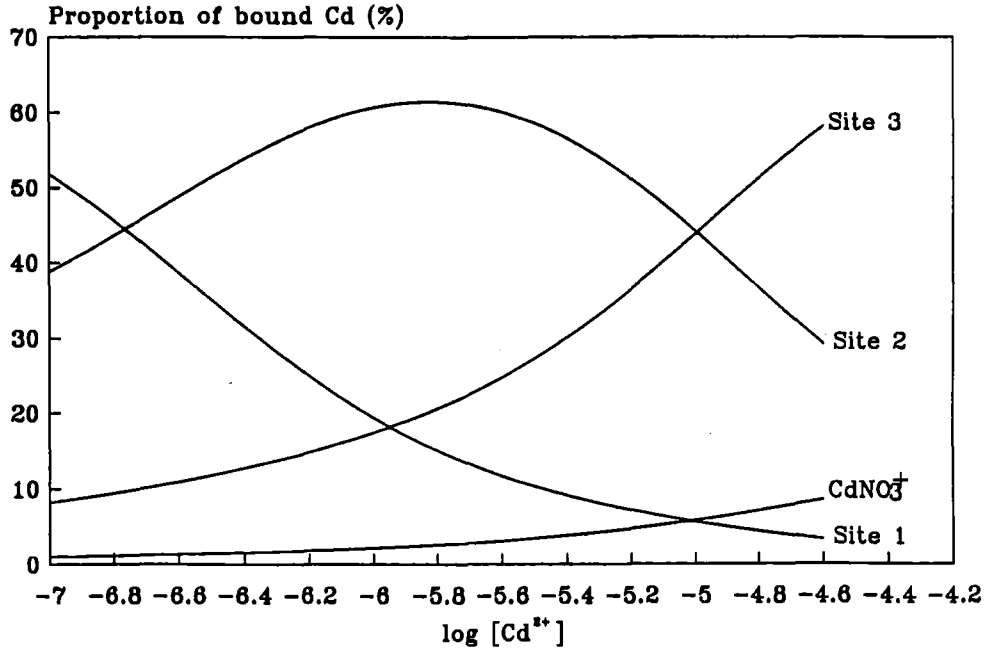

Figure 6.12 Hypothetical distribution of humate- and NO_3^- bound Cd^{2+} species, showing contribution of NO_3^- to complexation.

It is recognised that none of the models used to describe binding data explicitly involved mixed-ligand complexes. Such complexes (for example, humate-metal-hydroxy or humate-metal-nitrate) are dealt with implicitly when humate ligands are approximated to as mixtures of discrete sites, or as contributors to overall binding heterogeneity when models involve a continuous distribution of sites with respect to metal ion affinity.

Since the levels of metal ion addition in metal-humate titrations were intentionally kept low, binding curves showed no observable end points. As a result, no internally generated estimate of the total binding site density was available, in contrast with protonation data (Chapter 5). All of the modelling equations used allow C_L to be treated as an adjustable parameter and estimated from the experimental binding data. Owing to the relatively low levels of metal addition used, however, estimates of C_L from regressions are very likely to have high uncertainty. This may be illustrated qualitatively by inspecting estimates of C_L from regression analyses, for example using the lognormal distribution model (Table 6.9). For experiments involving the same ligand and metal ion, estimates of C_L from fits to this model vary by up to an order of magnitude. Since for many models, adjustable parameters may be highly correlated, fixing C_L at a nominal (but realistic) value may add stability to regressions and result in more realistic estimates for the remaining parameters. The arbitrary fixing of C_L values, on the basis of humic substance total acidity values, was recommended by Perdue (1989) for modelling of metal-humate binding data.

Conversely, it may not be physically unrealistic for observed values of C_L to vary somewhat with temperature, if binding reactions have not reached equilibrium over the timescale of the experiments used. Enhanced reaction rates at higher temperatures may allow a larger amount of humate binding sites to become occupied and thus the *effective* complexation capacity is increased.

6.4.3.1 Discrete ligand models

It was not considered to be unusual that copper-humate binding data was not described well by models incorporating a single type of noninteracting binding site. This observation has been made frequently by previous researchers (for example, Mantoura and Riley, 1975; Tuschall and Brezonik, 1983; Turner *et al.*, 1986) and fits in well with the concept that humic substances are chemically heterogeneous (see Chapter 2). It was somewhat surprising, then, to find that data from cadmium-humate binding experiments was, in some cases, described well by a single site model. In fact, it would be reasonable to conclude that sites on humic substances that bind Cd^{2+} to any significant extent, under the conditions of the experiments performed, exhibit a narrow range of affinities for cadmium ions. Cadmium(II) ions are 'soft' or 'Type B' metal ions (Cotton and Wilkinson, 1976), and as such would not be expected to form very strong complexes with the predominantly oxygen-containing donor atoms in the complex-forming functional groups present on humic substances. In addition, Cd^{2+} may be expected to form a substantial proportion of outer-sphere complexes with these ligands, and since the resulting complexes involve no direct metal-ligand electron sharing, differences in chemical environment may be suppressed. It is considered that these two factors combine to result in greatly decreased binding heterogeneity for Cd^{2+}-humate complexes compared with a more strongly complexing cation such as Cu^{2+}.

Refined values of the adjustable parameters found for various data sets appear to be physically realistic. When C_L was treated as an adjustable parameter, its refined values were substantially different than when C_L was fixed to be equal, on an equivalent basis, to the total acidity. A similar result was obtained on analysis of protonation data in Chapter 5; the explanation for metal binding data is the same, that is, absence of binding data at sufficiently high values of bound metal ion.

When the discrete ligand model was formulated to include a second site (as in classical Scatchard binding analysis (for example Mantoura and Riley, 1978) it provided an improved fit, relative to the single-site model, for all cadmium and copper humate binding data. In the case of cadmium(II)-calcium humate binding data, however, the refined values of the adjustable parameters often implied the

presence of a second 'site' which either: (i) is present as a small proportion (less than 1%) of sites; (ii) has a binding constant which means it would make a negligible contribution to binding under the experimental conditions, or; (iii) has a binding constant (almost) identical with the first site. In these cases, it was considered that the regression procedure had effectively 'rejected' the existence of the second site.

For those sets of Cd^{2+} and Cu^{2+} binding data where the second site was not effectively rejected, refined values for the adjustable parameters for the two ligand model (Table 6.4 and 6.5) appeared to be physically realistic, even when C_L was arbitrarily fixed. In addition, for these sets of data, the refined parameters always implied a lower density of sites for the site having a higher affinity for metal ions, compared with the site having lower affinity.

For those sets of titration data where the discrete binding model inferred two well-defined 'sites', attempts were made to fit a model incorporating three discrete ligands. In general, for cadmium-humate binding data, the three ligand model did not explain a greater proportion of variance of C_{CdL} (measured by R^2 values). For copper-humate binding data, however, the three site model provided significantly better fits to observed binding, measured by the F-test described in Chapter 3 (Section 3.6.6). For some data, a third site was also effectively rejected by the regression procedure (Tables 6.6 and 6.7).

It is recognised that the (C_i, log K_i) representations of hypothetical binding sites (Equation 6.1a,b) implied by discrete multiligand binding models are unlikely to represent true ligands in humic substances. Neither do they represent means values for 'classes' of binding sites (Perdue and Lytle, 1983). The finding that a discrete two ligand model generally provided the most significant description of cadmium binding data is likely to be a function of the experimental 'titration window' (Buffle, 1987; see Chapter 2, Section 2.4.3). Dzombak *et al.*,(1986) showed that the minimum number of discrete ligands required to adequately characterise binding of metal ions to ligand mixtures is approximated by the range of observed free metal ion concentrations in orders of magnitude. In this work, the range of $[Cd^{2+}]$ did not exceed three orders of magnitude (Figures 6.2 - 6.9) and thus, using the rule-of-thumb of

Dzombak *et al.*, (1986), two discrete sites should adequately describe cadmium-humate binding. Similarly, in copper-humate experiments, free copper concentrations spanned approximately three to four orders of magnitude (Figures 6.2 - 6.9), and thus copper-humate binding should be described adequately by a three to four ligand mixture. It should be noted that this rule-of-thumb is numerically derived, and has no physical justification.

The strictly empirical nature of discrete multiligand models, when applied to metal-humic substance complexation, does not mean that these models are not useful for predictive purposes. Turner *et al.* (1986) found that such models were best suited to predicting metal-humate speciation, on the basis of goodness of fit and ease of implementation. Care should be taken, however, not to extend predictions outside the ranges of reactant concentrations used in experiments (Dzombak *et al.*, 1986).

6.4.3.2 Continuous distribution multiligand models

In terms of goodness of fit, both the Sips and lognormal binding models provided a good description of cadmium- and copper-humate binding reactions. Copper(II)-humic substance binding has been found by other authors (for example, Perdue and Lytle, 1983; Fish *et al.*, 1986; Dobbs *et al.*, 1989a,b) to be described well by a mixture of ligands with a lognormal distribution of binding constants. In addition, the values of log K_{μ} and σ_K found by these researchers under similar experimental conditions for copper(II)-fulvate binding are in reasonable agreement with those found in this work; some values are listed in Table 6.15.

Table 6.15 Values of lognormal binding model parameters found by various authors for copper(II) binding to humic substances, pH 6.00.

Ligand	C_L/ mmol L^{-1}	log K_μ	σ_K	Reference
GPFA[a]	0.020	5.13	1.29	Fish *et al.*, 1986
TRFA[b]	0.04	3.82	2.01	Turner *et al.*, 1986
TRFA[b]	0.04	3.77	1.79	Turner *et al.*, 1986
SHNa	0.195	3.35[c]	2.58[c]	this work
WPNa	0.26	4.10[c]	2.10[c]	this work

[a] Grassy Pond Fulvic acid (USA); [b] Tamar River Fulvic acid (UK); [c]Mean values from replicate experiments

It is considered by some authors (for example, Marinsky and Ephraim, 1986) that the continuum of binding constants inferred by the lognormal or Sips models overestimates the functional-group heterogeneity of humic substances. The observation that such good fits are obtained, however, together with the probability that polyelectrolyte and aggregational effects are occurring in an already very complex ligand mixture, lead this author to consider that the physical implications of continuous multiligand models are feasible. This is especially true for humic acids, where the factors leading to heterogeneous binding (high molecular size and polydispersity, with associated extreme functional-group heterogeneity, and the possibility of aggregation processes and macro-ionic effects) are probably greater than for fulvic acids.

The refined parameters from fits of metal-humate binding data to the lognormal distribution (or Sips) model may be misleading, for the following reasons. Fish *et al.* (1986) found that, in a set of ligands which are normally distributed with respect to log K, only those ligands having log $K \geq \log K_\mu$ have any significant effect on metal ion speciation. As a result, refined values for log K_μ can appear to be lower than expected, and in effect log K_μ values represent a lower limit for sites involved in complexing reactions under the experimental conditions used. The standard normal distribution can be used to estimate, for example, the proportion of hypothetical ligands inferred by the lognormal model having log K higher than some arbitrary value. Conversely, a lower limit for log K for the strongest proportion (for example, 5%) of sites may be calculated in a similar fashion. For example, for Cu^{2+}-SHNa binding

at pH 6.0 and 20 ° C, the mean log K_μ (two replicates) is 3.36 and the mean σ_K is 2.58 (Table 6.8). Given these values, it may be estimated that:

(i) 0.5% of sites have log K ≥ 10.0, and

(ii) the strongest 5% of sites have log K ≥ 7.60.

Similar calculations may be used to estimate fractions of sites within arbitrary log K intervals, thus enabling approximation of the lognormal distribution using discrete ligands. Estimates of log K values from the Sips and lognormal binding models, and also discrete ligand models may be put into perspective by comparing with those of well-defined ligands. Using protonation and copper(II)-complex stability constants for various ligands (Perrin, 1979) it is possible to calculate pH and ionic strength dependent stability constants for these ligands. Table 6.16 contains conditional stability constants, valid for pH 6.0 and ionic strength = 0.1 mol L^{-1}, for various organic ligands.

Table 6.16 Conditional stability constants (log K') for selected organic ligands; pH 6.00, 25 ° C, I = 0.1 mol L^{-1}.

Ligand	log K'
Citrate	7.86
Ethylenediamine	5.44
EDTA	14.17
Nitrilotriacetate	9.65
Phthalate	3.11
Salicylate	3.20

A comparison of the range of effective binding constants found for ligands in humic substances with pH-dependent conditional stability constants for simple organic ligands shows that humic substances are able to bind at least a proportion of metal ions quite strongly. The finding that a significant proportion of humic substance ligands are predicted by models to have similar affinities for Cu^{2+} to chelating ligands such as citrate does not, however, prove the existence of such chelating moieties on humic substances. While it is quite possible that such structures exist, enhanced binding would also be expected for electrostatic reasons, due to the significant charge on humic substances at pH 6.0 as maintained in binding experiments (see Chapter 5, Table 5.3).

The finding that the lognormal distribution model is able to provide a good description of metal-humate binding with an equation having only three adjustable parameters means that the refined parameters may be used as useful comparisons between experimental treatments. A model having less adjustable parameters has less degree of freedom in regressions and parameters are often less highly correlated than in a model with more adjustable parameters. Even so, it is evident in qualitative and intuitive terms that the adjustable parameters for the lognormal distribution model (C_L, log K_μ, σ_K) will be correlated to some extent. For example, an increased density of sites with high affinity for metal ions on a humic substance may be accounted for in the model by an increase in any one of the adjustable parameters. The procedure of fixing a value of C_L in regressions is likely to reduce this effect.

It was shown in Chapter 5 (Section 5.4.4.3) that, for humic acid protonation, the parameters from the Sips binding model were simply related to those from the lognormal distribution model. For metal binding data, however, no simple relationship was found between the parameter estimates from these models unless data were categorised as shown in Figure 6.13.

6.4.3.3 Models based on aggregation processes

Aggregation processes have been implicated in metal-humic substance complexation reactions by several authors (for example: Rainville and Weber, 1982; Gamble *et al.*, 1985). Until the theoretical work of Teasdale (1987), however, no model had been developed which considered aggregation processes explicitly.

Even though no actual precipitates were observed to form during titration of sodium humates with cadmium(II) or copper(II) ions, it was considered that processes which allowed formation of soluble aggregates were quite feasible under titration conditions.

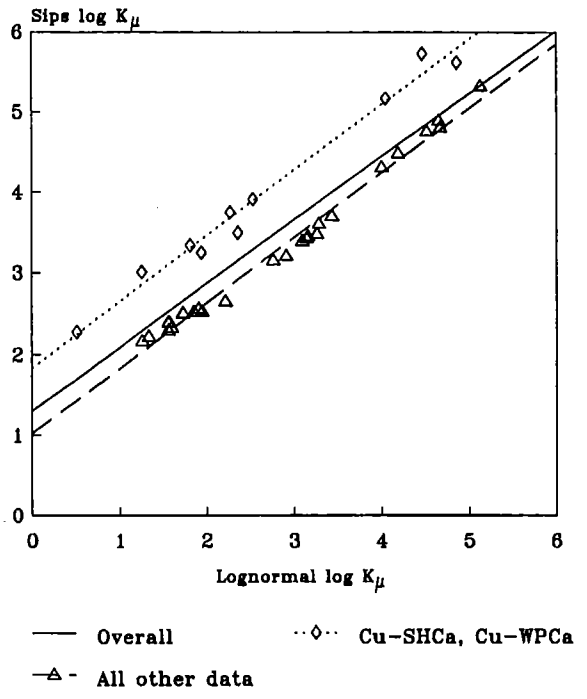

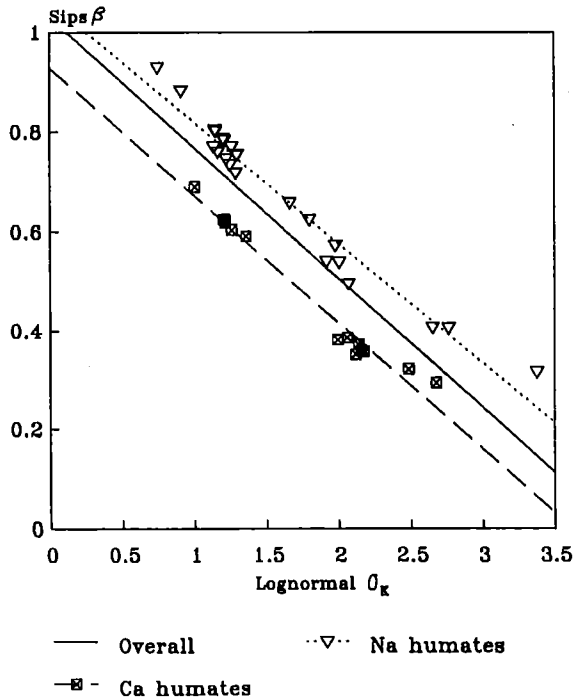

Figure 6.13 Relationship between parameters describing Sips and lognormal distributions for metal-humate binding.

It was somewhat surprising, then, to find that neither of the models proposed by Teasdale (1987) produced significantly improved fits of binding data compared with the single discrete site binding model. Although both the single site and Teasdale models explain binding in terms of a single ligand, it was expected that the greater number of adjustable parameters in the Teasdale models may have allowed closer agreement between observed and predicted binding. The form of the binding function implied by the modification/self association model (Teasdale, 1987), however, did not appear to be mimicked by any experimentally determined binding curve. In addition, the refined parameters derived from fits to this model are occasionally unrealistic. Values found for log K_S covered a very wide range (log K_S in the range 0.79 - 2.32 for Cu^{2+} binding; log K_S in the range 0.9 - 7.5 for Cd^{2+} binding), and a value of log K_S of c. 7.5, implying very strong self-association, is considered to be unlikely for cadmium(II)-humate binding. However, log K_S was not a well-defined parameter in regressions, and goodness of fit was almost independent of values for log K_S, indicating very broad minima in the residual sum of squares surface.

Similar behaviour was found for the crosslinking model. Although all adjustable parameters appeared to be well defined, refined values of f implied approximately 100 - 600 crosslinking sites per humate macromolecule for Cd^{2+} binding, and 0.6×10^5 - 4×10^5 crosslinking sites per humate macromolecule for Cu^{2+} binding. In addition, fits to this least restricted variant of the model often tended to diverge; this was shown by a tendency towards very small values for C_L combined with the large f values, and implied a strong (negative) correlation between these two parameters in regressions.

The number of potential binding (and therefore crosslinking) sites present on a humate macro-ion may be roughly estimated using the $Ba(OH)_2$ acidity (SHHA: 3.9 meq g^{-1}; WPHA: 5.2 meq g^{-1}; Chapter 5, Table 5.2) and assigning an arbitrary, but realistic (Stevenson, 1982; Hayes *et al.*, 1989b) number average molecular weight of 100 000 to the humic acid macromolecules. Given these two quantities, it may be calculated that the 'average humate macro-ion' contains 200-300 potential binding sites, assuming that metal ion binding is isoequivalent with proton binding. In light of this estimate, it is

considered that even 100 *active* crosslinking sites would be, on average, excessive since it is unlikely that all occupied binding sites could also act as crosslinking sites.

The poor fits to these aggregation-based models found for metal-humate binding data does not mean that aggregation processes are not occurring but rather that observed binding heterogeneity cannot be explained by aggregation alone, as recognised by Teasdale (1987) in developing these models. An extension of the models to include functional heterogeneity, macro-ionic effects and perhaps more than one mode of aggregation could provide an accurate and meaningful description of humic substance-metal ion complexation.

6.4.4 Temperature Dependence of Cadmium(II)/Copper(II) - Humate Binding Reactions

Any explanation of the observed dependence of the complexation reactions of Cd^{2+} and Cu^{2+} with sodium and calcium humates hinges on whether the reactions observed have reached equilibrium over the timescale of the experiments. If a true equilibrium has been achieved, then the changes in extent of metal-humate binding with temperature may be explained entirely in terms of thermodynamic considerations. The observed changes in apparent binding constants would, in an equilibrium situation, be directly related to the free energy of reaction, which in turn depends only on the enthalpy and entropy changes for the reaction(s) occurring.

The reaction systems observed, in combination with the method of observation, however, combine to give a situation where the results of experiments may be validly interpreted in terms of reactions which have not reached equilibrium. In the non-equilibrium case, the observed reaction temperature dependence would be explained in terms of reaction kinetics, that is, enhancement of reaction rates at higher temperature.

The results presented in this Chapter tend to support a kinetically based explanation for the observed decreases in free metal ion concentrations (at equivalent levels of bound metal) with increasing temperature.

6.4.4.1 Combined effect of increasing equilibration time and decreasing temperature

The results presented in Section 6.3.5 (Figure 6.10) show a trend in concentrations of unbound Cu^{2+} with temperature that is opposite to that expected from binding experiments at different temperature (for example, Figures 6.4 and 6.5). If the reactions had proceeded to a true equilibrium at all stages of this experiment, and binding was actually stronger at higher temperature, then the results should have indicated an increase in $[Cu^{2+}]$ with decreasing temperature (increasing reaction time). Instead, the decrease in $[Cu^{2+}]$ observed implies that the binding reactions are still proceeding after c. 150 hours of reaction time. This trend cannot be explained in terms of irreversibility of complex formation alone; such behaviour would result in the observed unbound Cu^{2+} concentrations being all equal, if the reaction systems attained equilibrium between temperature changes. To explain the observed behaviour, then, it is necessary to propose a mechanism for complex formation which is consistent with a proportion of metal ions being taken up very slowly by the humate macromolecule. It is important to note that the observation that kinetic factors are operative does not exclude the possibility that the position of equilibrium changes with changing temperature.

It is considered to be likely that the rate determining process for metal ion binding to solid phase calcium humates is diffusive in nature. It is unlikely that diffusion of solutes through the bulk solution, or the quiescent layer of solution surrounding humate particles, would be important on the timescale of either binding experiment in this work. In the case of Cd^{2+} and Cu^{2+} binding to solid phase calcium humates, it is probable that rate limiting particle diffusion is an important process in the later stages of metal binding reactions. Diffusion of metal ions through a particle of calcium humate is conceivable if the aggregations of humate macromolecules exist in gel form and are swollen by water uptake.

Diffusive processes would thus be driven by an activity gradient, in terms of the diffusing ion, between the surface and the interior of the gel. This activity gradient would be maintained as long as complexing sites remained available within the aggregates of humate macromolecules.

For metal - sodium humate complexation reactions occurring wholly in the solution phase, it is considered less likely that particle diffusion would be rate limiting. It is possible that the very slow complex formation reactions, implied by the results in this Chapter, occur through slow changes in conformation of the humate macromolecules as the free energy of the system is decreased by metal binding. Such processes may also be possible for complexation reactions of metal ions with a gel phase macromolecular ligand.

6.4.4.2 Comparison of temperature dependence of binding reactions with calcium and sodium humates

For copper(II) binding, the observed temperature dependence of the binding reactions is noticeably greater for binding to SHCa and WPCa than for binding to SHNa and WPNa (compare Figures 6.4 and 6.8; Figures 6.5 and 6.9). For example, for Cu^{2+} binding to WPCa, the vertical displacement in the ($\log[Cu^{2+}]$ *versus* bound Cu^{2+}) binding curves is approximately 1.1 $\log[Cu^{2+}]$ units when comparing binding at 20° C and 40° C. In contrast, the comparable binding curve displacement for the Cu^{2+}-WPNa reaction is approximately 0.6 $\log[Cu^{2+}]$ units. A similar situation exists for the cadmium(II) binding reactions. Cd^{2+} binding to SHCa and WPCa shows a significant temperature dependence (Figures 6.2 and 6.3). For Cd^{2+} binding to SHNa and WPNa, however, there is very little difference between binding at 20° C and 40° C.

This difference in temperature dependence for metal ion binding to gel-phase (SHCa and WPCa) and aqueous phase (SHNa and WPNa) humates is consistent with a hypothesis that the binding reactions observed are not at equilibrium at the time of observation. It is expected that humate-metal ion reactions

will proceed more slowly for solid and gel-phase humates because of the importance of processes such as particle diffusion. Particle diffusion should be less important for humate macromolecules in the solution phase, especially if the macromolecules are considered to be expanded, flexible polyanions. Diffusion through the solvated macromolecules will be facilitated, since their conformation is random with respect to time and space (Hayes and Swift, 1978), and thus a surface-interior concentration gradient would be less likely to form. This relative ease of diffusion through an expanded humate macromolecule will be maintained as long as complexation of metal ions does not induce significant aggregation.

This comparison of Cu^{2+} and Cd^{2+} binding behaviour between solid (gel) phase calcium humates and solution phase sodium humates is complicated by the possibility that thermodynamic factors are also operative. Since the phases, and ions being displaced, are different in each case, then any changes in the position of equilibrium with changing temperature may be of different magnitude for metal binding to either calcium or sodium humates.

6.4.4.3 Comparison of temperature dependence of copper(II) and cadmium(II) binding to humates

Copper(II) is a strongly complexing transition metal cation, facilitating large decreases in the free energy of the system when complexes are formed. As a result, it is expected that changes in conformation (such as intramolecular crosslinking by polyvalent metal ions, hydrogen bonding or non-polar attraction) of the humate macromolecules, which are normally unfavourable due to increases in free energy might become favourable if they allow *further* binding of Cu^{2+}. Binding of a more weakly complexing cation such as Cd^{2+} is not as favourable in terms of free energy decreases, and as such is not expected to induce substantial conformational change.

It is evident from comparison of Cd^{2+} and Cu^{2+} binding data to calcium humates (compare Figures 6.2 and 6.4; Figures 6.3 and 6.5) that the Cu^{2+} binding reactions show a greater temperature dependence than Cd^{2+} binding reactions. For Cd^{2+} binding to SHCa, the vertical displacement of ($\log[Cd^{2+}]$ *versus* bound Cd^{2+}) binding curves is approximately 0.5 $\log[Cd^{2+}]$ units between data obtained at 5 °C and 40 °C. In contrast, the corresponding binding curve displacement for Cu^{2+}-SHCa data is approximately 2.3 $\log[Cu^{2+}]$ units. Similar behaviour is observed when comparing Cd^{2+} and Cu^{2+} binding to sodium humates. For example, binding curves for Cu^{2+}-SHNa are displaced by c. 1.0 $\log[Cu^{2+}]$ units between data obtained at 20 °C and 40 °C. The binding curves for Cd^{2+}-SHNA binding, however, show a vertical displacement of $\leq$ 0.1 $\log[Cd^{2+}]$ units.

The difference in complexation behaviour described above for Cu^{2+} and Cd^{2+} binding to sodium humates are consistent with the hypothesis that the slow complex formation processes implied by the results presented in this Chapter involve rate-limiting conformational change. For metal ion binding to calcium humates, it would not be possible to separate any effects of diffusion and/or slow conformational change. Again, the situation is complicated by the possibility that the effect of temperature on Cu^{2+}-humate complexation equilibria may be different from that for Cd^{2+}-humate equilibria. Another point, which has relevance for design of experiments measuring metal ion - humic substance binding equilibria, is that the effect of slow complex formation processes will be more marked for reactions where the extent of complex formation is large. For example, if 99.9% of a metal ion is bound (not unreasonable for Cu^{2+}-humate complexes), and a slow conformational change allows the proportion of bound Cu^{2+} to increase by 0.05% to 99.95%, then the concentration of unbound Cu^{2+} would decrease by 50%. In contrast, for a more weakly bound metal ion where the proportion bound is 90% (for example, Cd^{2+}), a similar 0.05% increase in bound metal would decrease the unbound metal ion concentration by only 4.5%.

6.5 Summary

The reactions of copper(II) and cadmium(II) with both solid phase calcium humates, and solution phase sodium humates, have been found to be significant in that both metal ions form strong complexes with these macromolecular ligands. Binding of cadmium(II) to humates is characterised by a weaker complex formation, less extensive proton release, and a lesser degree of heterogeneity when compared with copper(II) binding. Binding of copper(II) shows extreme heterogeneity, and a proportion of the humate ligands show a very high affinity for Cu^{2+}, with substantial displacement of hydrogen ions. These trends in complexation behaviour are considered to be consistent with those expected for these metal ions.

The complexing reactions observed all show, to some extent, an increase in the amount and strength of complex formation with increasing temperature. This temperature dependence is consistent with kinetically controlled processes, and it is proposed that rate-limiting diffusion of ions through humic substances, and/or conformational changes induced by complexation, are responsible for this kinetic control. This hypothesis implies the existence of very slow components in metal-humic substance complex formation reactions, even in the solution phase. In addition, it emphasises that the design of experiments intended to observe metal ion - humic substance complexation equilibria must account for very slow reactions, particularly for solid or gel phase humic substances.

Description of metal-humate binding data using modelling equations resulted in strictly empirical representations of the complexation reactions, despite the physical basis of many of the models used. This is in accord with similar conclusions made when modelling protonation behaviour in the previous Chapter. The problem of defining complexation capacities (or ligand concentrations) for the humate ligands was successfully overcome by assigning complexation capacity the same value, on an equivalent basis, as the total acidity.

CHAPTER SEVEN

KINETICS OF COPPER(II) DISSOCIATION FROM SODIUM AND CALCIUM HUMATES

7.1 Introduction

The rates of metal ion - humic substance complexation reactions may be important in geochemical and ecological processes for several reasons. Biological availability of essential or toxic trace metal ions may, in some cases, be limited by dissociation kinetics of metal complexes rather than equilibrium metal speciation (Shuman *et al.*, 1983; Hering and Morel, 1990). In addition, if the kinetics of formation and/or dissociation are sufficiently slow, diffusion-controlled (van Genuchten and Wierenga, 1976) or chemical (Rao *et al.*, 1979) kinetics may be important factors in mass transport or immobilisation processes (van der Zee *et al.*, 1989). Individual slow processes may limit overall rates for subsequent processes in composite systems such as soils or natural waters (Pankow and Morgan, 1981). Factors such as these may invalidate the use of equilibrium models for predicting speciation in geochemical systems such as soils or natural waters (Wu and Gschwend, 1986). Unfortunately, a general dearth of kinetic data relating to reactions of humic substances (Plankey and Patterson, 1987) forestalls the possibility of including these non-equilibrium processes in environmental models.

This Chapter investigates rates of copper(II) dissociation from Summit Hill and Waimari Peat sodium humates, for a range of experimental conditions, using a continuous spectrophotometric monitoring technique. In addition, the rate of copper(II) dissociation from Waimari Peat calcium humate has been investigated using an intermittent sampling technique.

Also investigated in this Chapter is the description of observable copper(II)-humate complex dissociation kinetics using modelling equations. A model based on a continuous lognormal distribution of first-order dissociation rate constants is introduced and discussed.

7.2 Materials and Methods

7.2.1 Copper(II) Dissociation from Summit Hill and Waimari Peat Sodium Humates

The amount of copper(II) dissociating from copper(II)-sodium humate complexes was determined as a function of time using an adaptation of the technique described by Shuman *et al.* (1983). This technique is described in Chapter 3 (Section 3.5.1). The dissociation reaction was followed, for both sodium humates, over a range of copper:humate ratios, concentrations of $NaNO_3$ and pH. Combinations of these experimental conditions at which copper-humate complex dissociation was observed are shown in Figure 7.1. This experimental scheme allowed the investigation of the effects of varying a single experimental condition (pH, Cu^{2+}:humate ratio, or [$NaNO_3$]) while holding all others constant. In addition, for some experimental conditions, the copper(II)-humate solution was allowed to equilibrate for different lengths of time (24 h and 48-168 h) before reaction with PAR. For some preliminary experiments, the effect of ambient temperature on the dissociation reaction was observed. Copper(II)-humate solutions (before reaction with PAR) were always equilibrated at 20 °C, but dissociation was observed at 20 °C, 30 °C and 40 °C.

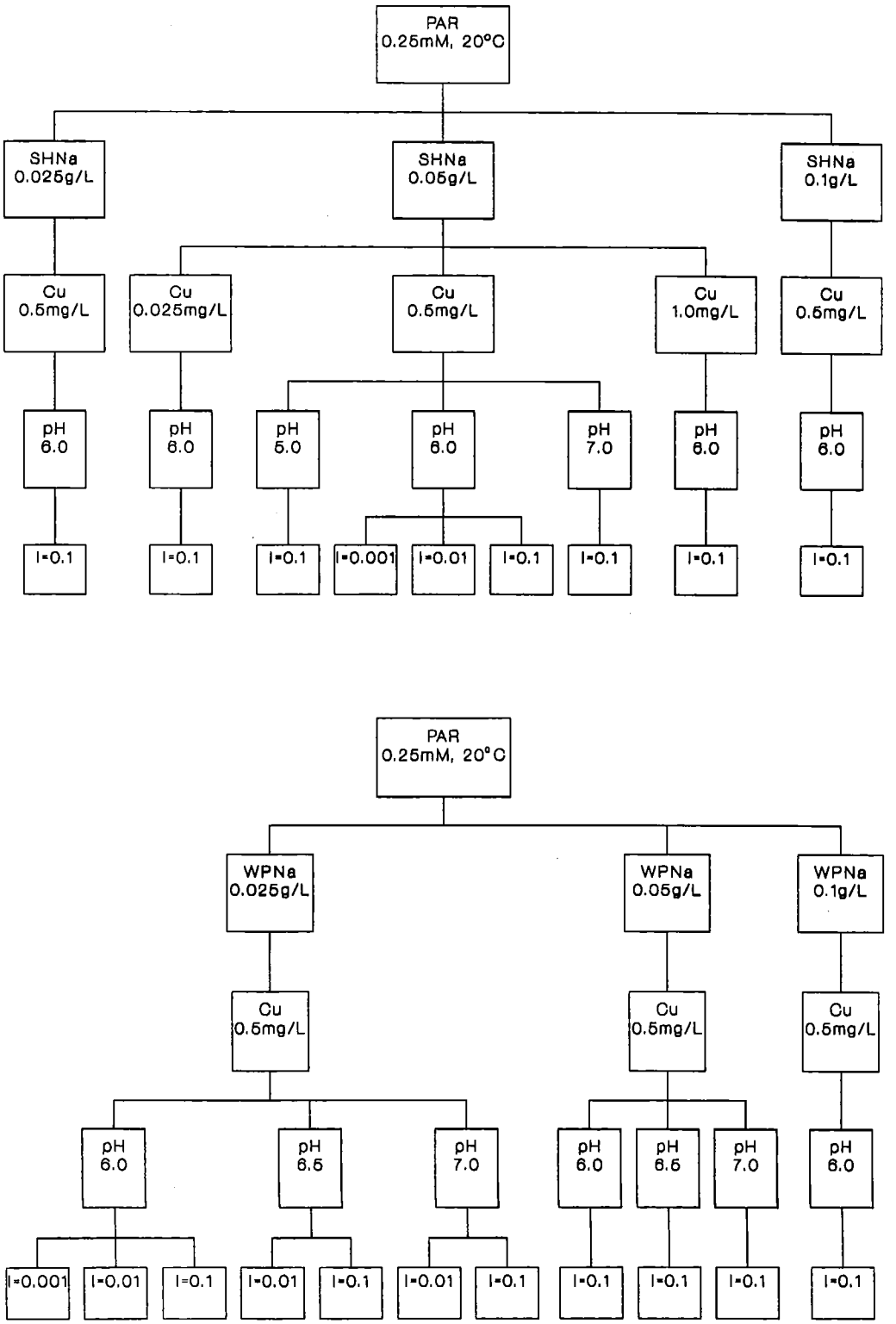

Figure 7.1 Treatments in experiments observing: (a) Cu^{2+}-SHNa complex dissociation kinetics, and; (b) Cu^{2+}-WPNa complex dissociation kinetics.

Initial concentrations of reactants were chosen such that PAR was always in large excess of the total copper concentration ([PAR]/[Cu] > 30), ensuring the predominance of pseudo-first-order conditions, and making any changes in the absorbance of uncomplexed PAR negligible compared with the overall absorbance change. Temperature was maintained throughout the observation of the reactions using a thermostatted cell block. Spectrophotometer output generated approximately 7000 absorbance-time data pairs which were equally spaced with respect to time. Such sets of data were reduced, for modelling purposes, to typically 50-100 data pairs (depending on constraints on processing time for more complex models) which were approximately equally spaced with respect to log(time) by using the program described in Chapter 3 (Section 3.6.2) and listed in Appendix 4.

The molar absorptivity (ϵ) for the Cu^{2+}-PAR complex in excess PAR (corresponding to the conditions used in kinetic experiments) was determined by measuring absorbance spectra for Cu^{2+}/PAR solutions, and from single-wavelength absorbance measurements at 510 nm. The protonation and Cu^{2+} complex stability constants for PAR (Perrin, 1979) were used to determine copper(II)-PAR complex speciation for all experimental conditions. Measurement of the molar absorptivity at 510 nm (ϵ_{510}) was used to determine the concentration of CuPAR, and hence dissociated Cu^{2+}, as a function of time.

7.2.2 Copper(II) Dissociation from Waimari Peat Calcium Humate

The procedures used to observe the dissociation of Cu^{2+} from an aqueous suspension of WPCa are given in Chapter 3 (Section 3.5.2). Approximately 25 (time, [Cu^{2+}]) data pairs were collected, at increasing time intervals, from t = 0-5400 s. Sampling time was taken as the total elapsed time when all of the sample aliquot had passed through the filter membrane.

7.2.3 Direct Spectrophotometric Observation of Copper(II)-Summit Hill Sodium Humate Complexation

In order to evaluate the possibility of direct spectrophotometric observation of Cu^{2+}-sodium humate complexing, with the intention of identifying a probe for following complex formation kinetics, the following experiment was performed. A series of solutions was prepared, containing identical concentrations of $NaNO_3$ (0.01 mol L^{-1}) and SHNa (0.10 g L^{-1}), with copper(II) concentrations in the range 0 - 2.5 × 10^{-4} mol L^{-1}. Using the solutions with zero Cu^{2+} addition as a reference, uv-visible absorbance spectra were determined for the remaining solutions in the wavelength range 250-800 nm. On the basis of the results obtained from this experiment, an attempt was made to follow the progress of the Cu-SHNa complex formation reaction as a function of time, using a method similar to that used to follow the reaction of Cu:humate with PAR (Section 7.2.1).

7.3 Treatment of Kinetic Data

7.3.1 Fitting Kinetic Data to Models

Observation of the dissociation reactions began a short (but significant in terms of reaction progress) time after reaction initiation for the experiments described in Section 7.2. The concentration *versus* time data derived from these experiments, therefore, described the progress of copper(II)-humate dissociation reactions over a timescale determined by the particular technique used. Data within this 'observation window' (with an upper limit defined by the maximum observation time) could be fitted to various models, some of which are outlined in Chapter 2 (Section 2.7.1).

Models based on chemical kinetics (as opposed to physical processes, such as diffusion) used in this work were always based on first-order processes. That is, at any time during a dissociation reaction, the rate of change in bound Cu^{2+} with respect to time was dependent only on the instantaneous concentration or mole fraction of bound Cu^{2+}. Departure from single-component first order kinetics was accounted for in models by involving a mixture of two or more copper(II)-humate species with different first order dissociation rate constants. Modelling of copper(II)-humate association reactions was not attempted, for reasons discussed later (Section 7.4.6).

7.3.1.1 Discrete Kinetic Models

The simplest model used in an attempt to describe copper(II)-humate complex dissociation kinetics was one involving complexes having a single first order rate constant. In this case, dissociation may be represented by:

$$\frac{-d[CuL]}{dt} = k_1[CuL] \qquad (7.1)$$

where k_1 is the first-order dissociation rate constant, and L represents the humate ligand. The integrated form of the equation may be written as:

$$[CuL]_t = [CuL]_0 \exp(-k_1 t) \qquad (7.2)$$

where $[CuL]_t$ is the concentration of CuL at any time t, and;

$[CuL]_0$ is the concentration of CuL at t=0.

Extending this model to account for kinetic heterogeneity is achieved by summing a series of exponential decay terms analogous to the right hand side of Equation 7.2. For a mixture of n sites (L_1, ..., L_n) dissociating simultaneously, a general discrete multisite equation is given by (Willis *et al.*, 1970):

$$\left(\sum_{i=1}^{n} [CuL_i] \right)_t = \sum_{i=1}^{n} [CuL_i]_0 \exp(-k_i t) \qquad (7.3)$$

where CuL_i is the complex of Cu^{2+} with the i^{th} humate ligand, and;

k_i is the first-order rate constant for dissociation of CuL_i.

If all sites in a discrete ligand mixture react after dissociation to form a common product CuZ, and formation of CuZ is not rate-determining, then the equation may be re-written as follows:

$$[CuZ]_t = [CuZ]_0 + \sum_{i=1}^{n} [CuL_i]_0 \exp(1 - k_i t) \qquad (7.4)$$

The term $[CuZ]_0$ may be taken to represent the concentration of species CuZ at the *effective*, rather than actual, time zero for the dissociation reaction. In such a case, it allows for dissociation of Cu^{2+} from sites which have rate constants too large to be observed by the particular experimental technique used. For the experiments described in Section 7.2, Z = PAR or NTA. If both sides of Equation 7.4 are multiplied by the molar absorptivity of CuZ, kinetic data obtained spectrophotometrically may be expressed in terms of absorbance measurements.

Equation 7.4 was applied to copper(II)-humate complex dissociation data in a form including either two or three discrete sites. Initial estimates of adjustable parameters for input into the nonlinear regression program were found using Guggenheim plots of $\ln([CuZ]_{t+\Delta t} - [CuZ]_t)$ *versus* time (Mak and Langford, 1983), where Δt is a constant time increment. Estimates of $[CuL_i]_0$ and k_i values were accessible from the intercepts and slopes respectively of rectilinear portions (resolvable for systems where k_i differ by $\geq$ 1 order of magnitude, otherwise arbitrarily defined) of Guggenheim plots. Although these plots can be noisy due to random fluctuations in sequential ([CuZ], time) data, they do not require that measurements are made until the experimental system reaches equilibrium (Mak and Langford, 1983), as in conventional $\ln([CuZ]_\infty - [CuZ]_t)$ *versus* time plots. In addition, increasing the Δt increment for calculation of the plot was found to result in reduced levels of noise. In this work, limiting slopes at the

shortest and longest measurement times provided estimates of two ($[CuL_i]_0$, k_i) pairs; for the three discrete site model, an intermediate k_i value and realistic $[CuL_i]_0$ value were also estimated.

7.3.1.2 Continuous multisite kinetic models

The extension of discrete multisite binding models to binding models involving a continuous distribution of sites was outlined in Chapter 2 (Section 2.4.5). By analogy, it is possible to apply a similar approach to formulating continuous multisite kinetic models. The general equation is given by (for example, Olson and Shuman, 1983):

$$[R]_t = \int_{-\infty}^{\infty} N(k) \exp(-kt)\, dk \qquad (7.5)$$

where R is a generalised reactant and N(k) is a site distribution function with respect to a first order rate constant, k (or log k) such that:

$$\int_{-\infty}^{\infty} N(k)\, dk = \left| [R]_0 - [R]_\infty \right| \qquad (7.6)$$

The specific form of Equation 7.5 used in this work was:

$$[CuZ]_t = [CuZ]_0 + \frac{L_{obs}}{\sigma_k \sqrt{2\pi}} \int_{-4\sigma_k}^{+4\sigma_k} \exp\left[\frac{-1}{2} \left(\frac{\kappa - \ln k_\mu}{\sigma_k} \right)^2 \right] (1-\exp(-(e^{\kappa}t)))\, .\, d\kappa \qquad (7.7)$$

where $\kappa = \ln k$, and;

L_{obs} is the total *observed* concentration of sites dissociating.

Equation 7.7 describes simultaneous dissociation of a mixture of Cu^{2+}-humate species, having first order dissociation rate constants, which are normally distributed with respect to ln k. The mean of the normal distribution is represented by $\ln k_\mu$, and the standard deviation by σ_k. The formation of a common product CuZ from dissociation of a hypothetical distribution of copper(II)-humate species, as a function

log k and t, is illustrated for ln k_μ = -4.605 ($\log_{10}k_\mu$ = -2.0) and σ_k = 2.303 in Figure 7.2. The concentration of CuZ at any point in the reaction is proportional to the cross-sectional area at instantaneous time t. By referring to the log (rate constant) axis, that portion of the log k distribution which dissociated to form this amount of CuZ may be found. It can be seen from the three-dimensional plot in Figure 7.2 that at short reaction times, the partial distribution of *reacted* sites is skewed to high log k values, since these react first. The remainder of the distribution is 'filled in' by dissociation of Cu^{2+} from sites with progressively smaller rate constants in the distribution as the reaction as a whole proceeds. It may also be seen from such a plot that, in contrast to a lognormal binding model (Section 2.4.5), all hypothetical sites implied by the distribution are important in determining rates of dissociation from the complex. Refined parameters derived from fitting kinetic data to this model were used to examine the effect of the various experimental conditions on copper(II)-humate dissociation reactions. Sets of data derived from copper(II)-humate dissociation experiments were also evaluated for fit to the the Elovich equation (Equation 2...) by linear regression of [CuZ] *versus* ln t. As mentioned in Chapter 2, the Elovich equation also implies a continuous distribution of rate constants, controlled by a linear relationship between activation energy and binding site occupancy.

7.3.1.3 Models based on diffusive processes

Reactions which proceed by rate-limiting diffusion are found to show a linear dependence on $t^{1/2}$, such that (Sparks, 1985):

$$[CuZ]_t = [CuZ]_0 + bt^{1/2} \qquad (7.8)$$

Copper(II)-humate dissociation kinetics data were evaluated for the existence of a single rate-determining diffusion process using plots of [CuPAR] (or [CuNTA]) *versus* √time.

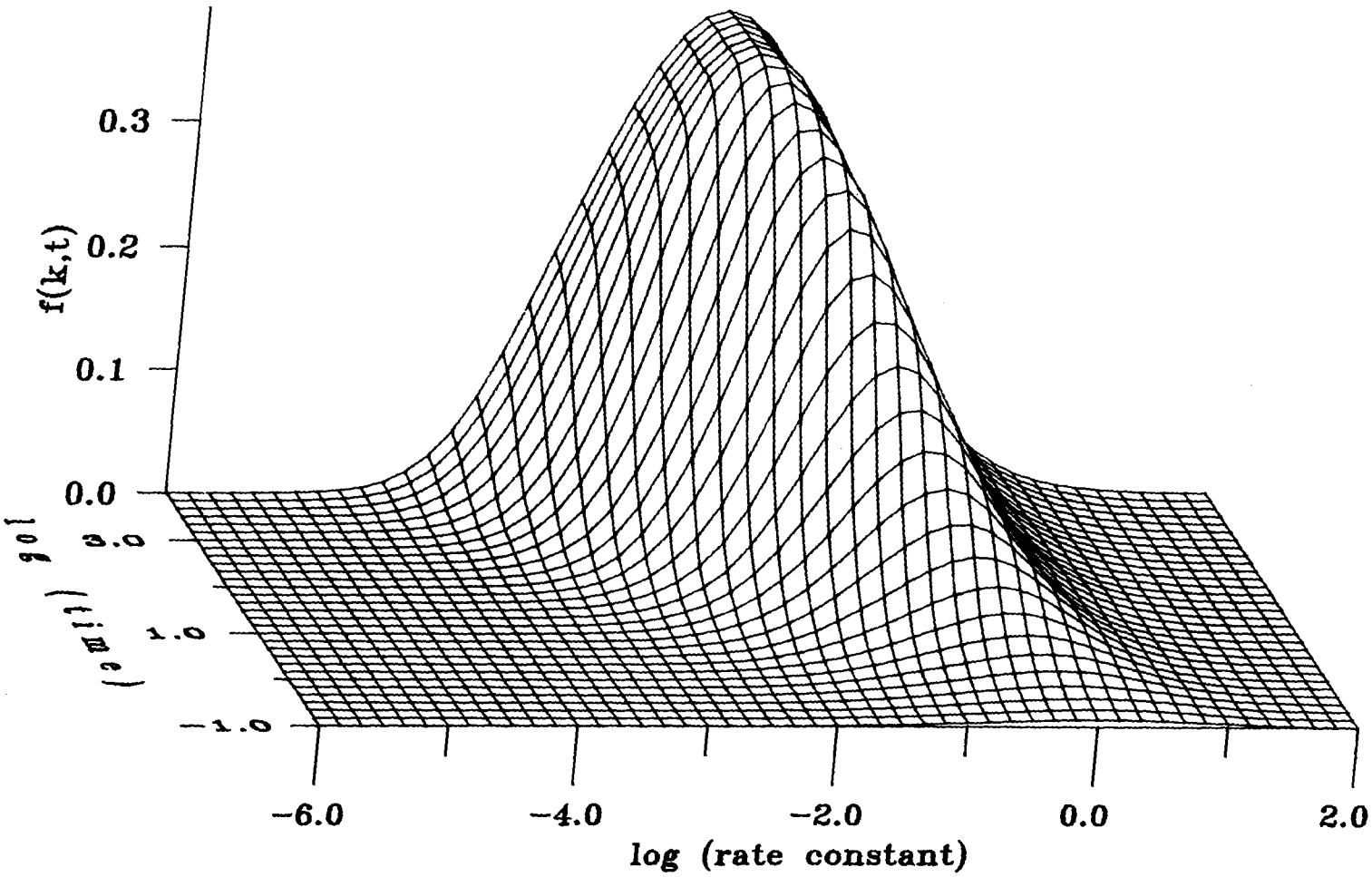

Figure 7.2 Hypothetical distribtion of *reacted* sites, as a function of rate constant and time, from dissociation of a mixture of complexes which are lognormally distributed with respect to first order dissociation rate constant. (See text for explanation.)

7.3.1.4 Kinetic Spectra

In order to approximate any distribution of dissociation rate constants that might describe the mixture of copper(II)-humate complexes reacting with PAR, a discrete kinetic spectrum analysis suggested by the work of Lavigne *et al.* (1987) and Cabaniss (1990) was used. This method was implemented in two ways: first, by the sequence of linear regression steps suggested by Cabaniss (1990); second, using the multidimensional simplex routine (Chapter 3) to optimise $\log_{10}[CuL_i]_0$ values for a set of fixed ten k_i values (Equation 7.4). Briefly, the method of Cabaniss (1990) involves fitting, by multiple linear regression, a series of (in this work, ten) exponential terms with fixed log k_i to kinetic data. (Since the k_i values are fixed, the equation becomes linear with respect to time). If a negative value of $[CuL_i]_0$ for a particular log k_i value is found, then that term is removed from the equation and the multiple linear regression repeated with one less 'site'. Poorly-defined sites giving $[CuL_i]_0$ values having a relative standard deviation of more than one third are also removed from the equation. Multiple regressions are performed on a decreasing number of fixed log k_i sites until all refined $[CuL_i]_0$ values are positive and well-defined (rsd $\leq$ 1/3). Use of this method was intended only as a technique for exploratory data analysis, and was not applied to all data.

When data from competing ligand-induced copper:humate dissociation experiments were fitted to the various models, the concentration of copper dissociated at the effective experimental time zero ($[CuZ]_0$) was fixed at experimentally determined values throughout the regression procedure. For copper-sodium humate dissociation induced by PAR, this value was accessible from the first absorbance measurement in the spectrophotometer output. For NTA-induced copper-calcium humate dissociation, the equilibrium copper concentration immediately prior to NTA addition was measured for each experiment, and $[CuZ]_0$ was fixed at this value throughout regressions.

7.3.2 Analysis of Kinetic Fractions in Copper(II)-Sodium Humate Dissociation Reactions

The nature of the experiment observing copper(II)-sodium humate reactions allowed the identification of three operationally defined fractions of copper(II)-humate species in terms of their behaviour under the experimental conditions. Two of these fractions were classified solely in terms of kinetic behaviour. The first of these kinetic fractions was defined as Cu^{2+} bound to sites on the humate macro-ion which dissociated before the effective zero time reading in experiments. This fraction was denoted *labile* Cu^{2+} (Cu_L). The second fraction was comprised of copper(II)-humate species which dissociated on a timescale such that their dissociation could be observed by the experimental technique used. This was the *non-labile* Cu^{2+} fraction (Cu_{NL}). A third fraction, which was not necessarily based on kinetic criteria, was denoted *non-reactive* Cu^{2+} (Cu_{NR}) and was considered to include: (i) copper(II)-humate species having extremely slow dissociation rates, and; (ii) copper(II)-humate complexes sufficiently stable to coexist in equilibrium with Cu^{2+}-PAR complexes.

The labile copper fraction includes Cu^{2+} which is not bound to sodium humate. Calculations based on a three-discrete site binding model, which has good predictive capability, (Chapter 6, Tables 6.6 and 6.7) indicated that the proportion of unbound Cu^{2+} would be negligible (< 1%) with respect to total solution copper, except for experiments where the Cu^{2+}:humate ratio was 20 mg g^{-1} (0.157 mmol g^{-1}). In these cases, copper not bound to SHNa was c. 12% of total solution copper; for WPNa experiments, this proportion was c. 2.5%. Use of the three-site model for predictive purposes was based on the fact that Cu^{2+}:sodium humate ratios used in kinetic experiments were within ranges used in binding experiments, and thus no potentially inaccurate extrapolation outside the titration window was necessary.

The boundary between the non-labile and non-reactive copper fractions was arbitrarily defined at 90 minutes reaction time, and it is recognised that this cut-off point may exclude some reactive copper. However, the maximum observed rate of CuPAR formation, at t=90 minutes, for any Cu^{2+}-humate dissociation reaction was approximately 10^{-10} mol L^{-1} s^{-1}, and thus any resulting errors should be small.

NOTE. This system of nomenclature for the kinetic fractions is in accord with the classical chemical definition of coordination complex lability (Cotton and Wilkinson, 1976), which refers to complexes which are able to dissociate very quickly, that is, within mixing time in conventional kinetic experiments. This restricted definition of lability, although clearly operational, is based solely on kinetic criteria. As such, it is more rigorously defined than in many scientific disciplines where 'labile' takes on a poorly defined range of meanings such as 'reactive', 'available' or 'exchangeable'. Since these definitions of lability are based on a combination of thermodynamic, kinetic or biological criteria, it is considered that use of this term in a chemical context should be restricted to being of purely kinetic significance.

The amount of labile copper, $[Cu]_L$, was calculated from:

$$[Cu]_L = ((A_{PAR} + A_{CuHumate}) - A_0)/\epsilon_{CuPAR} \quad (7.9)$$

where A_0 is the absorbance of the reacting solution of Cu^{2+}-sodium humate and PAR at the effective time zero; A_{PAR} is the absorbance of PAR alone; $A_{CuHumate}$ is the absorbance of Cu^{2+}-sodium humate alone, and ϵ_{CuPAR} is the molar absorptivity of the CuPAR complex (Section 7.2.1). Non-labile copper, $[Cu]_{NL}$, is given by:

$$[Cu]_{NL} = (A_\infty - A_0)/\epsilon_{CuPAR} \quad (7.10)$$

where A_∞ is the absorbance at the end of the experiment.

Non-reactive copper, $[Cu]_{NR}$, may be found using:

$$[Cu]_{NR} = ((A_{CuPAR} + A_{humate}) - A_\infty))/\epsilon_{CuPAR} \quad (7.11)$$

where A_{CuPAR} is the absorbance of CuPAR only, and A_{humate} is the absorbance of uncomplexed sodium humate. Only experiments having an observation time of 5400 s (90 minutes) were used in the estimation of the three fractions. The amount of copper(II) in each fraction was calculated, for each set of experimental conditions, as: (i) all three fractions as a proportion of total solution copper (Cu_T); and (ii) labile and non-labile copper as a proportion of *reactive* copper (= labile + non-labile copper, Cu_R).

Unless the effect of copper:humate reaction time prior to dissociation was being examined, only experiments where the copper:humate pre-equilibration time was 24h were used to compare the effects of experimental conditions on dissociation reactions.

Evaluation of whether or not the effect of changing an experimental condition produced a significant change in proportions of kinetically defined copper fractions was achieved using a conventional two sided t-test (Koopmans, 1981) based on the standard deviations in means of replicates.

7.4 Results

Representative results for kinetic runs observing Cu^{2+}-SHNa complex dissociation are shown as plots of ($[CuPAR]_t$-$[CuPAR]_0$) *versus* time in Figures 7.3 to 7.7. These plots qualitatively show effects of varying experimental conditions, as follows: pH (Figure 7.3); Cu^{2+}:humate ratio (Figure 7.4); $NaNO_3$ concentration (Figure 7.5); Cu^{2+}-humate reaction time prior to dissociation (Figure 7.6); and dissociation reaction temperature (Figure 7.7). Figure 7.8 compares Cu^{2+}-SHNa and Cu^{2+}-WPNa complex dissociation under identical experimental conditions.

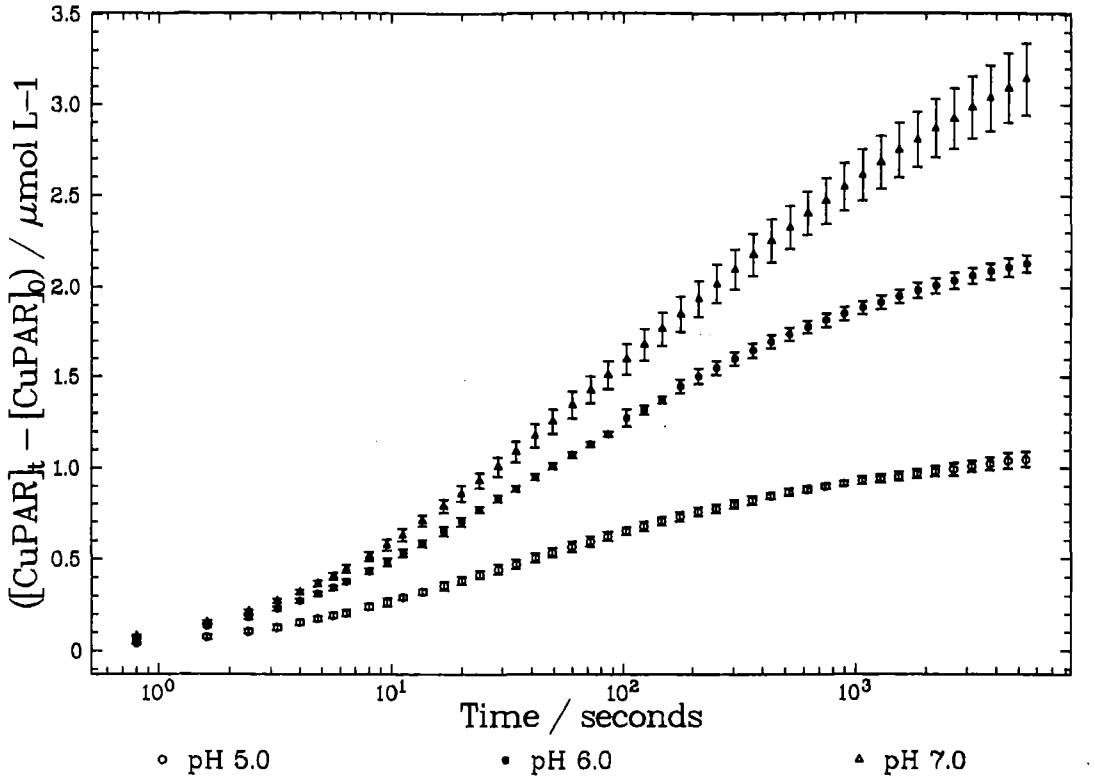

Figure 7.3 Effect of pH on Cu^{2+}-SHNa dissociation kinetics. SHNa 0.05 g L^{-1}, Cu_T 7.87 μmol L^{-1}, [$NaNO_3$] 0.1 mol L^{-1}. Error bars represent ± 1 standard deviation.

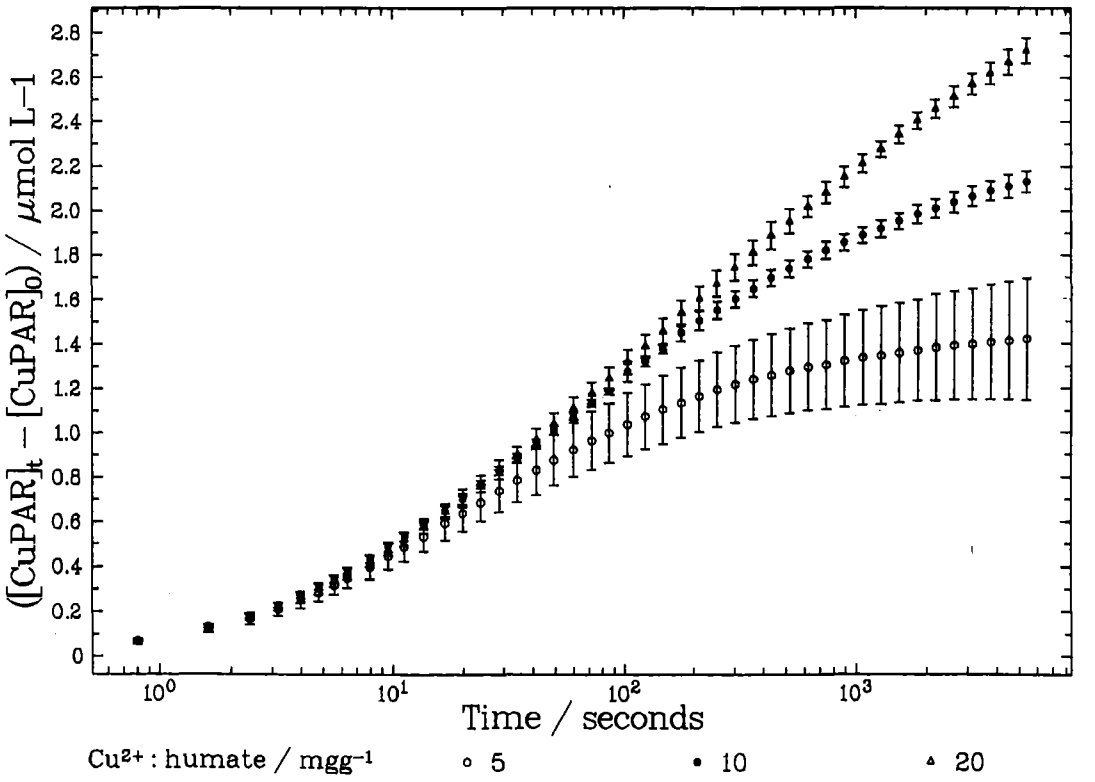

Figure 7.4 Effect of initial Cu^{2+}:humate ratio on Cu^{2+}-SHNa dissociation kinetics. Cu_T 7.87 μmol L^{-1}, pH 6.0, [$NaNO_3$] 0.1 mol L^{-1}; varying [SHNa]. Error bars represent ± 1 standard deviation.

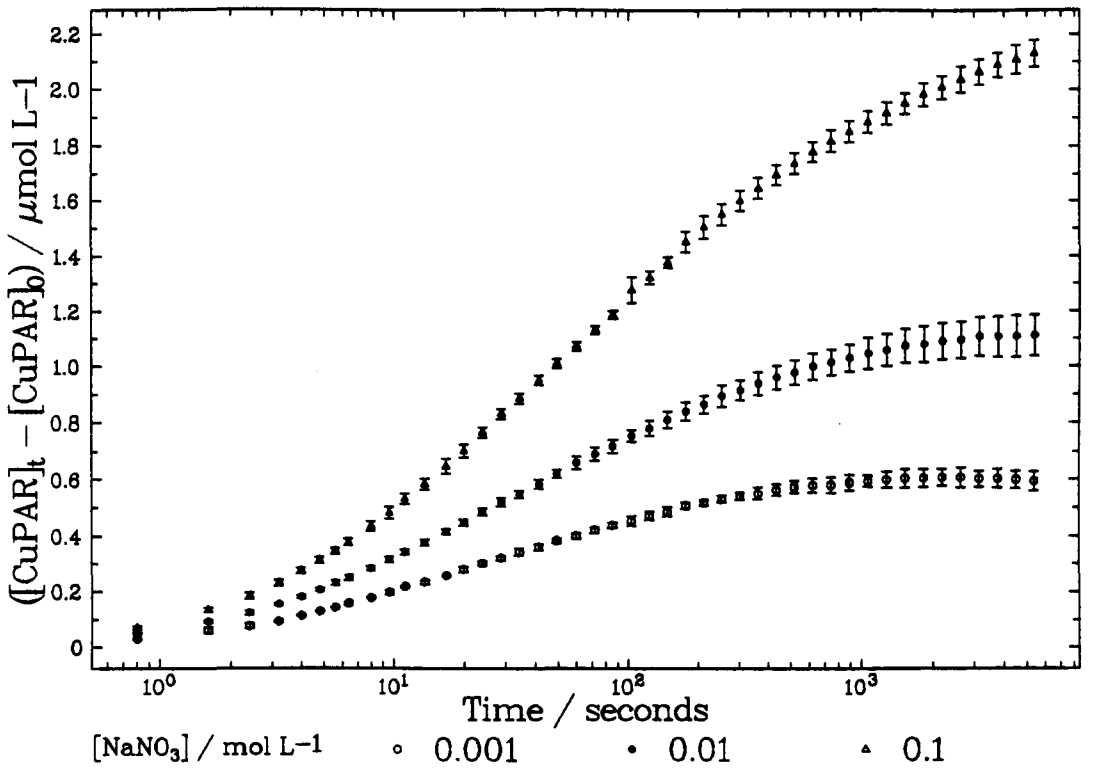

Figure 7.5 Effect of $NaNO_3$ concentration on Cu^{2+}-SHNa dissociation kinetics. SHNa 0.05 g L^{-1}, Cu_T 7.87 μmol L^{-1}, pH 6.0. Error bars represent ± 1 standard deviation.

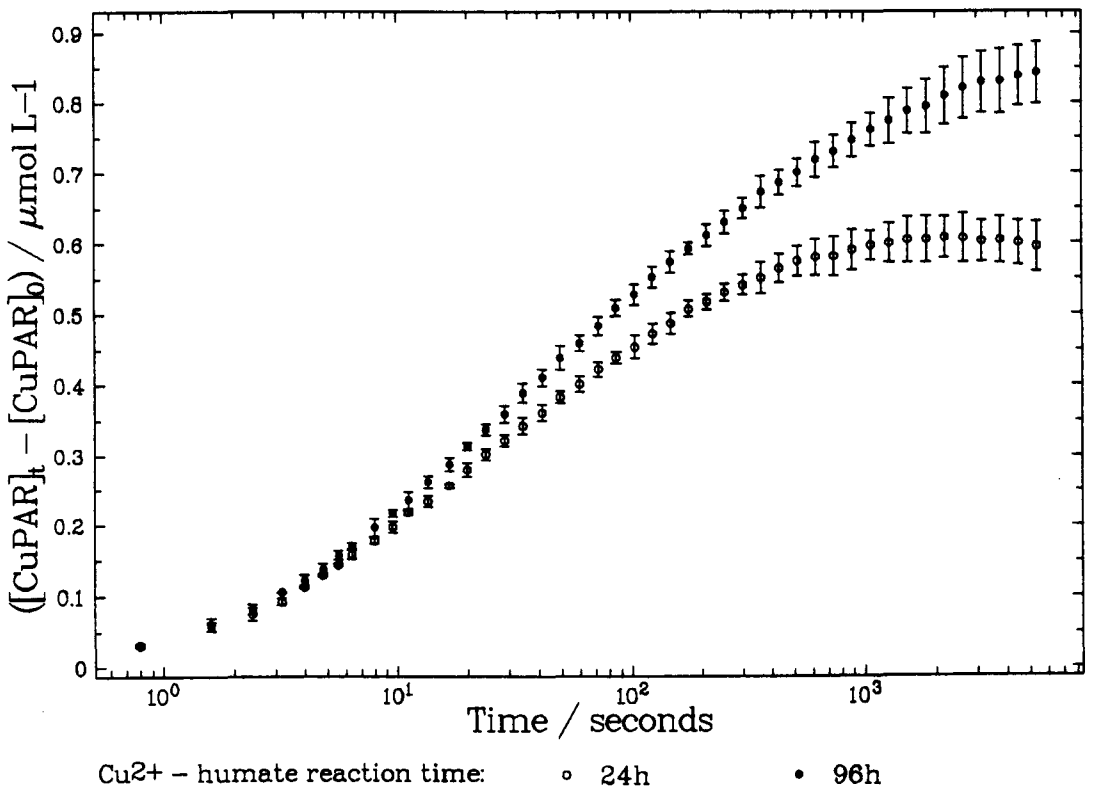

Figure 7.6 Effect of Cu^{2+}-humate reaction time (before dissociation) on Cu^{2+}-SHNa dissociation kinetics. SHNa 0.05 g L^{-1}, Cu_T 7.87 μmol L^{-1}, pH 6.0, [$NaNO_3$] 0.001 mol L^{-1}. Error bars represent ± 1 standard deviation.

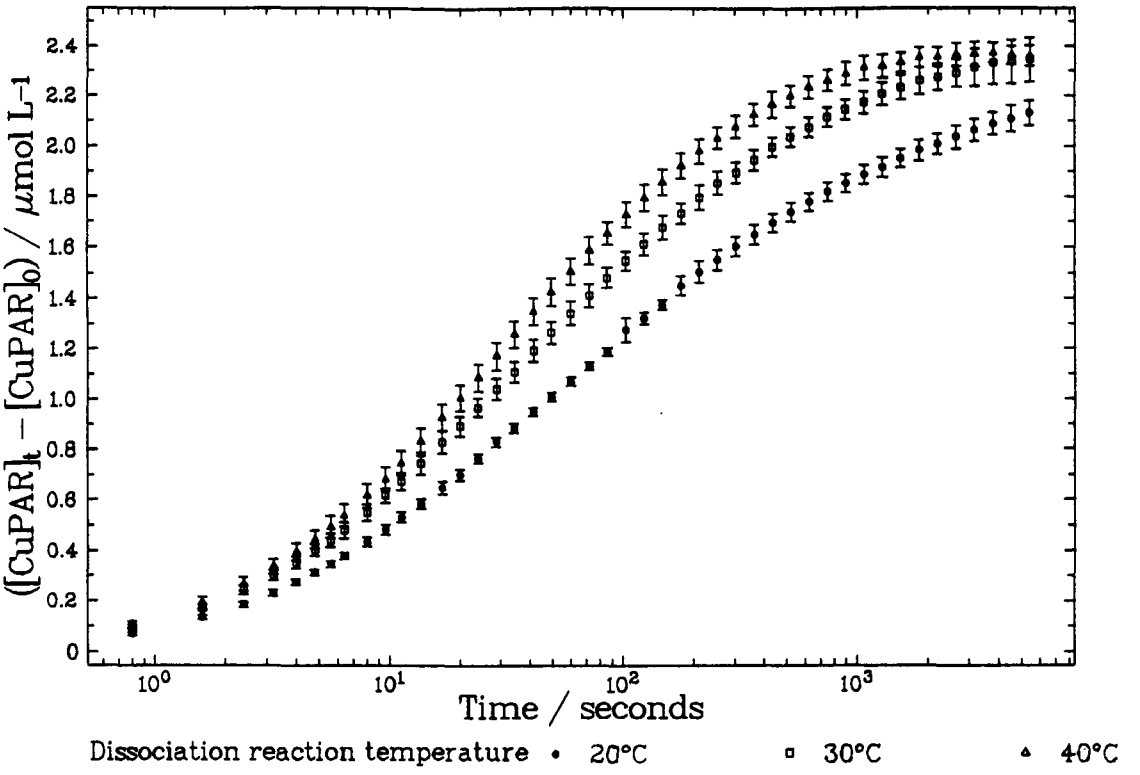

Figure 7.7 Effect of dissociation reaction temperature on Cu^{2+}-SHNa dissociation kinetics. SHNa 0.05 g L^{-1}, Cu_T 7.87 μmol L^{-1}, pH 6.0, [$NaNO_3$] 0.1 mol L^{-1}. Error bars represent ± 1 standard deviation.

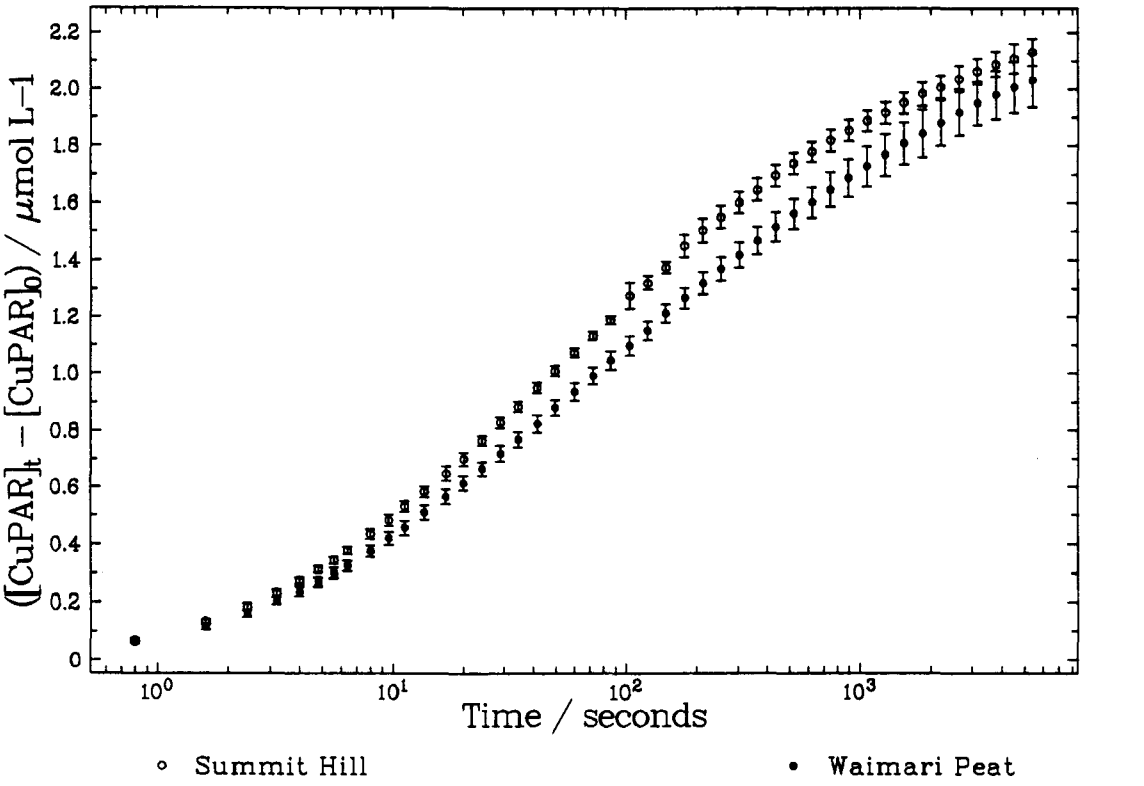

Figure 7.8 Comparison of Cu^{2+}-SHNa and Cu^{2+}-WPNa complex dissociation kinetics. [humate] 0.05 g L^{-1}, Cu_T 7.87 μmol L^{-1}, pH 6.0, [$NaNO_3$] 0.1 mol L^{-1}. Error bars represent ± 1 standard deviation.

Other results for Cu^{2+}-WPNa complex dissociation are not presented graphically, but were qualitatively similar to those obtained for Cu^{2+}-SHNa complex dissociation. Appendix 10 summarises results for Cu^{2+}-WPNa complex dissociation in tabular format.

7.4.1 Molar Absorptivity of Copper(II)-PAR Complex

The visible absorbance spectra of a series of buffered PAR solutions with increasing amounts of copper(II) is shown in Figure 7.9. The molar absorptivity, ϵ, of the CuPAR complex(es) present was obtained from a plot of CuPAR absorbance *versus* total copper concentration, ϵ being equal to the slope of this plot. The concentration of the CuPAR complex could be approximated by total copper concentration, since calculations using stability constants (Perrin, 1979) for PAR protonation and Cu^{2+} complexation showed that negligible copper remained uncomplexed, under the experimental conditions used. Absorbance values used to calculate ϵ_{CuPAR} were corrected for the small, but non-negligible, contribution of uncomplexed PAR. Speciation calculations indicated that CuPAR was the predominant complex at pH 7.0, and remained so until pH $\leq$ 5.0, where CuHPAR accounted for most complexed Cu^{2+}. Experiments at pH 4.8 (acetate/acetic acid buffer) gave ϵ_{510} for CuPAR of 24700±700 L mol^{-1} cm^{-1} at 20° C. Analysis of data from experiments at pH 6.8 ($HPO_4^{2-}/H_2PO_4^-$ buffer) gave ϵ_{510} for CuPAR of 37000±1000 L mol^{-1} cm^{-1} at 20° C. These results are in contrast to those determined by single-wavelength (510 nm) absorbance measurements on PAR-copper(II) solutions containing excess PAR (as was the case for kinetic experiments). Analysis of data from these measurements inferred substantially higher values of ϵ_{510} for CuPAR (ϵ_{510} in the range 40300±400 L mol^{-1} cm^{-1} for pH 6 and $[NaNO_3]$ = 0.1 mol L^{-1}, to 44100±300 L mol^{-1} cm^{-1} for pH 7 and $[NaNO_3]$ = 0.01 mol L^{-1}).

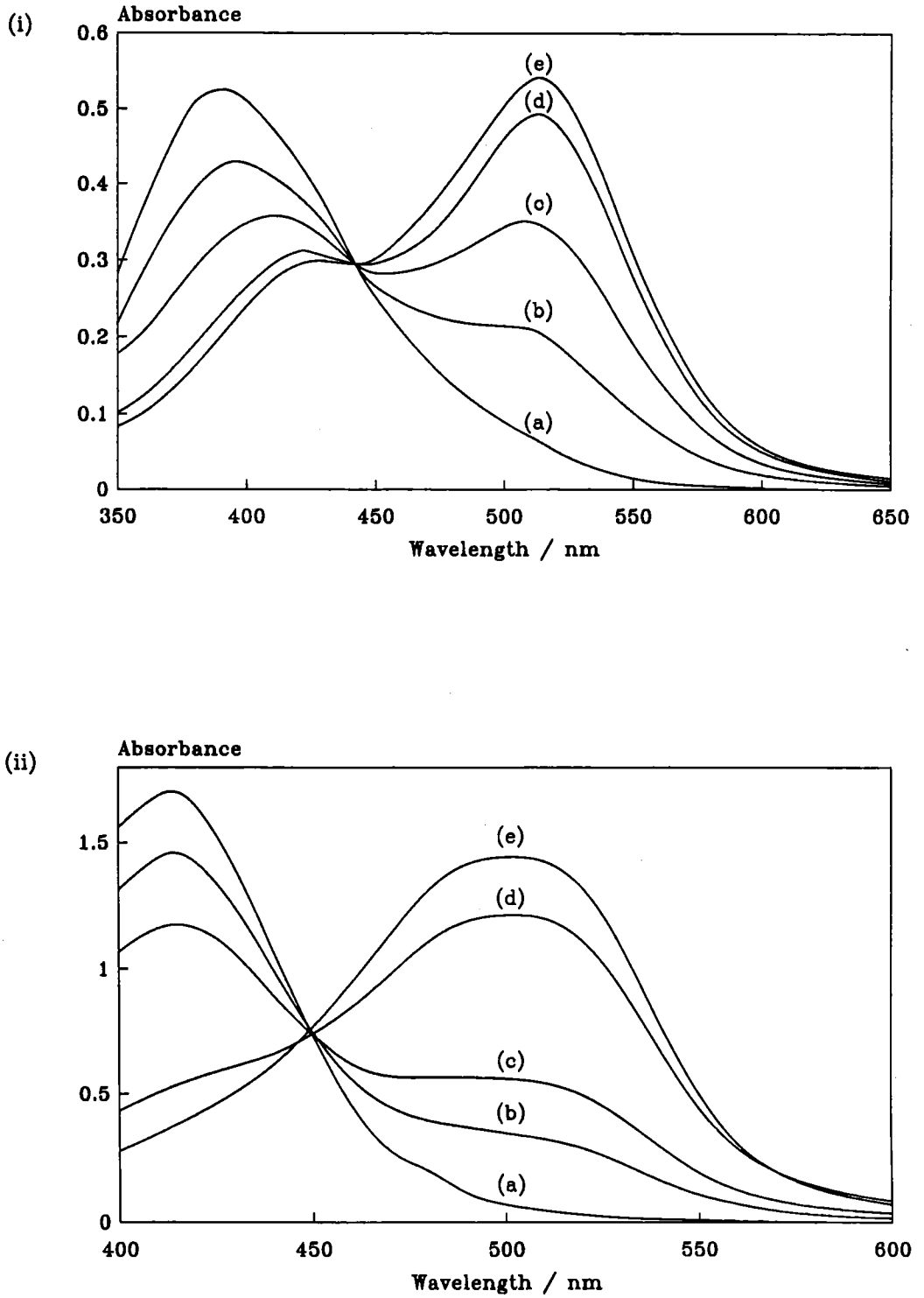

Figure 7.9 UV-visible absorbance spectra for solutions of PAR and varying amounts of Cu^{2+}:
(i) pH 4.8 (CH_3COOH/CH_3COO^- buffer); [Cu] = (a) 0, (b) 6.3, (c) 12.6, (d) 18.9, (e) 25.2 μmol L^{-1}.
(ii) pH 6.8 ($H_2PO_4^-/HPO_4^{2-}$ buffer); [Cu] = (a) 0, (b) 6.3, (c) 12.6, (d) 31.5, (e) 37.8 μmol L^{-1}.

7.4.2 Analysis of Kinetic Data in terms of Kinetic Fractions

Results are presented as proportions of copper(II) in each fraction, since the absolute amounts have no frame of reference and are thus of limited utility. However, the information required for calculation of absolute amounts of Cu^{2+} in the various fractions is contained within the sub-headings for Tables 7.1 to 7.5.

The amounts of Cu^{2+} dissociating from Cu^{2+}-SHNa and Cu^{2+}-WPNa complexes before the effective experimental time zero (the labile copper fraction) were found to be substantial for all experiments (Tables 7.1 to 7.5). Other workers have observed similar behaviour for Cu^{2+}-humic substance complex dissociation. For example, Olson and Shuman (1983) found that 57% of Cu^{2+}-humate complexes dissociated within 0.05s of reaction with PAR; Shuman *et al.* (1983) found that the proportion of Cu^{2+}-humate complexes dissociating within 0.05s was in the range 77-92%.

7.4.2.1 Effect of dissociation reaction pH

Data from PAR-induced copper(II)-humate complex dissociation experiments was analysed in terms of labile, non-labile and non-reactive copper as proportions of total solution copper. Non-labile copper (Cu_{NL}/Cu_T) was consistently found to increase with increasing pH for both Cu-SHNa and Cu-WPNa dissociation reactions (Table 7.1; Figure 7.3); in most cases, this increase was significant ($P \leq 0.05$). No consistent trends were found for either labile or non-reactive copper, as a proportion of total copper, as a function of pH. When labile and non-labile copper were calculated as fractions of reactive copper (Cu_R), both fractions showed consistent, and generally significant, trends. Labile copper (Cu_L/Cu_R) always decreased with increasing pH (equivalent to an increase in Cu_{NL}/Cu_R by definition) for Cu-SHNa and Cu-WPNa complex dissociation.

7.4.2.2 Effect of initial copper:humate ratio

As a proportion of total solution copper, non-labile copper was consistently found to decrease with increasing copper:humate ratio for Cu-SHNa and Cu-WPNa complex dissociation reactions (Table 7.2; Figure 7.4). Although in some cases significant trends were observed for labile and non-reactive copper (as a proportion of total copper), no consistent trend in these fractions described all dissociation reactions. In cases where significant trends were observed, Cu_L/Cu_R increased (Cu_{NL}/Cu_R decreased) with an increase in initial copper:humate ratio.

7.4.2.3 Effect of electrolyte concentration

Changing the concentration of $NaNO_3$ in the reaction systems produced discernible trends, for all kinetic fractions, for both Cu-SHNa and Cu-WPNa dissociation reactions (Table 7.3; Figure 7.5).

All trends in fractions were consistent between humates; Cu_L/Cu_T decreased, Cu_{NL}/Cu_T increased, Cu_{NR}/Cu_T decreased, Cu_L/Cu_R decreased and Cu_{NL}/Cu_R increased with increasing $NaNO_3$ concentration for both Cu-SHNa and Cu-WPNa dissociation reactions. The trends in all four of these fractions were significant ($P \leq 0.05$). The reductions in Cu_L/Cu_T with increasing [$NaNO_3$] were, however, small for both Cu-SHNa and Cu-WPNa dissociation.

Table 7.1 Effect of pH on proportions (percent ± standard error) of kinetic fractions found for copper(II)-sodium humate complex dissociation, 20° C. (*Probability P that value and preceding value are equal≤0.05; ^{ns}P>0.05. Symbols in column headings indicate the significance of overall trends.)

1. SHNa 0.05 g L^{-1}, Cu_T 7.87 μmol L^{-1}, [$NaNO_3$] 0.1 mol L^{-1}.

pH	Cu_L/Cu_T*	Cu_{NL}/Cu_T*	Cu_{NR}/Cu_T*	Cu_L/Cu_R*	Cu_{NL}/Cu_R*
5.0	55±1	12±2	33±1	82±3	18±3
6.0	63±1*	27±2*	10±1*	70±2*	30±2*
7.0	49.6±0.5*	38.6±0.9*	11.8±0.8^{ns}	56.3±0.8*	44±1*

2. WPNa 0.025 g L^{-1}, Cu_T 7.87 μmol L^{-1}, [$NaNO_3$] 0.1 mol L^{-1}.

pH	Cu_L/Cu_T*	Cu_{NL}/Cu_T^{ns}	Cu_{NR}/Cu_T^{ns}	Cu_L/Cu_R^{ns}	Cu_{NL}/Cu_R^{ns}
6.0	76.9±0.9	18±1	5.4±0.8	81±1	19±1
6.5	69±1*	21±2^{ns}	11±1*	77±2^{ns}	24±2^{ns}
7.0	71±1^{ns}	23±1^{ns}	6.6±0.4*	76±1^{ns}	24±1^{ns}

3. WPNa 0.025 g L^{-1}, Cu_T 7.87 μmol L^{-1}, [$NaNO_3$] 0.01 mol L^{-1}.

pH	Cu_L/Cu_T^{ns}	Cu_{NL}/Cu_T*	Cu_{NR}/Cu_T*	Cu_L/Cu_R*	Cu_{NL}/Cu_R*
6.0	78±1	9.9±0.7	12.4±0.2	89±1	11.3±0.8
6.5	83.5±0.8*	10.9±0.9^{ns}	5.6±0.6*	88±1^{ns}	11.6±0.9^{ns}
7.0	79.3±0.7*	14.1±0.9*	6.6±0.7^{ns}	85±1*	15±1*

4. WPNa 0.05 g L^{-1}, Cu_T 7.87 μmol L^{-1}, [$NaNO_3$] 0.1 mol L^{-1}

pH	Cu_L/Cu_T*	Cu_{NL}/Cu_T^{ns}	Cu_{NR}/Cu_T^{ns}	Cu_L/Cu_R^{ns}	Cu_{NL}/Cu_R^{ns}
6.0	63±1	26±2	11±1	71±2	29±3
6.5	61±1^{ns}	30±3^{ns}	9±2*	67±3^{ns}	33±4^{ns}
7.0	56±1*	32±3^{ns}	12±2^{ns}	64±3^{ns}	36±4^{ns}

Table 7.2 Effects of initial Cu:humate ratio on proportions (percent ± standard error) of kinetic fractions found for copper(II)-sodium humate complex dissociation, 20 °C. (*Probability P that value and preceding value are equal≤0.05; ^{ns}P>0.05. Symbols in column headings indicate the significance of overall trends.)

1. SHNa 0.05 g L^{-1}, pH 6.0, [$NaNO_3$] 0.1 mol L^{-1}; varying Cu_T.

Cu:humate /mg g^{-1}	Cu_L/Cu_T	Cu_{NL}/Cu_T	Cu_{NR}/Cu_T	Cu_L/Cu_R	Cu_{NL}/Cu_R
10	63±1	27±2	10±1	70±2	30±2
20	52.3±0.5*	22.0±0.7*	25.6±0.5*	70±1^{ns}	30±1^{ns}

2. Cu_T 7.87 μmol L^{-1}, pH 6.0, [$NaNO_3$] 0.1 mol L^{-1}; varying [SHNa].

Cu:humate /mg g^{-1}	Cu_L/Cu_T*	Cu_{NL}/Cu_T*	Cu_{NR}/Cu_T*	Cu_L/Cu_R*	Cu_{NL}/Cu_R*
5	42±1	45±2	13±1	48±2	52±3
10	63±1*	27±2*	10±1^{ns}	70±2*	30±2*
20	36.6±0.7*	21±1*	43±1*	64±2^{ns}	36±3^{ns}

3. Cu_T 7.87 μmol L^{-1}, pH 6.0, [$NaNO_3$] 0.1 mol L^{-1}; varying [WPNa].

Cu:humate /mg g^{-1}	Cu_L/Cu_T*	Cu_{NL}/Cu_T*	Cu_{NR}/Cu_T*	Cu_L/Cu_R*	Cu_{NL}/Cu_R*
5	52±2	34±3	14±2	61±3	39±4
10	63±1*	26±2^{ns}	11±1^{ns}	71±2*	29±3^{ns}
20	76.9±0.9*	18±1*	5.4±0.8*	81±1*	19±1*

Table 7.3 Effect of [$NaNO_3$] on proportions (percent ± standard error) of kinetic fractions found for copper(II)-sodium humate complex dissociation, 20° C. (*Probability P that value and preceding value are equal≤0.05; ^{ns}P>0.05. Symbols in column headings indicate the significance of overall trends.)

1. SHNa 0.05 g L^{-1}, Cu_T 7.87 μmol L^{-1}, pH 6.0.

[$NaNO_3$] /mol L^{-1}	Cu_L/Cu_T*	Cu_{NL}/Cu_T*	Cu_{NR}/Cu_T*	Cu_L/Cu_R*	Cu_{NL}/Cu_R*
0.001	71±1	9±1	20.4±0.4	81.4±1.3	18.6±0.9
0.01	62.1±0.9*	14.7±0.8*	23.2±0.4*	81±1*	19±1*
0.1	63±1^{ns}	27±2*	10±1*	70±2*	30±2*

2. WPNa 0.025 g L^{-1}, Cu_T 7.87 μmol L^{-1}, pH 6.0.

[$NaNO_3$] /mol L^{-1}	Cu_L/Cu_T^{ns}	Cu_{NL}/Cu_T*	Cu_{NR}/Cu_T*	Cu_L/Cu_R*	Cu_{NL}/Cu_R*
0.001	78±1	4±1	18.2±0.7	95.3±0.7	5±2
0.01	78±1^{ns}	9.9±0.7*	12.4±0.2*	89±1*	11.3±0.8*
0.1	76.9±0.9^{ns}	18±1*	5.4±0.8*	81±1*	19±1*

7.4.2.4 Effect of copper:humate reaction time before dissociation

Overall, allowing copper(II);humate solutions to react for a longer time resulted in an increase in Cu_{NL}/Cu_T, Cu_{NR}/Cu_T and Cu_{NL}/Cu_R. A corresponding decrease was found for the labile copper fraction; both Cu_L/Cu_T and Cu_L/Cu_R generally decreased with increasing copper(II):humate reaction time for both Cu-SHNa and Cu-WPNa dissociation (Table 7.4; Figure 7.6).

Table 7.4 Effect of copper(II)-humate reaction time on proportions (percent ± standard error) of kinetic fractions found for copper(II)-sodium humate complex dissociation, 20° C. (*Probability P that value and preceding value are equal≤0.05; ^{ns}P>0.05.)

1. SHNa 0.05 g L^{-1}, Cu_T 7.87 μmol L^{-1}, pH 6.0, [$NaNO_3$] 0.001 mol L^{-1}.

Reaction time / h	Cu_L/Cu_T	Cu_{NL}/Cu_T	Cu_{NR}/Cu_T	Cu_L/Cu_R	Cu_{NL}/Cu_R
24	71±1	9±1	20.4±0.4	81.4±1.3	18.6±0.9
96	49.7±0.7*	11.4±0.5^{ns}	38.9±0.4*	81±1*	18.6±0.9*

2. WPNa 0.05 g L^{-1}, Cu_T 7.87 μmol L^{-1}, pH 7.0, [$NaNO_3$] 0.1 mol L^{-1}.

Reaction time / h	Cu_L/Cu_T	Cu_{NL}/Cu_T	Cu_{NR}/Cu_T	Cu_L/Cu_R	Cu_{NL}/Cu_R
24	56±1	32±3	12±2	64±3	36±4
96	54±2^{ns}	32±2^{ns}	14.4±0.7^{ns}	63±2^{ns}	37±3^{ns}

3. WPNa 0.05 g L^{-1}, Cu_T 7.87 μmol L^{-1}, pH 6.5, [$NaNO_3$] 0.1 mol L^{-1}.

Reaction time / h	Cu_L/Cu_T	Cu_{NL}/Cu_T	Cu_{NR}/Cu_T	Cu_L/Cu_R	Cu_{NL}/Cu_R
24	61±1	30±3	9±2	67±3	33±4
48	62.6±0.6^{ns}	30.7±0.8^{ns}	7.1±0.6*	67.0±0.9^{ns}	33±1^{ns}

4. WPNa 0.025 g L^{-1}, Cu_T 7.87 μmol L^{-1}, pH 7.0, [$NaNO_3$] 0.1 mol L^{-1}.

Reaction time / h	Cu_L/Cu_T	Cu_{NL}/Cu_T	Cu_{NR}/Cu_T	Cu_L/Cu_R	Cu_{NL}/Cu_R
24	71±1	23±1	6.6±0.4	76±1	24±1
144	73±2^{ns}	20±3^{ns}	8±1^{ns}	79±3^{ns}	21±3^{ns}

5. WPNa 0.025 g L^{-1}, Cu_T 7.87 μmol L^{-1}, pH 6.5, [$NaNO_3$] 0.1 mol L^{-1}.

Reaction time / h	Cu_L/Cu_T	Cu_{NL}/Cu_T	Cu_{NR}/Cu_T	Cu_L/Cu_R	Cu_{NL}/Cu_R
24	69±1	23±2	6.6±0.4	76±1	24±1
168	60±1^{ns}	23.1±0.7^{ns}	16.5±0.2^{ns}	72±1^{ns}	27.7±0.8^{ns}

6. WPNa 0.025 g L^{-1}, Cu_T 7.87 μmol L^{-1}, pH 6.0, [$NaNO_3$] 0.01 mol L^{-1}.

Reaction time / h	Cu_L/Cu_T	Cu_{NL}/Cu_T	Cu_{NR}/Cu_T	Cu_L/Cu_R	Cu_{NL}/Cu_R
24	78±1	9.9±0.7	12.4±0.2	89±1	11.3±0.8
72	77±1^{ns}	9±1^{ns}	14.2±0.5	89±1^{ns}	11±1^{ns}

7. WPNa 0.025 g L^{-1}, Cu_T 7.87 μmol L^{-1}, pH 7.0, [$NaNO_3$] 0.01 mol L^{-1}.

Reaction time / h	Cu_L/Cu_T	Cu_{NL}/Cu_T	Cu_{NR}/Cu_T	Cu_L/Cu_R	Cu_{NL}/Cu_R
24	79.3±0.7	14.1±0.9	6.6±0.7	85±1	15±1
48	77.0±0.5*	15.5±0.5^{ns}	7.5±0.4^{ns}	83.2±0.7^{ns}	16.8±0.5^{ns}

8. WPNa 0.025 g L^{-1}, Cu_T 7.87 μmol L^{-1}, pH 6.5, [$NaNO_3$] 0.01 mol L^{-1}.

Reaction time / h	Cu_L/Cu_T	Cu_{NL}/Cu_T	Cu_{NR}/Cu_T	Cu_L/Cu_R	Cu_{NL}/Cu_R
24	83.5±0.8	10.9±0.9	5.6±0.6	88±1	11.6±0.9
96	78.8±0.9*	11.2±0.7^{ns}	10.0±0.4*	88±1^{ns}	12.5±0.8^{ns}

These trends were observed for most experiments but were not, however, found to be consistent for all dissociation reactions. Situations in which the opposite trends were observed, however largely involved small differences in amounts of fractions with large associated experimental errors.

7.4.2.5 Effects of temperature on dissociation reactions

An increase in the dissociation reaction temperature (Table 7.5, Figure 7.7) appeared to produce trends in all kinetic fractions (Cu_L/Cu_T and Cu_L/Cu_R decreased; Cu_{NL}/Cu_T, Cu_{NR}/Cu_T and Cu_{NL}/Cu_R increased). Significant trends ($P \leq 0.05$), however, were observed only for the decrease in Cu_L/Cu_T and the increase in Cu_{NR}/Cu_T. Changes in the proportions of all fractions were greater between 20 ° C and 30 ° C than between 30 ° C and 40 ° C.

Table 7.5 Effect of copper(II)-SHNa reaction temperature on proportions (percent ± standard error) of kinetic fractions found for copper(II)-SHNa complex dissociation (equilibration at 20 ° C). (*Probability P that value and preceding value are equal≤0.05; $^{ns}P>0.05$. Symbols in column headings indicate the significance of overall trends.)

SHNa 0.05 g L^{-1}, Cu_T 7.87 μmol L^{-1}, [$NaNO_3$] 0.1 mol L^{-1}, pH 6.0.

Temp / ° C	Cu_L/Cu_T*	Cu_{NL}/Cu_T^{ns}	Cu_{NR}/Cu_T^{ns}	Cu_L/Cu_R^{ns}	Cu_{NL}/Cu_R^{ns}
20	63±1	27±2^{ns}	10±1^{ns}	70±2^{ns}	30±2^{ns}
30	56±1*	30±2^{ns}	14±2^{ns}	65±2^{ns}	35±3^{ns}
40	56±3^{ns}	31±4^{ns}	14±2^{ns}	65±4^{ns}	36±6^{ns}

7.4.2.6 Comparison of copper(II) dissociation from Summit Hill and Waimari Peat sodium humates

Comparisons of CuPAR concentration *versus* ln t curves, obtained under identical experimental conditions, for Cu^{2+}-SHNa and Cu^{2+}-WPNa complex dissociation (for example, Figure 7.8) indicated that dissociation of Cu^{2+} from WPNa was slightly slower than from SHNa.

7.4.3 Description of Copper(II)-Humate Dissociation using Modelling Equations

7.4.3.1 Discrete multisite first-order models

The amount of Cu^{2+} dissociating from copper(II)-humate complexes as a function of time, over a timescale defined by the experimental window (Section 7.3.1), could not be predicted adequately by a model based on single-component first-order kinetics. (R^2 approximately 90%; Figure 7.10a). Inclusion of a second simultaneously dissociating copper(II)-humate species into this discrete site first-order model markedly improved the agreement between observed and predicted values (Table 7.6; Figure 7.10b). The same model formulated to include three discrete sites further improved the predictive capability (Table 7.7; see Figure 7.10c). For the three-site model, the values for the singly lagged residual autocorrelation (r_1) for kinetic experiments with an observation time of 600 s were in the range -0.2 - 0.25, and did not imply a significant autocorrelation (Chapter 3, Section 3.6.5.3). For experiments having observation times of 5400 s (90 minutes), however, the significance level of residual autocorrelations implied some systematic variability in the data that was not explained by the model.

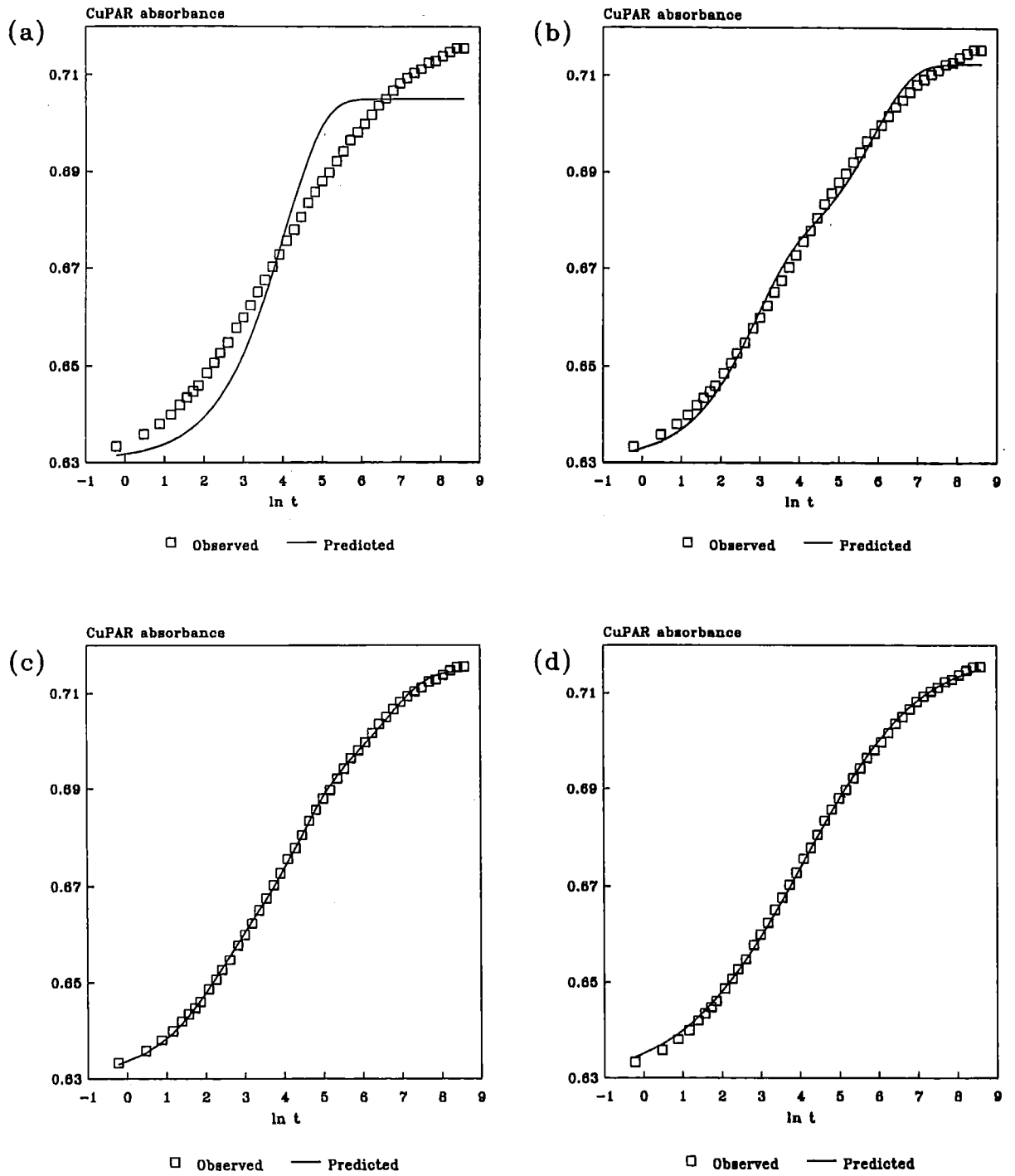

Figure 7.10 Comparison of observed Cu^{2+}-humate dissociation kinetics with that predicted by: (a) single site first-order model; (b) two site first-order model; (c) three-site first-order model, and; (d) lognormal first-order model.

Table 7.6 Summary of fits of representative copper(II)-sodium humate dissociation kinetics data (20 °C, pH=6.0, [$NaNO_3$]=0.1mol L^{-1}, [humate]=0.05g L^{-1}, Cu_T=7.87 μmol L^{-1}; observation time 5400 s; 46 data) to two discrete site first-order model. Adjustable parameters parameters shown as means (±sd) of replicates.

Complex	Cu^{2+}-SHNa	Cu^{2+}-WPNa
Replicates	3	4
$[CuL_1]_0$/μmol L^{-1}	1.02±0.02	0.92±0.04
$\log_{10}k_1$	-1.23±0.03	-1.28±0.01
$[CuL_2]_0$/μmol L^{-1}	1.07±0.05	1.01±0.07
$\log_{10}k_2$	-2.57±0.05	-2.73±0.04
$\Sigma_i[CuL_i]_0$/μmol L^{-1}	2.09±0.05	1.93±0.09
R^2 (%)	99.43	99.41
F ratio	2539	2393
r_1	0.887	0.901

Table 7.7 Summary of fits of representative copper(II)-sodium humate dissociation kinetics data (20 °C, pH=6.0, [$NaNO_3$]=0.1mol L^{-1}, [humate]=0.05g L^{-1}, Cu_T=7.87 μmol L^{-1}; observation time 5400 s; 46 data) to three discrete site first-order model. Adjustable parameters shown as means (±sd) of replicates.

Complex	Cu^{2+}-SHNa	Cu^{2+}-WPNa
Replicates	3	4
$[CuL_1]_0$/μmol L^{-1}	0.61±0.06	0.54±0.03
$\log_{10}k_1$	-0.93±0.06	-0.96±0.04
$[CuL_2]_0$/μmol L^{-1}	0.95±0.05	0.79±0.04
$\log_{10}k_2$	-1.96±0.09	-2.00±0.04
$[CuL_3]_0$/μmol L^{-1}	0.63±0.06	0.70±0.07
$\log_{10}k_3$	-3.05±0.08	-3.11±0.01
$\Sigma_i[CuL_i]_0$/μmol L^{-1}	2.18±0.06	2.02±0.09
R^2 (%)	99.96	99.97
F ratio	20592	24411
r_1	0.646	0.786

7.4.3.2 Continuous distribution first-order models

A model assuming the existence of a continuous mixture of copper(II)-humate species, which were lognormally distributed with respect to first-order dissociation rate constants, was able to provide an

excellent description of Cu-SHNa and Cu-WPNa dissociation reactions over the timescale defined by the experimental window ($R^2 \geq 99.36\%$; see Figure 7.10d). Residual autocorrelations were generally significant, however, especially for data where dissociation was observed for a longer time.

Refined values of the adjustable parameters in the lognormal first-order model (L_{obs}, $\ln k_\mu$ and σ_k) were found to vary with changing experimental conditions for Cu-SHNa and Cu-WPNa complex dissociation reactions, in most cases showing consistent and significant trends (Tables 7.8 - 7.12). With increasing reaction pH (Table 7.8), L_{obs} showed a consistent and significant increase; $\ln k_\mu$ and σ_k, however, showed no consistent pH trends. Changing the initial copper:humate ratio (Table 7.9) resulted in consistent and significant trends in all three parameters. As the copper:humate ratio was increased, L_{obs} (normalised with respect to total copper concentration) decreased, $\ln k_\mu$ increased and σ_k decreased. Increasing ionic strength for the dissociation reaction resulted in consistent increases in L_{obs} and σ_k, and decreases in $\ln k_\mu$, for both Cu-SHNa and Cu-WPNa dissociation (Table 7.10). Changes in $\ln k_\mu$ and σ_k for Cu-WPNa dissociation, however were not significant given the observed experimental variability. Increasing copper-humate reaction time before dissociation also produced, in most cases, significant changes in the adjustable parameters of the lognormal first-order model (Table 7.11). For instances where the changes observed were statistically significant, L_{obs} and σ_k both showed increases with increasing pre-equilibration time, while $\ln k_\mu$ decreased. Finally, comparison of refined parameters from fits of Cu-humate dissociation data obtained at different temperatures (Table 7.12) showed a significant trend in all three parameters. As the dissociation temperature increased, L_{obs} showed a small increase, $\ln k_\mu$ increased and σ_k decreased.

In addition, comparison of the refined parameter estimates from the lognormal model for Cu^{2+}-SHNa and Cu^{2+}-WPNa complex dissociation, under identical experimental conditions, confirmed the slower dissociation from WPNa inferred from inspection of [CuPAR] *versus* time plots (for example, Figure 7.8). Values of the adjustable parameters for the lognormal model for Cu^{2+}-SHNa and Cu^{2+}-WPNa dissociation under identical conditions are found in Table 7.13.

Table 7.8 Effect of pH on refined parameters (mean ± s.e.) derived from fits of copper(II)-sodium humate complex dissociation data, 20 °C, to a model incorporating a lognormal distribution of first-order rate constants. (*Probability (P) that value and preceding value are equal≤0.05; ^{ns}P>0.05. Symbols in column headings show significance of overall trends.)

1. SHNa 0.05 g L^{-1}, Cu_T 7.87 μmol L^{-1}, [$NaNO_3$] 0.1 mol L^{-1}.

pH	L_{obs}/μmol L^{-1}*	ln k_μ*	σ_k*
5.0	1.05±0.02	-4.43±0.05	2.15±0.08
6.0	2.23±0.03*	-4.66±0.07*	2.11±0.02^{ns}
7.0	3.4±0.1*	-5.37±0.05*	2.41±0.04*

2. WPNa 0.025 g L^{-1}, Cu_T 7.87 μmol L^{-1}, [$NaNO_3$] 0.1 mol L^{-1}.

pH	L_{obs}/μmol L^{-1}*	ln k_μ*	σ_k*
6.0	1.33±0.05	-3.92±0.10	1.82±0.04
6.5	1.64±0.02*	-4.16±0.01^{ns}	2.02±0.02*
7.0	1.72±0.06^{ns}	-3.98±0.02*	1.79±0.04*

3. WPNa 0.025 g L^{-1}, Cu_T 7.87 μmol L^{-1}, [$NaNO_3$] 0.01 mol L^{-1}.

pH	L_{obs}/μmol L^{-1}*	ln k_μ^{ns}	σ_k^{ns}
6.0	0.74±0.02	-3.77±0.08	1.79±0.08
6.5	0.82±0.02^{ns}	-4.00±0.06^{ns}	2.05±0.05^{ns}
7.0	1.08±0.03*	-3.91±0.01^{ns}	1.92±0.03^{ns}

4. WPNa 0.05 g L^{-1}, Cu_T 7.87 μmol L^{-1}, [$NaNO_3$] 0.1 mol L^{-1}.

pH	L_{obs}/μmol L^{-1}*	ln k_μ^{ns}	σ_k^{ns}
6.0	2.15±0.06	-5.09±0.05	2.39±0.06
6.5	2.23±0.03*	-5.03±0.04^{ns}	2.32±0.03^{ns}
7.0	2.47±0.08^{ns}	-4.90±0.04^{ns}	2.28±0.04^{ns}

Table 7.9 Effect of initial copper(II):humate ratio on refined parameters (mean ± s.e.) derived from fits of a model incorporating a lognormal distribution of first-order rate constants to copper(II)-sodium humate complex dissociation data, 20 °C. (*Probability (P) that value and preceding value are equal≤0.05; ^{ns}P>0.05. Symbols in column headings show significance of overall trends.)

1. SHNa 0.05 g L^{-1}, pH 6.0, [$NaNO_3$] 0.1 mol L^{-1}; varying Cu_T.

Cu:L/ mg g^{-1}	L_{obs}/μmol L^{-1}*	ln k_μ*	σ_k*
5	1.64±0.07	-6.4±0.1	2.87±0.09
10	2.23±0.03*	-4.66±0.05*	2.11±0.02*
20	3.31±0.04*	-4.08±0.03*	1.89±0.02*

2. Cu_T 7.87 μmol L^{-1}, pH 6.0, [$NaNO_3$] 0.1 mol L^{-1}; varying [SHNa].

Cu:L/ mg g^{-1}	L_{obs}/μmol L^{-1}*	ln k_μ*	σ_k*
5	3.00±0.07	-5.6±0.1	2.54±0.05
10	2.23±0.03*	-4.66±0.05*	2.11±0.02*
20	1.4±0.1*	-3.8±0.1*	1.73±0.08*

3. Cu_T 7.87 μmol L^{-1}, pH 6.0, [$NaNO_3$] 0.1mol L^{-1}; varying [WPNa].

Cu:L/ mg g^{-1}	L_{obs}/μmol L^{-1}*	ln k_μ*	σ_k*
5	2.88±0.02	-5.85±0.02	2.64±0.02
10	2.08±0.06*	-5.09±0.05*	2.39±0.06*
20	1.38±0.05*	-3.9±0.1*	1.82±0.04*

Table 7.10 Effect of [$NaNO_3$] on refined parameters (mean ± s.e.) derived from fits of a model incorporating a lognormal distribution of first-order rate constants to copper(II)-sodium humate complex dissociation data, 20 °C. (*Probability (P) that value and preceding value are equal≤0.05; ^{ns}P>0.05. Symbols in column headings show significance of overall trends.)

1. SHNa 0.05 g L^{-1}, Cu_T 7.87 μmol L^{-1}, pH 6.0.

[$NaNO_3$] mol L^{-1}	L_{obs}/μmol L^{-1}*	ln k_μ*	σ_k*
0.001	0.63±0.02	-3.75±0.05	1.68±0.05
0.01	1.16±0.03*	-4.16±0.06*	1.97±0.05*
0.1	2.23±0.03*	-4.66±0.05*	2.11±0.02^{ns}

2. WPNa 0.05 g L^{-1}, Cu_T 7.87 μ mol L^{-1}, pH 6.0.

[$NaNO_3$] mol L^{-1}	L_{obs}/μmol L^{-1}*	ln k_μ^{ns}	σ_k^{ns}
0.001	0.29±0.02	-3.6±0.2	1.7±0.3
0.01	0.74±0.02*	-3.77±0.08^{ns}	1.79±0.08^{ns}
0.1	1.33±0.05*	-3.9±0.1^{ns}	1.82±0.04^{ns}

Table 7.11 Effect of Cu-humate reaction time before dissociation on refined parameters (mean ± s.e.) derived from fits of a model incorporating a lognormal distribution of first-order rate constants to copper(II)-sodium humate complex dissociation data, 20 °C. (*Probability (P) that value and preceding value are equal≤0.05; ^{ns}P>0.05).

1. SHNa 0.05 g L^{-1}, Cu_T 7.87 μmol L^{-1}, pH 6.0, [$NaNO_3$] 0.001 mol L^{-1}.

Reaction time /h	L_{obs}/μmol L^{-1}	ln k_μ	σ_k
24	0.64±0.02	-3.75±0.05	1.68±0.05
96	0.90±0.03*	-4.44±0.08*	2.14±0.05*

2. WPNa 0.05 g L^{-1}, Cu_T 7.87 μmol L^{-1}, pH 7.0, [$NaNO_3$] 0.1 mol L^{-1}.

Reaction time /h	L_{obs}/μmol L^{-1}	ln k_μ	σ_k
24	2.47±0.08	-4.90±0.04	2.28±0.04
96	2.60±0.04^{ns}	-5.33±0.04*	2.47±0.04*

3. WPNa 0.05 g L^{-1}, Cu_T 7.87 μmol L^{-1}, pH 6.5, [$NaNO_3$] 0.1 mol L^{-1}.

Reaction time /h	L_{obs}/μmol L^{-1}	ln k_μ	σ_k
24	2.55±0.04	-5.03±0.04	2.32±0.03
48	2.78±0.08*	-5.27±0.14^{ns}	2.64±0.05*

4. WPNa 0.025 g L^{-1}, Cu_T 7.87 μmol L^{-1}, pH 7.0, [$NaNO_3$] 0.1 mol L^{-1}.

Reaction time /h	L_{obs}/μmol L^{-1}	ln k_μ	σ_k
24	1.64±0.06	-3.98±0.02	1.79±0.04
144	1.69±0.04^{ns}	-4.25±0.07*	2.00±0.08^{ns}

5. WPNa 0.025 g L^{-1}, Cu_T 7.87 μmol L^{-1}, pH 6.5, [$NaNO_3$] 0.1 mol L^{-1}.

Reaction time /h	L_{obs}/μmol L^{-1}	ln k_μ	σ_k
24	1.57±0.02	-4.16±0.02	2.02±0.02
168	1.90±0.02*	-4.86±0.05*	2.41±0.04*

6. WPNa 0.025 g L^{-1}, Cu_T 7.87 μmol L^{-1}, pH 6.0, [$NaNO_3$] 0.01 mol L^{-1}.

Reaction time /h	L_{obs}/μmol L^{-1}	ln k_μ	σ_k
24	0.74±0.02	-3.77±0.08	1.79±0.08
72	0.68±0.06^{ns}	-4.2±0.2^{ns}	2.1±0.3^{ns}

7. WPNa 0.025 g L^{-1}, Cu_T 7.87 μmol L^{-1}, pH 7.0, [$NaNO_3$] 0.01 mol L^{-1}.

Reaction time /h	L_{obs}/μmol L^{-1}	ln k_μ	σ_k
24	1.15±0.03	-3.91±0.01	1.92±0.03
48	1.35±0.02*	-4.38±0.05*	2.21±0.06*

8. WPNa 0.025 g L^{-1}, Cu_T 7.87 μmol L^{-1}, pH 6.5, [$NaNO_3$] 0.1 mol L^{-1}.

Reaction time /h	L_{obs}/μmol L^{-1}	ln k_μ	σ_k
24	0.81±0.02	-4.00±0.06	2.05±0.05
96	0.90±0.04^{ns}	-4.4±0.1*	2.2±0.1^{ns}

Table 7.12 Effect of Cu-SHNa reaction temperature on refined parameters (mean ± s.e.) derived from fits of a model incorporating a lognormal distribution of first-order rate constants to copper(II)-SHNa complex dissociation data, 20 ° C. (*Probability (P) that value and preceding value are equal≤0.05; ^{ns}P>0.05. Symbols in column headings show significance of overall trends.)

SHNa 0.05 g L^{-1}, Cu_T 7.87 μmol L^{-1}, [$NaNO_3$] 0.1 mol L^{-1}, pH 6.0.

Temp / ° C	L_{obs}/μmol L^{-1}*	ln k_μ*	σ_k*
20	2.23±0.03	-4.66±0.05	2.11±0.02
30	2.36+0.04*	-4.25+0.01*	1.93+0.04*
40	2.38+0.02^{ns}	-3.92+0.04*	1.65+0.02*

Table 7.13 Comparison of refined parameters (mean ± s.e.) derived from fits of a model incorporating a lognormal distribution of first-order rate constants to Cu^{2+}-SHNa and Cu^{2+}-WPNa complex dissociation data, 20 ° C. (*Probability (P) that value and preceding value are equal≤0.05; ^{ns}P>0.05.

1. [humate] 0.05 g L^{-1}, Cu_T 7.87 μmol L^{-1}, [$NaNO_3$] 0.1 mol L^{-1}, pH 6.0.

Complex	L_{obs}/μmol L^{-1}	ln k_μ	σ_k
Cu-SHNa	2.23±0.03	-4.66±0.05	2.11±0.02
Cu-WPNa	2.150±0.002^{ns}	-5.09±0.05*	2.39±0.06*

2. [humate] 0.025 g L^{-1}, Cu_T 15.74 μmol L^{-1}, [$NaNO_3$] 0.1 mol L^{-1}, pH 6.0.

Complex	L_{obs}/μmol L^{-1}	ln k_μ	σ_k
Cu-SHNa	1.4±0.1	-3.8±0.1	1.73±0.08
Cu-WPNa	1.33±0.05^{ns}	-3.9±0.1^{ns}	1.82±0.04^{ns}

3. [humate] 0.1 g L^{-1}, Cu_T 3.93 μmol L^{-1}, [$NaNO_3$] 0.1 mol L^{-1}, pH 6.0.

Complex	L_{obs}/μmol L^{-1}	ln k_μ	σ_k
Cu-SHNa	3.00±0.07	-5.6±0.1	2.54±0.05
Cu-WPNa	2.88±0.02^{ns}	-5.85±0.02^{ns}	2.64±0.02^{ns}

4. [humate] 0.05 g L^{-1}, Cu_T 7.87 μmol L^{-1}, [$NaNO_3$] 0.1 mol L^{-1}, pH 7.0.

Complex	L_{obs}/μmol L^{-1}	ln k_μ	σ_k
Cu-SHNa	3.3±0.1	-5.37±0.05	2.41±0.02
Cu-WPNa	2.47±0.08*	-4.89±0.04*	2.28±0.04*

Evaluation of the Elovich equation for description of copper(II)-sodium humate dissociation kinetics indicated (from inspection of [CuPAR] *versus* log(time) plots; Figures 7.3 - 7.8) that this equation was unsuitable for description of such data. These CuPAR concentration *versus* ln t plots were clearly curvilinear; linear regression of [CuZ] on ln t gave $R^2 \leq 98\%$.

7.4.3.3 Models based on diffusive processes

Under all experimental conditions, for copper(II)-sodium humate complex dissociation, plots of [CuPAR] *versus* √time were distinctly curvilinear (Figure 7.11). Linear regression of [CuZ] on $t^{1/2}$ gave $R^2 \leq 85\%$, suggesting the unsuitability of the general parabolic diffusion equation for description of these data.

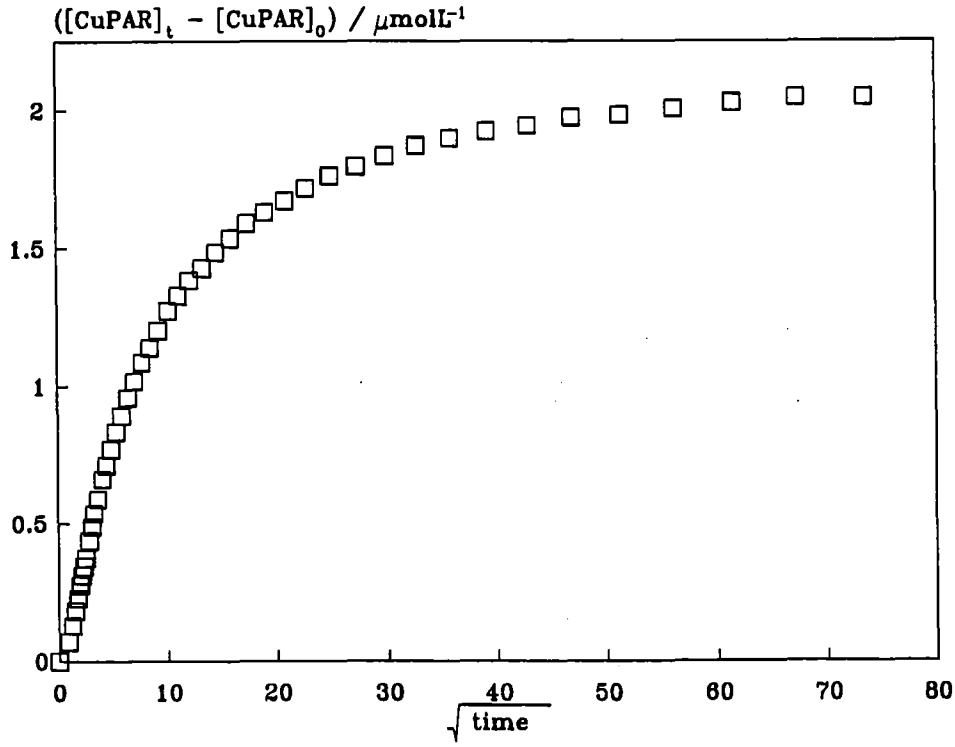

Figure 7.11 CuPAR concentration *versus* $t^{1/2}$ for PAR-induced Cu^{2+}-humate complex dissociation. SHNa 0.05 g L^{-1}, Cu_T 7.87 μmol L^{-1}, pH 6.0, [$NaNO_3$] 0.1 mol L^{-1}.

7.4.4 Discrete Kinetic Spectra

Despite the differences in approach, both methods used to generate discrete kinetic spectra gave similar results (Figures 7.12 to 7.14). Kinetic spectra derived using both methods appeared to be quite sensitive to data from near the end of a run where a reaction had not reached equilibrium (indicated by non-zero slope of [CuZ] *versus* t or log t plots). The effect of this sensitivity was that unrealistically large values of $[CuL_i]_0$ were estimated for sites having more negative log k_i values. $[CuL_i]_0$ values for these slower sites were unrealistic in that, when $[CuZ]_0$ values were taken into account, they implied a greater amount of total solution copper than was initially added to the reaction systems. Analysis of data from reactions that had apparently reached completion (or near-completion) did not result in such spurious values (Figure 7.12). This effect stresses the importance of the experimental observation window on estimates of modelling parameters; if a reaction component does not contribute significantly to the *observed* reaction, then the contribution of that component can not be modelled accurately. In contrast, Cabaniss (1990), whose Ni^{2+}-fulvic acid complex dissociation reactions reached near-completion, did not report spurious $[CuL_i]_0$ peaks for sites having small k_i values when using this modelling technique.

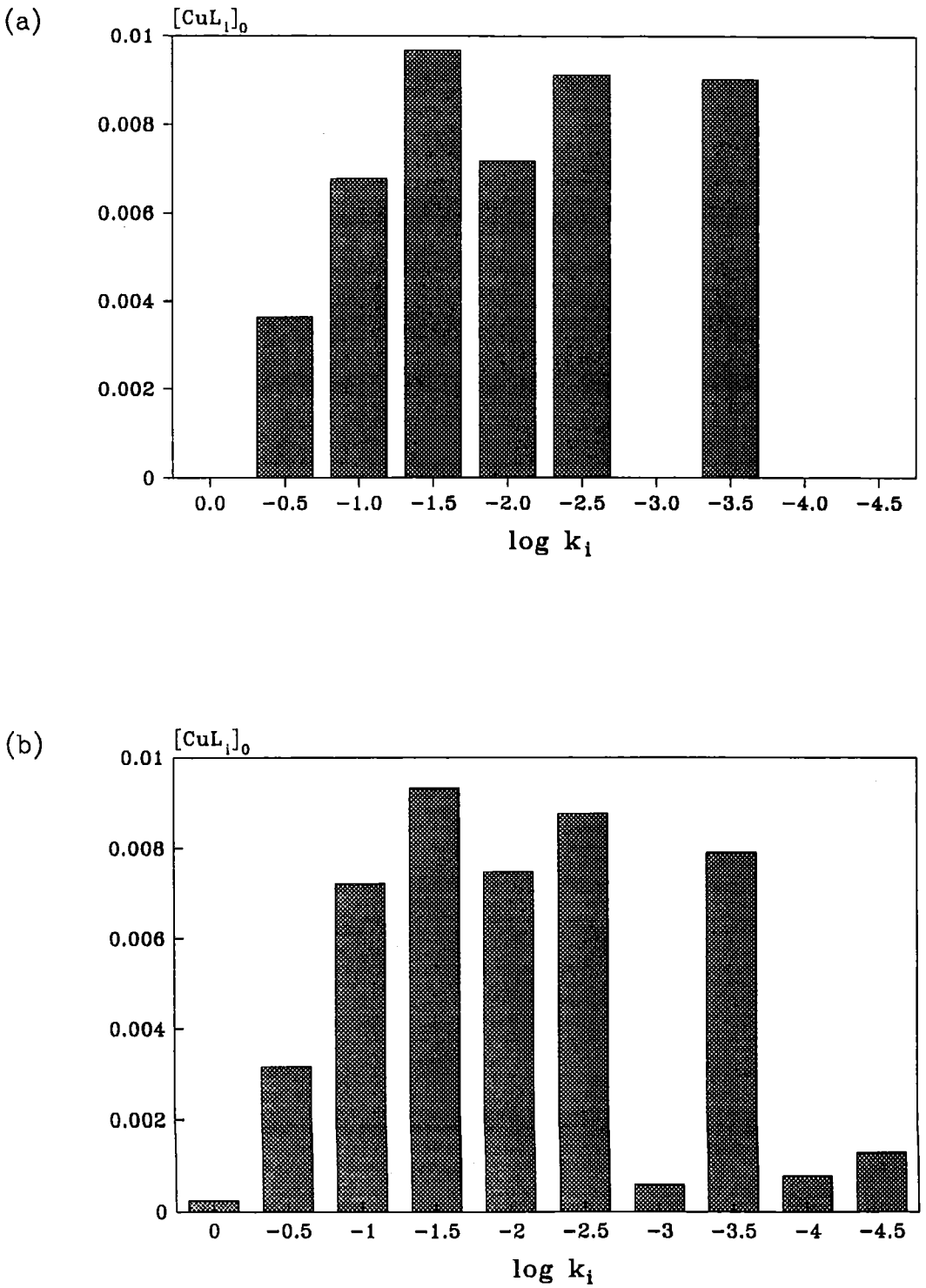

Figure 7.12 Discrete kinetic spectra derived from observations of Cu^{2+}-SHNa complex dissociation: (a) multiple linear regression; (b) multidimensional simplex optimisation. [SHNa] 0.05 g L^{-1}, Cu_T 7.87 μmol L^{-1}, pH 5.0, [$NaNO_3$] 0.1 mol L^{-1}.

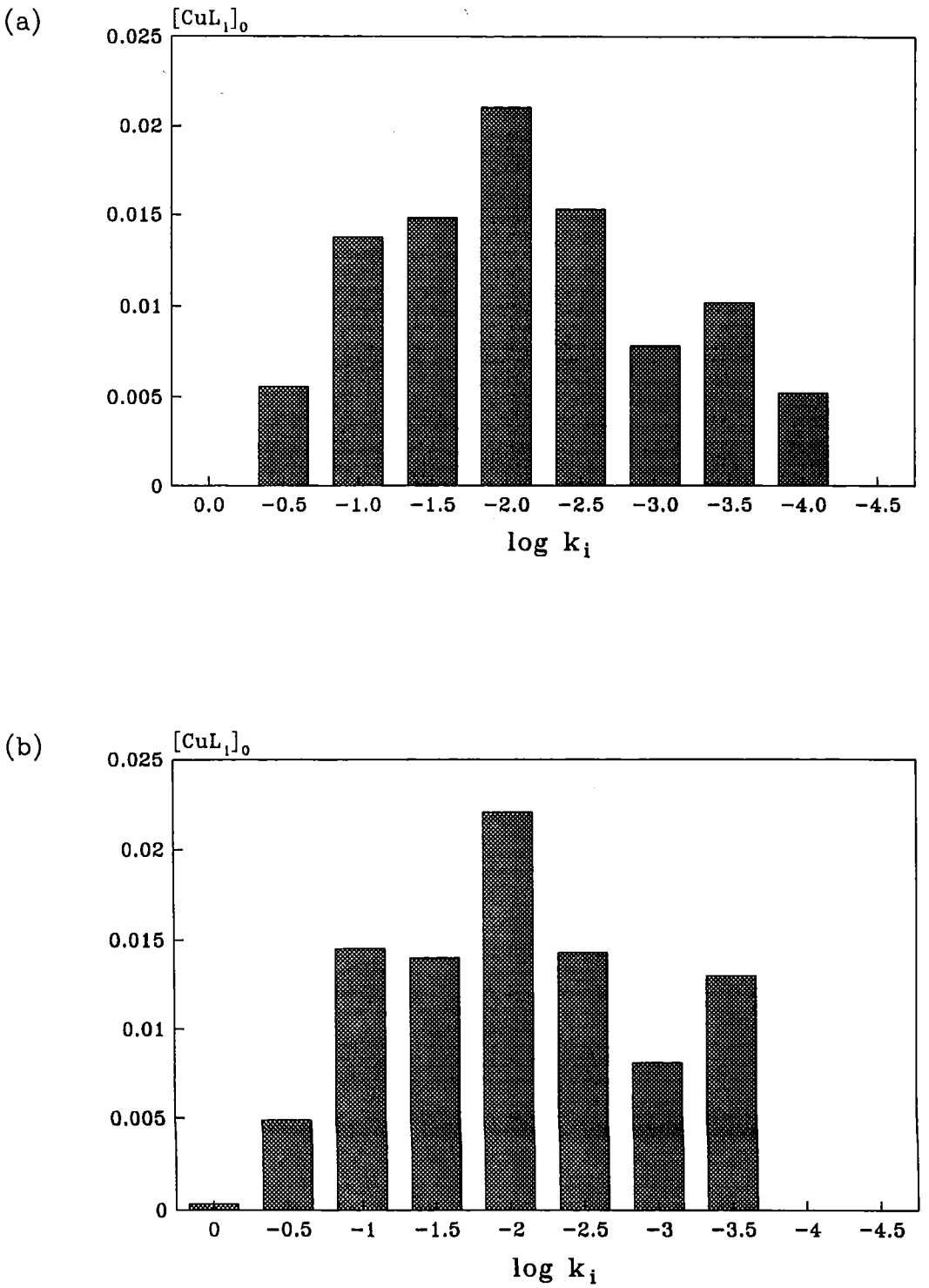

Figure 7.13 Discrete kinetic spectra derived from observations of Cu^{2+}-SHNa complex dissociation: (a) multiple linear regression; (b) multidimensional simplex optimisation. [SHNa] 0.05 g L^{-1}, Cu_T 7.87 μmol L^{-1}, pH 6.0, [$NaNO_3$] 0.1 mol L^{-1}.

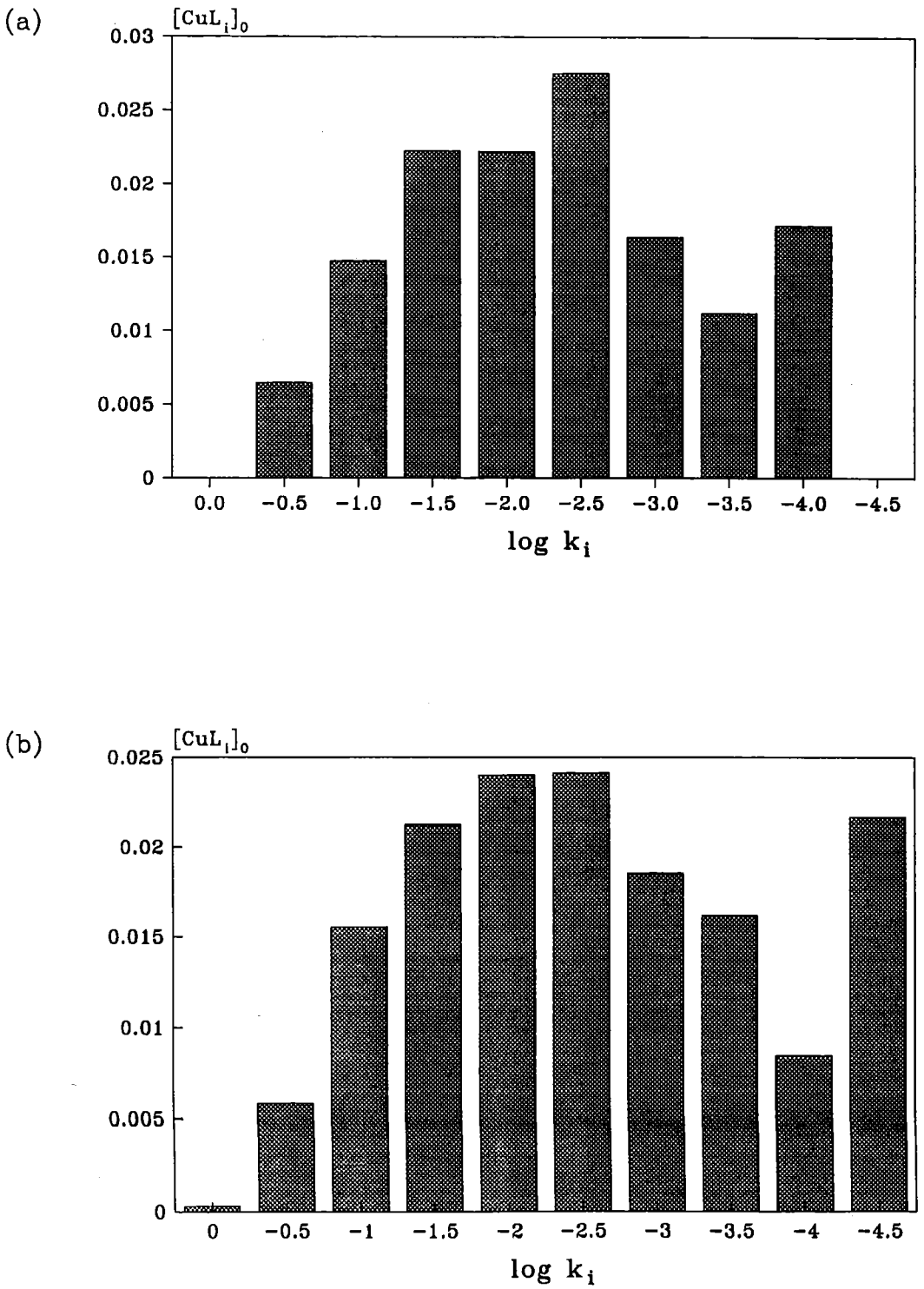

Figure 7.14 Discrete kinetic spectra derived from observations of Cu^{2+}-SHNa complex dissociation: (a) multiple linear regression; (b) multidimensional simplex optimisation. [SHNa] 0.05 g L^{-1}, Cu_T 7.87 μmol L^{-1}, pH 7.0, [$NaNO_3$] 0.1 mol L^{-1}.

If the $[CuL_i]_0$ values for the 'slow sites' derived from these methods are ignored, however, than discrete log k_i spectra derived by both methods were found to imply distributions which were approximately unimodal and symmetrical with respect to log k_i.

As a result of the large number of adjustable and fixed parameters required by these implementations of discrete multisite first-order models, agreement between observed and predicted values was always excellent ($R^2 \geq 99.95\%$). The same large number of adjustable parameters, however, caused parameter optimisation using the multidimensional simplex algorithm to be slow. Since only linear regression steps are necessary, it is considered that the method of Cabaniss (1990) is best suited to generation of discrete kinetic spectra.

This method is able to provide a reasonable and reproducible description of metal-humate complex dissociation kinetics using a fixed number of discrete rate constants, in a similar fashion to the description of binding *equilibria* presented by Eberle and Feuerstein (1979). This suggests that an approximation to a continuous distribution of rate constants may be accessible using an adaptation of the 'integral pK spectrometry' method of Leuenberger and Schindler (1986), which approximates a continuous distribution using fixed-width intervals. To the knowledge of this author, such an approach has not yet been applied to the kinetics of metal ion - humic substance interactions.

7.4.5 Dissociation of Copper(II) from Solid Phase Calcium Humates

Results indicate that approximately 80% of copper(II) bound to WPCa was dissociated by NTA over the 90 minute observation time of experiments (Figure 7.15). Reproducibility between replicates for these experiments was poorer than that observed for reaction of copper(II)-sodium humate complexes with PAR. Concentration *versus* time data was also subject to a greater degree of random fluctuation within experiments than for the solution phase data.

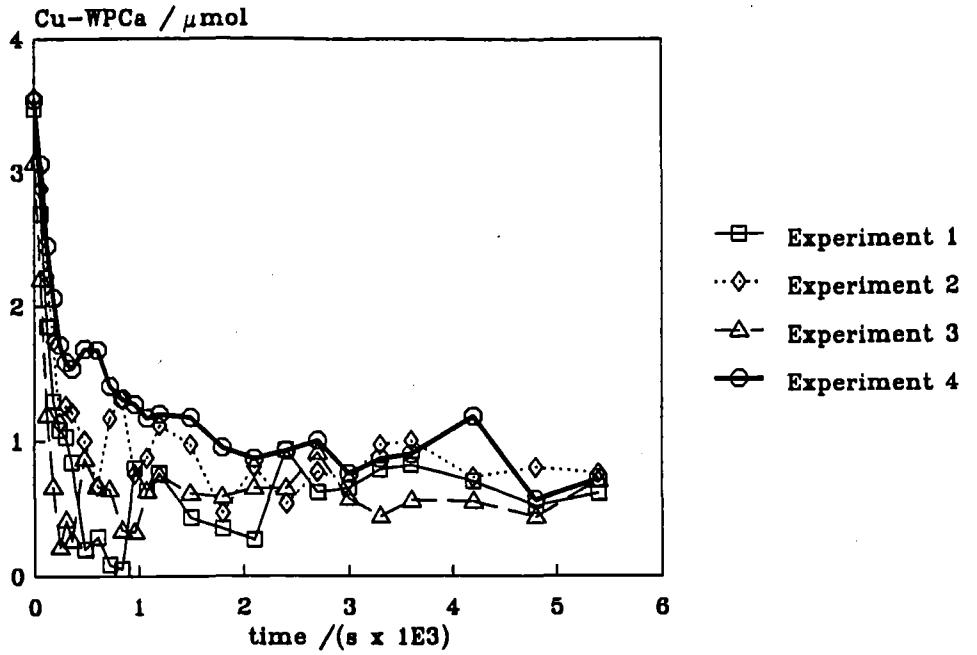

Figure 7.15 Dissociation of Cu^{2+}-WPCa complex as a function of time. Mass WPCa = 0.05 g, Cu_T = 3.93 μmol, $[Ca(NO_3)_2]$ = 0.05 mol L^{-1}, pH 6.0, 20° C.

Owing to the observed variability in Cu^{2+}-WPCa dissociation data (Figure 7.15), fits of any of the discrete-site first-order models to this data were poor relative to data from Cu^{2+}-sodium humate dissociation. For the single site first-order model, R^2 was in the range 84-93%. Inclusion of a second discrete site in the model only resulted in small improvements in fits, giving R^2 in the range 84-96%. It was considered that useful results would be not obtained by fitting a three discrete site first order model, due to the experimental variability.

Fits of the model based on a lognormal distribution of first-order dissociation rate constants (Equation 7.7) to Cu^{2+}-WPCa dissociation data resulted in R^2 values in the range 84-95%. For some replicates, refined estimates of σ_k were very low ($|\sigma_k| \leq 3.5 \times 10^{-4}$), and the associated estimates of $\ln k_\mu$ (mean±s.e. = 4.9±0.2) were effectively identical to estimates of $\ln k_1$ (mean±s.e. = 5.0±0.2) from the single discrete site model. Although this seems to imply negligible kinetic heterogeneity, it is considered that this effect is numerical. That is, the random variability inherent in this data is such that it makes the main contribution to the error sum of squares, and it is not possible to reduce this 'pure error' sum of squares term (Brook and Arnold, 1985) by using a more complicated model.

Evaluation of the Elovich Equation for description of Cu^{2+}-WPCa dissociation kinetics data, by linear regression of n(Cu-NTA) on ln t, gave $11\% \leq R^2 \leq 87\%$. The initial portions of n(Cu-NTA) *versus* ln t plots appeared to be approximately linear. It was considered, however, that the relatively poor quality of this data, and the small numbers of measurements from the initial stages of the reactions, did not justify any detailed analysis.

Plots of n(Cu-NTA) *versus* $t^{1/2}$ using data from the entire observed reaction were also curvilinear ($14\% \leq R^2 \leq 68\%$), suggesting that this range of data did not conform to simple diffusion-controlled kinetics. The initial portions of these plots were suggestive of a linear relationship between n(Cu-NTA) and √time; again, the poor quality of this data, and small numbers of measurements involved, did not justify further analysis.

7.4.6 Spectrophotometric Observation of Copper(II)-Sodium Humate Complexation

The UV-visible absorbance difference spectra obtained (Figure 7.16) showed that the presence of copper(II) ions in a solution of sodium humate caused observable changes in the humate absorbance spectrum. Peaks in the difference spectra (corresponding to increases in humate absorbance) were observed at approximately 280, 400, 500 and 620 nm. The height of all these peaks increased an an approximately linear fashion with respect to total solution copper concentration. It was confirmed that the changes in absorbance were due to chromophores on the humate macro-ion by measuring spectra for similar, but humate-free, solutions with the same levels of copper(II) addition.

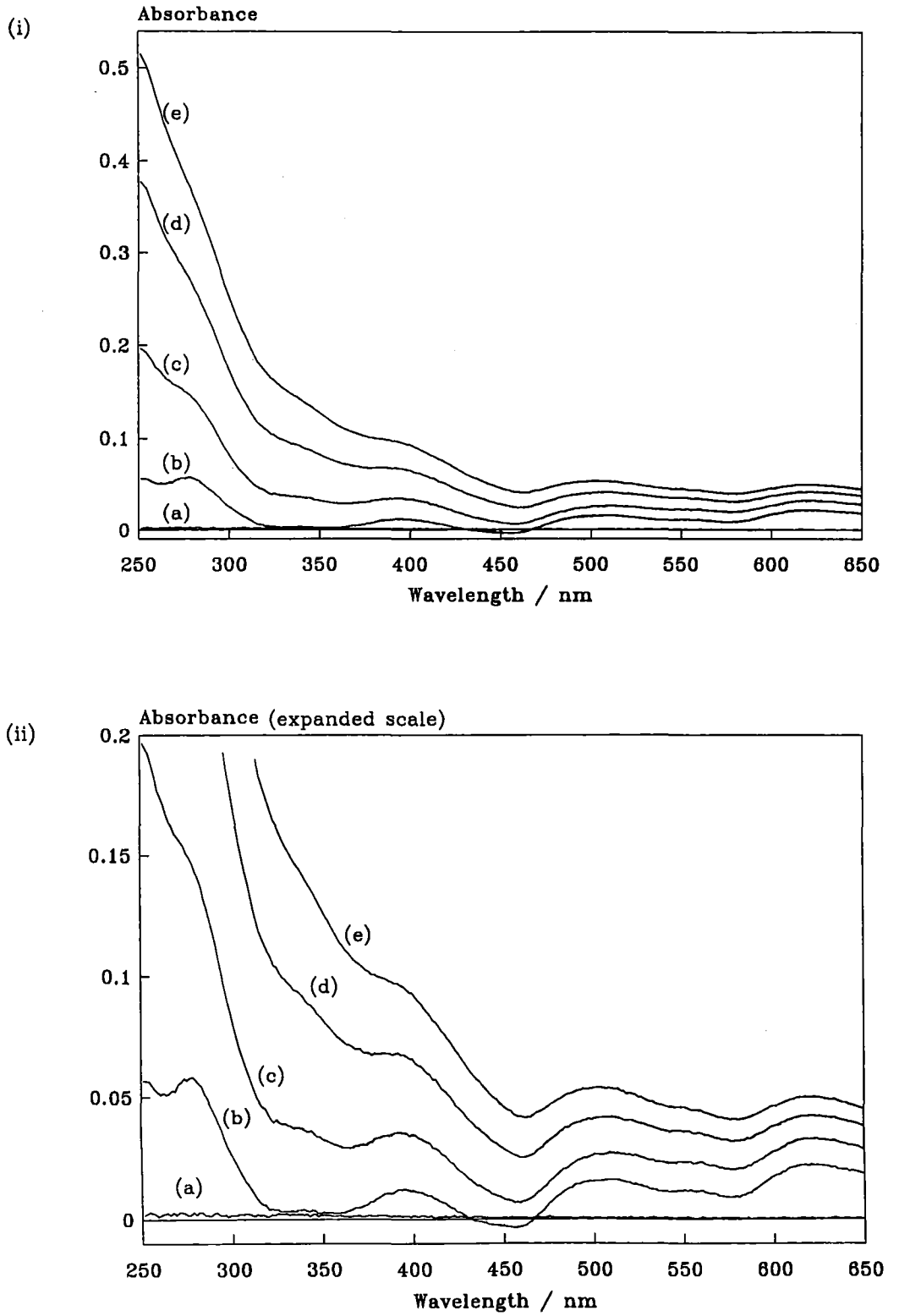

Figure 7.16 UV-visible spectra for solutions of SHNa containing varying amounts of Cu^{2+}. $[Cu^{2+}]$ = (a) 0, (b) 15.7, (c) 31.5, (d) 62.9, (e) 125.9 μmol L^{-1}.

A single peak was observed at c. 280 nm with absorbance approximately 25% of that observed for solutions with sodium humate present. Preliminary experiments designed to monitor the absorbance change on mixing Cu^{2+} and SHNa solutions as a function of time indicated that all absorbance changes took place before the effective time zero ($t \leq 0.5$ s) of experiments. The absorbance changes in the experimental observation window (effective time zero to 600 s) were negligible (monitoring absorbance change at 500 nm). As a result, no modelling of Cu^{2+}-humate association kinetics was possible.

7.5 Discussion

7.5.1 Experimental Methods

7.5.1.1 Assumptions in competing-ligand induced dissociation reactions

Inducement of copper(II)-humate dissociation using competing ligands makes several assumptions regarding the nature of the subsequent dissociation reaction. Firstly, it is assumed that formation of the copper(II)-competing ligand complex is not rate determining. In the case of copper-humate complex reaction with PAR, copper(II)-PAR complex formation has been shown (Olson and Shuman, 1983) to be complete in approximately 0.02s under similar experimental conditions to those used in this work. The zero-time uncertainty in experiments in this work is estimated to be of the order of 0.1 - 0.5s, and thus formation of Cu-PAR complexes should never be rate-determining for processes occurring within the observation window.

In the case of copper(II)-calcium humate complex reaction with NTA, Hering and Morel (1988b) found that formation of Cu-NTA in the presence of excess Ca^{2+} (as in this work) was essentially complete within 120 s. Although this is not an instantaneous reaction, it is unlikely that Cu-NTA formation would have been rate determining on the timescale of the experiments described here. This is in contrast to ligands such as EDTA; the rate of formation of CuEDTA is dramatically hindered by the

presence of Ca^{2+} in the system (Hering and Morel, 1988b). This emphasises the importance of choosing a suitable competing ligand for such experiments. It is interesting to note that Hering and Morel (1988) also found that the rate of Cu^{2+} complexation on an aquatic humic acid was unaffected by high Ca^{2+}:Cu^{2+} ratios in the reaction system.

The second assumption made for competing ligand-induced dissociation experiments is that dissociation rates are determined solely by dissociation of the copper(II)-humate complex and are strictly first-order processes. Both Olson and Shuman (1983) and Shuman *et al.* (1983) found that Cu-humate dissociation rate was independent of PAR concentration over a 10-fold range of [PAR], even if [PAR]:[Cu] was only c. 3:1 at the lower limit of the range. In this work PAR (or NTA) was always in approximately 25 - 30 fold molar excess over total Cu^{2+}, thus ensuring that pseudo first-order conditions prevailed, even if dissociation reactions were dependent on the concentration of PAR.

A third assumption, not stated explicitly by other researchers, is that the competing ligand does not react with the humic substance or the copper-humic substance complex (for example, to form a ternary humic substance-copper-competing ligand complex). The adsorption or partitioning of hydrophobic organic compounds on humic substances is well documented (for example, Chiou *et al.*, 1985; Wershaw, 1986). PAR (Figure 3.1) exists largely in a singly deprotonated form under the conditions of the experiments described (pK_1 = 5.60; Perrin (1979)), which means that the molecule is uncharged and is likely to have a certain degree of hydrophobic character. This makes hydrophobic sorption or partitioning of PAR in dissolved humates a possibility. In contrast, NTA is doubly deprotonated (pK_1 = 2.08, pK_2 = 2.95; Perrin (1979)) and therefore negatively charged under the conditions of the dissociation experiment, and hydrophobic interaction with calcium humate (itself having an overall negative charge) would tend to be unlikely. The possibility also exists for the formation of a mixed-ligand humate-Cu^{2+}-(PAR or NTA) complex in dissociation reaction systems. Such ternary complexes are proposed as reaction intermediates in induced dissociation reactions by Hering and Morel (1990).

Some results from PAR-induced copper(II)-humate complex dissociation in this work tend to suggest a minor interaction between PAR and sodium humate or PAR and Cu^{2+}-sodium humate complexes. During observation of Cu-WPNa dissociation at pH 6 and $[NaNO_3]$ = 0.001 mol L^{-1}, absorbance (510 nm) decreased after approximately 15 - 20 minutes (Figure 7.17), after the initial increase due to CuPAR formation. In addition, solutions of sodium humate, Cu^{2+} and PAR left to equilibrate over longer periods of time (≥24 h) consistently showed slightly lower absorbances than were observed at the termination of dissociation experiments under identical experimental conditions. Although these observations suggest that processes other than copper-humate complex dissociation are occurring, it is not possible to identify the nature of the process involved. The effect of these secondary processes on the large majority of experimental absorbance measurements is small, and it is considered reasonable to assume that copper-humate complex dissociation is the only process observed in experiments.

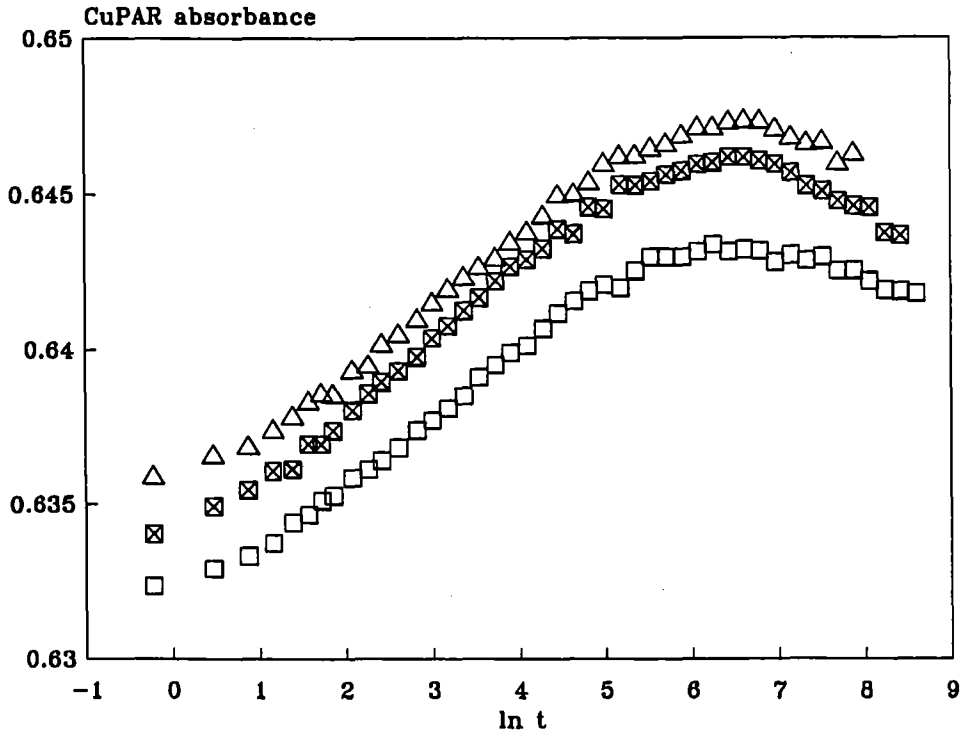

Figure 7.17 Absorbance decrease in experiments observing PAR-induced dissociation of Cu^{2+}-WPNa complexes. [WPNa] = 0.025 g L^{-1}, Cu_T = 7.87 μmol L^{-1}, pH 6.0, 20° C, $[NaNO_3]$ = 0.001 mol L^{-1}.

The zero time error of 0.1 - 0.5 seconds estimated for PAR induced Cu-humate dissociation experiments enables estimation of a minimum rate constant for complexes dissociating before the effective time zero. These complexes are calculated to have dissociation rate constants $\geq$ 4-20 s^{-1} ($\ln k \geq 1.4$).

7.5.1.2 Observation of the dissociation reactions from solid- or gel-phase humates

The relatively poor quality of data obtained from Cu^{2+}-WPCa dissociation kinetics experiments (Figure 7.15) suggested some shortcoming of the experimental technique (see Chapter 3, Section 3.5.2). It was considered that the method of reaction quenching in sample aliquots (phase separation by filtration through a 0.45 μm membrane) was a critical source of systematic error. For these experiments, the same filter was used, without washing, for successive samples from the early stages of the reaction. Residual Cu^{2+}-humate complex on filter membrane, being wetted with NTA solution, may have dissociated further and contributed to the amount of Cu-NTA in successive samples. As use of separate filter membranes for each sample would be wasteful and expensive, it is suggested that a two-stage filtration step be used. A relatively coarse (paper or glass fibre) filter at the end of the sampling tube which is immersed in the reaction suspension could offer the following advantages:

(i) most of the suspended Cu^{2+}-calcium humate complex would be removed before membrane filtration, suppressing contamination;

(ii) any Cu^{2+}-calcium humate complex entrained in the first filter would remain in contact with the NTA solution for further reaction, and;

(iii) any errors due to loss of humate from the reaction system would be minimised.

A further potential source of error in these experiments may have arisen from the presence of dissolved Cu^{2+}-humate species in the reaction suspension. Although such species would have made a negligible contribution to the overall Cu^{2+}-humate binding reaction, they would not have been removed by filtration. As such, they may have made a contribution to the copper determined in the sample aliquots; this may have been important in the early stages of the dissociation reaction.

7.5.2 Modelling of Kinetic Data

7.5.2.1 Discrete site first-order kinetic models

It was evident, from determination of apparent half-lives for the dissociation reactions, that the rate of dissociation of copper(II)-humate complexes did not conform to simple single-component first order kinetics. The time taken for the observable reactions to reach half-completion was generally of the order of 60 s; successive half-times for the remainder of the reactions were longer, exceeding 1000 s at the end of the observation window. The poor fits of the single site first order model to copper(II)-humate dissociation rate data were therefore expected. The much better fits of the two discrete site model are considered to be a purely empirical description of data, since refined values of k_1 and k_2 typically differed by at least an order of magnitude, and thus Guggenheim plots of experimental data should have shown two resolvable rectilinear portions (Mak and Langford, 1983). In fact Guggenheim (or $\ln([CuL]_t/[CuL]_0)$) plots were always concave upwards with no obvious linear trends. In contrast, Plankey and Patterson (1987) found that Al^{3+}-fulvic acid complex formation kinetics data, when plotted as $\ln([AlL]_\infty-[AlL]_t)$ *versus* time (qualitatively identical to Guggenheim plot) gave only two distinct rectilinear portions. Their measurements, however, were performed at lower pH, effectively decreasing the number and heterogeneity of fulvic acid sites available for Al^{3+} binding.

The three discrete site first-order model, although providing very close fits to experimental data, was also considered to have limited physical significance apart from indicating the extent of kinetic heterogeneity. The residual autocorrelations calculated for most regressions (except those from fits to data having observation windows of $\leq$ 600 s) implied non-random residual distributions and systematic trends which were either unexplained by the model or unjustified in the model given the complexity of the data. Similar behaviour was found when testing a four discrete site first-order model.

7.5.2.2 Continuous distribution first-order models

The proposal of a model involving copper-humate complexes with a lognormal distribution of first-order dissociation rate constants was based on several premises. The assumption was made that the degree of kinetic heterogeneity present in copper-humate complexes was sufficiently great to justify interpretation in terms of a continuous distribution model. This assumption is consistent with the degree of heterogeneity in binding site affinities, and is also supported by experimental data, for example, the continuous decrease in slope of Guggenheim or $\ln([CuL]_t/[CuL]_0)$ *versus* time plots. The choice of the standard normal equation for the form of the continuous distribution in log k was also based on independent analysis of kinetic data. Firstly, analysis of kinetic data in terms of three or four discrete sites (see Table 7.7) always implied that the fastest and slowest 'sites' were present at lower levels than sites having intermediate dissociation rate constants, suggesting some form of unimodal distribution which was approximately symmetrical with respect to log k.

Further analysis in terms of discrete sites with rate constants fixed in arbitrary increments, as suggested by Cabaniss (1990), revealed a similar pattern in the $[CuL_i]$ *versus* log K_i distribution. Finally, the finding that the application of the continuous lognormal distribution model to kinetic data provided, in general, very good agreement between observed and predicted values was further confirmation of the utility of what is essentially a conceptually simple model.

As stated by Albery *et al.* (1985), a lognormal distribution in rate constants implies a lognormal distribution in reaction activation energies, in this case for copper(II)-humate complex dissociation. In contrast with Albery *et al.* (1985), however, the model in this work uses the standard normal distribution to describe the dispersion in log k values, rather than a generalised Gaussian distribution. It is considered that the standard normal distribution provides the more conceptually simple and succinct description. Mean (k_μ) and standard deviation (σ_κ) log k values are explicitly stated in the adjustable parameters of the model, and the standard deviation is a more generally understood measurement than the dispersion parameter γ (Equation 2.48) used by Albery *et al.* (1985).

Previous studies measuring dissociation kinetics from humic substance-metal ion complexes (for example, Shuman *et al.*, 1983; Lavigne *et al.*, 1987; Cabaniss, 1990) have often indicated multimodal rate constant distributions, using the approximate Laplace transform method of Olson and Shuman (1983). The data of Cabaniss (1990), however, analysed in terms of discrete kinetic spectra, are also suggestive of a symmetrical, unimodal distribution of log k values for Ni^{2+}-fulvic acid complex dissociation. The tendency towards more discrete kinetic behaviour for metal ion-humic substance complex dissociation observed in these studies may reflect a lesser degree of kinetic heterogeneity for fulvic acids.

A comparison of observed dissociation behaviour with that predicted by the continuous lognormal model shows that this model slightly overestimates the amount of Cu^{2+} dissociated at the shortest reaction times (<10 s), and slightly underestimates at longer reaction times (>1000 s). This observation shows that the lognormal model implies faster reactions than are observed at short reaction times, and slower reactions than are observed at long reaction times. Combined with the calculated values of singly lagged residual autocorrelations from regressions, these observations indicated that the good fits achieved by this model are essentially empirical and do not necessarily have any physical significance. In fact the superficial similarity of the equations $y=(1-e^{-kx})$ and $y=\sqrt{x}$ may mean that a heterogeneous diffusion equation based on a continuous normal distribution would provide, in terms of simple goodness of fit, an equally good description of copper(II)-humate dissociation kinetics.

The lognormal model, along with discrete site models having at least three components do, however, offer good predictive capability within the range of experimental measurements. In addition, the lognormal model has been shown in this work to be useful for reducing kinetic data to a succinct set of parameters which may be used to compare the effects of different experimental treatments.

Refined values of the adjustable parameters derived from fits of kinetic data to all models indicated that the parameters and goodness of fit are dependent on the length of time over which dissociation was

observed. This again emphasises the empirical nature of the models used, and suggests that the resolution of kinetic experiments, in an analogy with binding experiments, shows considerable dependence on the analytical window. In other words, apparent kinetic heterogeneity will increase with increasing observation time.

7.5.3 Effect of Changing Experimental Conditions on Copper(II)-Humate Dissociation Kinetics

7.5.3.1 Effects of pH

An increase in pH was expected to affect the mixture of copper(II)-sodium humate complexes in different ways. At higher pH, complexing of Cu^{2+} by more weakly acidic ligands such as phenolates is likely to have been enhanced. As a result, equilibrium free copper concentrations would be decreased due to higher site occupancy and the heterogeneity of binding would increase. In addition, the humate macro-ion may exist in a more expanded conformation at higher pH (Hayes and Swift, 1978), and as a result, dissociation of Cu^{2+} may be less sterically hindered than for the more contracted macro-ions prevalent at lower pH. Titration data for both Summit Hill and Waimari Peat humic acids (Chapter 5) indicate that macro-ion charge increases measurably over the pH range employed in kinetics experiments.

The results obtained in this work (Sections 7.4.2.1 and 7.4.3) indicate that the proportion of non-labile (slowly dissociating) copper(II)-humate complex increases with increasing pH. Since there is expected to be less steric hindrance to dissociation of Cu^{2+} from the complex at higher pH, it is more logical to attribute the differences in proportions of non-labile Cu to chemical differences between sites. The increased charge on the macro-ion is likely to be an important factor (Olson and Shuman, 1983). In addition, because the humate macromolecules at higher pH probably contain a higher proportion of more strongly bound Cu^{2+}, it seems likely that more strongly bound copper dissociates more slowly.

While this may, intuitively, seem obvious, it is possible that strongly bound copper (having a high complex formation constant) may have a very fast formation reaction and thus may still dissociate quickly (for example, CuEDTA) according to Equation 2.42 (Cotton and Wilkinson, 1976). Some workers have assumed that thermodynamic and kinetic stability are equivalent (for example, Lehmann and Harter, 1984). While some results from this work indicate that this may be the case for copper(II)-humate complex dissociation, making this assumption in the absence of supporting evidence may, in some cases, be incorrect. If this assumption were strictly true, one could expect all sites in such a heterogeneous system to have very similar formation rate constants, which seems rather unrealistic.

The proportions of non-reactive copper showed only small variations with pH. Few useful conclusions may be made from this observation, however, since this operational fraction includes both very thermodynamically stable and very slowly dissociating complexes, and trends may reflect a combination of kinetic factors and the relative stabilities of copper-humate and copper-PAR complexes with changing pH.

Other workers have observed similar behaviour in metal-humate complex dissociation reactions. Both Lavigne *et al.* (1987) and Cabaniss (1990) observed an increase in the proportions of more slowly dissociating Ni^{2+}-fulvate complexes with increasing pH.

7.5.3.2 Effect of initial copper:humate ratio

Changes in initial copper:humate ratio, at constant pH and ionic strength, will produce changes in the speciation of the mixture of copper(II)-humate complexes present. At low copper:humate ratios, copper will be preferentially bound to sites having higher effective formation constants. As the Cu:humate ratio increases, sites on the humate macro-ion with lesser affinity for Cu^{2+} will be occupied; this increases the proportion of more weakly bound copper, and also increases heterogeneity with respect to complex stability. The proportion of non-labile copper-humate complexes present tended to decrease

with increasing copper:humate ratio, again suggesting that the more thermodynamically stable complexes were also the most kinetically stable. Increased copper(II) ion loading on the humate macro-ions may also lead to macromolecular contraction (Hayes and Swift, 1978). Since a more contracted macromolecule would hinder dissociation of Cu^{2+} sterically (thus giving an increased proportion of non-labile copper) it is unlikely that steric factors are rate-determining under the experimental conditions. It is interesting to note that non-reactive copper shows no consistent trend with Cu:humate ratio. It was expected that the proportion of non-reactive copper would decrease with increasing Cu:humate ratio, due to the decreased proportion of copper present in more stable copper(II)-humate complexes.

Analysis of the kinetics of the non-labile copper fraction, in terms of a lognormal distribution of first-order rate constants, showed significant trends in the refined parameters of this model with increasing Cu:humate ratio. Mean refined values of L_{obs} (Table 7.9), when normalised with respect to total solution copper, confirmed the decrease in non-labile copper with increasing Cu:humate ratio mentioned above. Mean values for $\ln k_{\mu}$ implied faster dissociation from this fraction as Cu:humate increased. The decrease in kinetic heterogeneity with increasing Cu:humate ratio, implied by mean σ_k values, is possibly related to either the smaller proportion of copper(II)-humate sites in the non-labile fraction, or to the possibility that additional bound copper is more quickly dissociating, thus skewing the distribution in ln k values and reducing apparent heterogeneity.

These results are in agreement with those of Lavigne *et al.* (1987) and Cabaniss (1990). These workers found that Ni^{2+}-fulvate complex dissociation rates increased with increasing Ni^{2+}-fulvate ratio. Cabaniss (1990) concluded that the more thermodynamically stable Ni^{2+}-fulvate complexes were also the most slowly dissociating.

7.5.3.3 Effect of electrolyte concentration

It was considered that increasing ionic strength would affect the copper(II)-sodium humate system in two ways. First, the masking of the humate macro-ion electrostatic potential at higher ionic strength would result in an overall decrease in affinity of humate ligands for Cu^{2+}. Second, the higher concentration of co-and counter-ions in the vicinity of the humate macroion would cause macromolecular contraction. The first expectation was confirmed by the trends in the non-reactive copper fraction, which consistently decreased with increasing ionic strength.

Analysis of dissociation data in terms of both kinetically defined fractions and the lognormal distribution first-order kinetic model, however, indicated that the proportions of more slowly dissociating sites, with respect to total copper, were lower at lower ionic strength. Unless the operationally defined non-reactive copper fraction contains a substantial proportion of relatively inert complexes, which increases as ionic strength is lowered, then it could be inferred, in this case, that conditions that cause Cu^{2+} to be more strongly bound also facilitate faster dissociation. This is in contrast to the effects of pH and Cu^{2+}:humate ratio discussed earlier (Sections 7.5.3.1 and 7.5.3.2).

It was observed, however, that the proportions of copper(II)-humate complexes in the labile fraction appear to show little decrease with changing $NaNO_3$ concentration. This suggests that the major change occurring with increasing ionic strength is a shift of Cu^{2+}-humate complexes from the non-reactive to the non-labile fraction, that is, a faster overall dissociation reaction. Such an observation agrees with data obtained by varying both ionic strength and pH, in that it appears that the solution conformation of humate macro-ions is not as important in determining the rate of copper(II)-humate complex dissociation as is complex stability. In other words, conditions which favour the formation of stronger complexes (in this case, low ionic strength) also tend to result in slower complex dissociation rates.

For description of dissociation data using the lognormal model, decreasing ionic strength resulted in increases in $\ln k_{\mu}$ and decreases in σ_k. This may reflect a shift of more slowly dissociating complexes to

the non-reactive (and non-modelled) fraction as electrolyte concentration decreased, thus decreasing effective kinetic heterogeneity, and resulting in an observed increase in dissociation rate for the remaining sites.

Cabaniss (1990) found that a decrease in the ionic strength at which Ni^{2+}-fulvate complex dissociation reactions took place decreased overall dissociation reaction rates, a finding consistent with that in this work. It was proposed (Cabaniss, 1990) that the rates of dissociation of only the more quickly dissociating components in the mixture of Ni^{2+}-fulvate complexes were affected significantly by changes in ionic strength. This second finding is not in agreement with the results in this work; the major changes occurring with changing ionic strength appeared to be within the more slowly dissociating components (non-labile and non-reactive copper) in the mixture of Cu^{2+}-humate complexes.

7.5.3.4 Effect of copper(II)-humate reaction time before dissociation

Results from analysis of copper(II)-humate complex dissociation data in terms of kinetically defined fractions (Table 7.4) generally indicated that, where significant changes occur, increasing reaction time results in a decrease in labile copper and an increase in non-reactive copper. Use of the lognormal first-order kinetics model for data analysis (Table 7.11) supports, and expands on, the kinetic fraction analysis. Changes in the mean refined parameters for this model (increasing L_{obs}, decreasing $\ln k_{\mu}$ and increasing σ_k) all imply that increasing Cu-humate reaction time slows down the subsequent dissociation reaction.

To explain this behaviour, it is proposed that the copper(II)-humic substance complex formation reaction includes some very slow processes. Elucidation of an unambiguous mechanism for the slow complexation reactions, however, is not possible from the data in this work. Some tentative hypotheses may, however, be made.

Previous workers observing metal ion dissociation from soils and soil components have found a similar effect. For example, the data presented by Lehmann and Harter (1984) indicated that increasing soil-copper reaction time, prior to dissociation, decreased the subsequent rate of desorption of copper from soil. Several possible mechanisms were proposed to explain this behaviour, including: movement of Cu^{2+} into more slowly dissociating or less sterically accessible sites; alteration of dissociation rates due to prolonged Cu^{2+} binding; or formation of a separate copper(II)-containing solid phase.

In this work, all components were in solution throughout the dissociation reaction; in addition, it is considered unlikely that complexation of Cu^{2+} could alter the *intrinsic* dissociation rate of particular sites. Unfortunately, any further hypothesis as to the mechanisms of a slow complex formation reaction (and subsequent retarded dissociation) is to some extent dependent on the concept of humic substance structure which is adopted. If solvated humate macro-ions are essentially linear, and coil randomly with respect to time and space (Hayes and Swift, 1978; Swift, 1989), then it is unlikely that accessibility of sites would be rate determining unless the timescale of conformational changes is long compared with that observed for complex formation or dissociation. The *effective* dissociation rate of certain sites may be influenced by Cu^{2+} binding if the binding reaction constrains the conformation of the complex in such a way that steric accessibility becomes important. Intramolecular crosslinking reactions could provide such conformational constraints; sites in the vicinity of the crosslinking complex may also become less sterically accessible (Teasdale, 1987). It has already been suggested (Chapter 6, Sections 6.4.4.1 and 6.4.4.3) that slow conformational change is an important factor in determining Cu^{2+}-humate complex formation rates, especially in the final stages of the formation reactions, and this hypothesis is supported by the data presented in this Chapter. The results discussed in this Section also imply that the processes which give rise to slow complex formation reactions also retard the rate of complex dissociation.

7.5.3.5 Temperature effects

Increasing the temperature at which the dissociation reaction took place was expected to increase reaction rates. This expectation was confirmed by analysis of kinetic data using the lognormal first-order model. The increase in mean first-order rate constants with temperature found corresponded satisfactorily to an Arrhenius-type expression (Atkins, 1978) (for linear regression of mean refined $\ln k_{\mu}$ *versus* reciprocal temperature, $R^2 = 0.998$). This enabled estimation of a mean activation energy (E_a) for the dissociation reaction of 28 ± 1 $kJmol^{-1}$ (pre-exponential factor in Arrhenius equation = 1030±50).

The magnitude of this estimate of E_a is within the range of 21-42 $kJmol^{-1}$ expected for rate-limiting intraparticle diffusion (Sparks, 1985). Since this value represents the centre of a continuous distribution, however, dissociation of a significant proportion of Cu^{2+} is controlled by activation energies outside this range, thus making any interpretations ambiguous. In addition, previous discussion in this Chapter has proposed that physical processes are less likely than chemical processes to be rate determining for aqueous copper(II)-humate complex dissociation. It should also be noted (Morgan and Stone, 1985) that in heterogeneous systems there is always a possibility that the reactions observed proceed by a sequence of unknown steps. In such a case, estimates of E_a may, in fact, represent *apparent* E_a values which combine actual E_a values and reaction enthalpies for non-rate determining steps.

The decrease in dissociation rate heterogeneity with increasing temperature implied by decreasing σ_k in the lognormal model was also expected. Slower sites (those having more negative $\ln k_i$) would have a larger activation energy, and thus the response of their dissociation rate to increasing temperature will be more marked. Similarly, copper(II)-humate complexes which dissociate quickly are controlled by smaller activation energies, and the rates of these dissociation reactions will be less sensitive to temperature change. These factors will tend to decrease the dispersion in dissociation rates at higher temperature with respect to the situation at lower temperature.

7.5.3.6 Comparison of copper(II) dissociation rates from Summit Hill and Waimari Peat sodium humates

Slower dissociation of Cu^{2+}-WPNa complexes, compared with Cu^{2+}-SHNa complexes, was implied by comparison of [CuPAR] *versus* time plots (Figure 7.8) or refined parameter estimates from the lognormal first-order model (Table 7.13). It is possible that the small but significant difference in dissociation rates is related to the higher charge density, at equivalent pH, of WPNa compared with SHNa (Chapter 5, Section 5.3.1.2). In turn, this implies that macro-ionic charge may be important in determining Cu^{2+}-humate dissociation rates. Cabaniss (1990) states that a strong ionic strength dependence of dissociation rates (implied by the results discussed in Section 7.5.3.3) may be expected if the rate-determining step for dissociation involves release of a 'territorially bound' ion from a polyelectrolyte, that is, removal of that ion from the influence of the macro-ionic electrostatic potential. In addition, Cu^{2+}-WPNa complexes were found to be more stable than Cu^{2+}-SHNa complexes (Chapter 6, Section 6.4.2), and the observed difference in dissociation rates is again consistent with a hypothesis that the more thermodynamically stable Cu^{2+}-humate complexes dissociate more slowly.

7.6 Summary

The formation and dissociation of copper(II)-humate complexes have been found to proceed by extremely heterogeneous processes with respect to reaction rates. In the case of both formation and dissociation reactions, a major proportion of the reaction is complete within the mixing time of conventional kinetics experiments. The results presented in this Chapter, however, also imply the existence of very slow formation and dissociation processes such that either process is incomplete over a timescale of hours to days. Such findings are in agreement with those presented in Chapter 6, and are explained by slow conformational change in Cu^{2+}-humate complexes which allows further complex formation and retards subsequent dissociation.

It has also been shown in this Chapter that the dissociation kinetics of copper(II)-humate complexes, over an observable timescale, may be described satisfactorily by a model based on a lognormal distribution of first-order dissociation rate constants. This model has also been found to be useful in identifying effects of changing experimental conditions on dissociation reaction rates.

In addition, analysis of copper(II)-humate complex dissociation kinetics data obtained under a range of systematically varied conditions has illustrated the importance of these conditions in determining dissociation rates. The rate of Cu^{2+}-humate complex dissociation was found to decrease with increasing pH or Cu^{2+}-humate reaction time before dissociation, and to increase with increasing overall Cu^{2+}:humate ratio, electrolyte concentration or temperature. These trends are consistent with slower dissociation of Cu^{2+} from more thermodynamically stable Cu^{2+}-humate complexes, and imply that the degree of expansion or contraction of solvated humate macro-ions may not be significant in determining complex dissociation rates.

CHAPTER EIGHT

CONCLUSIONS

8.1 Introduction

It is considered that the research objectives stated in Chapter 1 have been fulfilled satisfactorily in this work. New experimental approaches (for example, pH-potentiometric titration of size-fractionated humic acids) and strategies for data analysis (for example, use of a novel model to analyse kinetic data) were used to formulate conclusions regarding the nature of humic substance complexation reactions. Some shortcomings were apparent, however, for instance in the application of the theory developed by Marinsky and co-workers to humic acid protonation, or in the inability to resolve kinetic and thermodynamic effects when observing metal ion-humic substance complexation. Possibly the most important single conclusion gained from this work is the importance of kinetically controlled processes in humic substance-metal ion complexation reactions; this has both mechanistic, and practical or experimental implications, as outlined below.

8.2 Overall Conclusions

8.2.1 Numerical methods

The multidimensional simplex algorithm for function optimisation was found to be appropriate for parameter estimation in models of humic substance protonation, metal binding and metal complex

dissociation kinetics, by minimising a residual sum of squares term. Simulated metal-humate binding data were used to evaluate three different methods for calculating the residual sum of squares (minimisation of absolute and relative residual sum of squares with bound metal as the dependent variable, and absolute residual sum of squares with the log of free metal concentration as the dependent variable). Parameter estimates obtained using any of these methods were found to be acceptable given reasonable levels of random error.

8.2.2 Nature of Complexation Reactions between Protons or Metal Ions and Humic Acids

8.2.2.1 Humic substance protonation

The consistent presence of an inflection (pH 7.5 - 7.8) in the pH-potentiometric titration curves of all humic acid samples studied suggested that it was possible to separate the contributions to proton binding of carboxylic acid and more weakly acidic groups, such as phenolic hydroxyl. Protonation reactions also showed a clear ionic strength dependence with respect to proton binding affinity, consistent with macro-ionic behaviour. Measured carboxylic acid functional group contents were independent of solution ionic strength. Unfortunately, a detailed analysis of the ionic strength dependence of the protonation reactions failed to yield any unambiguous information regarding solution conformations.

An analysis of the protonation behaviour of molecular-size fractions of the Summit Hill IHSS Standard humic acid revealed that the differences in proton affinity were most likely to be due to differences in acidic functional groups than to charge characteristics. These molecular size fractions also showed a trend for carboxyl acidity to increase with decreasing molecular size.

8.2.2.2 Copper(II)- and cadmium(II)-complexation

The copper(II)- and cadmium(II)-humate complexation reactions were found to be important modifiers of metal ion speciation, with the major proportions of these metal ions being bound in humate complexes under the experimental conditions used. Both Cd^{2+} and Cu^{2+} were found to bind to the humic acids strongly enough to displace protons at pH 6, suggesting inner-sphere complexation and possibly chelation of Cu^{2+}. This behaviour was expected for Cu^{2+}, but inner-sphere complexation has not always been invoked for Cd^{2+} (Chapter 1). The differences in metal ion binding affinities for Summit Hill and Waimari Peat humic acids were considered to result from differences in macro-ionic charge, and therefore the degree of electrostatic attraction, although differences in the nature of binding sites present probably made some contribution. Although the possibility of aggregational effects could not be discounted for aqueous-phase complexation reactions, no direct evidence was found for such behaviour.

For Cd^{2+} and Cu^{2+} binding to both solution phase (sodium) and solid phase (calcium) humates, increasing the temperature at which the complexation reaction took place resulted in enhanced binding being observed, that is, more Cd^{2+} or Cu^{2+} was bound at higher temperature. Observation of such temperature-dependent behaviour in humic substance - metal ion complexation reactions is scarce in research literature. A decrease in the amount of bound Cu^{2+} was not observed, however, for systems where the temperature was decreased. It was proposed that slow formation kinetics for metal-humate complexes provided the most consistent explanation of the observed temperature dependence of these reactions. Thermodynamic effects on the temperature dependence of metal-humate complexation reactions were unable to be distinguished from these kinetic effects, however, and the relative contributions of these effects could not be determined. Rate determining steps for the final stages of complex formation reactions were postulated to involve slow complexation-induced conformational changes (allowing further metal binding) for reactions in the aqueous phase, and a combination of intraparticle diffusion and/or conformational change for solid phase complexation.

8.2.3 Heterogeneity of Complexation Reactions of Humic Substances

The proton and metal ion binding reactions of humic substances were found to be very heterogeneous with respect to binding affinity. Modelling studies implied a range of at least three to four orders of magnitude in conditional formation constants for humic acid protonation, Cu^{2+} complexation and Cd^{2+} complexation. The observed heterogeneity was consistent with both a mixture of many different complex-forming functional groups and macro-ionic behaviour of humic acid macromolecules.

The heterogeneity inherent in the binding reactions was also found to be a feature of the rates of copper(II)-humate complex dissociation reactions. A substantial proportion of components in the mixture of Cu^{2+}-humate complexes dissociated within c. 0.5s; other components were still dissociating after several hours. In addition, although a large proportion of Cu^{2+}-humate complexes formed almost instantaneously, the complex formation reactions were found to include some very slow processes which were not complete over a timescale of several days. As mentioned previously, these slow processes were attributed to rate-determining conformational change or diffusion.

8.2.4 Dissociation Kinetics

Data from competing-ligand induced Cu^{2+}-sodium humate complex dissociation kinetics experiments was analysed by two novel methods: in terms of operationally-defined kinetic fractions, and using a continuous lognormal distribution model. Such analyses revealed and quantified the sensitivity of the rates of these reactions to changing experimental conditions, in accord with objective 4 stated in Chapter 1 (Section 1.2.2). Faster dissociation was observed when Cu^{2+}:humate ratio, electrolyte concentration, or temperature were increased; dissociation became slower when pH, or Cu^{2+} reaction time before dissociation, were increased. Such trends were consistent with other recent research, and implied that more strongly bound Cu^{2+} dissociates more slowly. The strength of electrostatic attraction was also

considered to affect complex dissociation rates, dissociation being slower from a more highly charged humate macro-ion. The decrease in dissociation rates from Cu^{2+}-humate complexes which had reacted for longer periods before dissociation supports the hypothesis that the final stages of complex formation reactions are very slow.

8.2.5 Modelling of Complexation and Kinetic Behaviour

Despite the heterogeneity involved in both proton and metal binding affinities, and metal complex dissociation rates, it was found that a large number of models provided good numerical descriptions of experimentally derived data. It was considered, however, that no model which was applied provided an accurate physicochemical description of the processes involved, even though many of the models used had some reasonable chemical or physical basis. In addition, the adjustable parameters derived from fitting models to both binding and kinetic data were dependent on the range of experimental observations. This restricted these models to being of use primarily for predictive or comparative purposes. An evaluation of the models developed by Teasdale (1987) showed that further development of theory is necessary before aggregation processes are included explicitly in models designed to describe complexation reactions of humic substances. A new model for observable Cu^{2+}-humate complex dissociation kinetics, based on a lognormal distribution of first-order rate constants, was found to provide a good description of experimental data.

Some of the models applied to experimental data provided useful comparisons between experimental treatments, and provided quantitative or semi-quantitative confirmation of observed trends.

8.3 Implications for Future Research

8.3.1 Experimental Techniques

The very slow component found for the complexation reactions of metal cations and humic substances in this work suggests that experiments intended to observe *equilibria* in these reactions must allow for these slow processes. Although the long term increases in the amounts of *bound* metal ion may be negligible, the corresponding decreases in *uncomplexed* metal ion solution concentrations may be substantial, especially for strongly bound ions such as Cu^{2+} and/or solid or gel-phase humic substances. Failure to allow for slow complexation reactions will mean that parameter estimates derived from complexation models based on the attainment of equilibrium will be misleading. Research needs to be directed towards measurement of the timescale required for completion of metal ion - humic substance complexation reactions.

8.3.2 Humic acid protonation

It would be useful to more fully characterise the protonation behaviour of the IHSS Reference Summit Hill humic acid. This could involve measurement of carboxylic acid and phenolic hydroxyl group contents using methods other than those used in this work. In addition, this work involved detailed analysis of protonation in the pH range 4-8; the behaviour of more strongly acidic functional groups (at pH values less than 4) could be studied by titration with strong acid, and the titration range could be further extended into the high-pH region in order to more fully characterise phenolic and other similarly weak acidity.

A further area requiring investigation is the relationship between humic acid potentiometric properties and solution conformation. The analysis of protonation data developed by Marinsky and co-workers has been criticised by other workers, and was found in this work to give ambiguous conclusions; this

suggests that a refinement of the relevant theory is necessary. Such analysis is potentially useful in that it could provide a relatively simple method for following conformational changes of humate macro-ions in solution, or the transition from the solution to the solid phase, without requiring sophisticated equipment.

8.3.3 Humic Substance - Metal Ion Complexation Equilibria

Once experimental techniques which unambiguously observe complexation equilibria have been developed, it should be possible to evaluate the effect of temperature on the thermodynamic aspects of these reactions. Evaluation of reaction thermodynamics, however, would require simultaneous development of an accurate physicochemical description of metal ion - humic substance equilibria, another goal which has not yet been achieved. In the context of soil reactions, more research needs to be centered around reactions of solid- or gel-phase humic substances with metal ions.

8.3.4 Kinetics of Humic Substance - Metal Ion Complexation

Most kinetic investigations of metal-humate complexes, including this work, have centered on dissociation kinetics. Research needs to be directed towards measurement of complex formation rates; spectrofluorometric techniques may be best suited for solution phase reactions. Again, the study of complex formation and dissociation rates for solid phase humic substances is important in the context of soil processes, and more work needs to be done in this area. For completeness of understanding, the large proportion of very fast reactions should also be investigated; temperature- or pressure-jump relaxation techniques may be most suitable for such studies.

REFERENCES

Adriano, D.C. (1986). *Trace Elements in the Terrestrial Environment.* Springer-Verlag, New York.

Aiken, G.R., McKnight, D.M., Wershaw, R.L. and MacCarthy, P. (1985). An introduction to humic substances in soil, sediment and water. **In** *Humic Substances in Soil, Sediment and Water*, (edited by Aiken, G.R., McKnight, D.M., Wershaw, R.L. and MacCarthy, P.), Wiley-Interscience, New York, 1-9.

Albery, W.J., Bartlett, P.N., Wilde, C.P. and Darwent, J.R. (1985). A general model for dispersed kinetics in heterogeneous systems. *Journal of the American Chemical Society*, **107**, 1854-1858.

Anderson, H.A., Bick, W., Hepburn, A. and Stewart, M. (1989). Nitrogen in humic substances. **In** *Humic Substances II.* (edited by Hayes, M.H.B., MacCarthy, P., Malcolm, R.L. and Swift, R.S.), Wiley, Chichester, 223-253.

Atkins, P.W. (1978). *Physical Chemistry.* Oxford University Press, Oxford.

Avdeef, A., Zabronsky, J. and Stuting, H.H. (1983). Calibration of copper ion selective electrode response to pCu 19. *Analytical Chemistry*, **55**, 298-304.

Bauer, H.H., Christian, G.D. and O'Reilly, J.E. (1978). *Instrumental Analysis.* Allyn and Bacon, Boston.

Beckwith, R.S. (1955). Metal complexes in soils. *Australian Journal of Agricultural Research*, **6**, 685-698.

Bhattacharyya, G.K. and Johnson, R.A. (1977). *Statistical Concepts and Methods*, Wiley, New York.

Blaser, P. and Sposito, G. (1987). Spectrofluorometric investigation of trace metal complexation by an aqueous chestnut leaf litter extract. *Soil Science Society of America Journal*, **51**, 612-619.

Bloom, P.R. and McBride, M.B. (1979). Metal ion binding and exchange with hydrogen ions in acid washed peat. *Soil Science Society of America Journal*, **43**, 687-692.

Bollag, J-M. (1983). Cross-coupling of humus constituents and xenobiotic substances. **In** *Aquatic and Terrestrial Humic Materials* (edited by Christman, R.F. and Gjessing, E.T.), Ann Arbor, Michigan, 127-141.

Bolt, G.H. and van Riemsdijk, W.H. (1987). Surface chemical processes in soil. **In** *Aquatic Surface Chemistry* (edited by W. Stumm), Wiley-Interscience, New York, 127-164.

Brady, N.C. (1974). *The Nature and Properties of Soils.* MacMillan, New York.

Bremner, J.M., Heintze, S.G., Mann, P.J.G. and Lees, H. (1946). Metallo-organic complexes in soil. *Nature*, **158**, 790-791.

Brook, R.J. and Arnold, G.C. (1985). *Applied Regression Analysis and Experimental Design.* Marcel Dekker, New York.

Buffle, J. and Altmann, R.S. (1987). Interpretation of metal complexation by heterogeneous complexants. **In** *Aquatic Surface Chemistry* (edited by W. Stumm), Wiley-Interscience, New York, 351-383.

Buffle, J. Greter, F-L. and Haerdi, W. (1977). Measurement of complexation properties of humic and fulvic acids in natural waters with lead and copper ion-selective electrodes. *Analytical Chemistry*, **49**, 216-222.

Bunday, B.D. (1984). *Basic optimisation methods*. Edward Arnold, London.

Bunzl, K., Schmidt, W. and Sansoni, B. (1976). Kinetics of ion exchange in soil organic matter. IV. Adsorption and desorption of Pb^{2+}, Cu^{2+}, Cd^{2+}, Zn^{2+} and Ca^{2+} by peat. *Journal of Soil Science*, **27**, 32-41.

Cabaniss, S.E. (1990). pH and ionic strength effects on nickel-fulvic acid dissociation kinetics. *Environmental Science and Technology*, **24**, 583-588.

Cabaniss, S.E. and Shuman, M.S. (1988). Fluorescence quenching measurements of copper-fulvic acid binding. *Analytical Chemistry*, **60**, 2418-2421.

Cabaniss, S.E. and Morel, F.M.M. (1989). Comment on "A unified physicochemical description of the protonation and metal ion complexation equilibria of natural organic acids (humic and fulvic acids)." *Environmental Science and Technology*, **23**, 746-747.

Cameron, R.S., Thornton, B.K., Swift, R.S. and Posner, A.M. (1972). Molecular weight and shape of humic acid from sedimentation and diffusion measurements on fractionated extracts. *Journal of Soil Science*, **23**, 394-408.

Cavallaro, N. and McBride, M.B. (1978). Copper and cadmium adsorption characteristics of selected acid and calcareous soils. *Soil Science Society of America Journal*, **42**, 550-556.

Cheam, V. (1973). Chelation study of copper(II):fulvic acid system. *Canadian Journal of Soil Science*, **53**, 377-382.

Chen, Y. and Schnitzer, M. (1989). Sizes and shapes of humic substances by electron microscopy. **In** *Humic Substances II: In Search of Structure*, (edited by Hayes, M.H.B., MacCarthy, P., Malcolm, R.L. and Swift, R.S.), Wiley, Chichester, 621-638.

Chien, S.H., Clayton, W.R. and McLellan, G.H. (1980). Kinetics of dissolution of phosphate rocks in soils. *Soil Science Society of America Journal*, **44**, 260-264.

Chiou, C.T., Shoup, T.D. and Porter, P.E. (1985). Mechanistic roles for soil humus and minerals in the sorption of nonionic organic compounds from aqueous and organic solutions. *Organic Geochemistry*, **8**, 9-14.

Clark, M.E. (1979). *Contemporary Biology, Second Edition*, W.B. Saunders, Philadelphia.

Cotton, F.A. and Wilkinson, G. (1976). *Basic Inorganic Chemistry*, Wiley, New York.

Dempsey, B.A. and O'Melia, C.R. (1983). Proton and calcium complex formation of four fulvic acid fractions. **In** *Aquatic and Terrestrial Humic Materials*, (edited by Christman, R.F. and Gjessing, E.T.), Ann Arbor, Michigan, 239-273.

De Nobili, M., Gjessing, E. and Sequi, P. (1989). Sizes and shapes of humic substances by gel chromatography. **In** *Humic Substances II* , (edited by Hayes, M.H.B., MacCarthy, P., Malcolm, R.L. and Swift, R.S.), Wiley, Chichester, 561-591.

Dobbs, J.C., Susetyo, W., Knight, F.E., Castles, M.A., Carreira, L.A. and Azarraga, L.V. (1989a). Characterization of metal binding sites in fulvic acids by lanthanide ion probe spectroscopy. *Analytical Chemistry*, **61**, 483-488.

Dobbs, J.C., Susetyo, W., Carreira, L.A. and Azarraga, L.V. (1989b). Competitive binding of protons and metal ions in humic substances by lanthanide ion probe spectroscopy. *Analytical Chemistry*, **61**, 1519-1524.

Dzombak, D.A., Fish, W. and Morel, F.M.M. (1986). Metal-humate interactions. 1. Discrete ligand and continuous distribution models. *Environmental Science and Technology*, **20**(7), 669-675.

Eberle, S.H. and Feuerstein, W. (1979). On the pK spectrum of humic acid from natural waters. *Naturwissenschaften*, **66**, 572-573.

Ennis, M.T. and Brogan, J.C. (1985). The availability of copper from copper - humic acid complexes. In *Soil Nutrient Availability*, (edited by Y.K. Soon), Van Nostrand Reinhold, New York, 153-160.

Ephraim, J. and Marinsky, J.A. (1986). A unified physicochemical description of the protonation and metal ion complexation equilibria of natural organic acids (humic and fulvic acids). 3. Influence of polyelectrolyte properties and functional heterogeneity on the copper ion binding equilibria in an Armadale horizons B_h fulvic acid sample. *Environmental Science and Technology*, **20**, 367-376.

Ephraim, J., Alegret, S., Mathuthu, A., Bicking, M., Malcolm, R.L. and Marinsky, J.A. (1986). A united physicochemical description of the protonation and metal ion complexation equilibria of natural organic acids (humic and fulvic acids). 2. Influence of polyelectrolyte properties and functional group heterogeneity on the protonation equilibria of fulvic acid. *Environmental Science and Technology*, **20**, 354-366.

Fish, W., Dzombak, D.A. and Morel, F.M.M. (1986). Metal-humate interactions. 2. Application and comparison of models. *Environmental Science and Technology*, **20**, 676-683.

Flaig, W., Beutelspacher, H. and Rietz, E. (1975). Chemical composition and physical properties of humic substances. In *Soil Components: Volume 1. Organic Components* (edited by J.E. Gieseking), Springer-Verlag, New York, 1-211.

Gamble, D.S. (1970). Titration curves of fulvic acid: the analytical chemistry of a weak acid polyelectrolyte. *Canadian Journal of Chemistry*, **48**, 2662-2669.

Gamble, D.S., Schnitzer, M. and Hoffman, I. (1970). Cu^{2+}-fulvic acid chelation equilibrium in 0.1*M* KCl at 25 °C. *Canadian Journal of Chemistry*, **48**, 3197-3204.

Gamble, D.S., Underdown, A.W. and Langford, C.H. (1980). Copper(II) titration of fulvic acid ligand sites with theoretical, potentiometric and spectrophotometric analysis. *Analytical Chemistry*, **52**, 1901-1908.

Gamble, D.S., Schnitzer, M., Kerndorff, H. and Langford, C.H. (1983). Multiple metal ion exchange equilibria with humic acid. *Geochimica et Cosmochimica Acta*, **47**, 1311-1323.

Gamble, D.S., Langford, C.H. and Underdown, A.W. (1985). Light scattering measurements of Cu(II)-fulvic acid complexing: the interdependence of apparent complexing ability and aggregation. *Organic Geochemistry*, **8**, 35-39.

Genstat 5 Committee, (1987). *GENSTAT 5 Reference Manual* (Statistics Department, Rothamsted Experimental Station), Oxford University Press, Oxford.

Goodman, B.A. and Cheshire, M.V. (1976). The occurrence of copper-porphyrin complexes in soil humic acids. *Journal of Soil Science*, **27**, 337-347.

Gran, G. (1952). Determination of the equivalence point in potentiometric titrations. *Analyst*, **77**, 661-671.

Gregor, J.E. and Powell, H.K.J. (1988a). Application of sampled-DC anodic stripping voltammetry to metal/fulvic acid equilibria. *Analytica Chimica Acta*, **211**, 141-154.

Gregor, J.E. and Powell, H.K.J. (1988b). Protonation reactions of fulvic acids. *Journal of Soil Science*, **39**, 243-252.

Griffith, S.M. and Schnitzer, M. (1989). Oxidative degradation of soil humic substances. **In** *Humic Substances II.* (edited by Hayes, M.H.B., MacCarthy, P., Malcolm, R.L. and Swift, R.S.), Wiley, Chichester, 69-78.

de **Haan**, F.A.M. and Zwerman, P.J. (1976). Pollution of soil. **In** *Soil Chemistry. A. Basic Elements*, (edited by Bolt, G.H. and Bruggenwert, M.G.M.), Elsevier, Amsterdam, 192-271.

Hansen, A.M., Leckie, J.O., Mandelli, E.F. and Altmann, R.S. (1990). Study of copper(II) association with dissolved organic matter in surface waters of three Mexican coastal lagoons. *Environmental Science and Technology*, **24**, 683-688.

Harter, R.D. (1989). A new modeling-compatible solution for the first-order kinetics equation. *Soil Science*, **147**, 97-102.

Harvey, G.R. and Boran, D.A. (1985). Geochemistry of humic substances in seawater. **In** *Humic Substances in Soil, Sediment and Water*, (edited by Aiken, G.R., McKnight, D.M., Wershaw, R.L. and MacCarthy, P.), Wiley-Interscience, New York, 233-247.

Hayes, M.H.B. (1985). Extraction of humic substances from soil. **In** *Humic Substances in Soil, Sediment and Water*, (edited by Aiken, G.R., McKnight, D.M., Wershaw, R.L. and MacCarthy, P.), Wiley-Interscience, New York, 329-362.

Hayes, M.H.B. and Himes, F.L. (1986). Nature and properties of humus-mineral complexes. **In** *Interactions of Soil Minerals with Natural Organics and Microbes*, SSSA Special Publication Number 17, (edited by Huang, P. and Schnitzer, M.), SSSA, Madison, 103-158.

Hayes, M.H.B. and O'Callaghan, M.R. (1989). Degradations with sodium sulfide and with phenol. **In** *Humic Substances II.* (edited by Hayes, M.H.B., MacCarthy, P., Malcolm, R.L. and Swift, R.S.), Wiley, Chichester, 143-180.

Hayes, M.H.B. and Swift, R.S. (1978). The chemistry of soil organic colloids. **In** *The Chemistry of Soil Constituents*, (edited by Greenland, D.J. and Hayes, M.H.B.), Wiley-Interscience, New York, 179-320.

Hayes, M.H.B., MacCarthy, P., Malcolm, R.L. and Swift, R.S. (1989a). The search for structure: setting the scene. **In** *Humic Substances II.* (edited by Hayes, M.H.B., MacCarthy, P., Malcolm, R.L. and Swift, R.S.), Wiley, Chichester, 3-31.

Hayes, M.H.B., MacCarthy, P., Malcolm, R.L. and Swift, R.S. (1989b). Structures of humic substances: the emergence of 'forms'. **In** *Humic Substances II.* (edited by Hayes, M.H.B., MacCarthy, P., Malcolm, R.L. and Swift, R.S.), Wiley, Chichester, 689-733.

Hering, J.G. and Morel, F.M.M. (1988a). Humic acid complexation of calcium and copper. *Environmental Science and Technology*, **22**, 1234-1237.

Hering, J.G. and Morel, F.M.M. (1988b). Kinetics of trace metal complexation: role of alkaline-earth metals. *Environmental Science and Technology*, **22**, 1469-1478.

Hering, J.G. and Morel, F.M.M. (1990). Kinetics of trace metal complexation: ligand-exchange reactions. *Environmental Science and Technology*, **24**, 242-252.

Himes, F.L. and Barber, S.A. (1957). Chelating ability of soil organic matter. *Soil Science Society of America, Proceedings*, **21**, 368-373.

Hogg, D.S. (1989). *Sorption Behaviour and Plant Availability of Copper in Soils*. Unpublished Ph.D. Thesis, University of Canterbury, New Zealand.

Hunston, D.L. (1975). Two techniques for evaluating small molecule - macromolecule binding in complex system. *Analytical Biochemistry*, **63**, 99-109.

Kerndorff, H. and Schnitzer, M. (1980). Sorption of metals on humic acid. *Geochimica et Cosmochimica Acta*, **44**, 1701-1708.

Kielland, J. (1937). Individual activity coefficients of cations in aqueous solutions. *Journal of the American Chemical Society*, **59**, 1675-1678.

Koopmans, L.H. (1981). *An Introduction to Contemporary Statistics*. Duxbury Press, Boston.

Kumada, K. (1987). *Chemistry of Soil Organic Matter*. Japan Scientific Societies Press, Elsevier, Amsterdam.

Langford, C.H. and Khan, T.R. (1975). Kinetics and equilibrium of binding of Fe^{3+} by a fulvic acid: a study by stopped flow methods. *Canadian Journal of Chemistry*, **53**, 2979-2984.

Lavigne, J.A., Langford, C.H. and Mak, M.K.S. (1987). Kinetic study of nickel(II) bound to a fulvic acid. *Analytical Chemistry*, **59**(21), 2616-2620.

Lehmann, R.G. and Harter, R.D. (1984). Assessment of copper-soil bond strength by desorption kinetics. *Soil Science Society of America Journal*, **48**, 769-772.

Leuenberger, B. and Schindler, P.W. (1986). Application of integral pK spectrometry to the titration curve of fulvic acid. *Analytical Chemistry*, **58**, 1471-1474.

Lindsay, W.L. (1979) *Chemical Equilibria in Soils*. Wiley, New York.

Low, M.J.D. (1960). Kinetics of chemisorption of gases on solids. *Chemical Reviews*, **60**, 267-271.

MacCarthy, P. and Rice, J.A. (1985). Spectroscopic methods (other than NMR) for determining functionality in humic substances. **In** *Humic Substances in Soil, Sediment and Water*, (edited by Aiken, G.R., McKnight, D.M., Wershaw, R.L. and MacCarthy, P.), Wiley-Interscience, New York, 527-559.

McLaren, R.G. and Crawford, D.V. (1973). Studies on copper. II. The specific adsorption of copper by soils. *Journal of Soil Science*, **24**, 443-452.

McLaren, R.G., Swift, R.S. and Williams, J.G. (1981). The adsorption of copper by soil materials at low equilibrium solution concentrations. *Journal of Soil Science*, **32**, 247-256.

Mak, M.K.S. and Langford. C.H. (1983). Kinetic analysis applied to aluminium citrate complexing. *Inorganica Chimica Acta*, **70**, 237-246.

Malcolm, R.L. (1985). Geochemistry of stream humic and fulvic substances. **In** *Humic Substances in Soil, Sediment and Water*, (edited by Aiken, G.R., McKnight, D.M., Wershaw, R.L. and MacCarthy, P.), Wiley, New York, 181-209.

Mantoura, R.F.C. and Riley, J.P. (1975) Use of gel filtration in the study of metal binding by humic acids and related compounds. *Analytica Chimica Acta*, **78**, 193-200.

Malcolm, R.L. (1989). Applications of solid-state ^{13}C NMR spectroscopy to geochemical studies of humic substances. **In** *Humic Substances II.* (edited by Hayes, M.H.B., MacCarthy, P., Malcolm, R.L. and Swift, R.S.), Wiley, Chichester, 339-372.

Mantoura, R.F.C. and Riley, J.P. (1975). The use of gel filtration in the study of metal binding by humic acids and related compounds. *Analytica Chimica Acta*, **78**, 193-200.

Marinsky, J.A. (1987). A two phase model for the interpretation of proton and metal ion interaction with charged polyelectrolyte gels and their linear analogs. **In** *Aquatic Surface Chemistry* (edited by W. Stumm), Wiley-Interscience, New York, 49-81.

Marinsky, J.A. (1989). Reply to a comment on 'A unified physicochemical description of the protonation and metal ion complexation equilibria of natural organic acids (humic and fulvic acids)'. *Environmental Science and Technology*, **23**, 747-748.

Marinsky, J.A. and Ephraim, J. (1986). A unified physicochemical description of the proton and metal ion complexation equilibria of natural organic acids. 1. Analysis of the influence of polyelectrolyte properties on protonation equilibria in ionic media: fundamental concepts. *Environmental Science and Technology*, **20**, 349-354.

Marinsky, J.A., Gupta, S. and Schindler, P. (1982). A unified physicochemical description of the equilibria encountered in humic acid gels. *Journal of Colloid and Interface Science*, **89**(2), 412-426.

Mathur, S.P. and Farnham, R.S. (1985). Geochemistry of humic substances in natural and cultivated peatlands. **In** *Humic Substances in Soil, Sediment and Water*, (edited by Aiken, G.R., McKnight, D.M., Wershaw, R.L. and MacCarthy, P.), Wiley-Interscience, New York, 53-85.

Merle, Y. and Marinsky, J.A. (1984). Gel speciation studies - I. The intrinsic dissociation constant of weakly acidic cation-exchange gels. *Talanta*, **31**(3), 199-204.

Midgley, D. (1976). Comparison of copper(II) ion selective electrodes for measurements at micromolar concentrations. *Analytica Chimica Acta*, **87**(1), 7-17.

Morawetz, H. (1975). *Macromolecules in Solution, Second Edition*, Wiley-Interscience, New York, 344-396.

Morgan, J.J. and Stone, A.T. (1985). Kinetics of chemical processes of importance in lacustrine environments. **In** *Chemical Processes in Lakes*, (edited by W. Stumm), Wiley-Interscience, New York, 389-426.

Murray, K. and Linder, P.W. (1983). Fulvic acids: structure and metal binding. I. A random molecular model. *Journal of Soil Science*, **34**, 511-523.

Murray, K. and Linder, P.W. (1984). Fulvic acids: structure and metal binding. II. Predominant metal binding sites. *Journal of Soil Science*, **35**, 217-222.

Nelder, J.A. and Mead, R. (1965). A simplex method for function minimization. *The Computer Journal*, **7**, 308-313.

Ninomiya, K. and Ferry, J.D. (1959). Phenomenological treatment of linear viscoelastic data. *Journal of Colloid Science*, **14**, 36-48.

Olson, D.L. and Shuman, M.S. (1983). Kinetic spectrum method for analysis of simultaneous, first order reactions and application to copper(II) dissociation from aquatic macromolecules. *Analytical Chemistry*, **55**, 1103-1107.

O'Melia, C.R. (1987). Particle-particle interactions. **In** *Aquatic Surface Chemistry*, (edited by W. Stumm), Wiley-Interscience, New York, 385-403.

Pankow, J.F. and Morgan, J.J. (1981). Kinetics for the aquatic environment. *Environmental Science and Technology*, **15**, 1155-1164.

Parsons, J.W. (1989). Hydrolytic degradations of humic substances. **In** *Humic Substances II.* (edited by Hayes, M.H.B., MacCarthy, P., Malcolm, R.L. and Swift, R.S.), Wiley, Chichester, 99-120.

Perdue, E.M. (1985). Acidic functional groups of humic substances. **In** *Humic Substances in Soil, Sediment and Water*, (edited by Aiken, G.R., McKnight, D.M., Wershaw, R.L. and MacCarthy, P.), Wiley-Interscience, New York, 493-526.

Perdue, E.M. (1989). Effects of humic substances on metal speciation. **In** *Aquatic Humic Substances*, (edited by Suffet, H. and MacCarthy, P.), American Chemical Society, Washington, 281-295.

Perdue, E.M. and Lytle, C.R. (1983b). Distribution model for binding of protons and metal ions by humic substances. *Environmental Science and Technology*, **17**, 654-660.

Perrin, D.D. (1979). *Stability constants of metal-ion complexes. Part B. Organic ligands.* IUPAC Chemical Data Series No.22, Pergamon Press, Oxford.

Plankey, B.J. and Patterson, H.H. (1987). Kinetics of aluminium-fulvic acid complexation in acidic waters. *Environmental Science and Technology*, **21**, 595-601.

Posner, A.M. (1964). Titration curves of humic acid. **In** *Proceedings of the 8th International Congress of Soil Science Part II.* Bucharest, Romania, 161-174.

Press, W.H., Flannery, B.P., Teukolsky, S.A. and Vetterling, W.T. (1986). *Numerical Recipes - the Art of Scientific Computing.* Cambridge University Press, Cambridge.

Purves, D. (1985). *Trace Element Contamination of the Environment (Revised Edition).* Elsevier, Amsterdam.

Rainville, D.P. and Weber, J.H. (1982). Complexing capacity of soil fulvic acid for Cu^{2+}, Cd^{2+}, Mn^{2+}, Ni^{2+} and Zn^{2+} measured by dialysis titration: a model based on soil fulvic aggregation. *Canadian Journal of Chemistry*, **60**, 1-5.

Randle, K. and Hartmann, E.H. (1987). Applications of the continuous flow stirred cell (CFSC) technique to adsorption of zinc, cadmium and mercury on humic acids. *Geoderma*, **40**, 281-296.

Rao, P.S.C., Davidson, J.M., Jessup, R.E. and Selim, H.M. (1979). Evaluation of conceptual models for describing nonequilibrium adsorption-desorption of pesticides during steady flow in soils. *Soil Science Society of America Journal*, **43**, 22-28.

Ratkowsky, D.A. (1983). *Nonlinear Regression Modeling. A Unified Practical Approach.* Marcel Dekker, New York, 135-151.

Ritchie, G.S.P. and Posner, A.M., (1982). The effect of pH and metal binding on the transport properties of humic acids. *Journal of Soil Science*, **33**, 233-247.

Saar, R.A. and Weber, J.H. (1979). Complexation of cadmium(II) with water and soil derived fulvic acids: effect of pH and fulvic acid concentration. *Canadian Journal of Chemistry*, **57**, 1263-1268.

Saar, R.A. and Weber, J.H. (1980). Comparison of spectrofluorometry and ion-selective electrode potentiometry for determination of complexes between fulvic acid and heavy-metal ions. *Analytical Chemistry*, **52**, 2095-2100.

Salim, R. and Cooksey, B.G. (1980). Kinetics of the adsorption of lead on river mud. *Plant and Soil*, **54**, 399-417.

Sanders, J.R. (1980). The use of adsorption equations to describe copper complexing by humified organic matter. *Journal of Soil Science*, **31**, 633-641.

Sanders, J.R. (1982). The effect of pH upon the copper and cupric ion concentrations in soil solutions. *Journal of Soil Science*, **33**, 679-689.

Schneider, S.H. (1989). *Global Warming*. Sierra Club, San Francisco.

Schnitzer, M. (1969). Reactions between fulvic acid, a soil humic compound and inorganic soil constituents. *Soil Science Society of America Proceedings*, **33**, 75-81.

Schnitzer, M. (1978). Humic substances: chemistry and reactions. **In** *Soil Organic Matter*, (edited by Schnitzer, M. and Khan, S.U.), Elsevier/North Holland, Amsterdam, 1-64.

Schnitzer, M. (1980). Effect of low pH on the chemical structure and reactions of humic substances. **In** *Effects of Acid Precipitation on Terrestrial Ecosystems*, (edited by Hutchinson, T.C. and Havas, M.), Plenum Press, New York, 203-222.

Schnitzer, M. (1985). Nature of nitrogen in humic substances. **In** *Humic Substances in Soil, Sediment and Water*, (edited by Aiken, G.R., McKnight, D.M., Wershaw, R.L. and MacCarthy, P.), Wiley-Interscience, New York, 303-325.

Schnitzer, M. and Hansen, E.H. (1970). Organo-metallic interactions in soils. **8.** An evaluation of methods for he determination of stability constants of metal-fulvic acids complexes. *Soil Science*, **109**, 333-340.

Schnitzer, M. and Khan, S.U. (1972). *Humic Substances in the Environment*, Marcel Dekker, New York.

Scraton, R.E. (1984). *BASIC Numerical Methods: an Introduction to Numerical Mathematics on a Microcomputer*. Edward Arnold, London.

Senesi, M., Griffith, S.M. and Schnitzer, M. (1977). Binding of Fe^{3+} by humic materials. *Geochimica et Cosmochimica Acta*, **41**, 969-976.

Shuman, M.S. and Michael, L.C. (1978). Application of the rotated disk electrode to measurement of copper complex dissociation rate constants in marine coastal samples. *Environmental Science and Technology*, **12**, 1069-1072.

Shuman, M.S. and Cromer, J.L. (1979). Copper association with aquatic fulvic and humic acids. Estimation of conditional formation constants with a titrimetric anodic stripping voltammetry procedure. *Environmental Science and Technology*, **13**, 543-545.

Shuman, M.S., Collins, B.J., Fitzgerald, P.J. and Olson, D.L. (1983). Distribution of stability constants and dissociation rate constants among binding sites on estuarine copper-organic complexes: rotated disk electrode studies and an affinity spectrum analysis of ion selective electrode and photometric data. **In** *Aquatic and Terrestrial Humic Materials* (edited by Christman, R.F. and Gjessing, E.T.), Ann Arbor, Michigan, 349-370.

Sikora, F.J. and Stevenson, F.J. (1988). Silver complexation by humic substances: conditional stability constants and nature of reactive sites. *Geoderma*, **42**, 353-363.

Sillen, L.G. and Martell, A.E. (1971). *Stability Constants of Metal-Ion Complexes. Supplement No. 1*, Chemical Society, London.

Sips, R. (1948). On the structure of a catalyst surface. *Journal of Chemical Physics*, **16**, 490-495.

Sparks, D.L. (1985). Kinetics of ionic reactions in clay minerals and soils. **In** *Advances in Agronomy, Volume 38*, Academic Press, 231-266.

Sposito, G. (1982). On the use of the Langmuir equation in the interpretation of 'adsorption' phenomena: II. The 'two surface' Langmuir equation. *Soil Science Society of America Journal*, **46**, 1147-1152.

Sposito, G. (1984). *The Surface Chemistry of Soils*. Oxford University Press, New York.

Sposito, G. (1986). Sorption of trace metals by humic materials in soils and natural waters. *CRC Critical Reviews in Environmental Control*, **16**(2), 193-228.

Sposito, G. and Holtzclaw, K.M. (1977). Titration studies on the polynuclear, polyacidic nature of fulvic acid extracted from sewage sludge - soil mixtures. *Soil Science Society of America Journal*, **41**, 330-336.

Sposito, G., Holtzclaw, K.M. and Keech, D.A. (1977). Proton binding in fulvic acid extracted from sewage sludge - soil mixtures. *Soil Science Society of America Journal*, **41**, 1119-1125.

Sposito, G., Holtzclaw, K.M. and LeVesque, C.S. (1979). Cupric ion complexation by fulvic acid extracted from sewage sludge - soil mixtures. *Soil Science Society of America Journal*, **43**, 1148-1155.

Steelink, C. (1985). Implications of elemental characteristics of humic substances. **In** *Humic Substances in Soil, Sediment and Water*, (edited by Aiken, G.R., McKnight, D.M., Wershaw, R.L. and MacCarthy, P.), Wiley-Interscience, New York, 457-476.

Steinberg, C. and Muenster, U. (1985). Geochemistry and ecological role of humic substances in lakewater. **In** *Humic Substances in Soil, Sediment and Water*, (edited by Aiken, G.R., McKnight, D.M., Wershaw, R.L. and MacCarthy, P.), Wiley, New York, 105-145.

Stevenson, F.J. (1982). *Humus Chemistry - Genesis, Composition, Reactions*. Wiley-Interscience, New York.

Stevenson, F.J. (1985). Geochemistry of soil humic substances. **In** *Humic Substances in Soil, Sediment and Water*, (edited by Aiken, G.R., McKnight, D.M., Wershaw, R.L. and MacCarthy, P.), Wiley-Interscience, New York, 13-52.

Stevenson, F.J. (1989). Reductive cleavage of humic substances. **In** *Humic Substances II*. (edited by Hayes, M.H.B., MacCarthy, P., Malcolm, R.L. and Swift, R.S.), Wiley, Chichester, 121-142.

Stevenson, F.J. and Ardakani, M.S. (1972). Organic matter reactions involving micronutrients in soils. In *Micronutrients in Agriculture*, (edited by Mortvedt, J.J., Giordano, P.M. and Lindsay, W.L.), Soil Science Society of America, Madison, 79-114.

Stevenson, F.J. and Fitch, A. (1986). Chemistry of complexation of metal ions with soil solution organics. In *Interactions of Soil Minerals with Natural Organics and Microbes*, SSSA Special Publication Number 17, (edited by Huang, P. and Schnitzer, M.), SSSA, Madison, 29-58.

Stevenson, F.J., Krastonav, S.A. and Ardakani, M.S. (1973). Formation constants of Cu(II) complexes with humic and fulvic acids. *Geoderma*, **9**, 129-141.

Susetyo, W., Dobbs, J.C., Carreira, L.A., Azarraga, L.V. and Grimm, D.M. (1990). Development of a statistical model for metal-humic interactions. *Analytical Chemistry*, **62**, 1215-1221.

Swift, R.S. (1989). Molecular weight, size, shape and charge characteristics of humic substances: some basic considerations. In *Humic Substances II.* (edited by Hayes, M.H.B., MacCarthy, P., Malcolm, R.L. and Swift, R.S.), Wiley, Chichester, 449-465.

Swift, R.S. and Posner, A.M. (1972). Autoxidation of humic acid under alkaline conditions. *Journal of Soil Science*, **23**, 381-393.

Tanford, C. (1961). *Physical Chemistry of Macromolecules*, Wiley, New York.

Teasdale, R.D. (1987). Copper-induced indefinite aggregation of humic substances: theoretical consequences for copper-binding behaviour. *Journal of Soil Science*, **38**, 433-442.

Thakur, A.K., Munson, P.J., Hunston, D.L. and Rodbard, D. (1980). Characterisation of ligand - binding systems by continuous affinity distributions of arbitrary shape. *Analytical Biochemistry*, **103**, 240-254.

Thurman, E.M. (1985) *Organic Geochemistry of Natural Waters*, Martinus Nijhoff/Dr. W. Junk Publishers, Dordrecht, The Netherlands.

Thurman, E.M. and Malcolm, R.L. (1983). Structural study of humic substances: new approaches and methods. In *Aquatic and Terrestrial Humic Materials*, (edited by Christman, R.F. and Gjessing, E.T.), Ann Arbor Science, Ann Arbor, Michigan, 1-23.

Tipping, E., Backes, C.A. and Hurley, M.A. (1988). The complexation of protons, aluminium and calcium by aquatic humic substances: a model incorporating binding-site heterogeneity and macroionic effects. *Water Research*, **22**, 597-611.

Turner, D.R., Varney, M.S., Whitfield, M., Mantoura, R.F.C. and Riley, J.P. (1986). Electrochemical studies of copper and lead complexation by fulvic acid. I. Potentiometric measurements and a critical comparison of metal binding models. *Geochimica et Cosmochimica Acta*, **50**, 289-297.

Tuschall, J.R.(Jr.) and Brezonik, P.L. (1983). Complexation of heavy metals by aquatic humus: a comparative study of five analytical methods. In *Aquatic and Terrestrial Humic Materials*, (edited by Christman, R.F. and Gjessing, E.T.), Ann Arbor Science, Ann Arbor, Michigan, 275-294.

Underdown, A.W., Langford, C.H. and Gamble, D.S. (1985). Light scattering studies of the relationship between cation binding and aggregation of a fulvic acid. *Environmental Science and Technology*, **19**, 132-136.

Van der Zee, S.E.A.T.M., Van Riemsdijk, W.H. and Van Grimsven, J.J.M. (1989). Extrapolation and interpolation by time scaling in systems with diffusion-controlled kinetics and first-order reaction rates. *Netherlands Journal of Agricultural Science*, **37**, 47-60.

van Genuchten, M.T. and Wierenga, P.J. (1976). Mass transfer studies in sorbing porous media. I. Analytical solutions. *Soil Science Society of America Journal*, **40**, 473-480.

Vogel, A.I. (1979). *A Textbook of Quantitative Inorganic Analysis Including Elementary Instrumental Analysis, 4th Edition.* (Revised by Bassett, J., Denney, R.C., Jeffery, G.H. and Mendham, J.). Longman, London.

Waite, T.D. and Morel, F.M.M. (1983). Characterisation of complexing agents in natural waters by copper(II)/copper(I) amperometry. *Analytical Chemistry*, **55**, 1268-1274.

Weast, R.C., Astle, M.J. and Beyer, W.H. (editors) (1983). *CRC Handbook of Chemistry and Physics*, 64th Edition, CRC Press, Boca Raton.

Weber, J.H. (1988). Binding and transport of metals by humic substances. **In** *Humic Substances and Their Role in the Environment*, (edited by Frimmel, F.H. and Christman, R.F.), Wiley-Interscience, New York, 165-178.

Wershaw, R.L. (1986). A new model for humic materials and their interactions with hydrophobic organic chemicals in soil-water or sediment-water systems. *Journal of Contaminant Hydrology*, **1**, 29-45.

Wershaw, R.L., Pinckney, D.J. and Booker, S.E. (1977). Chemical structure of humic acids - Part 1, a generalized structural model. *Journal of Research of the U.S. Geological Survey*, **5**, 565-569.

Wilkins, R.G. (1970). Mechanisms of ligand replacement in octahedral nickel(II) complexes. *Accounts of Chemical Research*, **3**, 408-416.

Willis, B.G., Woodruff, W.H., Frysinger, J.R., Margerum, D.W. and Pardue, H.L. (1970). Simultaneous kinetic determination of mixtures by on-line regression analysis. *Analytical Chemistry*, **42**, 1350-1355.

Wilson, D.E. and Kinney, P. (1977). Effects of polymeric charge variations on the protonation - metal ion equilibria of humic materials. *Limnology and Oceanography*, **22**, 281-289.

Wilson, M.A. (1989). Solid-state nuclear magnetic resonance spectroscopy of humic substances: basic concepts and techniques. **In** *Humic Substances II.* (edited by Hayes, M.H.B., MacCarthy, P., Malcolm, R.L. and Swift, R.S.), Wiley, Chichester, 309-338.

Wu, S-C. and Gschwend, P.M. (1986). Sorption kinetics of hydrophobic organic compounds to natural sediments and soils. *Environmental Science and Technology*, **20**, 717-725.

Zazoski, R.J. and Burau, R.G. (1978). A technique for studying the kinetics of adsorption in suspensions. *Soil Science Society of America Journal*, **42**, 372-374.

APPENDIX ONE

International Humic Substances Society: Procedure for Extraction of Standard and Reference Humic Substances from Soils.

The procedure is initiated using a sieved bulk soil sample (roots removed).

Step 1 *Acid Pretreatment*: Add 1 mol L^{-1} HCl to soil sample so that equilibrium pH is between 1 and 2 and final solution:dry soil ratio is 10 ml:1 g. Shake 1 hour.

Step 2 Separate supernatant from residue by settling and decantation or centrifugation.

Step 3 Slurry residue in c. 200 mL distilled water. Neutralise this slurry with 1 mol L^{-1} NaOH to pH 7.0; add *under* N_2 0.1 mol L^{-1} NaOH to a final extractant:residue ratio of 10:1.

Step 4 Extract suspension from Step 3 under N_2 with intermittent shaking for 12-16 hours. Allow alkaline suspension to settle overnight under N_2 and decant or centrifuge to isolate supernatant.

Step 5 Acidify supernatant with 6 mol L^{-1} HCl with constant stirring to pH 1.0. Let stand for 12-16 hours in cool conditions.

Step 6 Centrifuge and separate humic (solid) and fulvic (supernatant) fractions.

Step 7 *Humic acid treatment*: Slurry humic fraction in distilled water. Add KCl so that final KCl concentration is 0.3 mol L^{-1}. Add 0.3 mol L^{-1} KOH *under* N_2 until pH is 12.0. Centrifuge to remove suspended solids.

Step 8 Reprecipitate humic acid as in Step 5. Centrifuge and discard supernatant.

Step 9 Suspend humic acid in 0.1 mol L^{-1} HCl/0.3 mol L^{-1} HF solution in a *plastic* container. Shake 24 hours, room temperature. Centrifuge suspension and discard supernatant. Repeat this HCl/HF treatment once (24 hours shaking) and twice (48 hours shaking).

Step 10 Transfer humic acid to a Visking dialysis tube. Dialyze against distilled water to a negative Cl^- test with $AgNO_3$. Alternatively, test conductivity of solution outside dialysis tube.

Step 11 Shell-freeze humic acid in round bottomed flask(s) and freeze-dry.

Step 12 *Fulvic acid treatment*: Readjust pH of supernatant (from Step 6) to pH1 with 6 mol L^{-1} HCl. Pass this supernatant (degassed) through a column of XAD-8 resin at a $k'_{0.5R}$ of 7 (1.0 mL of resin per g of initial sample dry weight).

Step 13 Back-elute XAD-8 resin column with one column volume of 0.1 mol L^{-1} NaOH, followed by 2-3 column volumes of distilled water.

Step 14 Immediately acidify with 6 mol L^{-1} HCl to pH 1. Add HF to a final concentration of 0.3 mol L^{-1} HF. Solution volume should be sufficient to maintain fulvic acid solubility.

Step 15 Pass fulvic acid/HCl/HF solution through XAD-8 resin in *plastic* column (column volume should be 1/5 of sample volume; this yields $k'_{0.5R} \sim 2$). Rinse fulvic acid on resin with distilled water until eluate shows negative Cl^- test with $AgNO_3$.

Step 16 Back elute with 1 column volume of 0.1 mol L^{-1} NaOH followed by sufficient distilled water to remove most of the fulvic acid from the resin; collect alkaline fulvic acid solution under N_2. Pass alkaline fulvic acid solution through H^+-saturated cation exchange resin column (Bio-Rad AG-MP-50; capacity = 3 × Na^+ ions in solution on equivalent basis).

Step 17 Freeze-dry H^+-saturated fulvic acid after shell freezing in round bottomed flask(s). Redissolve fulvic acid in minimum volume of distilled water, shell freeze in round bottomed flask(s) and freeze-dry again.

GENERAL NOTE: Due to fluoride contamination, the whole fulvic acid fraction was redissolved at pH 1 in HCl (HF was omitted). The procedure was then continued from Step 15.

APPENDIX TWO

DETAILS OF THE SOIL USED FOR THE EXTRACTION OF SUMMIT HILL HUMIC ACID

1. *Soil Description*

Soil Series: Summit Soil

N.Z. Classification	Yellow Brown Earth
U.S. Taxonomy	Typic Dystrochept, fine loamy, mixed, mesic

Profile Description:

A_h	0 - 25 cm	Very dark grey (10YR 3/1) silt loam; friable; moderately developed nut structure; few small fragments of tuff; numerous roots;diffuse boundary.
B_w	25 - 40 cm	Yellowish brown (10YR 5/4) silt loam; friable; weakly developed nut structure; many very dark greyish brown (10YR 3/2) worm casts from above; diffuse boundary.
B/C	40 - 48 cm	Yellowish brown (10YR 5/4) silt loam; friable; massive; few fine and coarse distinct strong brown (7.5YR 5/6) mottles; few small fragments of tuff; sharp boundary.
R	48 - 137+ cm	Light olive brown (2.5Y 5/4) loamy sand; firm to very firm *in situ* but once broken the fragments are friable; massive; at top end of horizon few grey veins running horizontally with iron staining on edge.

2. *Depth of sample taken for extraction of humic acid*

0 - 20 cm

3. *Analytical data*

Horizon	pH	TOC	C/N	CEC	TEB	BS
		%		me%	me%	%
A_h (0-25 cm)	5.4	5.2	14	24.9	9.6	40

4. *Analytical characteristics of humic acid*

(i) Elemental composition (mean values on ash-free basis)

C = 49.5%, H = 5.01%, N = 4.67%, S = 0.59%.

Ash content = 1.15%.

(ii) Total acidity ($Ba(OH)_2$ adsorption)

TH = c. 4.5(±0.5) meq g^{-1}

NOTES: Summit soils have developed from loess parent material overlying basalt at an elevation above 270-300 m, where the mean annual rainfall ranges from 890-1140 mm. The soil moisture is at or above field capacity for 7 months (March-September) and below field capacity for 5 months (October to February) but seldom drops to wilting point. Climate is at the lower end of the humid class, and aspect has a marked effect on soil moisture, so that the soils on the north-facing slopes are drier than those facing south and approach the intergrade between yellow-grey and yellow-brown earths. The soils were probably formed under podocarp forest which was later destroyed by fire and replaced by silver tussock.

APPENDIX THREE

DETAILS OF THE SOIL USED FOR THE EXTRACTION OF **WAIMARI PEAT** HUMIC ACID

1. Soil Description

Soil Series: Waimari Peaty Loam

N.Z. Classification	Organic Soil
U.S. Taxonomy (O horizon)	Typic medihemist

Profile description

O	0 - 25 cm	Black (5Y 2/1) peaty loam; friable; strongly developed medium and fine granular structure; less peaty in lower 7 cm; wood fragments common; distinct boundary.
G1	23 - 42 cm	Dark grey (5Y 4.1) coarse sandy loam; many distinct diffuse yellowish brown (10YR 5/4) mottles; massive with very weak medium nutty structure; plastic; distinct boundary.
G2	42+ cm	Grey (N5) sandy loam; firm; massive.
C	on	Very wet grey (N5) sandy to loamy sand

Analytical Data

Horizon	pH	TOC %	C/N me%	CEC me%	TEB me%	BS %
O (0-25 cm)	5.0	n.a.	22	75.5	45.1	60

NOTES: This soil is formed on decomposed or partly decomposed plant residues which occur in low-lying areas where the ground water is high and there is little or no deposition of alluvium. The textures vary from peat to peaty loam, depending on the content of mineral matter. The depth of peat overlying the mineral soil also varies from 25 cm to 1.5 m.

APPENDIX FOUR

GW-BASIC program (written to run under MS-DOS) to convert binary datafiles from a Philips PU8700 spectrophotometer into ASCII. As written, the program produces (absorbance,time) data pairs spaced in approximately equal log(time) intervals.

```
10        KEY OFF
20        REM     program to convert PU8700 datafiles
30        CLS
35  '     __________ NB: screen 10 requires EGA ____________'
40        SCREEN 10
50        COLOR 1,0,0
60        LINE (1,1)-(630,340),1,B:LINE(100,140)-(530,180),1,B
70        LOCATE 7,22:PRINT "PU8700 BINARY RATE FILE CONVERTER"
80        COLOR 2,0,0:LOCATE 12,21:PRINT "INSERT DATA DISKETTE INTO DRIVE A:"
90        COLOR 1,0,0:LOCATE 17,26:PRINT "Press any key to continue"
100       CMD$=INKEY$
110       IF CMD$="" GOTO 100  ELSE GOTO 120
120       SCREEN 10
130       CLS
140       LINE (1,1)-(630,340),1,B
150       FILES"A:\*.dat"
180       COLOR 1,0,0
190       ON ERROR GOTO 2010
210       DIR$="A:\"
230       LINE (1,1)-(630,340),1,B
240       LOCATE 22,13:INPUT "    Enter code number for binary input file";FIL$
250       DIM D%(15000)
260       CLS
270       LINE (1,1)-(630,340),1,B
290       FF$="F:\SOSC\RATE\UTIL\RATE" + FIL$ + ".PRN"
300       OPEN "O",2,FF$
310       N$=DIR$+FIL$+".dat"
330       LOCATE 8,20:PRINT "Reading binary data from ";N$;" ..."
340       BLOAD N$,VARPTR(D%(0))
350       IF D%(232) <> 82 THEN CLS:LOCATE 10,20:PRINT "NOT A PU8700 RATE
          FILE!!":GOTO 860
360       NPTS=D%(9)*2+254
370       HIABS=LOG(100/(D%(NPTS)+(D%(NPTS+1)/1000)))/2.30258
380       LOABS=LOG(100/(D%(256)+(D%(257)/1000)))/2.30258
390       CT%=0:U$="#.####"
400       ZABS=.05:TMAX=12
410       NDATA=D%(202)+(D%(203)/1000)
420       DW=D%(208)+(D%(209)/1000)
430       TINT=INT(NDATA*DW)
440       NK=4
450       C%=256
460       L%=INT(LOG(NDATA))+1
470       LOCATE 8,20:PRINT "Calculating - please wait...                    "
480       DAT=D%(C%)+(D%(C%+1)/1000)
490       XABS=(LOG(100/DAT))/2.30258
500       TIME=0!
510       PRINT #2,USING "####.#";TIME;
520       PRINT #2,"     ";USING "#.######";XABS
530       ' _____________Conversion loop _____________________________
540       FOR I=0 TO L% STEP 9.000001E-02
550            C%=(2*(INT(EXP(2*I))))+256     'Ensures even C%
```

```
570           DAT=D%(C%)+(D%(C%+1)/1000)
580         ' ____Conversion of %transmittance to relative absorbance_______
590           IF DAT = 0 THEN XABS = 0:GOTO 630
600           XABS=(LOG(100/DAT))/2.30258
610           TIME=((C%-256)/2)*DW
620           IF TIME=TOLD THEN GOTO 720
630           TQ$=INKEY$
640           IF TQ$="Q" OR TQ$="q" THEN GOTO 780
650           IF XABS=0 THEN GOTO 730
660           PRINT #2,USING "####.#";TIME;
670           PRINT #2,"     ";USING "#.######";XABS
680           CT%=CT%+1
690           LOCATE 10,25:PRINT "    Time/s: ";USING "####.#";TIME
700           LOCATE 11,25:PRINT "Absorbance: ";USING "#.####";XABS
710           TOLD=TIME
720         NEXT I
730         DAT=D%(NPTS)+(D%(NPTS+1)/1000)
740         XABS=(LOG(100/DAT))/2.30258
750         TIME=INT(NDATA*DW)
760         PRINT #2,USING "####.#";TIME;
770         PRINT #2,"     ";USING "#.######";XABS
780         SOUND 16000,.1
790         LOCATE 8,13:PRINT "Length of dataset = ";TINT;" seconds"
800         LOCATE 11,13:PRINT SPACE$(50)
810         LOCATE 12,20:PRINT "Zero time absorbance = ";USING "#.####";LOABS
820         LOCATE 13,20:PRINT "  Maximum absorbance = ";USING "#.####";HIABS
830         LOCATE 5,6:PRINT (CT%+2);"Absorbance vs time results"
840         LOCATE 6,6:PRINT "Output to ASCII file ";FF$
850         COLOR 3,0,0
860         LOCATE 22,13:INPUT "                    Another dataset (yes or no) ";T2$
870         LOCATE 22,13:PRINT SPACE$(60)
880         IF LEFT$(T2$,1)="n"OR LEFT$(T2$,1)="N"THEN GOTO 900
890         CLEAR:GOTO 170
900         CLS:LINE(1,280)-(630,320),1,B
910         COLOR 1,0,0
920         FILES "F:\SOSC\RATE\UTIL\RATE*.PRN"
930         COLOR 3,0,0
940         LOCATE 22,13:INPUT "      Return to DOS (yes or no)                ";T4$
950         LOCATE 22,13:PRINT SPACE$(60)
960         IF LEFT$(T4$,1)="N" OR LEFT$(T4$,1)="n" GOTO 860
970         LOCATE 22,13:INPUT "                Sure?                          ";T5$
980         IF LEFT$(T5$,1)="Y" OR LEFT$(T5$,1)="y" THEN CLOSE:CLEAR:SYSTEM ELSE GOTO
            860
990         CLOSE
1000        END
2000        '_____________Error trapping routine_____________
2010        COLOR 2,0,0
2020        IF ERR=53 THEN CLS:SOUND 50,1:LOCATE 10,20:PRINT "No such file!":RESUME
            850
2030        IF ERR<>53 THEN CLS:LOCATE 10,20:PRINT "Hit any key to quit";ERR;ERL
2040        T$=INKEY$
2050        IF T$="" THEN GOTO 2040
2060        CLEAR:SYSTEM
```

APPENDIX FIVE

Representative driver module for regression programs (in this case for fitting metal-humate binding data to a three discrete site model). Program has following functions: input of experimental data and adjustable parameter estimates; generation of initial n-dimensional simplex (using subroutine CALC); invoking optimisation procedure (subroutine AMOEBA); and, output of results.

```
      PROGRAM MB3
C
C     Using AMOEBA routine (Numerical Recipes; Press et al) to fit
C     experimental data to nonlinear equations (VAX-11 Fortran)
C
      PARAMETER(NP=6,MP=7,IP=100,DFAC=0.11D+01,DTOL=1.0D-07)
C     Don't forget to alter NP,MP if equation in routine CALC changed
      REAL*8 P(MP,NP),X(NP),Y(MP),XO(IP),YO(IP),VT(IP),YC(IP),RES(IP),
     *  VZ,YBAR,FRNG,MSR,MSE,SSR,SST,SSE,RSQ,FRATIO,RBAR,ACFTOP,CL,
     *  SSLAG,ACF,C1,C2,C3,K1,K2,K3,CX,KMX,KMX2,PH,KOH1,KOH2,KOH3,KM2OH,
     *  KM2OH2,CH
      CHARACTER*10 CDAT,CTIM
      CHARACTER*36 DATFILE,INFILE,OUTFILE,PATH
      LOGICAL FEX
      COMMON CH,KOH1,KOH2,KOH3,KM2OH,KM2OH2
      WRITE(*,*) ' '
2     WRITE(*,*) '>>> Input filename?'
      READ(*,3) DATFILE
3     FORMAT(A)
      INQUIRE(FILE=DATFILE,EXIST=FEX)
      IF(.NOT.FEX) THEN
           WRITE(*,*) 'No such file as ',DATFILE
           GOTO 2
      ELSE
           OPEN(UNIT=3,FILE=DATFILE,STATUS='OLD')
      ENDIF
5     READ(UNIT=3,FMT=6,ERR=500,END=1000) INFILE
6     FORMAT(A)
      IF(INFILE.EQ.'END'.OR.INFILE.EQ.'end') GOTO 500
      PATH='[RATE.DATA]'//INFILE
      OPEN(UNIT=1,FILE=PATH,STATUS='OLD')
C     Input OH- & NO3- complexation parameters...
      READ(UNIT=3,FMT=*,ERR=500,END=500) CX,KMX,KMX2
      READ(UNIT=3,FMT=*,ERR=500,END=500) PH,KOH1,KOH2,KOH3,KM2OH,KM2OH2
      CH=10.**(-1.*PH)
C     Adjust maximum arraysize (IP) at line 2 if necessary
      IF (NPTS.GT.IP) PAUSE 'Too many points; type EXIT '
      DO 10 I=1,100
           READ(UNIT=1,FMT=*,END=15,ERR=20) XO(I),YO(I),VT(I)
C          Calc true [M] using [X-] & M(X)n stability constants
           XO(I)=XO(I)/(1. + KMX*CX + KMX2*(CX**2))
10    CONTINUE
15    NPTS=I-1
20    CLOSE(UNIT=1,STATUS='KEEP')
      YBAR=0.0
      DO 40 I=1,NPTS
           YBAR=YBAR+(YO(I)/NPTS)
40    CONTINUE
```

```
C           READ(UNIT=3,FMT=*,END=500,ERR=500) CL
            DO 80 J=1,NP
                 READ(UNIT=3,FMT=*,END=500,ERR=500) P(1,J)
80          CONTINUE
C           Generate initial simplex using first-guess points and expansion
C           by factor DFAC in each dimension (adjust DFAC if necessary).
            DO 100 I=2,NP+1
                 DO 90 J=1,NP
                      IF (J.EQ.(I-1)) THEN
                           P(I,J) = P(1,J)*DFAC
                      ELSE
                           P(I,J)=P(1,J)
                      ENDIF
90               CONTINUE
100         CONTINUE
            NDIM=NP
C           Find function values at simplex vertices
            DO 120 I=1,MP
                 DO 110 J=1,NP
                      X(J)=P(I,J)
110              CONTINUE
                 CALL CALC(XO,YO,VT,VZ,NPTS,IP,NP,X,YC,RES,Y(I),CL)
120         CONTINUE
            CALL AMOEBA(XO,YO,VT,VZ,NPTS,IP,P,Y,MP,NP,NDIM,DTOL,ITER,
       *     X,YC,RES,ILO,FRNG,CL)
            CALL DATE(CDAT)
            CALL TIME(CTIM)
C           Changing suffix of input file to name output file
            J=INDEX(INFILE,'.')
            K=INDEX(INFILE,'  ')
            OUTFILE=INFILE(1:J)//'M3U'
            OPEN(UNIT=2,FILE=OUTFILE,STATUS='UNKNOWN')
            WRITE(2,*) '=====================================',
       *     '====================================='
            WRITE(2,*) '_'
            WRITE(2,'(1X,A,A,A,I2,A)')'*** Input_file was ',INFILE(1:K),
       *     'containing ',NPTS,' data ***'
            WRITE(2,'(1X,I1,A,I1,A)') (NP/2),' site (',NP,
       *     ' parameter) binding model: accounts for OH- & NO3- complexation'
            WRITE(2,'(1X,A,2X,A,2X,A)') 'A.W.Rate ',CDAT,CTIM
            IF(ITER.GE.500) THEN
                 WRITE(2,'(1X,A)')'MAXIMUM_ITERATIONS (500) EXCEEEDED'
            ELSE
                 WRITE(2,'(1X,A,I3)') 'Iterations: ',ITER
            ENDIF
            WRITE(2,'(1X,A,E14.6)') 'Convergence test = ',FRNG
            WRITE(2,'(1X,A)') '_'
C           WRITE(2,'(1X,A,E12.4)') 'Fixed_LT = ',CL
            DO 150 J=1,NP
                 WRITE(2,140) 'log P_(',J,') = ',P(ILO,J),
       *          ';     P_(',J,') = ',(10.**P(ILO,J))
140              FORMAT(1X,A,I1,A,F10.5,A,I1,A,E12.6)
              X(J)=P(ILO,J)
150         CONTINUE
            SST=0.0D+00
            SSE=0.0D+00
            K1=1.0D+01**X(2)
            K2=1.0D+01**X(4)
            K3=1.0D+01**X(6)
C           Recalculation of SSE(unweighted) ...
            DO 155 I=1,NPTS
                 C1=(10.**X(1))*(VZ/VT(I))
                 C2=(10.**X(3))*(VZ/VT(I))
                 C3=(10.**X(5))*(VZ/VT(I))
                 YC(I)= C1*K1*XO(I)/(1.0D+00 + K1*XO(I))
       *       + C2*K2*XO(I)/(1.0D+00 + K2*XO(I))
       *       + C3*K3*XO(I)/(1.0D+00 + K3*XO(I))
       *       + KOH1*XO(I)/CH + KOH2*XO(I)/(CH**2) + KOH3*XO(I)/(CH**3)
```

```
     *       + KM2OH*(XO(I)**2)/CH + KM2OH2*(XO(I)**2)/(CH**2)
                 RES(I)=YO(I)-YC(I)
                 SSE=SSE+(RES(I)**2)
155          CONTINUE
             RBAR=0.0D+00
             DO 160 I=1,NPTS
                 SST=SST+((YO(I)-YBAR)**2)
                 RBAR=RBAR+(RES(I)/NPTS)
160          CONTINUE
             SSR=SST-SSE
             MSE=SSE/(NPTS-NP)
             MSR=SSR/(NP-1)
             FRATIO=MSR/MSE
             RSQ=1.0D+02*(1.0D+00-(SSE/SSR))
             WRITE (2,170) 'Residual sum of squares (SSE) =',Y(ILO)
170          FORMAT(1X,A,1X,E14.6)
             ACFTOP=0.0D+00
             SSLAG=0.0D+00
             DO 175 I=1,NPTS
                 IF(I.GE.2) THEN
                     ACFTOP=ACFTOP+((RES(I-1)-RBAR)*(RES(I)-RBAR))
                     SSLAG=SSLAG+((RES(I)-RBAR)**2)
                 ELSE
                     SSLAG=SSLAG+((RES(I)-RBAR)**2)
              ENDIF
175          CONTINUE
             ACF=ACFTOP/SSLAG
             WRITE(2,'(1X,A)') ' '
             WRITE(2,180) 'X(obs)','Y(obs)','Y(calc)','Residual'
180          FORMAT(5X,A,8X,A,8X,A,7X,A)
             WRITE(2,*) '-----------------------------------',
     *       '--------------------'
             DO 200 I=1,NPTS
                 WRITE(2,190) XO(I),YO(I),YC(I),RES(I)
190              FORMAT(4(E14.6))
200          CONTINUE
             WRITE(2,*) '_'
             WRITE(2,*) '*** ANALYSIS_OF_VARIANCE ***'
             WRITE(2,220) '  SOV_      |','DF','SS','MS','F'
220          FORMAT(1X,A,6X,A,10X,A,14X,A,14X,A)
             WRITE(2,*) '----------|------------------------',
     *       '-----------------------------------_'
             WRITE(2,230) 'Regression_|',(NP-1),SSR,MSR,FRATIO
230          FORMAT(1X,A,5X,I3,5X,2(E14.6),F14.2)
             WRITE(2,240) 'Error_     |',(NPTS-NP),SSE,MSE
240          FORMAT(1X,A,5X,I3,5X,2(E14.6))
             WRITE(2,250) 'Total_     |',(NPTS-1),SST
250          FORMAT(1X,A,5X,I3,5X,E14.6)
             IF(RSQ.LE.0..OR.RSQ.GT.100.) THEN
                 WRITE(2,'(1X,A,A)')'NB!_Error sum of squares exceeds ',
     *           'sum of squares for regression'
             ELSE
                 WRITE(2,'(1X,A,1X,F7.3,1X,A)') 'R_squared =',RSQ,'%'
             ENDIF
             WRITE(2,'(1X,A,1X,F7.3)') 'Residual_autocorrelation (lag 1) =',ACF
             WRITE(2,*) '=====================================',
     *       '=====================================_'
             WRITE(*,490) '>>> Find results in file ',OUTFILE
490          FORMAT(1X,A,1X,A)
500          CLOSE(UNIT=2,STATUS='KEEP')
             IF (INFILE.EQ.'END'.OR.INFILE.EQ.'end') THEN
                 GOTO 1000
             ELSE
                 GOTO 5
             ENDIF
1000         CLOSE(UNIT=3,STATUS='KEEP')
             END
```

APPENDIX SIX

FORTRAN module in the form of a subroutine (AMOEBA) incorporating the multidimensional simplex optimisation method of Nelder and Mead (1965), adapted from Press *et al.*, (1986). This module is called by a driver routine (Appendix Five) which inputs experimental data and estimates of model parameters. The subroutine CALC formulates the modelling equation and calculates a residual sum of squares which is minimised by subroutine AMOEBA.

```
      SUBROUTINE AMOEBA(XO,YO,VT,VZ,NPTS,IP,P,Y,MP,NP,NDIM,DTOL,ITER,
     *  X,YC,RES,ILO,FRNG,CL)
      PARAMETER (NMAX=10,ALPHA=1.0D+00,BETA=0.5D+00,GAMMA=2.0D+00,
     *  ITMAX=500)
C     NMAX is max expected no. of dimensions, ALPHA is reflecion factor,
C     BETA is contraction factor, GAMMA is expansion factor
      INTEGER NPTS,MPTS,IP,MP,NP,NDIM,ITER,ILO,IHI,INHI,I,J
      REAL*8 P(MP,NP),Y(MP),PR(NMAX),PRR(NMAX),PBAR(NMAX),X(NP),
     *  XO(IP),YO(IP),VT(IP),YC(IP),RES(IP),FRNG,VZ,CL,YPR,YPRR,
     *  CH,KOH1,KOH2,KOH3,KM2OH,KM2OH2
      COMMON CH,KOH1,KOH2,KOH3,KM2OH,KM2OH2
      MPTS=NDIM+1
      ITER=0
10    ILO=1
C     Determine highest (worst), next-highest and lowest (best) points
      IF(Y(1).GT.Y(2))THEN
            IHI=1
            INHI=2
      ELSE
            IHI=2
            INHI=1
      ENDIF
      DO 80 I=1,MPTS
            IF(Y(I).LT.Y(ILO)) ILO=I
            IF(Y(I).GT.Y(IHI))THEN
                  INHI=IHI
                  IHI=I
            ELSE IF(Y(I).GT.Y(INHI))THEN
                  IF(I.NE.IHI) INHI=I
            ENDIF
80    CONTINUE
C     Convergence test based on fractional range of function values at
C     simplex vertices
      FRNG=2.0D+00*DABS(Y(IHI)-Y(ILO))/(DABS(Y(IHI))+DABS(Y(ILO)))
      IF (FRNG.LT.DTOL) RETURN
      IF(ITER.GE.ITMAX) RETURN
      ITER=ITER+1
C     Begin a new iteration
      DO 120 J=1,NDIM
            PBAR(J)=0.0D+00
120   CONTINUE
C     Find 'centroid'; vector average of all points except highest
C     (worst); transformations involve high point and centroid
      DO 140 I=1,MPTS
            IF(I.NE.IHI)THEN
      DO 130 J=1,NDIM
            PBAR(J)=PBAR(J)+P(I,J)
130               CONTINUE
            ENDIF
140   CONTINUE
C     Reflect simplex from high point through centroid
      DO 150 J=1,NDIM
```

```
            PBAR(J)=PBAR(J)/NDIM
            PR(J)=(1.0D+00+ALPHA)*PBAR(J)-ALPHA*P(IHI,J)
150         CONTINUE
            CALL CALC(XO,YO,VT,VZ,NPTS,IP,NMAX,PR,YC,RES,YPR,CL)
C           Evaluate reflected point; if better extrapolate by factor gamma
            IF(YPR.LE.Y(ILO))THEN
                  DO 160 J=1,NDIM
                        PRR(J)=GAMMA*PR(J)+(1.0D+00-GAMMA)*PBAR(J)
160               CONTINUE
C           Check function value after extrapolation...
                  CALL CALC(XO,YO,VT,VZ,NPTS,IP,NMAX,PRR,YC,RES,YPRR,CL)
C           ...if it's better than high point, do a swap
                  IF(YPRR.LT.Y(ILO))THEN
                        DO 170 J=1,NDIM
                              P(IHI,J)=PRR(J)
170                     CONTINUE
                        Y(IHI)=YPRR
C           If extrapolated point is worse, use the first reflected point
                  ELSE
                        DO 180 J=1,NDIM
                              P(IHI,J)=PR(J)
180                     CONTINUE
                  Y(IHI)=YPR
                  ENDIF
C           Compare 1st reflected point and second-worst
            ELSE IF(YPR.GE.Y(INHI))THEN
C           If 1st reflected point better than high point then swap
                  IF(YPR.LT.Y(IHI))THEN
                        DO 190 J=1,NDIM
                              P(IHI,J)=PR(J)
190                     CONTINUE
                        Y(IHI)=YPR
                  ENDIF
C           Look for intermediate lower point by contracting simplex along
C           one dimension...
                  DO 210 J=1,NDIM
                        PRR(J)=BETA*P(IHI,J)+(1.0D+00-BETA)*PBAR(J)
210               CONTINUE
C           Evaluate function after contraction
                  CALL CALC(XO,YO,VT,VZ,NPTS,IP,NMAX,PRR,YC,RES,YPRR,CL)
C           If contracted point better than high point do a swap
                  IF(YPRR.LT.Y(IHI))THEN
                        DO 220 J=1,NDIM
                              P(IHI,J)=PRR(J)
220                     CONTINUE
                        Y(IHI)=YPRR
                  ELSE
C           Contraction around lowest (best) point
                        DO 240 I=1,MPTS
                              IF(I.NE.ILO)THEN
                                    DO 230 J=1,NDIM
                                          PR(J)=0.5D+00*(P(I,J)+P(ILO,J))
                                          P(I,J)=PR(J)
230                                 CONTINUE
C           Evaluate function after contraction
                                    CALL CALC(XO,YO,VT,VZ,NPTS,IP,NMAX,X,YC,RES,Y(I),CL)
                              ENDIF
240                     CONTINUE
                  ENDIF
            ELSE
C           Original reflection has given a middling point; replace old high point
                  DO 250 J=1,NDIM
                        P(IHI,J)=PR(J)
250               CONTINUE
                  Y(IHI)=YPR
            ENDIF
C           Go back to start and test for convergence
            GO TO 10
            END
```

APPENDIX SEVEN

Representative subroutine for formulating a model with an analytical solution (in this case, a three discrete site binding model) and calculating the residual sum of squares to be minimised using the AMOEBA subroutine in Appendix Six.

```
      SUBROUTINE CALC(XO,YO,VT,VZ,NPTS,IP,NMAX,X,YC,RES,Z,CL)
      REAL*8 X(NMAX),XO(IP),YO(IP),VT(IP),YC(IP),RES(IP),CL,C1,C2,C3,
     *  K1,K2,K3,Z,VZ,CH,KOH1,KOH2,KOH3,KM2OH,KM2OH2
      COMMON CH,KOH1,KOH2,KOH3,KM2OH,KM2OH2
C     X contains altering values of parameters, XO the independent
C     variable, YO the experimental values, YC the calculated values,
C     RES the residuals and Z is the sums of squares of residuals
      Z=0.0D+00
      K1=1.0D+01**X(2)
      K2=1.0D+01**X(4)
      K3=1.0D+01**X(6)
C     Alter this equation where necessary, but don't forget to alter
C     the other relevant parameters in the main program, e.g. NP, MP
      DO 100 I=1,NPTS
           C1=(10.**X(1))*(VZ/VT(I))
           C2=(10.**X(3))*(VZ/VT(I))
           C3=(10.**X(5))*(VZ/VT(I))
           YC(I)= C1*K1*XO(I)/(1.0D+00 + K1*XO(I))
     *     + C2*K2*XO(I)/(1.0D+00 + K2*XO(I))
     *     + C3*K3*XO(I)/(1.0D+00 + K3*XO(I))
     *     + KOH1*XO(I)/CH + KOH2*XO(I)/(CH**2) + KOH3*XO(I)/(CH**3)
     *     + KM2OH*(XO(I)**2)/CH + KM2OH2*(XO(I)**2)/(CH**2)
           RES(I)=YO(I)-YC(I)
C     Can apply weighting factor to Z, eg. 1/YC(I)
           Z=Z+(RES(I)**2)
100   CONTINUE
      RETURN
      END
```

APPENDIX EIGHT

Representative subroutine for formulating a model requiring a Newton-Raphson iterative solution (in this case, a three discrete site binding model rearranged to solve for [M]) and calculating the residual sum of squares to be minimised using the AMOEBA subroutine in Appendix Six. The Newton-Raphson algorithm used is adapted from Press *et al.* (1986).

```
      SUBROUTINE CALC(XO,YO,VT,VZ,NPTS,IP,NMAX,X,YC,RES,Z,CL)
      INTEGER I,NPTS,IP,NMAX
      REAL*8 X(NMAX),XO(IP),YO(IP),VT(IP),YC(IP),RES(IP),
     *  X1,X2,YEST,Z,Q,VZ
C     X contains altering values of parameters, XO the independent
C     variable, YO the experimental values, YC the calculated values,
C     RES the residuals and Z is the sums of squares of residuals
      Z=0.0D+00
C     Logical bounds (X1,X2) for [M] are (0, [M](total))
      X1=0.0D+00
      DO 100 I=1,NPTS
           X2=XO(I) + (1.0D+01**YO(I))
           YEST = (1.0D+01**YO(I))
           CALL NEWTON(XO,VT,VZ,IP,YEST,X1,X2,I,NMAX,X,Q)
           YC(I)=DLOG10(YEST)
           RES(I)=YO(I)-YC(I)
C          _____NB: No weighting factor applied to Z_____
           Z=Z+(RES(I)**2)
100   CONTINUE
      RETURN
      END

      SUBROUTINE NEWTON(XO,VT,VZ,IP,YEST,X1,X2,I,NMAX,X,Q)
      INTEGER I,NMAX,IP,J,K
      REAL*8 XO(IP),VT(IP),VZ,X1,X2,X(NMAX),YEST,F,FL,FH,DF,XL,XH,
     *  SWAP,DX,DXOLD,TEMP,Q
C     _____Polynomial solution by bisection/Newton-Raphson_____
      PARAMETER (MAXIT=100,XACC=1.0D-06)
C     X1, X2 are approximate logical bounds for root
      K=0
      CALL FUNCD(XO,VT,VZ,IP,X1,FL,DF,X,NMAX,I,Q)
10    CALL FUNCD(XO,VT,VZ,IP,X2,FH,DF,X,NMAX,I,Q)
C     IF(FL*FH.GE.0.0D+00) PAUSE 'Root must be bracketed'
C     Orient the search so that f(XL) < 0
      IF(FL.LT.0.0D+00)THEN
           XL=X1
           XH=X2
      ELSE
           XH=X1
           XL=X2
           SWAP=FL
           FL=FH
           FH=SWAP
      ENDIF
      DXOLD=DABS(X2-X1)
      DX=DXOLD
      CALL FUNCD(XO,VT,VZ,IP,YEST,F,DF,X,NMAX,I,Q)
C     Initial Newton step
```

```
      DX=F/DF
      TEMP=YEST
      YEST=YEST-DX
      IF(TEMP.EQ.YEST)RETURN
      DO 110 J=1,MAXIT
C           Check whether Newton is (i) out of bounds or
C           (ii) not decreasing fast enough
            IF(((YEST-XH)*DF-F)*((YEST-XL)*DF-F).GE.0.0D+00
     *       .OR. DABS(2.0D+00*F).GT.DABS(DXOLD*DF) ) THEN
C           Bisection step necessary and implemented
                DXOLD=DX
                DX=0.5D+00*(XH-XL)
                YEST=XL+DX
                IF(XL.EQ.YEST)RETURN
            ELSE
C           Newton step acceptable and implemented
                DXOLD=DX
                DX=F/DF
                TEMP=YEST
                YEST=YEST-DX
                IF(TEMP.EQ.YEST)RETURN
            ENDIF
C     Test for convergence
            IF(DABS(DX).LT.XACC) RETURN
            CALL FUNCD(XO,VT,VZ,IP,YEST,F,DF,X,NMAX,I,Q)
            IF(F.LT.0.0D+00) THEN
                XL=YEST
                FL=F
            ELSE
                XH=YEST
                FH=F
            ENDIF
110   CONTINUE
      PAUSE 'NEWTON exceeding maximum (100) iterations'
      RETURN
      END

      SUBROUTINE FUNCD(XO,VT,VZ,IP,YEST,F,DF,X,NMAX,I,Q)
C     Calculates f([M]) and f'([M]) for rearranged binding model which
C     is in form f([M])=0
      INTEGER IP,NMAX,I
      REAL*8 XO(IP),VT(IP),VZ,YEST,F,DF,X(NMAX),C1,C2,C3,K1,K2,K3,A,B,C,D
C     Three-site binding model rearranged to cubic in [M]
C     Defining conventional symbols
      C1=(10.**X(1))*(VZ/VT(I))
      C2=(10.**X(3))*(VZ/VT(I))
      C3=(10.**X(5))*(VZ/VT(I))
      K1=1.0D+01**X(2)
      K2=1.0D+01**X(4)
      K3=1.0D+01**X(6)
C     Formulating cubic function
      A = XO(I)
      B = (XO(I)*(K1+K2+K3)) - (C1*K1 + C2*K2 + C3*K3)
      C = K1*K2*(XO(I)-(C1+C2))
     *  + K1*K3*(XO(I)-(C1+C3))
     *  + K2*K3*(XO(I)-(C2+C3))
      D = K1*K2*K3*(XO(I)-(C1+C2+C3))
      F = A + B*YEST + C*(YEST**2) + D*(YEST**3)
      DF = B + 2*C*YEST + 3*D*(YEST**2)
10    RETURN
      END
```

APPENDIX NINE

Representative subroutine for formulating a model requiring iterative solution of an integral (in this case, a kinetic model involving formation of a common product from a mixture of complexes having a continuous lognormal distribution of first-order rate constants) and calculating a residual sum of squares to be minimised using the AMOEBA subroutine in Appendix Six. Integral solution is by Romberg integration, using adaptations of routines presented by Press *et al.* (1986).

```
      SUBROUTINE CALC(XO,YO,YF,NP,IP,XX,YC,RES,NPTS,ZW,K)
      REAL*8 XX(NP),XO(IP),YO(IP),YC(IP),RES(IP),YF,A,B,SS,ZW,K(NP)
C     XX contains altering values of parameters, XO the independent
C     variable, YO the experimental values, YC the calculated values,
C     RES the residuals and ZW the weighted residual sum of squares
      ZW=0.0D+00
      A=XX(2)-(4.*XX(3))
      B=XX(2)+(4.*XX(3))
      DO 100 I=1,NPTS
            IF(XO(I).GT.0.01) THEN
                  CALL QROMB(A,B,XX,I,IP,XO,NP,SS)
                  YC(I) = YF + (0.39894228D+00*XX(1)/XX(3))*SS
            ELSE
                  YC(I)=YF
            ENDIF
            RES(I) = YO(I)-YC(I)
C           Apply weighting factor to ZW if required
C            (eg. divide by YC(I))
            ZW=ZW+(RES(I)**2)
100   CONTINUE
      RETURN
      END

      SUBROUTINE QROMB(A,B,XX,I,IP,XO,NP,SS)
      PARAMETER(EPS=1.E-6,JMAX=20,JMAXP=JMAX+1,K=5,KM=4)
      REAL*8 S(JMAXP),H(JMAXP),A,B,XX(NP),SS,DSS,XO(IP)
      H(1)=1.
      DO 11 J=1,JMAX
            CALL TRAPZD(A,B,S(J),J,XX,I,IP,XO,NP)
            IF (J.GE.K) THEN
                  L=J-KM
                  CALL POLINT(H(L),S(L),K,0.,SS,DSS)
                  IF (DABS(DSS).LT.EPS*DABS(SS)) RETURN
            ENDIF
            S(J+1)=S(J)
            H(J+1)=0.25*H(J)
11    CONTINUE
      PAUSE 'Too many QROMB steps.'
      END

      SUBROUTINE TRAPZD(A,B,S,N,XX,I,IP,XO,NP)
      REAL*8 A,B,S,XX(NP),FA,FB,FX,TNM,DEL,X,SUM,XO(IP)
C     Generation of successive approximations to integral by halving
C     trapezoid width at each cycle
      IF (N.EQ.1) THEN
            CALL KGAUSS(A,I,IP,XX,XO,NP,FA)
            CALL KGAUSS(B,I,IP,XX,XO,NP,FB)
            S=0.5*(B-A)*(FA+FB)
            IT=1
```

```
      ELSE
            TNM=IT
            DEL=(B-A)/TNM
            X=A+0.5*DEL
            SUM=0.
            DO 11 J=1,IT
                  CALL KGAUSS(X,I,IP,XX,XO,NP,FX)
                  SUM=SUM+FX
                  X=X+DEL
11          CONTINUE
            S=0.5*(S+(B-A)*SUM/TNM)
            IT=2*IT
      ENDIF
      RETURN
      END

      SUBROUTINE POLINT(XA,YA,N,X,Y,DY)
      PARAMETER (NMAX=10)
      REAL*8 XA(N),YA(N),C(NMAX),D(NMAX),X,Y,DY,DIF,DIFT,W,HO,HP,DEN
C     Polynomial fitting of successive approximations to integral for
C     extrapolation to zero trapezoid width
      NS=1
      DIF=DABS(X-XA(1))
      DO 11 I=1,N
            DIFT=DABS(X-XA(I))
            IF (DIFT.LT.DIF) THEN
                  NS=I
                  DIF=DIFT
            ENDIF
            C(I)=YA(I)
            D(I)=YA(I)
11    CONTINUE
      Y=YA(NS)
      NS=NS-1
      DO 13 M=1,N-1
            DO 12 I=1,N-M
                  HO=XA(I)-X
                  HP=XA(I+M)-X
                  W=C(I+1)-D(I)
                  DEN=HO-HP
                  IF(DEN.EQ.0.)PAUSE 'Pause in routine POLINT'
                  DEN=W/DEN
                  D(I)=HP*DEN
                  C(I)=HO*DEN
12          CONTINUE
            IF (2*NS.LT.N-M)THEN
                  DY=C(NS+1)
            ELSE
                  DY=D(NS)
                  NS=NS-1
            ENDIF
            Y=Y+DY
13    CONTINUE
      RETURN
      END

      SUBROUTINE KGAUSS(K,I,IP,XX,XO,NP,ANS)
      REAL*8 K,ANS,XX(NP),XO(IP)
C     Formulation of lognormal equation to be integrated
      ANS = DEXP(-0.5*((K-XX(2))/XX(3))**2)
     *      * (1. - DEXP(-1.*(DEXP(K)*XO(I))))
      RETURN
      END
```

APPENDIX TEN

Data derived from spectrophotometric observation of PAR-induced Cu^{2+}-WPNa complex dissociation, 20°C; 90 minute experiments only. $A_b = (A_{PAR} + A_{CuHumate})$; A_{PAR}, $A_{CuHumate}$ and A_∞ defined in Section 7.3.2; RT=Cu^{2+}-WPNa reaction time before PAR-induced dissociation.

1. [WPNa]=0.05gL^{-1}; Cu_T=7.87μmolL^{-1}; pH=6.0; [$NaNO_3$]=0.1molL^{-1}; RT=24h; A_b=0.458; A_∞=0.775.

Time /s	CuPAR Absorbance (510nm)	Standard deviation (n=4)
0.0	0.658	0.008
0.8	0.661	0.008
1.6	0.663	0.008
2.4	0.665	0.008
3.2	0.666	0.008
4.0	0.668	0.008
4.8	0.669	0.008
5.6	0.670	0.008
6.4	0.671	0.008
8.0	0.673	0.008
9.6	0.675	0.008
11.2	0.677	0.008
13.6	0.679	0.008
16.8	0.681	0.008
20.0	0.683	0.008
24.0	0.685	0.008
28.8	0.687	0.007
34.4	0.689	0.008
41.6	0.691	0.007
49.6	0.694	0.007
60.0	0.696	0.007
72.0	0.698	0.007
85.6	0.700	0.007
103.2	0.702	0.007
123.2	0.705	0.007
147.2	0.707	0.008
176.8	0.709	0.008
212.0	0.711	0.008
253.6	0.713	0.008
303.2	0.715	0.008
363.2	0.717	0.007
435.2	0.719	0.007
520.8	0.721	0.007
624.0	0.723	0.007
747.2	0.725	0.007
894.4	0.726	0.007
1071.2	0.728	0.007
1282.4	0.729	0.007
1535.2	0.731	0.007
1838.4	0.732	0.007
2200.8	0.734	0.007
2635.2	0.735	0.007
3155.2	0.737	0.007
3777.6	0.738	0.007
4522.4	0.739	0.007
5400.0	0.740	0.007

2. [WPNa]=0.025gL^{-1}; Cu_T=7.87μmolL^{-1}; pH=6.0; [$NaNO_3$]=0.1molL^{-1}; RT=24h; A_b=0.393; A_∞=0.709.

Time /s	CuPAR Absorbance (510nm)	Standard deviation (n=3)
0.0	0.637	0.001
0.8	0.640	0.001
1.6	0.642	0.001
2.4	0.644	0.001
3.2	0.645	0.001
4.0	0.647	0.001
4.8	0.648	0.001
5.6	0.649	0.001
6.4	0.650	0.001
8.0	0.652	0.001
9.6	0.654	0.001
11.2	0.655	0.001
13.6	0.657	0.001
16.8	0.659	0.002
20.0	0.661	0.002
24.0	0.663	0.002
28.8	0.664	0.002
34.4	0.666	0.002
41.6	0.668	0.002
49.6	0.670	0.002
60.0	0.672	0.002
72.0	0.673	0.002
85.6	0.675	0.002
103.2	0.676	0.002
123.2	0.678	0.002
147.2	0.679	0.002
176.8	0.681	0.002
212.0	0.682	0.002
253.6	0.683	0.002
303.2	0.684	0.003
363.2	0.685	0.003
435.2	0.687	0.003
520.8	0.687	0.003
624.0	0.688	0.003
747.2	0.689	0.003
894.4	0.689	0.003
1071.2	0.690	0.003
1282.4	0.691	0.004
1535.2	0.691	0.004
1838.4	0.692	0.004
2200.8	0.692	0.004
2635.2	0.692	0.004
3155.2	0.692	0.004
3777.6	0.693	0.004
4522.4	0.693	0.004
5400.0	0.693	0.005

3. [WPNa]=0.10gL^{-1}; Cu_T=7.87μmolL^{-1}; pH=6.0; [$NaNO_3$]=0.1molL^{-1}; RT=24h; A_b=0.593; A_∞=0.919.

Time /s	CuPAR Absorbance (510nm)	Standard deviation (n=5)
0.0	0.764	0.014
0.8	0.766	0.014
1.6	0.769	0.014
2.4	0.771	0.014
3.2	0.772	0.014
4.0	0.774	0.014
4.8	0.775	0.014
5.6	0.777	0.014
6.4	0.778	0.014
8.0	0.780	0.014
9.6	0.782	0.014
11.2	0.783	0.014
13.6	0.786	0.014
16.8	0.788	0.014
20.0	0.790	0.014
24.0	0.793	0.014
28.8	0.795	0.014
34.4	0.798	0.014
41.6	0.800	0.014
49.6	0.803	0.014
60.0	0.806	0.014
72.0	0.808	0.014
85.6	0.811	0.014
103.2	0.814	0.014
123.2	0.816	0.014
147.2	0.819	0.014
176.8	0.822	0.014
212.0	0.825	0.014
253.6	0.828	0.014
303.2	0.830	0.014
363.2	0.833	0.014
435.2	0.836	0.013
520.8	0.839	0.013
624.0	0.842	0.013
747.2	0.845	0.013
894.4	0.847	0.013
1071.2	0.850	0.013
1282.4	0.853	0.013
1535.2	0.855	0.013
1838.4	0.858	0.013
2200.8	0.860	0.012
2635.2	0.863	0.012
3155.2	0.865	0.012
3777.6	0.868	0.012
4522.4	0.870	0.012
5400.0	0.872	0.012

4. [WPNa]=0.05gL^{-1}; Cu_T=7.87μmolL^{-1}; pH=7.0; [$NaNO_3$]=0.1molL^{-1}; RT=24h; A_b=0.388; A_∞=0.728.

Time /s	CuPAR Absorbance (510nm)	Standard deviation (n=2)
0.0	0.581	0.003
0.8	0.585	0.003
1.6	0.588	0.003
2.4	0.590	0.003
3.2	0.592	0.003
4.0	0.594	0.004
4.8	0.596	0.004
5.6	0.597	0.004
6.4	0.599	0.004
8.0	0.601	0.004
9.6	0.604	0.005
11.2	0.606	0.005
13.6	0.609	0.005
16.8	0.611	0.005
20.0	0.614	0.005
24.0	0.617	0.006
28.8	0.620	0.006
34.4	0.622	0.006
41.6	0.625	0.006
49.6	0.628	0.007
60.0	0.631	0.007
72.0	0.634	0.007
85.6	0.637	0.007
103.2	0.640	0.007
123.2	0.643	0.008
147.2	0.645	0.008
176.8	0.648	0.008
212.0	0.651	0.009
253.6	0.654	0.009
303.2	0.656	0.009
363.2	0.658	0.010
435.2	0.661	0.010
520.8	0.663	0.010
624.0	0.665	0.010
747.2	0.667	0.011
894.4	0.669	0.011
1071.2	0.670	0.011
1282.4	0.672	0.011
1535.2	0.674	0.011
1838.4	0.675	0.011
2200.8	0.677	0.010
2635.2	0.679	0.010
3155.2	0.681	0.010
3777.6	0.682	0.010
4522.4	0.684	0.010
5400.0	0.686	0.010

5. [WPNa]=0.05gL^{-1}; Cu_T=7.87μmolL^{-1}; pH=6.0; [$NaNO_3$]=0.1molL^{-1}; RT=96h; A_b=0.388; A_∞=0.728.

Time /s	CuPAR Absorbance (510nm)	Standard deviation (n=3)
0.0	0.575	0.005
0.8	0.578	0.005
1.6	0.581	0.005
2.4	0.583	0.005
3.2	0.585	0.005
4.0	0.586	0.005
4.8	0.588	0.005
5.6	0.589	0.005
6.4	0.591	0.005
8.0	0.593	0.005
9.6	0.595	0.005
11.2	0.597	0.005
13.6	0.599	0.005
16.8	0.602	0.005
20.0	0.604	0.005
24.0	0.607	0.005
28.8	0.610	0.005
34.4	0.612	0.004
41.6	0.615	0.005
49.6	0.618	0.004
60.0	0.621	0.005
72.0	0.624	0.004
85.6	0.626	0.004
103.2	0.629	0.004
123.2	0.632	0.004
147.2	0.635	0.004
176.8	0.637	0.004
212.0	0.640	0.004
253.6	0.643	0.004
303.2	0.645	0.004
363.2	0.647	0.004
435.2	0.650	0.004
520.8	0.652	0.004
624.0	0.655	0.004
747.2	0.657	0.004
894.4	0.659	0.004
1071.2	0.661	0.004
1282.4	0.663	0.004
1535.2	0.665	0.004
1838.4	0.667	0.004
2200.8	0.669	0.004
2635.2	0.671	0.004
3155.2	0.673	0.004
3777.6	0.675	0.004
4522.4	0.677	0.003
5400.0	0.679	0.003

6. [WPNa]=0.05gL^{-1}; Cu_T=7.87μmolL^{-1}; pH=6.5; [$NaNO_3$]=0.1molL^{-1}; RT=24h; A_b=0.403; A_∞=0.739.

Time /s	CuPAR Absorbance (510nm)	Standard deviation (n=3)
0.0	0.610	0.003
0.8	0.613	0.003
1.6	0.616	0.003
2.4	0.618	0.003
3.2	0.620	0.003
4.0	0.622	0.003
4.8	0.623	0.004
5.6	0.625	0.004
6.4	0.626	0.003
8.0	0.629	0.003
9.6	0.631	0.003
11.2	0.632	0.004
13.6	0.635	0.003
16.8	0.638	0.003
20.0	0.640	0.004
24.0	0.643	0.003
28.8	0.645	0.003
34.4	0.648	0.003
41.6	0.651	0.004
49.6	0.653	0.003
60.0	0.656	0.003
72.0	0.659	0.003
85.6	0.661	0.003
103.2	0.664	0.003
123.2	0.667	0.003
147.2	0.669	0.003
176.8	0.672	0.003
212.0	0.675	0.003
253.6	0.677	0.003
303.2	0.679	0.003
363.2	0.682	0.003
435.2	0.684	0.003
520.8	0.687	0.003
624.0	0.689	0.003
747.2	0.691	0.002
894.4	0.693	0.002
1071.2	0.695	0.002
1282.4	0.697	0.002
1535.2	0.699	0.002
1838.4	0.700	0.002
2200.8	0.702	0.002
2635.2	0.703	0.002
3155.2	0.705	0.002
3777.6	0.706	0.002
4522.4	0.707	0.002
5400.0	0.709	0.002

7. [WPNa]=0.05gL^{-1}; Cu_T=7.87μmolL^{-1}; pH=6.5; [$NaNO_3$]=0.1molL^{-1}; RT=48h; A_b=0.403; A_∞=0.739.

Time /s	CuPAR Absorbance (510nm)	Standard deviation (n=3)
0.0	0.625	0.022
0.8	0.628	0.021
1.6	0.631	0.021
2.4	0.633	0.021
3.2	0.635	0.021
4.0	0.638	0.023
4.8	0.642	0.029
5.6	0.644	0.028
6.4	0.645	0.028
8.0	0.648	0.028
9.6	0.649	0.028
11.2	0.651	0.028
13.6	0.654	0.028
16.8	0.656	0.028
20.0	0.659	0.028
24.0	0.661	0.029
28.8	0.664	0.029
34.4	0.666	0.029
41.6	0.669	0.028
49.6	0.671	0.029
60.0	0.674	0.029
72.0	0.677	0.029
85.6	0.679	0.029
103.2	0.682	0.029
123.2	0.685	0.029
147.2	0.687	0.029
176.8	0.690	0.029
212.0	0.693	0.029
253.6	0.695	0.029
303.2	0.698	0.029
363.2	0.700	0.029
435.2	0.703	0.029
520.8	0.705	0.029
624.0	0.708	0.029
747.2	0.710	0.029
894.4	0.712	0.029
1071.2	0.715	0.029
1282.4	0.717	0.029
1535.2	0.719	0.029
1838.4	0.721	0.029
2200.8	0.723	0.029
2635.2	0.725	0.028
3155.2	0.727	0.029
3777.6	0.729	0.029
4522.4	0.731	0.029
5400.0	0.733	0.029

8. [WPNa]=0.025gL^{-1}; Cu_T=7.87μmolL^{-1}; pH=7.0; [$NaNO_3$]=0.1molL^{-1}; RT=24h; A_b=0.328; A_∞=0.644.

Time /s	CuPAR Absorbance (510nm)	Standard deviation (n=3)
0.0	0.5522	0.0042
0.8	0.5552	0.0039
1.6	0.5578	0.0035
2.4	0.5599	0.0034
3.2	0.5619	0.0030
4.0	0.5637	0.0032
4.8	0.5653	0.0032
5.6	0.5668	0.0030
6.4	0.5679	0.0030
8.0	0.5702	0.0029
9.6	0.5724	0.0027
11.2	0.5741	0.0026
13.6	0.5765	0.0026
16.8	0.5792	0.0023
20.0	0.5813	0.0022
24.0	0.5836	0.0022
28.8	0.5859	0.0022
34.4	0.5882	0.0021
41.6	0.5906	0.0020
49.6	0.5929	0.0018
60.0	0.5952	0.0017
72.0	0.5975	0.0017
85.6	0.5994	0.0015
103.2	0.6014	0.0014
123.2	0.6033	0.0013
147.2	0.6050	0.0013
176.8	0.6068	0.0012
212.0	0.6083	0.0011
253.6	0.6097	0.0010
303.2	0.6112	0.0008
363.2	0.6124	0.0007
435.2	0.6135	0.0006
520.8	0.6146	0.0004
624.0	0.6156	0.0006
747.2	0.6164	0.0006
894.4	0.6170	0.0005
1071.2	0.6177	0.0004
1282.4	0.6184	0.0007
1535.2	0.6188	0.0007
1838.4	0.6196	0.0008
2200.8	0.6200	0.0010
2635.2	0.6205	0.0011
3155.2	0.6210	0.0009
3777.6	0.6214	0.0010
4522.4	0.6220	0.0012
5400.0	0.6225	0.0013

9. [WPNa]=0.025gL^{-1}; Cu_T=7.87μmolL^{-1}; pH=7.0; [$NaNO_3$]=0.1molL^{-1}; RT=144h; A_b=0.328; A_∞=0.644.

Time /s	CuPAR Absorbance (510nm)	Standard deviation (n=3)
0.0	0.558	0.010
0.8	0.560	0.010
1.6	0.563	0.010
2.4	0.565	0.010
3.2	0.566	0.010
4.0	0.568	0.010
4.8	0.569	0.010
5.6	0.571	0.010
6.4	0.572	0.010
8.0	0.574	0.011
9.6	0.576	0.011
11.2	0.577	0.011
13.6	0.579	0.011
16.8	0.582	0.011
20.0	0.584	0.011
24.0	0.586	0.011
28.8	0.588	0.010
34.4	0.590	0.011
41.6	0.592	0.011
49.6	0.594	0.011
60.0	0.596	0.010
72.0	0.599	0.010
85.6	0.601	0.010
103.2	0.603	0.010
123.2	0.605	0.010
147.2	0.606	0.010
176.8	0.608	0.010
212.0	0.609	0.010
253.6	0.611	0.010
303.2	0.612	0.010
363.2	0.613	0.010
435.2	0.614	0.010
520.8	0.615	0.010
624.0	0.616	0.010
747.2	0.617	0.010
894.4	0.618	0.010
1071.2	0.619	0.011
1282.4	0.620	0.011
1535.2	0.621	0.011
1838.4	0.621	0.011
2200.8	0.622	0.011
2635.2	0.623	0.011
3155.2	0.624	0.011
3777.6	0.625	0.012
4522.4	0.626	0.012
5400.0	0.627	0.012

10. [WPNa]=0.025gL^{-1}; Cu_T=7.87μmolL^{-1}; pH=6.5; [$NaNO_3$]=0.1molL^{-1}; RT=24h; A_b=0.346; A_∞=0.679.

Time /s	CuPAR Absorbance (510nm)	Standard deviation (n=3)
0.0	0.601	0.046
0.8	0.604	0.046
1.6	0.607	0.046
2.4	0.609	0.046
3.2	0.611	0.046
4.0	0.612	0.046
4.8	0.614	0.046
5.6	0.615	0.046
6.4	0.616	0.046
8.0	0.619	0.046
9.6	0.621	0.046
11.2	0.622	0.046
13.6	0.625	0.046
16.8	0.627	0.046
20.0	0.629	0.046
24.0	0.631	0.046
28.8	0.633	0.047
34.4	0.636	0.047
41.6	0.638	0.047
49.6	0.640	0.047
60.0	0.642	0.047
72.0	0.644	0.047
85.6	0.646	0.047
103.2	0.648	0.047
123.2	0.650	0.047
147.2	0.651	0.047
176.8	0.653	0.047
212.0	0.654	0.047
253.6	0.656	0.047
303.2	0.657	0.047
363.2	0.658	0.047
435.2	0.659	0.047
520.8	0.661	0.047
624.0	0.662	0.047
747.2	0.663	0.047
894.4	0.664	0.048
1071.2	0.665	0.048
1282.4	0.666	0.047
1535.2	0.667	0.047
1838.4	0.668	0.047
2200.8	0.668	0.047
2635.2	0.669	0.048
3155.2	0.670	0.047
3777.6	0.670	0.048
4522.4	0.671	0.047
5400.0	0.671	0.047

11. [WPNa]=0.025gL^{-1}; Cu_T=7.87μmolL^{-1}; pH=6.5; [$NaNO_3$]=0.1molL^{-1}; RT=168h; A_b=0.346; A_∞=0.679.

Time /s	CuPAR Absorbance (510nm)	Standard deviation (n=2)
0.0	0.5496	0.0006
0.8	0.5520	0.0005
1.6	0.5542	0.0007
2.4	0.5561	0.0006
3.2	0.5577	0.0004
4.0	0.5592	0.0006
4.8	0.5606	0.0007
5.6	0.5618	0.0008
6.4	0.5630	0.0008
8.0	0.5648	0.0006
9.6	0.5667	0.0004
11.2	0.5683	0.0005
13.6	0.5701	0.0006
16.8	0.5725	0.0005
20.0	0.5745	0.0006
24.0	0.5762	0.0003
28.8	0.5785	0.0007
34.4	0.5805	0.0004
41.6	0.5826	0.0003
49.6	0.5847	0.0003
60.0	0.5867	0.0004
72.0	0.5886	0.0002
85.6	0.5905	0.0005
103.2	0.5926	0.0004
123.2	0.5941	0.0003
147.2	0.5959	0.0005
176.8	0.5979	0.0001
212.0	0.5994	0.0001
253.6	0.6012	0.0002
303.2	0.6027	0.0004
363.2	0.6042	0.0003
435.2	0.6059	0.0001
520.8	0.6075	0.0003
624.0	0.6091	0.0006
747.2	0.6106	0.0004
894.4	0.6121	0.0006
1071.2	0.6137	0.0006
1282.4	0.6149	0.0005
1535.2	0.6162	0.0004
1838.4	0.6175	0.0006
2200.8	0.6187	0.0004
2635.2	0.6198	0.0004
3155.2	0.6209	0.0006
3777.6	0.6221	0.0009
4522.4	0.6236	0.0014
5400.0	0.6251	0.0023

12. [WPNa]=0.025gL^{-1}; Cu_T=7.87μmolL^{-1}; pH=6.0; [$NaNO_3$]=0.01molL^{-1}; RT=24h; A_b=0.372; A_∞=0.695.

Time /s	CuPAR Absorbance (510nm)	Standard deviation (n=2)
0.0	0.6245	0.0022
0.8	0.6260	0.0023
1.6	0.6272	0.0025
2.4	0.6282	0.0024
3.2	0.6293	0.0024
4.0	0.6304	0.0018
4.8	0.6312	0.0016
5.6	0.6320	0.0019
6.4	0.6324	0.0020
8.0	0.6336	0.0021
9.6	0.6345	0.0020
11.2	0.6352	0.0021
13.6	0.6363	0.0021
16.8	0.6373	0.0018
20.0	0.6385	0.0021
24.0	0.6393	0.0023
28.8	0.6409	0.0014
34.4	0.6413	0.0017
41.6	0.6424	0.0019
49.6	0.6434	0.0020
60.0	0.6443	0.0020
72.0	0.6453	0.0020
85.6	0.6461	0.0016
103.2	0.6469	0.0016
123.2	0.6475	0.0019
147.2	0.6484	0.0018
176.8	0.6492	0.0015
212.0	0.6500	0.0015
253.6	0.6505	0.0017
303.2	0.6510	0.0015
363.2	0.6515	0.0015
435.2	0.6520	0.0015
520.8	0.6524	0.0014
624.0	0.6527	0.0011
747.2	0.6529	0.0011
894.4	0.6533	0.0008
1071.2	0.6539	0.0010
1282.4	0.6539	0.0006
1535.2	0.6541	0.0006
1838.4	0.6545	0.0006
2200.8	0.6544	0.0005
2635.2	0.6546	0.0003
3155.2	0.6548	0.0001
3777.6	0.6548	0.0001
4522.4	0.6548	0.0002
5176.0	0.6546	0.0002

13. [WPNa]=0.025gL^{-1}; Cu_T=7.87μmolL^{-1}; pH=6.0; [$NaNO_3$]=0.01molL^{-1}; RT=72h; A_b=0.372; A_∞=0.695.

Time /s	CuPAR Absorbance (510nm)	Standard deviation (n=3)
0.0	0.6203	0.0036
0.8	0.6216	0.0034
1.6	0.6229	0.0032
2.4	0.6236	0.0029
3.2	0.6246	0.0026
4.0	0.6253	0.0027
4.8	0.6258	0.0029
5.6	0.6263	0.0026
6.4	0.6270	0.0029
8.0	0.6278	0.0026
9.6	0.6287	0.0023
11.2	0.6294	0.0024
13.6	0.6301	0.0025
16.8	0.6313	0.0023
20.0	0.6321	0.0026
24.0	0.6331	0.0025
28.8	0.6340	0.0024
34.4	0.6348	0.0024
41.6	0.6357	0.0024
49.6	0.6365	0.0026
60.0	0.6372	0.0024
72.0	0.6381	0.0023
85.6	0.6388	0.0024
103.2	0.6395	0.0022
123.2	0.6403	0.0020
147.2	0.6409	0.0022
176.8	0.6414	0.0022
212.0	0.6422	0.0021
253.6	0.6425	0.0020
303.2	0.6432	0.0019
363.2	0.6435	0.0019
435.2	0.6441	0.0017
520.8	0.6446	0.0019
624.0	0.6450	0.0016
747.2	0.6455	0.0013
894.4	0.6460	0.0010
1071.2	0.6464	0.0009
1282.4	0.6467	0.0006
1535.2	0.6473	0.0005
1838.4	0.6478	0.0002
2200.8	0.6478	0.0001
2635.2	0.6483	0.0002
3155.2	0.6485	0.0007
3777.6	0.6487	0.0007
4522.4	0.6487	0.0011
5400.0	0.6488	0.0011

14. [WPNa]=0.025gL^{-1}; Cu_T=7.87μmolL^{-1}; pH=6.0; [$NaNO_3$]=0.001molL^{-1}; RT=24h; A_b=0.364; A_∞=0.700.

Time /s	CuPAR Absorbance (510nm)	Standard deviation (n=3)
0.0	0.628	0.003
0.8	0.629	0.003
1.6	0.629	0.003
2.4	0.630	0.003
3.2	0.630	0.003
4.0	0.631	0.003
4.8	0.631	0.003
5.6	0.631	0.003
6.4	0.631	0.003
8.0	0.632	0.003
9.6	0.632	0.003
11.2	0.633	0.003
13.6	0.633	0.003
16.8	0.634	0.003
20.0	0.634	0.003
24.0	0.634	0.003
28.8	0.635	0.003
34.4	0.635	0.003
41.6	0.636	0.003
49.6	0.636	0.003
60.0	0.637	0.003
72.0	0.637	0.004
85.6	0.637	0.004
103.2	0.638	0.004
123.2	0.638	0.004
147.2	0.638	0.004
176.8	0.638	0.004
212.0	0.639	0.004
253.6	0.639	0.004
303.2	0.639	0.004
363.2	0.639	0.004
435.2	0.639	0.004
520.8	0.639	0.004
624.0	0.640	0.004
747.2	0.640	0.004
894.4	0.640	0.004
1071.2	0.640	0.004
1282.4	0.640	0.004
1535.2	0.640	0.004
1838.4	0.640	0.004
2200.8	0.640	0.004
2635.2	0.640	0.004
3155.2	0.640	0.003
3777.6	0.640	0.004
4522.4	0.640	0.004
5400.0	0.640	0.004

15. [WPNa]=0.025gL^{-1}; Cu_T=7.87μmolL^{-1}; pH=7.0; [$NaNO_3$]=0.01molL^{-1}; RT=24h; A_b=0.311; A_∞=0.659.

Time /s	CuPAR Absorbance (510nm)	Standard deviation (n=3)
0.0	0.589	0.002
0.8	0.591	0.002
1.6	0.593	0.002
2.4	0.594	0.002
3.2	0.596	0.002
4.0	0.597	0.002
4.8	0.598	0.002
5.6	0.600	0.002
6.4	0.600	0.002
8.0	0.602	0.002
9.6	0.604	0.002
11.2	0.605	0.002
13.6	0.606	0.002
16.8	0.608	0.002
20.0	0.609	0.002
24.0	0.611	0.002
28.8	0.612	0.003
34.4	0.614	0.003
41.6	0.616	0.003
49.6	0.617	0.003
60.0	0.618	0.003
72.0	0.620	0.003
85.6	0.621	0.003
103.2	0.622	0.003
123.2	0.623	0.003
147.2	0.625	0.003
176.8	0.626	0.003
212.0	0.627	0.003
253.6	0.628	0.003
303.2	0.629	0.004
363.2	0.630	0.004
435.2	0.630	0.004
520.8	0.631	0.004
624.0	0.632	0.004
747.2	0.632	0.004
894.4	0.633	0.004
1071.2	0.634	0.004
1282.4	0.634	0.004
1535.2	0.634	0.004
1838.4	0.635	0.004
2200.8	0.635	0.004
2635.2	0.635	0.004
3155.2	0.636	0.004
3777.6	0.636	0.004
4522.4	0.636	0.003
5400.0	0.636	0.003

16. [WPNa]=0.025gL^{-1}; Cu_T=7.87μmolL^{-1}; pH=7.0; [$NaNO_3$]=0.01molL^{-1}; RT=48h; A_b=0.311; A_∞=0.659.

Time /s	CuPAR Absorbance (510nm)	Standard deviation (n=3)
0.0	0.578	0.001
0.8	0.581	0.001
1.6	0.583	0.001
2.4	0.584	0.001
3.2	0.586	0.001
4.0	0.587	0.001
4.8	0.588	0.001
5.6	0.589	0.001
6.4	0.590	0.001
8.0	0.592	0.001
9.6	0.594	0.001
11.2	0.595	0.001
13.6	0.596	0.001
16.8	0.598	0.001
20.0	0.600	0.001
24.0	0.601	0.001
28.8	0.603	0.001
34.4	0.604	0.001
41.6	0.606	0.001
49.6	0.607	0.001
60.0	0.609	0.001
72.0	0.611	0.001
85.6	0.612	0.001
103.2	0.613	0.001
123.2	0.615	0.001
147.2	0.616	0.001
176.8	0.618	0.001
212.0	0.619	0.001
253.6	0.620	0.001
303.2	0.621	0.001
363.2	0.622	0.001
435.2	0.624	0.001
520.8	0.625	0.001
624.0	0.626	0.001
747.2	0.627	0.001
894.4	0.627	0.001
1071.2	0.628	0.001
1282.4	0.629	0.001
1535.2	0.630	0.002
1838.4	0.631	0.002
2200.8	0.631	0.002
2635.2	0.632	0.002
3155.2	0.632	0.002
3777.6	0.633	0.002
4522.4	0.633	0.002
4820.0	0.633	0.002

17. [WPNa]=0.025gL^{-1}; Cu_T=7.87μmolL^{-1}; pH=6.5; [$NaNO_3$]=0.01molL^{-1}; RT=24h; A_b=0.337; A_∞=0.658.

Time /s	CuPAR Absorbance (510nm)	Standard deviation (n=3)
0.0	0.605	0.001
0.8	0.607	0.001
1.6	0.608	0.001
2.4	0.609	0.001
3.2	0.610	0.001
4.0	0.611	0.001
4.8	0.612	0.001
5.6	0.613	0.001
6.4	0.613	0.001
8.0	0.615	0.001
9.6	0.615	0.001
11.2	0.616	0.001
13.6	0.617	0.001
16.8	0.618	0.001
20.0	0.619	0.001
24.0	0.620	0.001
28.8	0.621	0.001
34.4	0.622	0.001
41.6	0.623	0.001
49.6	0.624	0.001
60.0	0.625	0.002
72.0	0.626	0.001
85.6	0.627	0.001
103.2	0.628	0.002
123.2	0.629	0.001
147.2	0.630	0.002
176.8	0.631	0.002
212.0	0.631	0.002
253.6	0.632	0.002
303.2	0.633	0.002
363.2	0.633	0.002
435.2	0.634	0.002
520.8	0.634	0.002
624.0	0.635	0.002
747.2	0.635	0.002
894.4	0.636	0.002
1071.2	0.636	0.002
1282.4	0.636	0.002
1535.2	0.636	0.002
1838.4	0.637	0.002
2200.8	0.637	0.002
2635.2	0.637	0.002
3155.2	0.638	0.002
3777.6	0.638	0.002
4522.4	0.639	0.002
5400.0	0.640	0.003

18. [WPNa]=0.025gL^{-1}; Cu_T=7.87μmolL^{-1}; pH=6.5; [$NaNO_3$]=0.01molL^{-1}; RT=96h; A_b=0.337; A_∞=0.658.

Time /s	CuPAR Absorbance (510nm)	Standard deviation (n=4)
0.0	0.589	0.003
0.8	0.591	0.003
1.6	0.592	0.002
2.4	0.593	0.002
3.2	0.594	0.002
4.0	0.595	0.002
4.8	0.596	0.002
5.6	0.596	0.002
6.4	0.597	0.002
8.0	0.598	0.002
9.6	0.599	0.002
11.2	0.600	0.002
13.6	0.601	0.002
16.8	0.602	0.002
20.0	0.603	0.002
24.0	0.604	0.002
28.8	0.605	0.002
34.4	0.606	0.002
41.6	0.607	0.002
49.6	0.608	0.002
60.0	0.610	0.002
72.0	0.611	0.002
85.6	0.611	0.002
103.2	0.612	0.002
123.2	0.613	0.002
147.2	0.614	0.002
176.8	0.615	0.002
212.0	0.616	0.002
253.6	0.617	0.002
303.2	0.617	0.002
363.2	0.618	0.002
435.2	0.619	0.002
520.8	0.619	0.001
624.0	0.620	0.001
747.2	0.621	0.001
894.4	0.621	0.001
1071.2	0.622	0.001
1282.4	0.622	0.001
1535.2	0.623	0.001
1838.4	0.623	0.001
2200.8	0.624	0.001
2635.2	0.624	0.001
3155.2	0.624	0.001
3777.6	0.625	0.001
4522.4	0.625	0.001
5400.0	0.626	0.001